Martin Waldhör

Hennentalweg 19
72070 Tübingen

The SMALL-CIRCLE RECONSTRUCTION

in Palaeomagnetism

and its Application to Palaeomagnetic Data from the Pamirs

Tübingen, 1998

Abstract

Through tilting, in-situ remanences become distributed on a small circle (*remanence small circle*), which is perpendicular to the tilt axis. Small-circle distributions can be observed in folded sequences, single sites and single specimens. This aspect and its consequences for the interpretation of palaeomagnetic remanences obviously have not been discovered before, though it is a common property of in-situ remanences in folded sequences. The position of a remanence small circle is a function of the acquisition field (D/I) and the trend of the tilt axis. With the assumption that tilting and block rotation occur around horizontal and vertical axes, tilting and block rotation of an in-situ remanence can be reconstructed. This *small-circle reconstruction* is ambiguous, but equivalent reconstructions can be resolved by additional information, e.g. upright or overturned bedding, results from adjacent sites and local geology. From originally E-W or close to E-W tilted sites, the inclination of the palaeofield can be estimated, thus, providing an alternative approach to the palaeoinclination, no matter if remanences are primary or secondary. Finally, if in-situ remanence components of one site have recorded different increments of the displacement, they directly give a path of displacement. The small-circle concept provides a comprehensive approach to the interpretation of palaeomagnetic remanences. The conventional aspects of palaeomagnetism such as the two-dimensional Gaussian distribution, Fisher statistics and bedding correction, are fully incorporated. The new method allows the analysis of a much broader range of data and is the key to the use of secondary remanences. Data which up to now had to be discarded as statistically non-significant or meaningless, can now be interpreted.

Palaeoremanences of 90 analysed sites from the Pamirs, mostly carried by magnetite, show an overall secondary character. According to geochronological data, overprinting probably took place 20 Ma ago throughout the Pamirs. The small-circle reconstruction indicates that the palaeoinclination at the time of remanence acquisition unlikely exceeded 55° in the southern Pamirs, implying a minimum of about 440 km of N-S oriented crustal shortening in the past 20 Ma between the southern Pamirs and stable Eurasia. In the southern and central Pamirs, the tilt axes at present have a preferred trend around E-W. After reconstruction, the trends of the tilt axes show a much broader distribution. Hence, the present orientation of the tilt axes around E-W most probably is (1) at least partly a product of the block rotations and (2) a consequence of N-S shortening. This implies that, to some extent, tilting and block rotation must have occurred simultaneously, or in alternating increments. On the assumption that a uniform N-S shortening regime aligned the tilt axes through block rotation, the amount of shortening is estimated to about 60% in the southern Pamirs, and to about 40% in the central Pamirs.

With at least three to four different remanence components, Jurassic limestones from the central Pamirs show a possibly continuous, tape-like record of tectonic displacement, revealing the relation of the remagnetisation to the Miocene uplift of the adjacent metamorphic dome. The distribution of normal and reverse polarity remanences in these displacement paths indicates that the duration of their acquisition and thus folding unlikely exceeded 2 Ma. Since then, no further folding can have occurred there, because the last acquired remanences today still are close to the reference field direction.

For the tectonic evolution of the Pamirs, the following sequence of events is proposed: Northward convergence affects first the southern and central Pamirs, pushes them against the northern Pamirs and causes intense internal N-S shortening. Folding ends - at least in the central Pamirs - already in the Early Miocene. Then, active shortening shifts to the northern frontal thrust zone and the whole Pamirs move en-bloc to the north.

Kurzfassung

Faltung bewirkt die Verteilung von In-situ-Remanenzen auf Kleinkreisen (*Remanenzkleinkreisen*) senkrecht zur Verkippungsachse. Die Kleinkreisverteilung ist eine allgemeine Eigenschaft von In-situ-Remanenzen in gefalteten Abfolgen, sie ist aber auch in einzelnen Sites und sogar in Einzelproben anzutreffen. Ihre umfassende Bedeutung für die Auswertung paläomagnetischer Daten ist offensichtlich bisher unerkannt geblieben.
Die Lage eines Remanenzkleinkreises ist eine Funktion des Erwerbsfeldes (D/I) und des Azimuths der Verkippungsachse. Unter der Voraussetzung, daß die Verkippung und Blockrotation um horizontale bzw. vertikale Achsen erfolgen, können die Verkippung und die Blockrotation rekonstruiert werden. Für diese sog. *Kleinkreisrekonstruktion* gibt es immer mehrere Lösungen. Äquivalente Rekonstruktionen können durch zusätzliche Informationen ausgeschlossen werden, wie beispielsweise die Lagerungsverhältnisse (aufrecht, überkippt), Ergebnisse von benachbarten Sites oder der lokale geologische Kontext.
Im Fall von in E-W bzw. nahe in E-W Richtung gefalteten Sites kann die Paläoinklination des Erwerbsfeldes bzw. ihre Obergrenze rekonstruiert werden. Damit besteht ein alternatives Verfahren zur Bestimmung der Paläoinklination, ganz gleich, ob die Remanenzen primär oder sekundär sind. Wenn Remanenzkomponenten Inkremente der Verstellung aufgezeichnet haben, geben sie direkt den Pfad der Verstellung an. Das Konzept der Kleinkreisrekonstruktion ist ein vereinheitlichender Ansatz zur Interpretation von primären und sekundären Remanenzen. Die konventionellen Aspekte und Verfahren der Paläomagnetik (zweidimensionale Gaussverteilung, Fisher Statistik, Schichtlagenkorrektur) sind darin vollständig enthalten. Das neue Verfahren ermöglicht die Verwertung einer wesentlich größeren Bandbreite von Daten, die bisher als statistisch nicht signifikant oder bedeutungslos angesehen wurden. Vor allen Dingen sekundäre Remanenzen, die zuvor nicht korrekt interpretierbar waren, können jetzt wesentlich besser ausgewertet werden.
Paläoremanenzen von 90 analysierten Sites aus dem Pamirgebirge, überwiegend von Magnetit getragen, zeigen einen insgesamt sekundären Charakter. Ar-Ar- und Spaltspurendatierungen deuten darauf hin, daß die Remagnetisierung vermutlich vor 20 Ma im gesamten Pamir erfolgte. Die Kleinkreisrekonstruktion ergibt, daß die Paläoinklination am Probenort zu dieser Zeit sehr wahrscheinlich nicht größer war als 55°. Dies wiederum bedeutet eine minimale Krustenverkürzung von ca. 440 km seit 20 Ma zwischen dem südlichen Pamir und stabilem Eurasien im Norden. Im südlichen Pamir liegen die Verkippungsachsen heute in einer Orientierung vorwiegend um E-W (90°) vor. Mit der Rekonstruktion wird jedoch die Streuung erheblich breiter. Die heutige Orientierung der Verkippungsachsen um E-W ist daher (1) das zumindest teilweise Resultat von Blockrotationen und (2) eine Folge der N-S Verkürzung. Dies bedeutet wiederum, daß Faltung und Blockrotation in gewissem Ausmaß gleichzeitig oder in alternierenden Teilschritten erfolgt sind. Unter der Annahme, daß N-S Verkürzung die Verkippungsachsen in Richtung E-W einrotiert hat, wurde der Verkürzungsbetrag im südlichen Pamirs zu 60% und im zentralen Pamir zu 40% bestimmt.
In jurassischen Kalken des zentralen Pamirs zeigen die Remanenzen mit mindestens drei bis vier inkrementellen Remanenzkomponenten eine detaillierte, möglicherweise sogar kontinuierliche Aufzeichnung der tektonischen Verstellung. Dabei zeigt sich, daß die Remagnetisierung von dem angrenzenden metamorphen Dom verursacht wurde, der im Miozän aufgestiegen ist. Die Häufigkeit von normal und invers polaren Remanenzen legt nahe, daß die Zeitdauer des Remanenzerwerbs und damit der Faltung 2 Ma nicht überstiegen hat. Danach kann keine Faltung mehr erfolgt sein, da die zuletzt erworbenen Remanenzen heute immer noch nahe der Referenzfeldrichtung liegen.
Für die tektonische Entwicklung des Pamirs erscheint folgender Ablauf plausibel: Nordgerichtete Konvergenz erfaßt zuerst den südlichen und zentralen Pamir, schiebt diese Einheiten gegen den nördlichen Pamir und verkürzt sie stark. Die Faltung endet - zumindest im zentralen Pamir - im frühen Miozän. Danach springt die aktive Eingengung nach Norden und der gesamte Pamir wird en-bloc nach Norden geschoben.

Resumen

El plegamiento de capas geológicas resulta en la distribución de remanencias „in-situ“ en un círculo pequeño (*círculo pequeño de remanencia*) perpendicular al eje de rotación. Esta distribución se encuentra

en secuencias plegadas, en sitios individuales y en especímenes particulares. Este aspecto y sus consecuencias para la interpretación de remanencias paleomagnéticas no fueron descubiertos antes, aunque es un atributo general de las remanencias „in-situ“ en terrenos plegados. La posición de un círculo pequeño de remanencias es una función del campo magnético de adquisición (D/I) y del azimut del eje de rotación. Bajo la condición que el plegamiento y la rotación de los bloques ocurrieron alrededor de ejes horizontales y verticales, el plegamiento y la rotación de los bloques de una remanencia „in-situ“ pueden ser reconstruidos. Esta *reconstrucción de círculo pequeño* es ambigua, pero las reconstrucciones equivalentes pueden ser resueltas con informaciones adicionales, p. ej. con la orientación de las capas (normal o invertida), con los resultados de sitios adyacentes y con la geología local. Sitios que originalmente fueron plegados en la dirección E-W, proveen la inclinación del campo magnético, de esta manera, se tiene un acceso alternativo a la paleoinclinación, no importa si las remanencias son de origen primario o secundario. Finalmente, si las remanencias de los componentes de uno de los sitio han registrado los incrementos del movimiento tectónico, ellos directamente demuestran trayectoria del desplazamiento. El concepto de la distribución en círculos pequeños provee un acceso comprensivo a la interpretación de remanencias primarias y secundarias. Los aspectos convencionales paleomagnéticos - distribución bidimensional Gaussiana, estadística Fisher, corrección tectónica de estratos - se integran por completo. El concepto permite el análisis de un rango de datos mucho más amplio y a la vez es la llave al uso de remanencias de origen secundario. Datos que fueron calificados como insignificantes en el sentido estadístico, pueden ser interpretados ahora.

Paleoremanencias de 90 sitios analizados en el Pamir, principalmente llevado por magnetita, muestran en total un carácter secundario. Según Ar-Ar y „fisson track“ análisis geochronólogicos, la remagnetización probablemente se efectuó hace 20 Ma en todo el Pamir. La reconstrucción de círculos pequeños indica que la paleoinclinacíon en el momento de la adquisición de la remanencia probablemente no fue mayor que los 55° en el Pamir sureño, implicando un mínimo de aproximadamente 440 km de acortamiento de la corteza en los pasados 20 Ma entre el Pamir sureño y la estable Eurasia en el norte. En el Pamir sureño, los ejes de rotación en la actualidad tienen una orientación preferencial E-W. Después de la reconstrucción, los ejes demuestran una dispersión mucho mas amplia.

Por ende, la orientación presente de los ejes es (1) al menos en parte un effecto de la rotación de los bloques y (2) una consecuencia de la convergencia N-S. El plegamiento y la rotación de los bloques deben haber ocurrido simultaneamente o en pequeños pasos alternados. Con la suposición de que la convergencia N-S ha alineado los ejes mediante la rotación de bloques, la magnitud de la convergencia es aproximadamente de un 60% en el Pamir sureño, y cercana al 40% en el Pamir central. La orientación actual de los ejes alrededor de E-W probablemente es la consecuencia de convergencia orientada N-S, alineando los ejes.

En calizas jurásicas del Pamir central, las remanencias posiblemente muestran un registro continuo de los movimientos tectónicos, presentando una relación entre la remagnetización Miocénica y el domo metamórfico adyacente. La distribución de las remanencias de polaridad normal e inversa adquiridas durante la deformación tectónica, indica que la duración de la adquisición y del plegamiento probablemente no ha durado más de 2 Ma. Desde entonces, ningún plegamiento adicional puede haber ocurrido ya que las remanencias adquiridas al final, actualmente están cerca del campo magnético de referencia. Con respecto a la evolución tectónica del Pamir, proponemos la siguiente secuencia: La convergencia N-S afecta inicialmente el Pamir sureño y central, empujándolos contra el Pamir norteño y causando una intensa deformación interna. El plegamiento cesa - al menos en el Pamir central - ya en el Mioceno. La convergencia activa se desplaza a la zona frontal del Pamir norteño y el Pamir como una unidad avanza hacia el norte.

Introduction

Remagnetisation is one of the main problems in palaeomagnetism. If, after time consuming measurements, an overall secondary character of the remanences turns out, most efforts are thought to be in vain. This thesis introduces the *small-circle reconstruction*, a new approach to the tectonic interpretation of in-situ remanences.

Section 1 presents the concept of the small-circle distribution of in-situ remanences as the consequence of tilting and/or block rotation, providing a comprehensive explanation for the distribution of in-situ remanences in folded terrains. The conventional concepts of palaeomagnetism are fully incorporated. Given an appropriate data set basically the same information can be extracted from secondary data as from primary data.

Section 2 presents a palaeomagnetic investigation in the Pamirs, still a rather blank area on the palaeomagnetic map of the India-Asia collision zone. The results of the rock- and palaeomagnetic measurements with fold tests will be documented according to the conventional procedures.

Section 3 applies the small-circle reconstruction to the palaeomagnetic data of the investigated area, showing the new concept to be an effective tool for analysis and interpretation in palaeomagnetism.

1. The Small-Circle Concept

1.1 Introduction

Palaeomagnetic analysis and interpretation almost exclusively focus on bedding corrected remanence directions. Bedding (or tilt) correction tilts the rock layer with its remanence vector back to the horizontal around the strike of the bedding plane. If the remanence is primary, it will be restored to its original inclination and can be interpreted in terms of N-S movement and block rotation. If secondary, tilt correction gives a meaningless result. Secondary in-situ remanences have been interpreted only, if the remanences were acquired after folding was completed.

This procedure overlooks two basic aspects of in-situ remanences:

(a) In-situ remanences reflect a true net amount of rotational displacement since their acquisition.

(b) The distribution of in-situ remanences is related to the direction, angle and sense of tilting.

The following concept outlines how tilting and block rotation control the distribution of in-situ remanences. With a known acquisition field, this relationship allows tectonic rotations to be extracted from in-situ remanences alone. The concept bases on two assumptions which in nature mostly are reasonable and also are part of the established data processing and interpretation procedure in palaeomagnetism:

(a) Tilting occurs around horizontal axes.

(b) Block rotation occurs around vertical axes.

These assumptions are certainly valid in general for deformation at shallow depth and moderate metamorphism. Possible exceptions such as deformation in shear zones have to be avoided by adequate sampling.

The fold test according to McFadden (1990) bases on a correlation of remanence direction and tectonic tilt, but does not denote the small-circle distribution of remanences due to tectonic displacement. Mardia & Gadsden (1977) report a possible small-circle distribution of palaeomagnetic directions, but not related to tectonic displacement. Statistical treatment of small-circle distributions has been described by Mardia & Gadsden (1977), Gray et al. (1980) and Fisher et al. (1987). MacDonald (1980) discusses net tectonic rotation and tilt correction in palaeomagnetism. He notes that palaeomagnetic poles (in bedding coordinates) can have a small-circle distribution, but attributes this to an inappropriate tilt correction. Ménard & Rochette (1992) and Crouzet et al. (1996) report the scatter of secondary remanences due to rotational displacement around a horizontal axis, but do not note their obvious small-circle distribution. They determine tilt angles between the remanences and an expected reference palaeofield using a projection method not described in detail.

Therefore, it seems the small-circle distribution of in-situ remanences due to tectonic displacement and i.e. the consequences on palaeomagnetic methodology have not been recognised before.

1.2 Terminology and Conventions

The conventions used from here on are illustrated in Fig. 1.1. *Tilting* will refer to rotation around horizontal axes and *block rotation* will refer to rotation around vertical axes. *Displacement* means rotational rigid body displacement including *tilting* and *block rotation*. The term *displacement path* denotes the path of these rotations. The term *tilting direction* denotes the projection of the *dip vector* of a layer to the horizontal x-y plane. The tilting direction is perpendicular to the corresponding tilt axis. The Cartesian coordinate system and the rotation senses will be defined as shown in Fig. 1.1. The trend of the tilt axis varies between 0° and 180°. The rotation angle is clockwise negative and counterclockwise positive when viewed from the sphere centre (downwards for block rotation). The angular distance *d* (defined in the next section) is positive to the right of the Π-circle (mean great circle for a distribution of bedding poles) or tilting direction (in the case of one bedding pole), and negative to the left of it. Theoretical considerations will always be presented in orthographic projections, where small circles parallel to the z-axis show up as straight lines. Real data will be shown in equal-area projections.

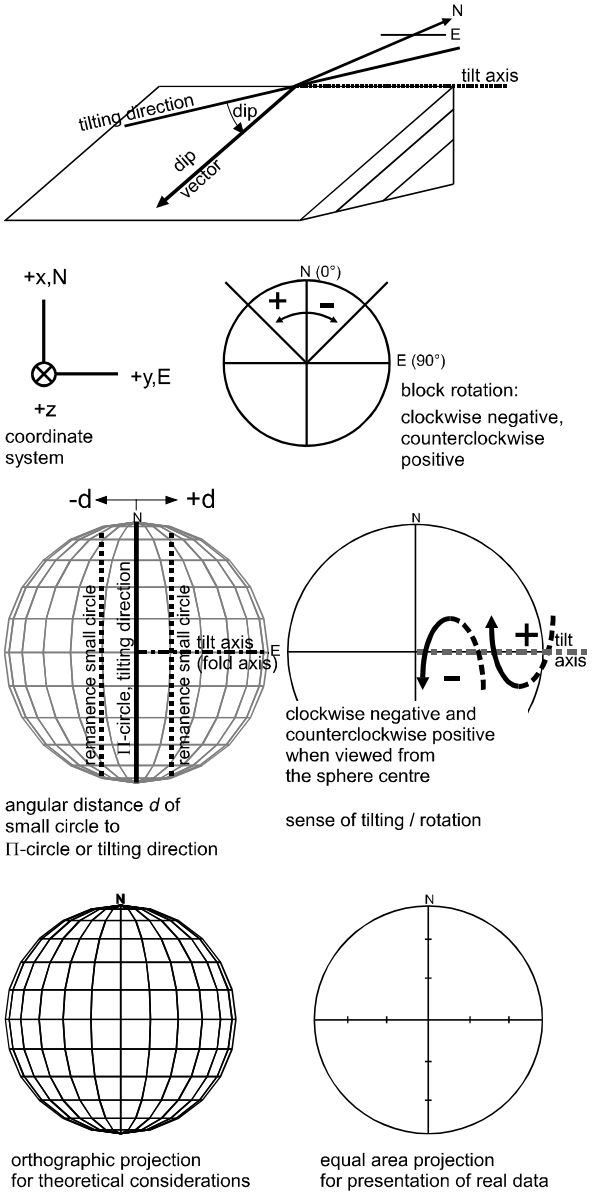

Fig. 1.1: Conventions for coordinate system, block rotation, tilting, rotation senses and projections. The term *tilting direction* denotes the projection of the *dip vector* of a layer to the horizontal plane. The trend of the tilt axis varies between 0° and 180°. Rotations (tilting and block rotation) are clockwise negative and counterclockwise positive, when viewed from the sphere centre (downwards for block rotation). For graphical presentation of theoretical considerations, the orthographic projection will be used. Real data will be shown in equal-area projections.

Further on, four types of palaeomagnetic data will be under consideration. To avoid confusion, the following terms will be used:

- *Site mean* as calculated by Fisher statistics (Fisher 1953) for a number of single specimen remanence components.
- *Remanence component* from a single specimen obtained by component analysis.
- *Remanence direction* as measured at a single step during the demagnetisation of single specimens (raw data).

- *Differential vector* as calculated from the remanence directions of subsequent steps during demagnetisation.

Remanence will be used as a general term encompassing all these kinds of directional palaeomagnetic data. D_{bc}/I_{bc} and D_{is}/I_{is} denote declination and inclination in bedding coordinates and in-situ coordinates, respectively. A glossary at the end of this thesis lists the most relevant and partly new terms as well as frequently used abbreviations.

1.3 The Small-Circle Distribution of In-Situ Remanences

Palaeomagnetic remanences in rocks are thought to be acquired in a geomagnetic dipole field. Assuming an axial geocentric dipole and averaged on secular variation, this field has a zero declination and an inclination as a function of the latitude. Tilting and block rotation will rotate the in-situ remanence away from the original position. Primary remanences undergo all sequences of displacement, secondary remanences only that part which occurs after their acquisition.

The control on the distribution of in-situ remanences by the tilting direction (or tilt axis) and the field of acquisition is illustrated in Fig. 1.2. In a three-dimensional perspective view, Fig. 1.2a shows remanence directions acquired at a field of $I_{acq} = 60°$, that rotate on small circles around three different tilt axes. Each remanence small circle is perpendicular to its corresponding tilt axis. For each field polarity, one small circle exists (Fig. 1.2b-d). Both small circles are parallel to the tilting direction. For a given field inclination, the angular distance *d* of the small circles to the tilting direction is a function of the trend of the tilt axis. N-S oriented tilting produces a zero distance, E-W oriented tilting the largest distance.

The trend of the tilt axis *t* and the angular distance *d* as a fraction of the radius of the sphere (*r* = 1) are given by:

$$d = \cos t \quad \cos I_{acq} \qquad (1)$$

t trend of the tilt axis; I_{acq} inclination of the acquisition field

Hence, with a known acquisition field, the original tilt axis can be determined from the angular distance *d*. A subsequent block rotation can be inferred by comparison of the calculated tilt axis with the present one.

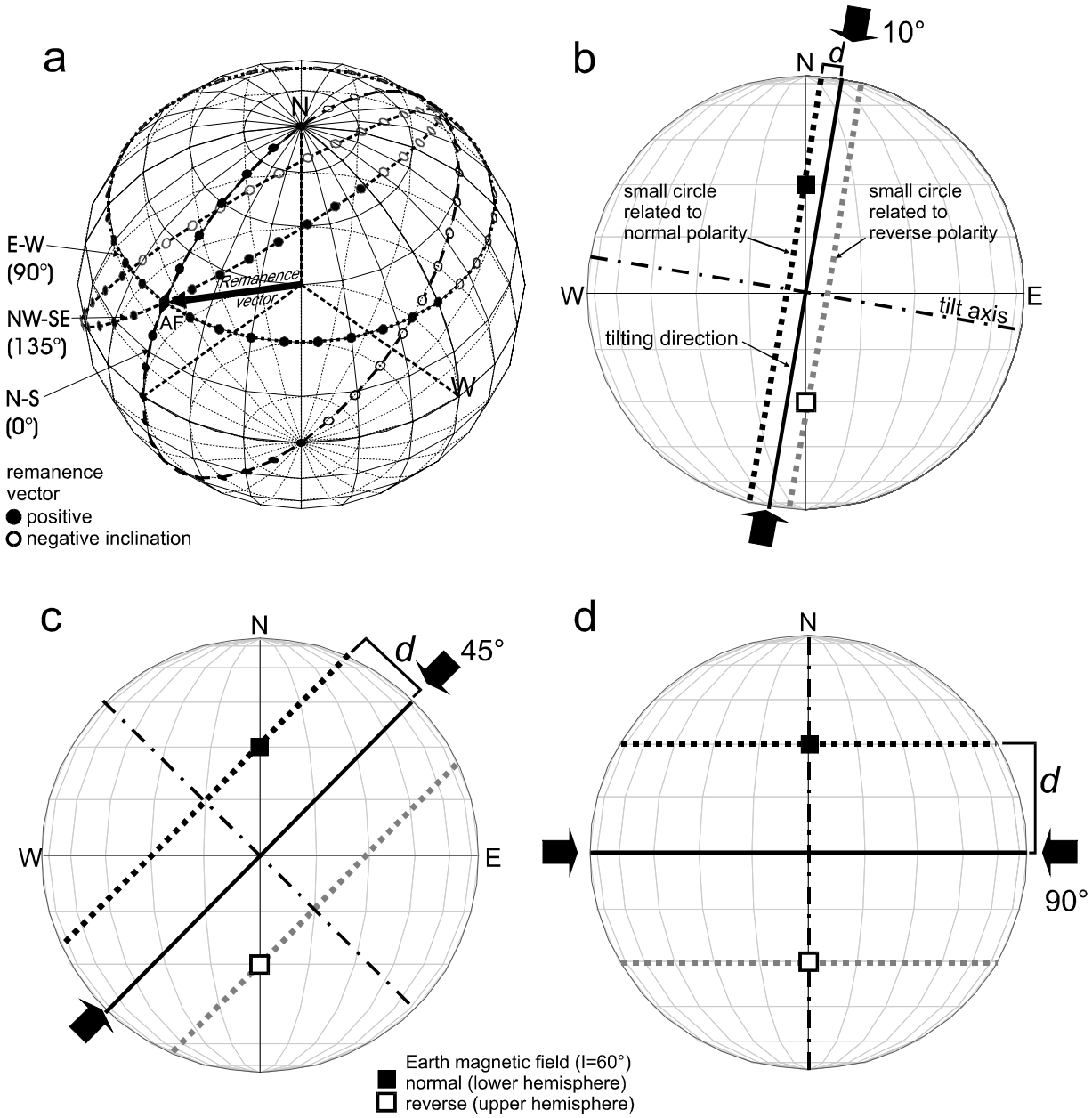

Fig. 1.2: Rotation of remanence directions on small circles by tilting. Acquisition field at D/I = 0°/60° (assumed to be normal) and reverse. (a) Perspective view of a sphere showing rotation of remanence directions in 10° steps. Hidden lines are dashed. Tilting directions are N-S (0°), NW-SE (135°) and E-W (90°) oriented. AF: Normal acquisition field with I_{acq} = 60°. Note that the hemisphere of the positive inclination (lower hemisphere in equal-area plots) is rotated to the front. (b) Orthographic projection showing the two small circles for 10° oriented tilting, one related to normal, the other to reverse field polarity. (c) 45° (NE-SW) tilting. (d) 90° (E-W) tilting. For a given field inclination I_{acq}, the angular distance *d* between the small circles and the tilting direction is related to the direction of tilting.

The positions of in-situ remanences on a small circle are further controlled by the angle and sense of tilting. Fig. 1.3 illustrates four possible constellations. For a primary remanence the dip angle of the layer and the tilt angle of the remanence direction coincide (Fig. 1.3a). The remanence will be restored to its original position by 100% untilting. A secondary remanence underwent only part of the tilting (Fig. 1.3b) and will be restored by <100% untilting. The situation in Fig. 1.3c implies that bedding is overturned. A negative percentage of untilting is required. The constellation in Fig. 1.3d can be explained in two ways. If tilting is allowed only in one sense, its angle must have exceeded 180°. The other solution is tilting first in one sense and then back in the opposite. If tilted sufficiently, remanences can change the hemisphere. This has to be considered, when a polarity is to be attributed to an in-situ remanence.

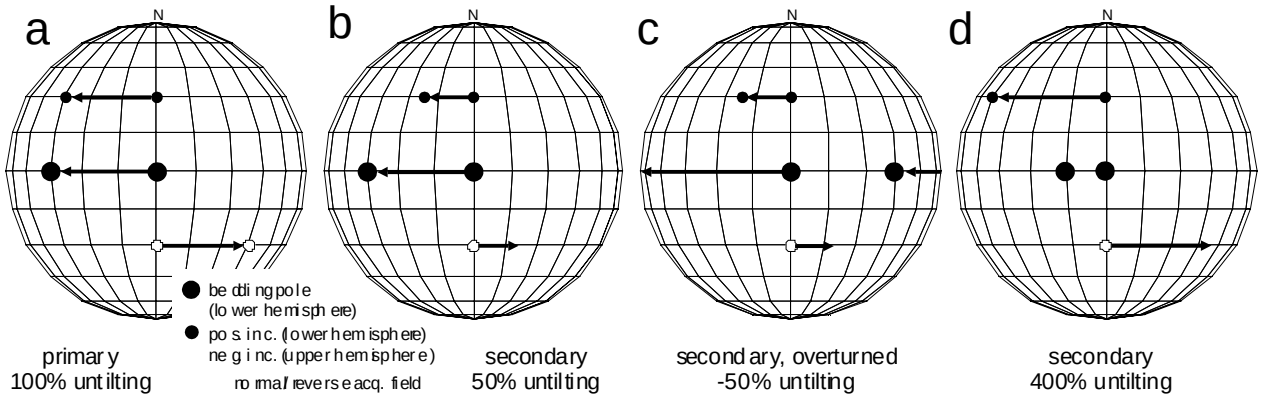

Fig. 1.3: Comparison of bedding and remanence with respect to the rotation sense for E-W tilting. Normal and reverse acquisition field is shown for I_{acq} = 60°. Percentage of untilting refers to the actual dip assumed to be upright. (a) A primary remanence undergoes the whole tilting and can be restored by 100% untilting (=angle of dip). (b) A secondary remanence acquired at 50% tilting. (c) A secondary remanence of an overturned layer requiring -50% untilting, leading to a steeper dip of the layer. (d) Untilting of the remanence direction exceeds the dip of bedding but has the same sense. This can be explained by either more than 180° of net tilting of the layer in one sense or tilting first in one and then back in the opposite sense. Real examples for this situation will be shown behind. Note that remanences can change the hemisphere through tilting.

Hence, tilting back until the reference inclination is achieved gives the stage of tilting where a remanence direction has been acquired. Comparison of the in-situ remanence with the bedding allows the identification of upright and overturned layers and gives information about the process of folding.

1.4 Examples

The following examples show small-circle distributions of in-situ remanences on several scales. All data are from this work and will be discussed in detail in sections 2 and 3.

1.4.1 Small-Circle Distribution within a Folded Sequence

Fig. 1.4 shows 107 remanence components from 12 sites in a unidirectionally folded sequence. The bedding poles define a Π-circle which is nearly perpendicular (plunge of fold axis of 1°). The fold test for this data set (see section 2) clearly shows a secondary character of the palaeoremanences.

The distribution of the in-situ remanence components (Fig. 1.4b) can be explained by a mean small circle parallel to the Π-circle of the bedding poles. The distribution around this small circle is broad, as well as the distribution of the bedding poles. As long as this is caused by a second, perpendicular phase of folding or initial heterogeneity in tilting, the position of the mean small circle will not be affected. All remanence components seem to originate from a normal acquisition field belonging to a small circle of normal polarity. With an assumed acquisition field of D/I = 10°/55° and the azimuth of the Π-circle as tilting direction, the whole sequence most probably experienced a counterclockwise block rotation of about 20°. However, this amount of rotation is an average over the whole sequence. Variations in tilting as well as possible block rotations between the sites, as might be supposed from the distribution of the bedding poles, are not resolved. This can be accounted for by considering the single sites with their tilt axes in the same way. As in the bedding correction of palaeomagnetic data, it is assumed that the tilt occurred around a horizontal axis.

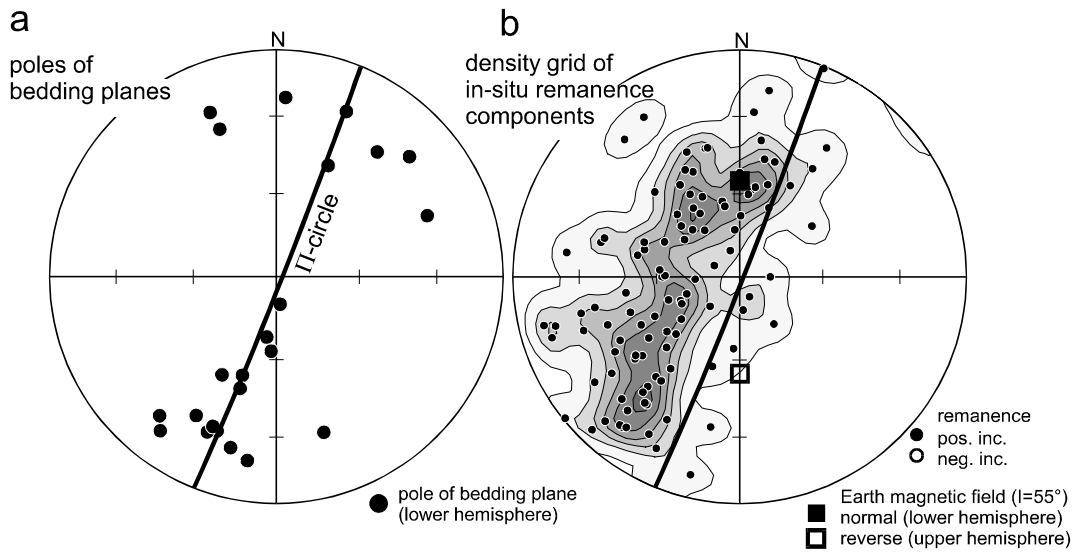

Fig. 1.4: Example of a data set of 12 sites in a unidirectionally folded sequence. (a) Bedding poles and Π-circle. (b) Density grid of 107 single in-situ remanence components in in-situ coordinates (positive inclination on lower hemisphere. Distribution is around a mean small circle parallel to the Π-circle of the bedding poles (thick line). Assuming an acquisition field of D/I = 10°/55°, the folded sequence most probably underwent an average counterclockwise rotation of about 20°. Detailed discussion in section 3.

1.4.2 Small-Circle Distribution in Single Sites

Palaeomagnetism uses Fisher statistics (Fisher 1953) to calculate a mean value for a distribution and to estimate whether this mean value is statistically significant. Fisher statistics assume that the remanence vectors represent a two-dimensional Gaussian distribution (Fisher distribution) on a sphere due to secular variation of the Earth's magnetic field and/or non-systematic errors.

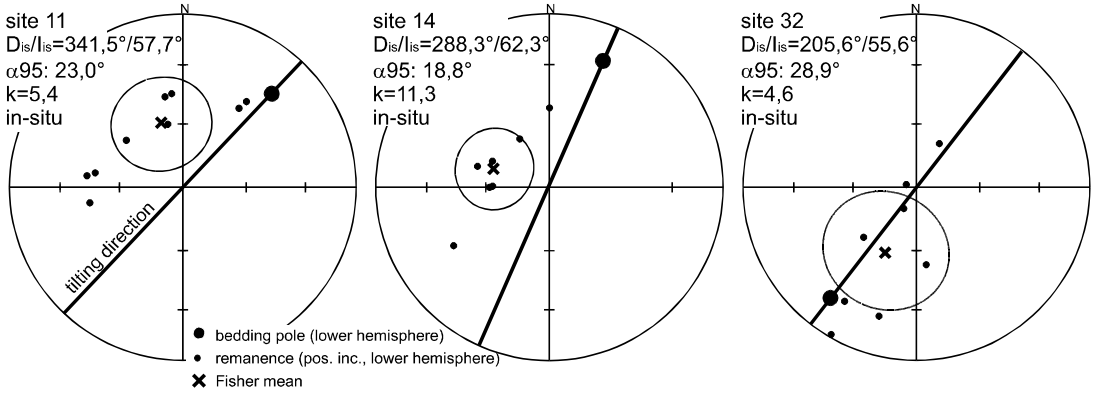

Fig. 1.5: Small-circle distributions of in-situ remanence components in single sites. Distribution is on a small circle roughly parallel to the corresponding tilting direction. Components obviously have different ages recording different increments of displacement. Each site was taken from a close succession of layers with the bedding as indicated. Specimens of each site are only a few metres apart. Fisher statistics give invalid means. Note that bedding in sites 11 and 14 is most probably overturned and in site 32 upright.

If the rock is rotated during the time interval of remanence acquisition, the remanences become distributed on a small circle, and application of Fisher statistics is no more valid. Examples for small-circle distributions of remanence components in single sites are shown in Fig. 1.6. Using Fisher statistics, sites 11 and 32 would be discarded because of a precision parameter *k* below 10. The remanence components in the sites

11, 14 and 32 (Fig. 1.5) obviously do not have a Fisher distribution. Acquired at different stages of tilting, they represent a magnetic record of tectonic displacement, thus defining a displacement path.

1.4.3 Small-Circle Distributions during Demagnetisation of Single Specimens

Small-circle distributions of remanences can even be observed in single specimens during stepwise demagnetisation. Fig. 1.6 depicts the demagnetisation behaviour of several specimens (Jurassic limestones, see section 3).

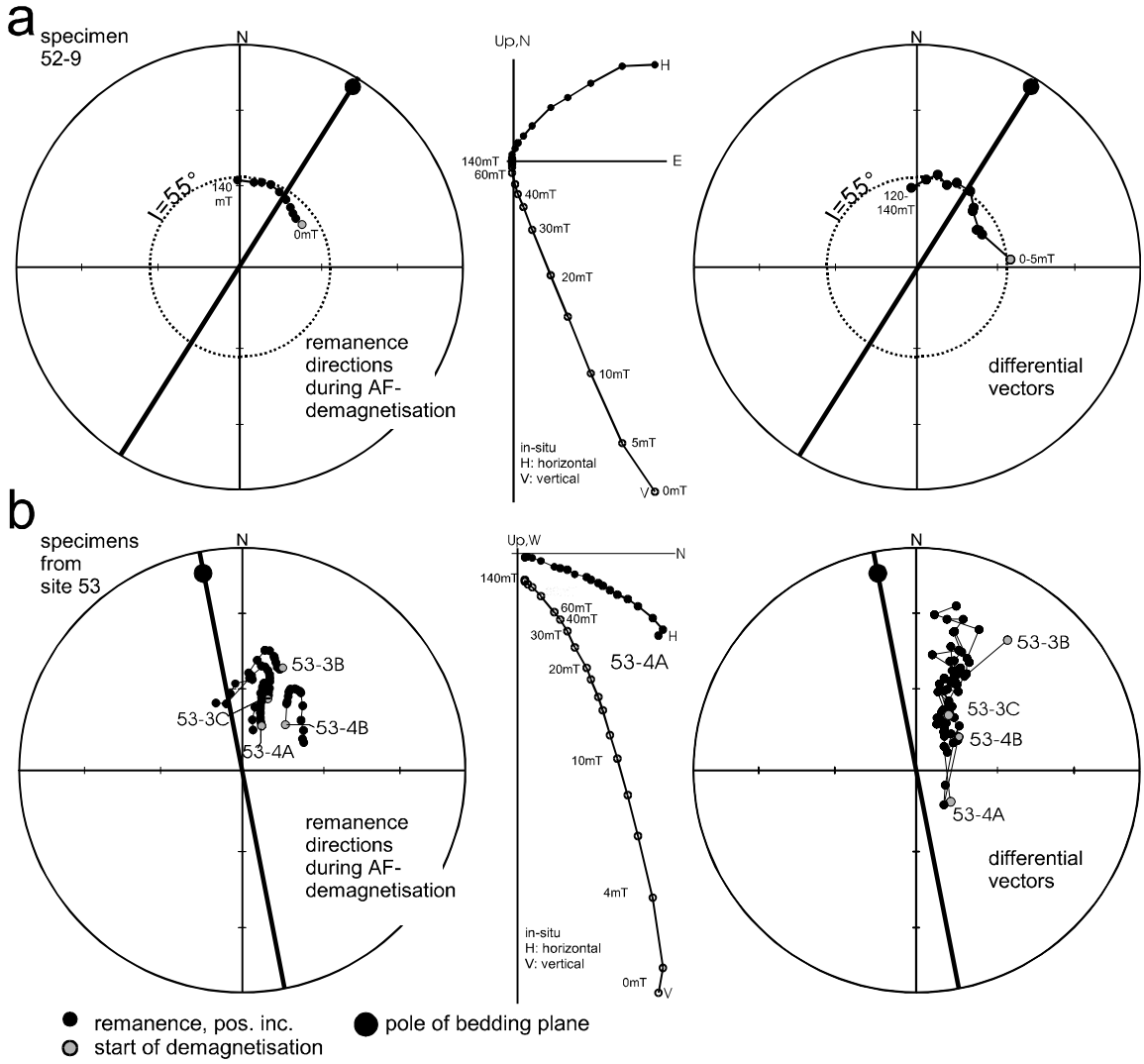

Fig. 1.6: Small-circle distributions of remanences in single specimens during AF-demagnetisation. Demagnetisation behaviour in equal-area plots demonstrated by the remanence directions (sum vectors, left), the differential vectors (right) and the Zijderveld plot (middle). (a) The differential vectors during demagnetisation seem to follow a horizontal small circle of about I = 55°. This behaviour requires at least three different remanence components to define the small circle. Note that the lowest-coercive component is the oldest, because it records most displacement. (b) Four specimens from the nearby site 53. Differential vectors during demagnetisation move on small circles roughly parallel to the tilting direction, hence are a consequence of tilting. A reversal of the tilting sense has occurred (better reflected by the remanence directions). Tilting as recorded has been first to the north and then back to the south. For discussion see text and section 3.

The overall trend of block rotation in the surroundings is clockwise up to about -60°. All specimens of this lithology exhibit a very well-defined and stable demagnetisation path. This permits the calculation of differential vectors between the measured remanence directions of the single demagnetisation steps.

Differential vectors in Fig. 1.6a follow a horizontal small circle of approximately I = 55°. At least three different remanence components must be present to define the horizontal small circle. Alternatively, it is possible that the remanences are not composed of a few components only, but constitute a continuous or partly continuous record, showing as much components as have been sampled by the demagnetisation steps. This would imply a steady remanence acquisition in the course of tectonic displacement, rather than the acquisition of single discrete components. Then, the specimens in Fig. 1.6a would represent a continuous magnetic record of a clockwise block rotation. Surprisingly, the lowest-coercive component reflects the highest rotation and thus must be oldest. The fold tests indicate that an overall primary character of the remanences has not been preserved. However, as will be shown behind, some primary remanences are likely to have persisted in these rocks. Overprinting did not add the new components to the existing remanence, but replaced them. It seems the old magnetic record fades out while the new one is printed over, very much like overwriting a magnetic tape. This in turn supports the concept of a continuous remanence acquisition.

The differential vectors of the four specimens from the nearby site 53 (Fig. 1.6b) move mostly on a vertical small circle parallel to the tilting direction, and thus are clearly related to tilting. As before, at least three different remanence components are necessary to define the small circle. Alternatively, a steady remanence acquisition might have performed, giving a continuous record of tilting. If interpreted in this way, the demagnetisation behaviour reflects a reversal of the tilting sense. Tilting as recorded has been first to the north and then back to the south. This is further confirmed by the reconstruction of the site means of this site, as will be seen in section 3.

1.5 Reconstruction of Small-Circle Distributions and Ambiguity

The purpose of reconstruction is to obtain the angles of tilting and block rotation of an in-situ remanence, and to infer the path of displacement. Fig. 1.7 introduces the basic steps of reconstruction for the two extreme cases of N-S and E-W tilting. Both data sets underwent clockwise block rotation by -30°. Reconstruction is done by tilting back the remanence until it reaches the inclination of the assumed acquisition field. This is given at the intersection of the remanence small circle with the small circle of constant field inclination. The angle of block rotation results from the difference between the declination of the reconstructed position and the declination of the reference field. For N-S tilting (Fig. 1.7a) the remanence small circles and the tilting direction coincide, implying that the angle of block rotation determined is independent from the inclination of the acquisition field. In this case, a wrong assumption of the inclination will not affect the block rotation determined. When the distance between the small and great circles becomes larger, reconstruction gets more sensitive to a variation of the inclination of the acquisition field. E-W tilting is most sensitive (Fig. 1.7b). In practice, variation of the field inclination within a range of 5° around the true value will not affect the results significantly. In most areas, the palaeofield is known within this range from the APWP, and thus reasonable assumptions can be made. Moreover, in Alpine and Himalayan fold belts, N-S convergence is common, which is the most insensitive case for the reconstruction of the declination.

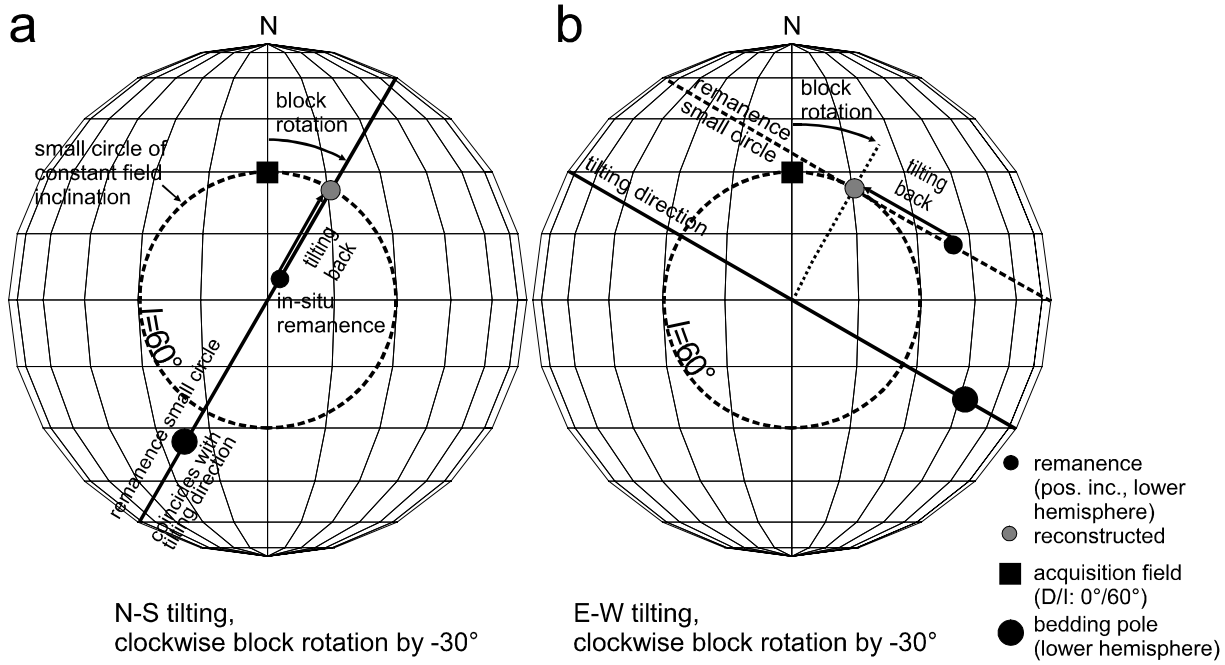

Fig. 1.7: Reconstruction of -30° clockwise block-rotated secondary in-situ remanences. (a) N-S tilting with zero distance between remanence small circle and tilting direction. (b) E-W tilting with largest distance of remanence small circles to tilting direction. The reconstructed position is at the intersection of the remanence small circle with the small circle of constant field inclination. For N-S tilting where remanence small circles and tilting direction coincide, the angle of block rotation is independent from the inclination of the acquisition field.

Up to this point, only positive inclinations on the lower hemisphere coming from a normal polarity field have been examined. However, both field polarities have to be considered as possible origins. Fig. 1.8 shows a three-dimensional representation of this problem. Remanence small circles are shown for 0° (N-S), 135° (NW-SE) and 90° (E-W) oriented tilting. The small circles of constant field inclination are for I_{acq}= ±60°. Apart from E-W tilted remanences having only two touching intersections, each remanence small circle has four intersections, two with the small circle of positive inclination, and two with the small circle of negative inclination.

Hence, up to four direct reconstructions (tilting/block rotation < 180°) exist for each remanence small circle. While at N-S tilting a block rotation of 180° is needed to exchange the intersection points, this angle decreases with the distance *d* of the remanence small circle and gets zero at the maximum distance cos I_{acq}. In practice, this means that at N-S tilting, the possible reconstructions are easier to distinguish upon probability. In the case of tilting close to E-W, equivalent reconstructions come close to each other and are more difficult to assess.

Thus, for each angular distance *d* there are two reconstructed tilting directions. Each tilting direction can be related either to the normal polarity or the reverse polarity field, giving two possible block rotations for each tilting direction.

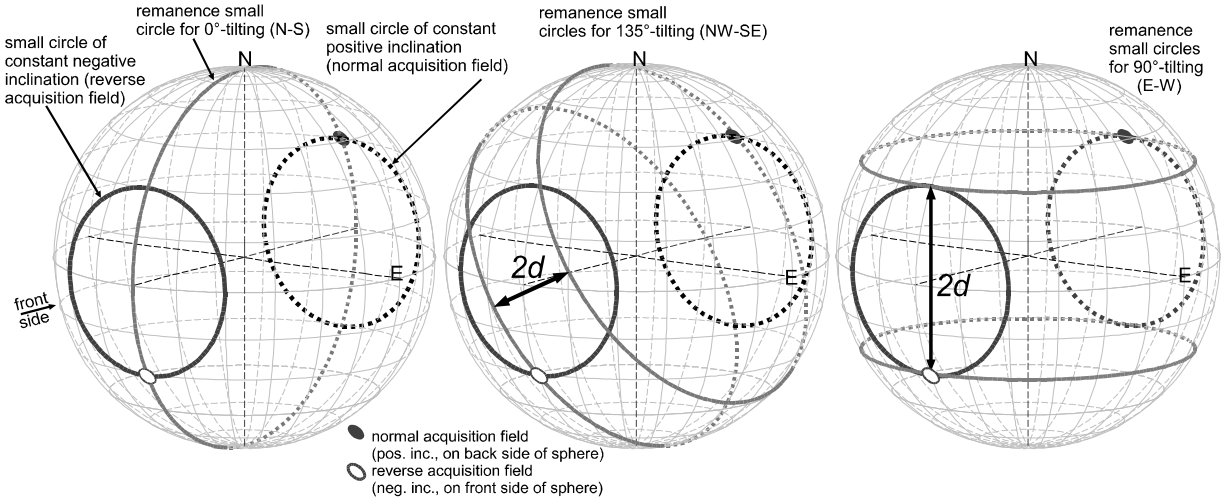

Fig. 1.8: Three-dimensional views of a sphere with the hidden lines dashed. Small circles of constant field inclination for a normal and reverse acquisition field at I_{acq} = ±60°. Full circle at backside: normal polarity field, open circle on front side: reverse polarity field. Remanence small circles for normal and reverse polarity are shown for 0° (N-S), 135° (NW-SE) and 90° (E-W) oriented tilting. Except for the maximum angular distance *d* in the case of E-W tilting, the small circles of the normal and reverse field polarities are intersected by each remanence small circle at four points. This gives four possible direct reconstructions (tilting/rotation < 180°), two of which belong to the normal and two to reverse field polarity.

Altogether, this gives four possibilities for tilting and block rotation < 180°, further on called *direct reconstructions*. The trends *t´* of the tilt axes of the two reconstructed tilting directions at a given distance *d* are:

$$t_1' = \arccos(+d / \cos I_{acq}) + D_{acq} \qquad (2a)$$

$$t_2' = \arccos(-d / \cos I_{acq}) + D_{acq} \qquad (2b)$$

Addition of equations (2a) and (2b) shows that the trends of the two tilt axes are complementary to 180° + 2 D_{acq}:

$$t_2' = 180° - t_1' + 2\,D_{acq} \qquad (3)$$

t_1' trend of the first reconstructed tilt axis;

t_2' trend of the complementary second reconstructed tilt axis;

d distance of a remanence small circle to its corresponding tilting direction or Π-circle ;

D_{acq}, I_{acq} normal reference field with positive inclination

Each of the two reconstructed tilt axes is rotated to match the present tilt axis either in one sense, e.g. implying normal polarity, or in the opposite sense, implying reverse polarity. The block rotations (*br*) of one reconstructed tilt axis for normal polarity and reverse polarity reconstruction are inverse complementary to ±180°:

$$br_n - br_r = \pm 180° \qquad (4)$$

br_n, br_r block rotation from normal and reverse polarity reconstruction

If block rotation up to 360° is allowed, the possible direct reconstructions sum up to eight. Reconstructions have to be assessed according to their probability, mainly by considering the angles of backtilting and block rotation. Geological information such as upright or overturned bedding and a comparison to magnetic data

from nearby sites in most cases resolve ambiguity. If reconstruction is done using Fisher site means, the angle of backtilting for each solution can be determined. This allows the reconstruction of the bedding at the time of remanence acquisition.

The following examples (Fig. 1.9 and Fig. 1.10) illustrate the procedure of reconstruction and assessment. The remanence components of the sites are supposed to have a Fisher distribution giving a site mean, for which the angles of backtilting can be calculated. Conventions on rotations are as previously defined in Fig. 1.1 (again shown in Fig. 1.9 and 1.10). Fig. 1.9a gives remanence components, site mean, tilting direction, remanence small circle and the small circle of constant field inclination for site 22. Fig. 1.9b-e represent the four direct reconstructions with the angles of backtilting and resulting angles of block rotation.

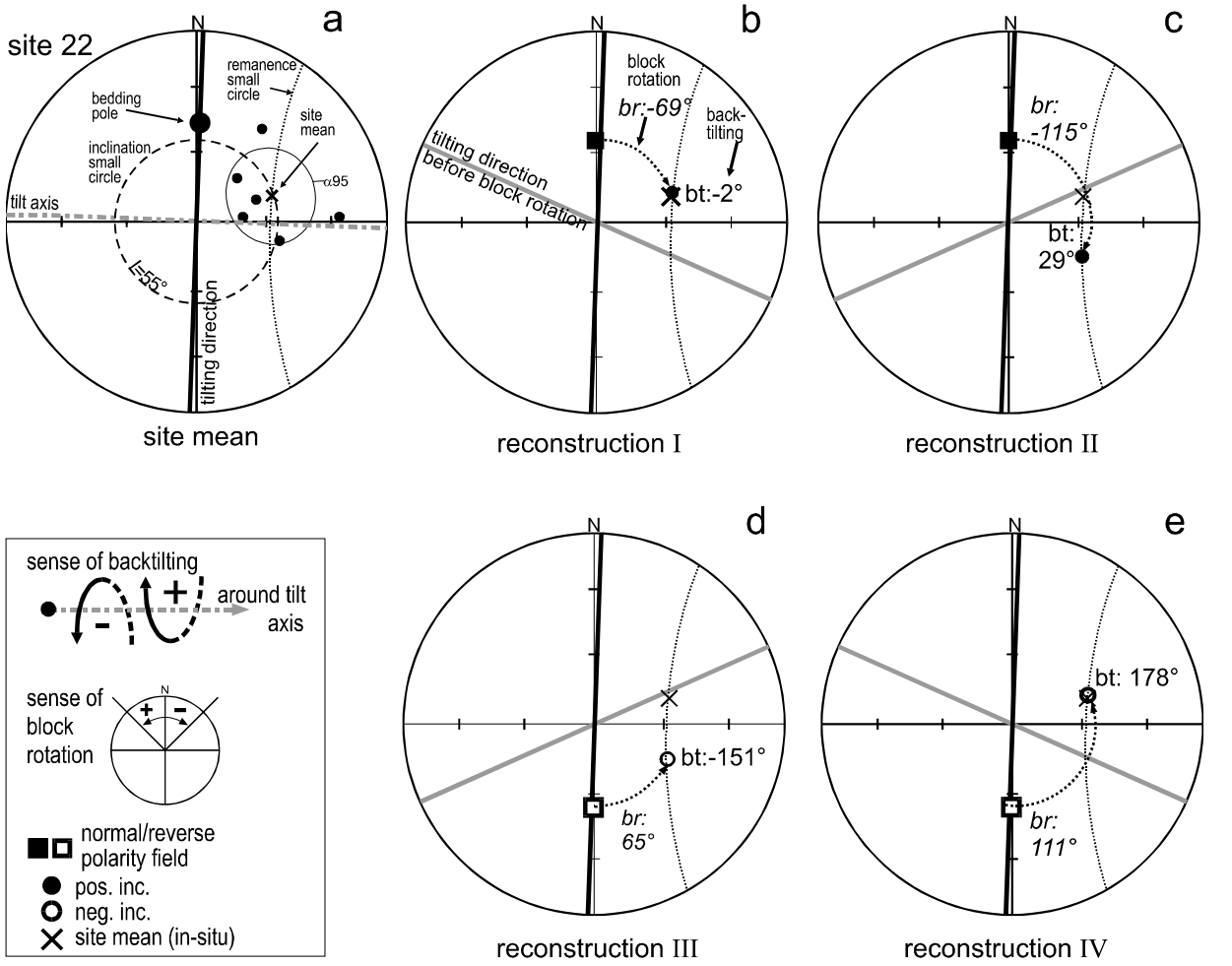

Fig. 1.9: The four direct reconstructions for site 22. Acquisition field at D/I = 0°/55° and reverse. Angle of backtilting calculated for the site mean. Percent of untilting relates to present dip assumed to be upright. Reconstructed positions shown for site mean (open/full circles) and tilting direction (thick grey line). (a) Remanence components, site mean, tilting direction, remanence small circle and inclination small circle. Sense and angle of backtilting (bt) and resulting block rotation (br) as indicated in b-e. (b) Shortest path by -2° (-4%) of backtilting giving a clockwise block rotation of -69°. (c) Next possible reconstruction by 29° (67%) backtilting giving a -115° clockwise block rotation. (d) -151° (-351%) of backtilting giving a 65° counterclockwise block rotation. (e) 178° (415%) of backtilting giving a counterclockwise block rotation of 111°. The angles of backtilting of b and e, and c and d are inverse complementary to 180°.

Reconstruction I (Fig. 1.9b) requires the smallest angle of backtilting and block rotation (2° = -4% untilting and -69° block rotation) The small negative percentage of untilting is too small to be significant for overturned bedding. In this reconstruction, the remanence was acquired after tilting of the layer, and the magnetic record is constrained to the block rotation or to a part of it. This solution gives the shortest displacement and thus is the most probable reconstruction. Reconstruction II (Fig. 1.9c) gives 29° (67%) of

untilting and -115° of block rotation. Bedding would be normal. Reconstructions III and IV (Fig. 1.9d and e) give tilting angles of -151° (-351%) and 178° (415%). The present bedding dip of 43° does not allow the reconstruction positions to be reached within the range of untilting for an upright bedding dip of 43° and an overturned bedding dip of 137°. Hence, either tilting by more than 180° or tilting in two phases with opposite senses must be allowed to explain these solutions (see also Fig. 1.3d for this constellation).

Analogous to the angles of block rotation, the angles of untilting of reconstructions I and IV, and II and III are inverse complementary to 180° (see also equation 5), thus, it is sufficient to determine the tilting angles of the first two reconstructions and calculate the others through the symmetry.

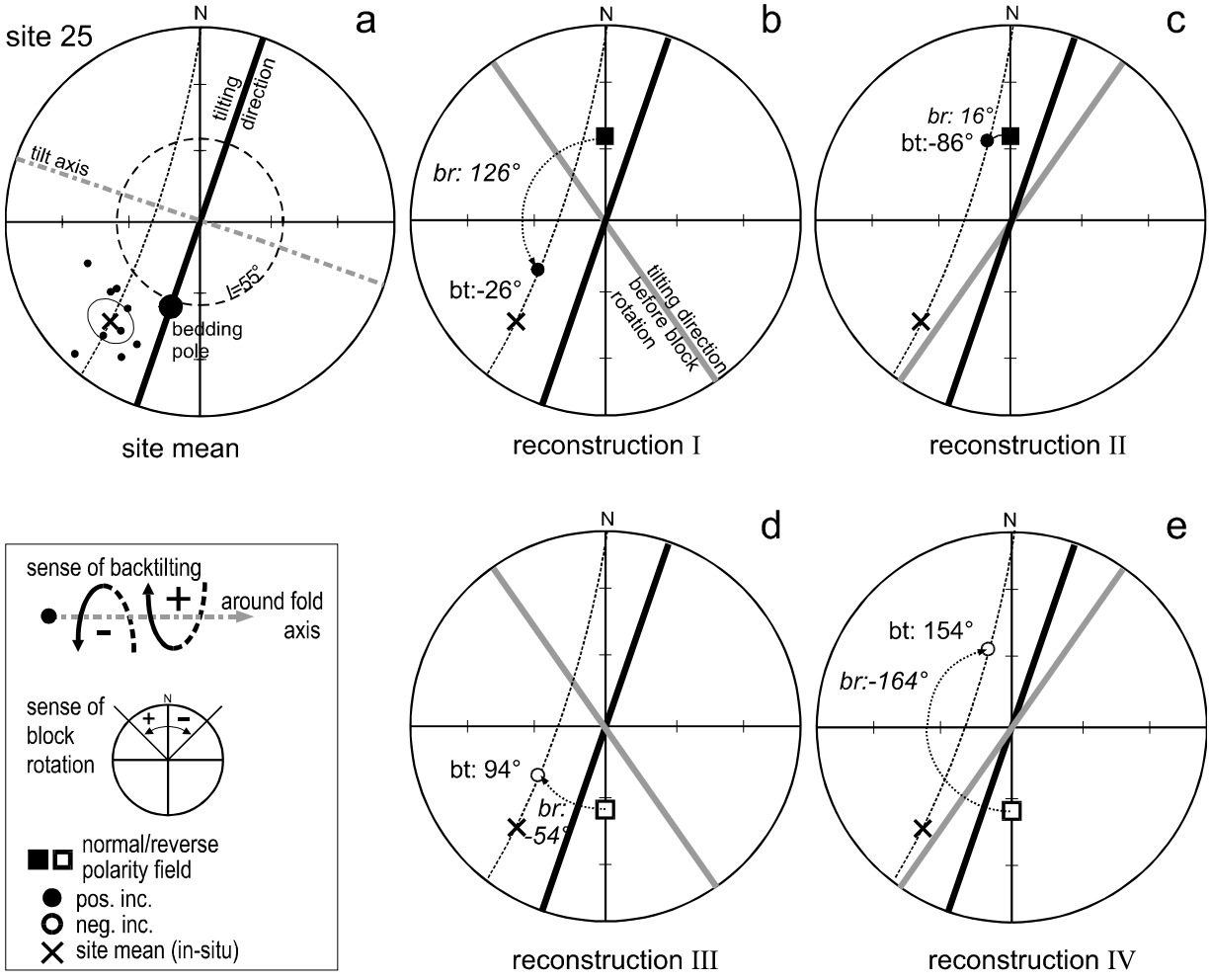

Fig. 1.10: The four direct reconstructions for site 25. For conventions see Fig. 1.9. (a) Site results and site mean. (b) -26° (69%) of backtilting giving a counterclockwise block rotation of 126°. (c) -86° (226%) of backtilting giving a 16° counterclockwise block rotation. (d) 94° (-248%) of backtilting giving a -54° clockwise block rotation. (e) 154° (-404%) of backtilting giving a clockwise block rotation of -164°.

The reconstruction of site 25 is shown in Fig. 1.10. This example illustrates how different reconstructions can achieve similar probability when displacements become high. Reconstruction I (Fig. 1.10b) requires -26° (69%) of backtilting giving a 126° counterclockwise block rotation and upright bedding. Reconstruction II (Fig. 1.10c) requires -86° (226%) of backtilting giving a 16° block rotation. The tilting sense with its positive percentage implies upright bedding, but backtilting significantly exceeds the dip of 38°. This reconstruction could only be explained by a tilt of more than 180°, or a tilt first to a southward dip direction may have occurred and then, after remanence acquisition, back northward to the present dip direction.

Reconstruction III (Fig. 1.10c) implies overturned bedding: Backtilting of 94° (-248%) is below the overturned tilt angle of 142°. This constitutes the most moderate solution in terms of rotation and backtilting

angles. Reconstruction IV (Fig. 1.10e) requires 154° backtilting (-404%) which does not significantly exceed the overturned tilt angle of 142°.

Reconstruction III would be chosen as the most probable since it requires the smallest angles of displacement and no reversal of the tilting sense. However, site 25 is part of the unidirectionally folded sequence of Fig. 1.4, from which a mean counterclockwise rotation of about 20° has been obtained. Thus, reconstruction II (Fig. 1.10c) is likely to be the correct solution. Either the site has been tilted by more than 180°, or two phases of tilting below 180° with opposite senses must have occurred.

1.6 Subsequent Tilt, Two Folding Phases and Simultaneous Displacement

In the following, possible complications will be discussed. The first two usually can be identified from the analysis of the bedding within a folded sequence.

1.6.1 Subsequent Overall Tilting

Any subsequent tilt of a whole folded sequence affects both bedding data and palaeomagnetic data. However, it will not affect the angular distance between in-situ remanence and Π-circle. If known to have occurred, both bedding data and remanence directions need to be tilted back until the Π-circle reaches its orientation prior to the overall tilt.

1.6.2 Second Phase of Tilting

A second folding phase with tilting perpendicular to the first phase rotates a remanence direction away from an initial small circle on a further small circle perpendicular to the first one. This affects also the distribution of the bedding poles. The broader distribution will show up in both data sets and can be identified. If symmetrical, the small-circle distribution of the remanences becomes broader, but the mean small circle remains the same. Definition of this small circle can still be done, but is possible only if secondary tilting is not too intense and if representative sampling is done across the sequence. This should be true also for a second folding phase at an angle ≠90° to the first.

1.6.3 Simultaneous Tilting and Block Rotation

Basically, the small-circle reconstruction does not indicate if block rotation occurred before or after tilting. In principle, there are three possibilities:

1. Block rotation after tilting, thought to be the general case.
2. Block rotation before tilting, implying a primary character of such an in-situ remanence.
3. Simultaneous block rotation and tilting.

Generally, changing the temporal sequence of rotations also will change the final result, because rotations are not commutative. However, there is an exception, thought to be represented by the process of tectonic folding (Fig. 1.11): The tilt axis rotates with the block rotation. Both axes are perpendicular to each other. The axis of the block rotation is not affected by tilting. If tilting and block rotation are exchanged, the final result will be the same (Fig. 1.11a).

Moreover, if these steps are exchangeable, they can be subdivided into incremental steps, combined alternatively and still will give the same final result. Eventually, subdivided into infinitesimals and arranged

alternatively, a simultaneous process of tilting and block rotation is obtained. The final result is always the same, but the path is different (Fig. 1.11b).

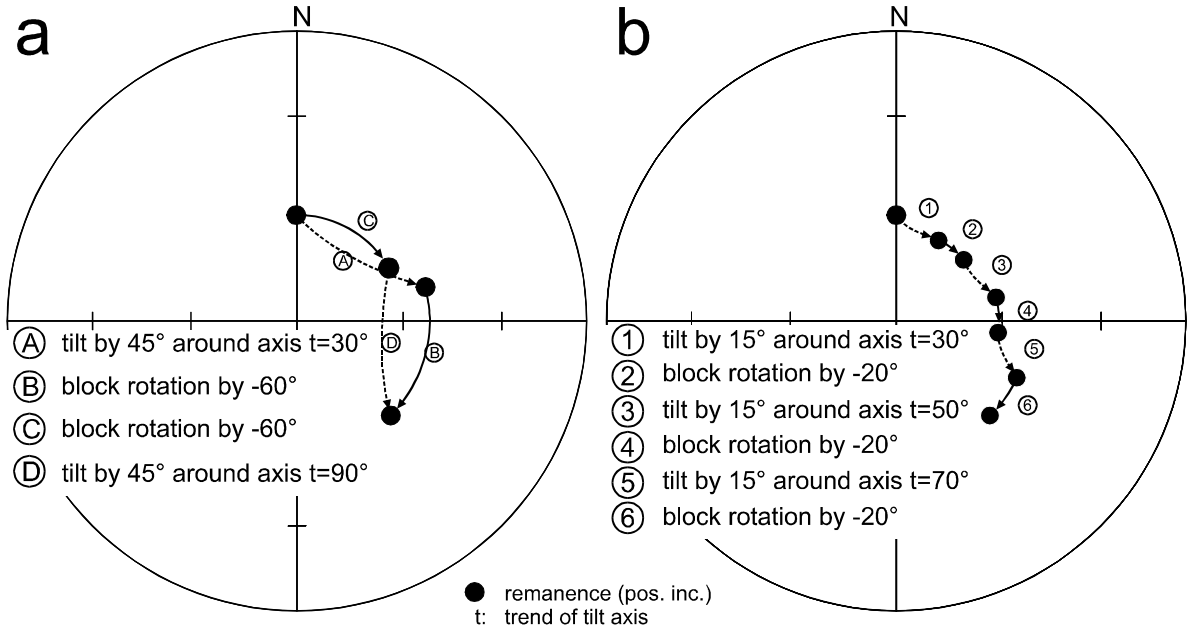

Fig. 1.11: Exchanging and subdividing tilting and block rotation. Block rotation rotates the tilt axis, but tilting does not affect the axis of the block rotation. In this case, block rotation and tilting can be exchanged and still will give the same result (a). Subdivision into increments still yields the same final result (b). The displacement path is always different.

Hence, also in the case of simultaneous or alternating block rotation and tilting, the small-circle reconstruction gives the correct angles of net tilt and net block rotation. This simultaneous process is likely to perform during folding (Fig. 1.12). Strata which are not parallel to the fold axis, must undergo block rotation during tilting in order to reach a tighter arrangement of the layers.

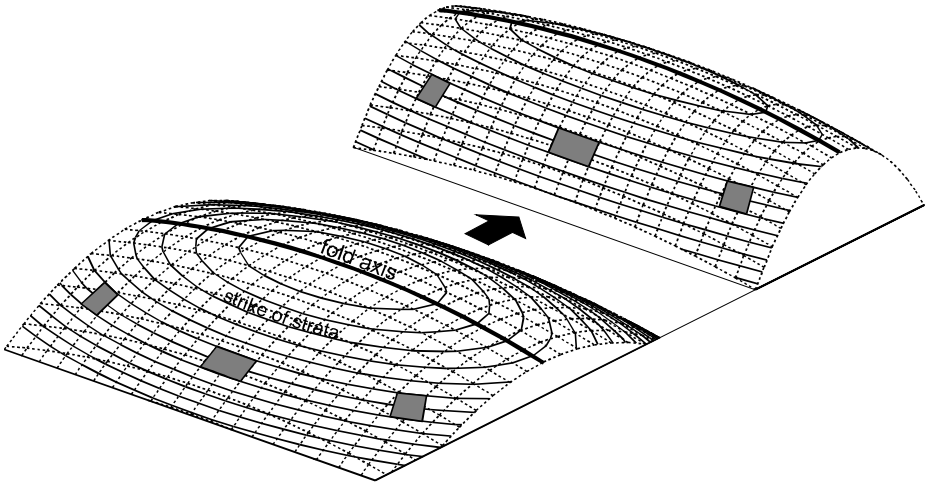

Fig. 1.12: Schematic view of a fold with hinge culmination. Shaded rectangles shall represent internally rigid layer elements. During folding, layer elements which are not parallel to the fold axis, must undergo block rotation in order to reach a tighter arrangement of the layers. Tilting and block rotation will occur simultaneously.

Fig. 1.13 shows remanence components of two sites that might have recorded simultaneous tilting and block rotation. The sites are taken from a fold and are some 50 m apart. Distributions seem to be on small circles, but not parallel to the corresponding tilting direction. If each remanence direction is tilted back, different amounts of block rotation are obtained. With the exception of one specimen in site 12 and two in site 14, the angle of backtilting seems to correlate with the obtained block rotation. The remanences that recorded the largest tilting, also exhibit the largest block rotation. However, secular variation is contained in these distributions. To proof the relation between block rotation and tilting, more remanence components

are necessary. Nevertheless, from the further results (see section 3.1), it is plausible that block rotation went along with folding in this area. Therefore, the remanence components shown in Fig. 1.13 could reflect this simultaneous displacement.

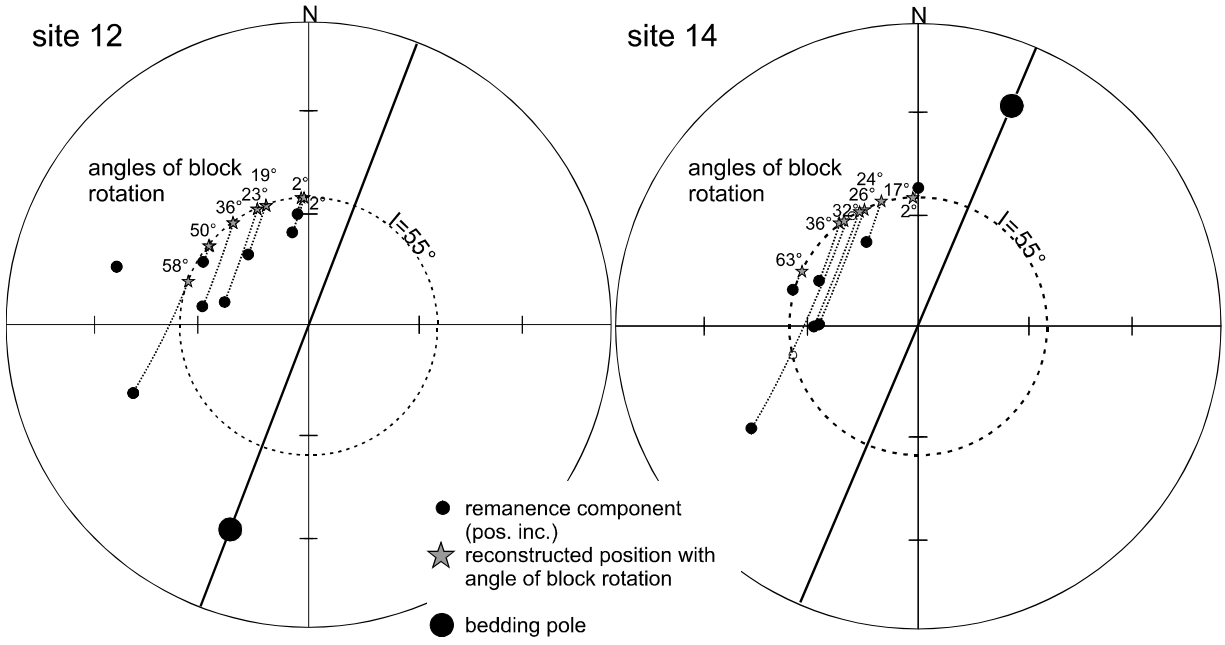

Fig. 1.13: Remanence components from sites 12 and 14, both in red beds from the opposite limbs of one fold. Distributions seem to be on a small circle which is not parallel to the tilting direction. Each component has been backtilted to intersect a small circle of I_{acq} = 55° giving a block rotation as indicated. One remanence component of site 12 is outside the possible range. The angle of backtilting correlates roughly with the angle of block rotation. Thus, tilting and block rotation may have occurred simultaneously.

1.7 Finding a Mean Small Circle

If remanence components of a site are considered that show a Fisher distribution, the site mean can be taken for the calculation of the *d*-angle and the small-circle reconstruction. As usual, the *α95* divided by *cos* I_{acq} is taken as the confidence interval for the block rotation.

In order to reconstruct a given small-circle distribution parallel to its corresponding tilting direction or Π-circle, a mean small circle has to be calculated first. The small-circle distribution of remanence components in a site is a one-dimensional Gaussian distribution parallel to the tilt axis. It is obtained by allowing the remanence directions to rotate around the tilt axis. In this way, a former two-dimensional Gaussian distribution is reduced to a one-dimensional one. (Fig. 1.14).

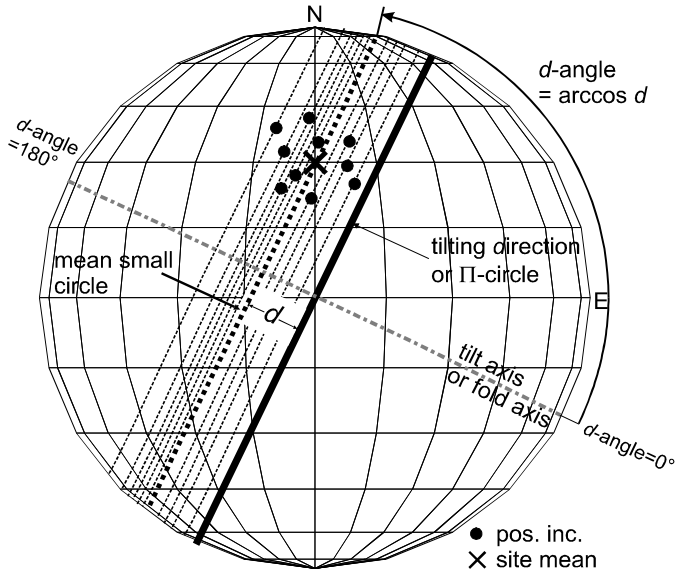

Fig. 1.14: Geometry of small-circle distributions. By allowing the remanences to rotate freely around the tilt axis, the two-dimensional Gaussian distribution is reduced by one dimension. Each remanence component can be seen to have its own small circle defined by the angular distance *d* or the *d*-angle *arccos d.* Tilting direction (or Π-circle) and small circle intersect the tilt axis (or fold axis) at an angle of 90°. At a field inclination of I_{acq} = 0° *d* can vary between -1 and +1, and the *d*-angle between 180° and 0°.

Each remanence component can be seen to have its own small circle defined by the angular distance *d* or the *d*-angle *arccos d.* Tilting direction and small circle intersect the tilt axis at an angle of 90°. The angular distance *d* is a fraction of the radius, which equals the cosine of the so called *d-angle* (Fig. 1.14). At a field inclination of I_{acq} = 0°, *d* can vary between -1 and +1, and the *d*-angle between 180° and 0°. The distance *d* of each remanence is:

$$d = \cos (D - t) \cos I \qquad (5)$$

d angular distance as a fraction of the radius (=1), *D/I* declination and inclination of the in-situ remanence, *t* trend of the present tilt axis ($0° \le t \le 180°$)

The *d*-angle of a mean small circle is found by calculating the arithmetic mean of the *d*-angles *arccos* d_n of *n* remanences:

$$arccos\ d_{mean} = \frac{1}{n}\sum_{n} arccos\ d_n \qquad (6)$$

The 95%-confidence interval can be calculated using the usual approximation:

$$\alpha_{95} \approx \pm\ 1{,}96\ \frac{S_d}{\sqrt{n}} \qquad S_d \text{ standard deviation of d-angle} \qquad (7)$$

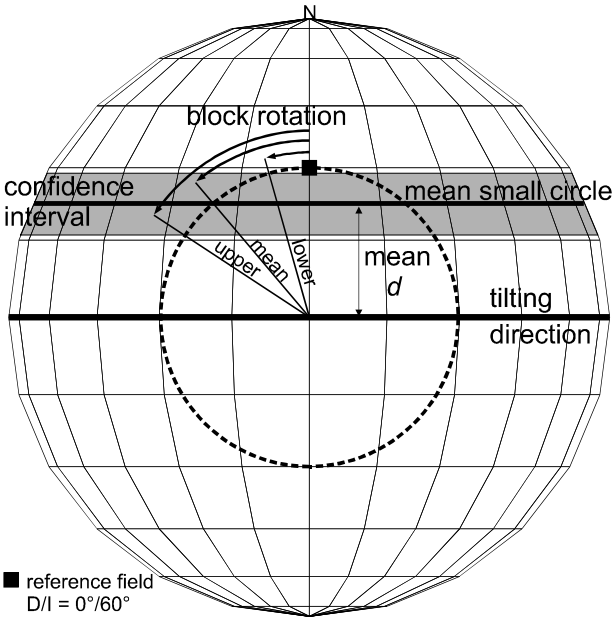

For the azimuth of the reconstructed tilt axis and the resulting block rotation, the confidence interval is asymmetric, except for a zero angular distance (Fig. 1.15). If one of the interval limits of the *d*-angle is below the maximum I_{acq}, the corresponding confidence limit for the reconstructed tilt axis cannot be calculated.

Fig. 1.15: The confidence interval for the mean *d*-angle is symmetric, but results in an asymmetric confidence interval for the azimuth of the reconstructed tilt axis and the block rotation. Asymmetry is zero at *d*=0 and increases with the mean angular distance.

1.8 Estimation of the Field Inclination from In-Situ Remanences

Secondary palaeoremanences have been acquired at an unknown stage of tilting and cannot be restored to their original orientation without knowing the acquisition field. Therefore, the determination of the palaeofield inclination does not seem possible from an in-situ remanence. However, the angular distance of a remanence puts an upper limit on the field inclination (maximum I_{acq} = arccos I*d*I, I*d*I amount of *d*). In the case of an originally E-W tilted site, this upper limit is the inclination of the acquisition field (Fig. 1.16): The inclination of the acquisition field is arccos |*d*|. Since it is never known if a site has been block-rotated, always an upper constraint will be obtained.

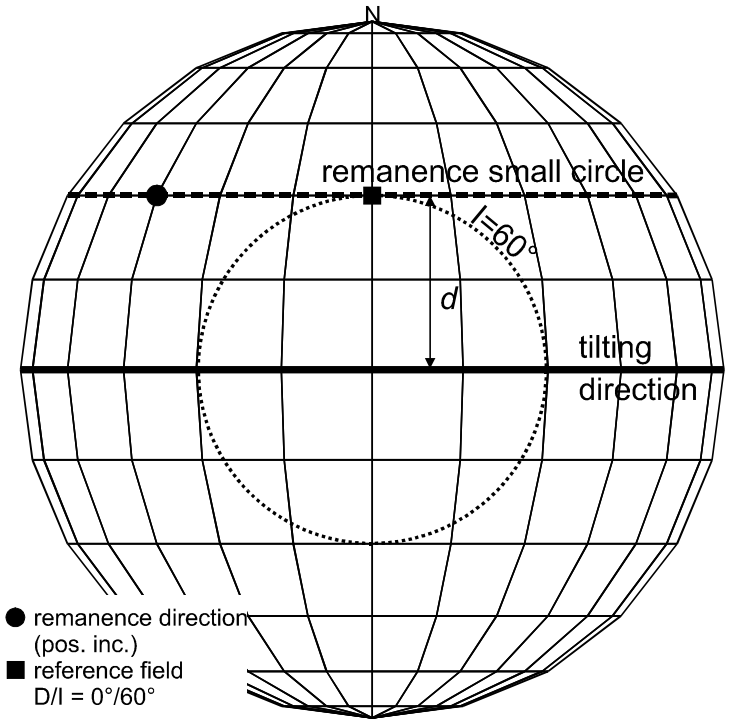

Fig. 1.16. In the case of an E-W tilted remanence, the *d*-angle (arccos *d*) is the inclination of the acquisition field. If not E-W tilted, an upper constraint on the field inclination (maximum I_{acq}) is given. As block rotation could have changed the original tilting direction, the angular distance is always an upper constraint.

Consequently, within a number of remanences, tilted in various directions between N-S and E-W, the inclination of the acquisition field will be found in the angular distance of the E-W tilted sites. If no originally E-W tilted sites are represented, an upper constraint on the field inclination will be found.

Fig. 1.17a depicts theoretical curves for the cumulative distribution of the maximum I_{acq} for a number of in-situ remanences, that have been tilted in directions uniformly distributed between E-W and N-S. The uniform distribution of the tilting directions makes the cumulative curve a straight line for each I_{acq}. Fig. 1.17b presents the cumulative distribution of the maximum I_{acq} of 43 sites from the southern Pamirs. The curve exhibits a significant increase in the cumulative number of sites above a maximum I_{acq} of 55°. The cumulative curve above 55° resembles a straight line indicating a rather uniform distribution of the reconstructed tilting directions. Hence, these 55° can be taken as the upper constraint on the field inclination at the time of remanence acquisition. Three sites have an I_{acq} below 55°. Reasons can be:

- Acquisition at a lower field inclination, possibly indicating a primary character.
- Displacement around inclined axes.
- Rockmagnetic and other reasons such as inclination shallowing, not averaged secular variation, and statistical and physical errors.

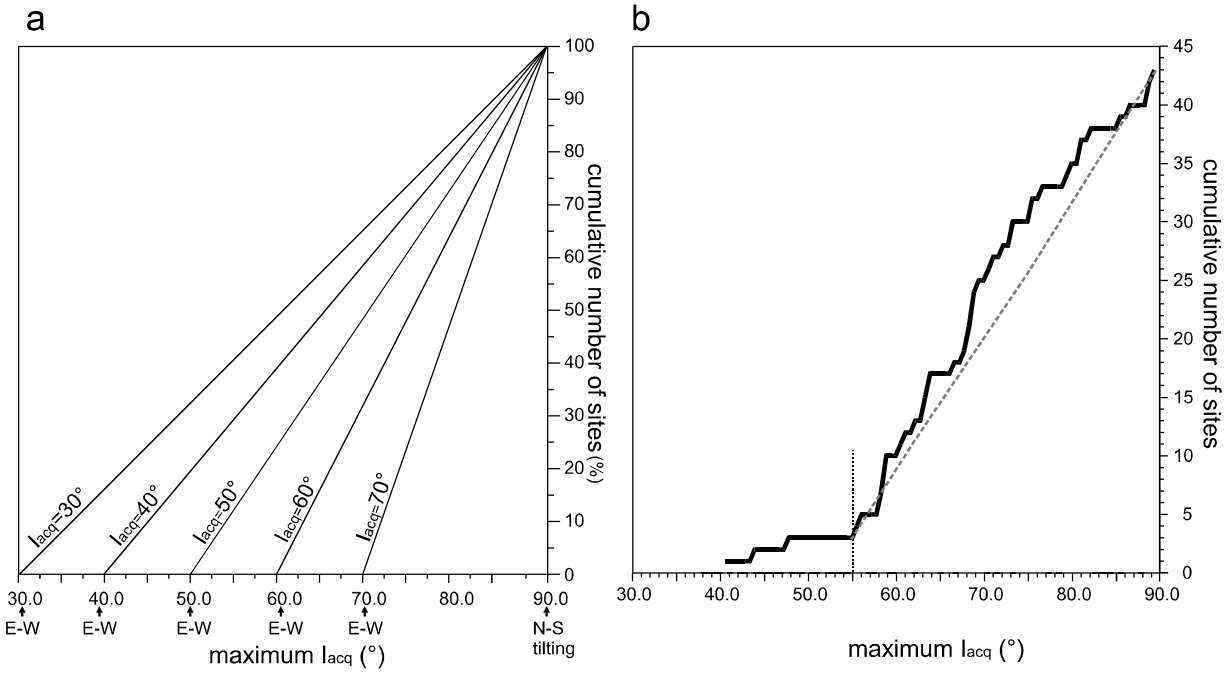

Fig. 1.17: Constraints on the palaeofield inclination from tilted in-situ remanences. Each angular distance of a remanence implies a maximum I_{acq}. The field inclination at the time of remanence acquisition is obtained from originally E-W tilted sites. (a) Theoretical curves for the cumulative distribution of the maximum I_{acq} of 100 in-situ remanences acquired at an inclination as indicated and tilted in directions that are uniformly distributed between N-S and E-W. The cumulative distribution curves are lines. (b) Example of the 43 sites from the southern Pamirs. The marked increase in the cumulative number of sites above 55° indicates that the field inclination unlikely exceeded this value. The curve resembles a line indicating a rather uniform distribution of the reconstructed tilting directions.

In practice, a site does not have to be exactly E-W tilted to give a reasonable constraint on the field inclination. The angular distance *d* is a cosine function of the azimuth of the tilt axis (equation (1) in section 1.3). Changing the azimuth from 0° to 10° reduces the maximum I_{acq} only to 1,01 of the original value, an azimuth of 20° still gives 1,06.

1.9 Further Aspects

The concept, that in-situ remanences effectively represent a magnetic record of net tectonic displacement, that can be reconstructed, adds new possibilities to palaeomagnetic and tectonic investigations, such as:

- Palaeomagnetic investigations can be extended to metamorphic sequences (e.g. using schistosity instead of bedding).
- Investigation of the increments and kinematics of folding and block rotation.
- Direct correlation of palaeomagnetic data to structural data from the same outcrop, e.g. brittle deformation data, cleavage, schistosity. Temporal sequences of folding and block rotation, formation of cleavage, brittle deformation, etc. can be resolved.
- Rock- and palaeomagnetic studies related to the processes of remanence acquisition and overprinting during metamorphism and deformation.

Besides this, sampling in the field must already account for originally supposedly E-W tilted sites to get the palaeoinclination. Field information on upright and overturned bedding is important.

1.10 A Modified Way of Data Processing

In the conventional procedure the interpretation depends greatly upon the primary character of the remanence which is assessed by fold tests. However, these tests can be misleading. Secondary remanences can be interpreted only if acquired completely after folding. With the techniques outlined so far, palaeomagnetic data processing can be rearranged. The conventional procedure is not replaced, but integrated (Fig. 1.18).

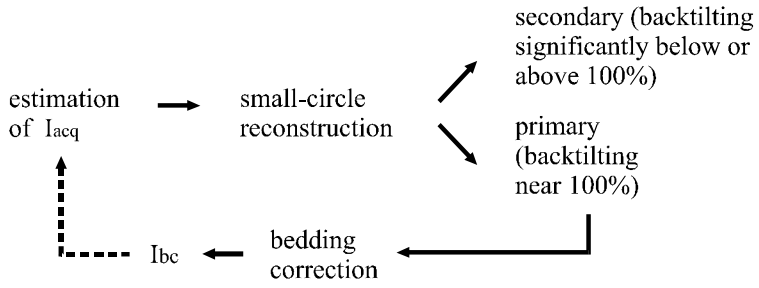

Fig. 1.18. Modified way of data processing. For discussion see text.

The small-circle reconstruction bases on the estimation of the palaeoinclination (I_{acq}) which is assessed from the in-situ remanences. This has to be ensured by appropriate sampling. In contrast to the conventional procedure, a primary character is not a prerequisite for the interpretation. The information on the character of the remanence comes out as a final result and can be checked by fold tests. A remanence is primary, if the percentage of backtilting is around 100%. In this case, the inclination in bedding coordinates can be taken to optimise the small-circle reconstruction. Ideally, the palaeoinclination and block rotation derived from the small-circle reconstruction coincide with the values given by the bedding corrected site mean. Such a remanence is undoubtedly primary, and tilting and block rotation have performed around a horizontal and a vertical axis. Hence, the initial assumptions for the small-circle reconstruction can be checked in turn. Finally, when I_{acq} is known, the character of the remanence can be determined separately for each remanence direction, hence, a fold test is not absolutely necessary.

2. Palaeomagnetic Investigation in the Pamirs

Starting with a brief geologic history of the investigation area, this section documents the results of the rock- and palaeomagnetic measurements in the Pamirs. Fold tests will be applied at the end of the section.

2.1 Geology, Tectonics and Drift History of the Investigation Area

A detailed review of the geology and tectonics of the Pamirs is given by Burtman & Molnar (1993). The following outline compiles aspects relevant for this work. All geochronological ages given below are yet unpublished, preliminary results from the project, provided by M. Schwab (fission track ages) and L. Ratschbacher (Ar-Ar ages).

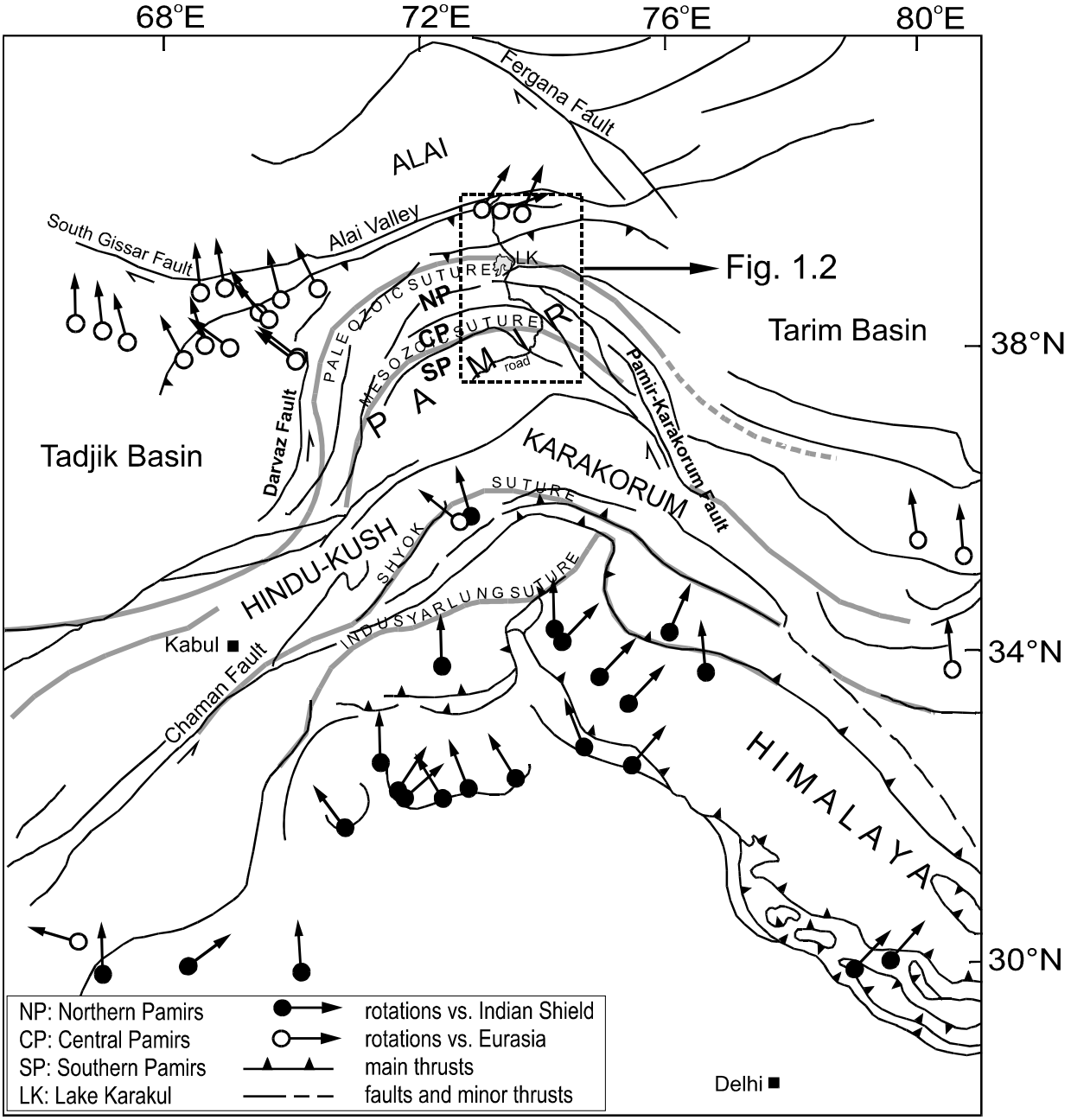

Fig. 2.1: Area of investigation (dashed rectangle) in the western part of the India-Asia collision zone. Structural map from Klootwijk et al. 1986, 1991 and 1994. Sutures taken from Burtman & Molnar (1993), map of palaeomagnetic rotations from Klootwijk et al. (1986, 1991 and 1994), Thomas et al. (1994) and Patzelt et al. (1996).

The Pamir mountains are part of the north-western edge of the India-Asia collision zone. They comprise at least three crustal segments successively accreted to the southern Eurasian margin in the Palaeozoic and Mesozoic. The corresponding sutures which are reported to continue to the east and the west (Burtman & Molnar 1993 and references therein), have been subsequently bent and displaced northward by the indentation of the Indian plate. Based on these sutures, the Pamirs are subdivided into a northern, central and southern part (Fig. 2.1). Fig. 2.2 shows a simplified geologic map of the investigation area.

The northern Pamirs consist mainly of Late Triassic to Early Jurassic granites and Palaeozoic metamorphic rocks. Biotites in these granites show Ar-Ar cooling ages around 200 Ma (Early Jurassic). Fission track ages of apatites reveal Oligocene to Miocene cooling ages. At the northern rim, folded and northward thrusted Cretaceous limestones and red beds, and Tertiary sandstones and red beds occur (Burtman & Molnar 1993, Strecker et al. 1995, own observations).

The northern part of the central Pamirs comprises an intensely folded sequence of Palaeozoic and Mesozoic sedimentary rocks, occasionally with imbricated layers of Tertiary red beds. The boundary between the central and the southern Pamirs is delineated by a dome of high-grade metamorphic rocks. Ar-Ar dating yields cooling ages of 15 - 25 Ma for amphiboles within these rocks. Fission track dating of apatites from the same rocks provides cooling ages of mostly around 20 Ma. The metamorphic rocks are intruded by granites whose biotites give an Ar-Ar cooling age also of around 20 Ma. The northern boundary of the dome is characterised by northward dextral normal faulting, the southern boundary by southward thrusting with prominent dextral strike-slip. To both sides of the dome, the rocks underwent intense folding and metamorphism with rapidly increasing grade toward the dome. The metamorphic and intensely folded sediments to the south of the dome are referred to as the *Rushan-Pshart zone* (see Fig. 2.2).

The southern Pamirs comprise Carboniferous to Permian sandstones and Triassic to Jurassic limestones in their eastern part. Intrusions of granites are frequent. Fission track dating on apatites shows a cooling age of about 20 Ma. Tertiary sandstones and red beds occur concentrated in the Rushan-Pshart zone along the southern boundary of the metamorphic dome. The Early Miocene age of about 20 Ma concurrently turns up as Ar-Ar cooling age of biotites in granites and as fission track cooling age in apatites from rocks of the northern, central and southern Pamirs. This indicates that a thermal event, probably associated with intense deformation, occurred around this time in the Pamirs. Furthermore, this age coincides with the Early to Middle Miocene age given by Wang et al. (1992) for the begin of thrusting in the adjacent Tarim basin farther east.

Since the first contact of India with Eurasia 55 - 65 Ma ago (e.g. Besse & Courtillot 1988, Beck et al. 1995, Patzelt et al. 1996), total convergence between the two plates is assumed to be 2500 - 3000 km (e.g. Molnar & Tapponnier 1975, Chen et al. 1993a,1993b). From the northward displacement of the sutures, and from fault displacements and balanced cross sections, a total of 300 - 700 km of convergence is supposed to have been absorbed within the area from the southern Pamirs to the Alai range (Burtman & Molnar 1993). As inferred from fault displacements and balanced cross sections, a minimum of 160 km of shortening is attributed to the area south of the Rushan-Pshart zone, at least 80 km to the Rushan-Pshart zone itself, and a minimum of 100 km to the area between the central and the northern Pamirs (Burtman & Molnar 1993 and references therein).

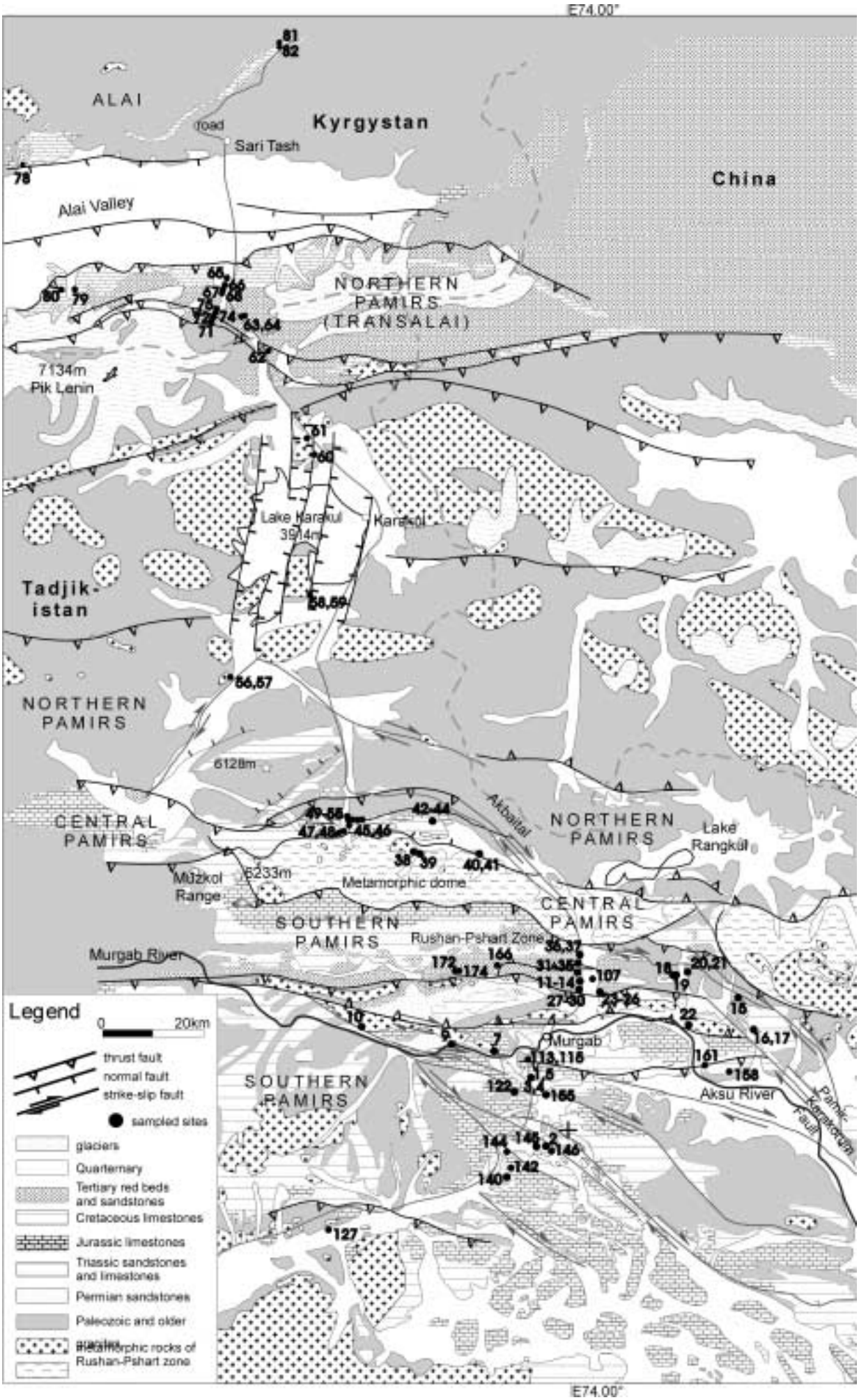
E74.00°
ALAI
road
Kyrgystan
Sari Tash
China
Alai Valley
NORTHERN PAMIRS (TRANSALAI)
7134m Pik Lenin
Lake Karakul 3914m
Karakol
Tadjik-istan
NORTHERN PAMIRS
6128m
CENTRAL PAMIRS
Akbaital
NORTHERN PAMIRS
Lake Rangkul
Muzkol Range
6233m
Metamorphic dome
CENTRAL PAMIRS
SOUTHERN PAMIRS
Rushan-Pshart Zone
Murgab River
Murgab
SOUTHERN PAMIRS
Aksu River
Panjsk Kamarovsk Fault
Legend
0 20km
thrust fault
normal fault
strike-slip fault
sampled sites
glaciers
Quaternary
Tertiary red beds and sandstones
Cretaceous limestones
Jurassic limestones
Triassic sandstones and limestones
Permian sandstones
Paleozoic and older
Metamorphic rocks of Rushan-Pshart zone
E74.00°

Fig. 2.2 (preceding page): Geologic map of the investigation area with palaeomagnetic site localities. Simplified from the geologic maps 1:500.000 of the Russian Geology Ministery (1980 and 1984) and from maps of Strecker et al. (1995).

In the western part of the India-Asia collision zone, the present N-S convergence between India and Eurasia is estimated to be 44±5 mm/a (DeMets et al. 1990), being transferred due north by the sinistral Chaman and Darvaz faults to the west of the Pamirs and the dextral Pamir-Karakorum fault to the east (Fig. 2.1). Present convergence in this region is partitioned into northward subduction of India beneath the Himalaya, southward subduction of Eurasia below the Pamirs, thrusting in the Alai range, and distributed crustal shortening in the Pamirs and the Karakorum/Hindukush mountains (Burtman & Molnar 1993, Strecker et al. 1995).

Existing palaeomagnetic declination data point to an overall oroclinal bending (see Fig. 2.1), thought to be caused by the northward indentation of the Indian into the Eurasian plate.

According to the ages of the sutures, the northern and central Pamirs are part of Eurasia since the Late Palaeozoic, and the southern Pamirs since the Late Cretaceous. There is no information regarding the drift history of these crustal segments before they became part of Eurasia. Hence, in the southern Pamirs, palaeoremanences must be younger than Late Cretaceous to be referenced to the Eurasian polar wander path. Within the central Pamirs, palaeoremanences must be younger than Late Palaeozoic to be referenced. Fig. 2.3 shows the expected palaeofield declination and inclination for a reference location now at a longitude/latitude E74,00°/N38,00° on Eurasia, calculated according to the APWP from Besse & Courtillot (1991). These curves will be taken as the reference for the palaeomagnetic data of this work.

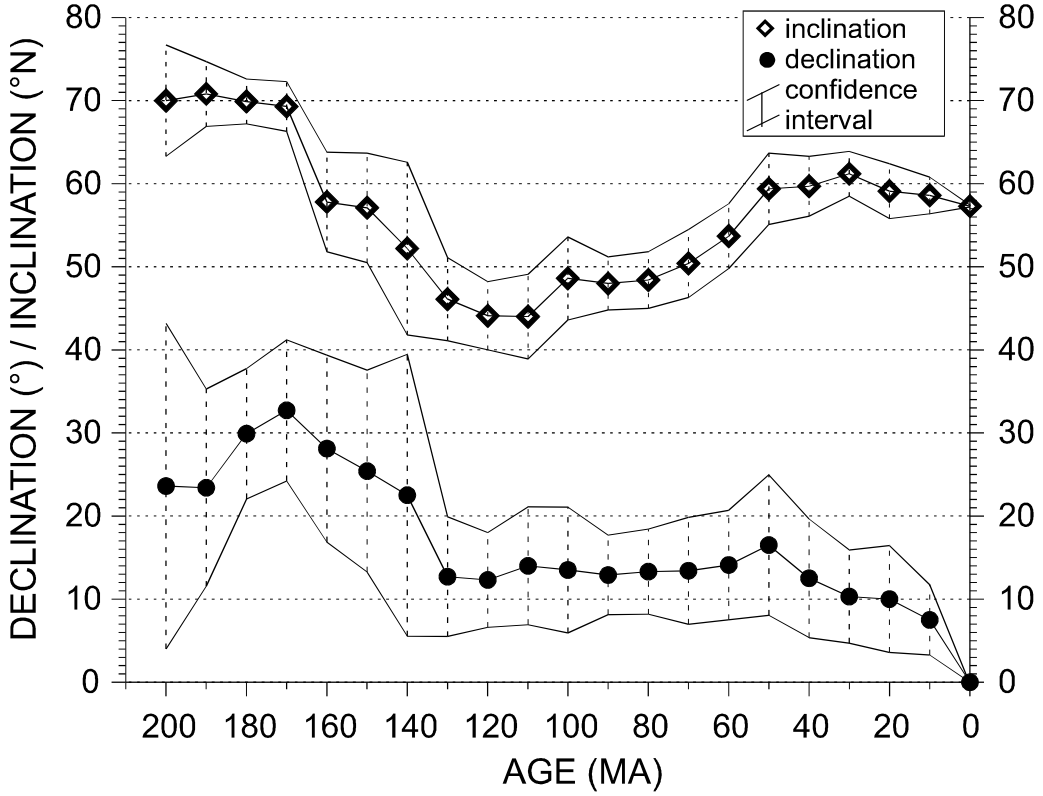

Fig. 2.3: Expected palaeofield declination and inclination from Triassic to present for a reference location now at a longitude/latitude of E74,00°/N38,00° on Eurasia. Calculated according to the APWP for stable Eurasia from Besse & Courtillot (1991). Confidence intervals for the inclination are ±A95. For the declination, the approximation A95/cos I has been used instead of the true asymmetric confidence interval.

2.2 Sampled Sites

Sampling has been carried out with a portable drilling machine. Coordinates were taken by a GPS-device with a horizontal accuracy of about 100 m. The site locations are shown in Fig. 2.2. Table 2.1 lists all analysed sites with localities, lithologies and ages of the rocks. The ages of the Tertiary sediments as given by the Russian maps are uncertain. Therefore, the whole time interval of the Tertiary has been assumed for these sites.

Table 2.1: Location, lithology and ages of the analysed sites. Coordinates taken by GPS. Lithology and ages from geologic maps 1:500.000 of the Russian Geology Ministery (1980, 1984). Numerical ages according to time table from Ogg (1995). demag.: demagnetisation, AF: in alternating field, TH: thermal. The right column indicates whether a significant site mean with a precision parameter of $k \geq 10$ according to Fisher statistics (Fisher 1953) in in-situ coordinates has been obtained.

site	location		lithology	geologic	num. age		demag.	k≥10
	lat.	long.		age	(Ma)			+/-
1	38,09	73,90	sandstone	Early Permian	290 -	256	TH	+
2	37,96	73,96	limestone	Early to middle Jur.	208 -	157	AF	+
3	38,11	73,91	limestone	Early to middle Jur.	208 -	157	AF	+
4	38,11	73,91	limestone	Early to middle Jur.	208 -	157	AF	+
5	38,10	73,90	sandstone	Early Permian	290 -	256	AF	+
6	38,10	73,90	sandstone	Early Permian	290 -	256	TH	+
7	38,13	73,85	granite	Late Jur. - Early Cret.	146 -	97	AF	+
9	38,14	73,74	sandstone	Early Permian	290 -	256	TH	+
10	38,17	73,57	granite	Late Jur. - Early Cret.	146 -	97	TH	+
11	38,27	74,04	red beds	Tertiary	65 -	2	TH	-
12	38,27	74,04	red beds	Tertiary	65 -	2	TH	-
13	38,27	74,04	red beds	Tertiary	65 -	2	TH	+
14	38,27	74,05	red beds	Tertiary	65 -	2	TH	+
15	38,23	74,37	red beds	Tertiary	65 -	2	TH	+
16	38,16	74,41	red beds	Tertiary	65 -	2	TH	+
17	38,16	74,41	red beds	Tertiary	65 -	2	TH	+
18	38,27	74,25	sandstone	Tertiary	65 -	2	AF	+
19	38,27	74,25	sandstone	Tertiary	65 -	2	AF	+
20	38,27	74,27	red beds	Tertiary	65 -	2	TH	-
21	38,27	74,27	red beds	Tertiary	65 -	2	TH	-
22	38,16	74,29	limestone	Early to Middle Jur.	208 -	157	AF	+
23	38,25	74,06	basalt	Tertiary	65 -	2	TH	+
24	38,25	74,06	red beds	Tertiary	65 -	2	TH	+
25	38,25	74,06	red beds	Tertiary	65 -	2	TH	+
27	38,25	74,05	red beds	Tertiary	65 -	2	TH	+
28	38,25	74,05	basalt	Tertiary	65 -	2	TH	+
29	38,26	74,05	red beds	Tertiary	65 -	2	TH	+
30	38,26	74,05	red beds	Tertiary	65 -	2	TH	+
31	38,28	74,08	sandstone	Tertiary	65 -	2	TH	+
32	38,27	70,04	red beds	Tertiary	65 -	2	TH	-
33	38,27	70,04	sandstone	Tertiary	65 -	2	AF	-
34	38,31	74,04	sandstone	Tertiary	65 -	2	TH	+
35	38,31	74,04	sandstone	Tertiary	65 -	2	TH	+
36	38,31	74,04	basalt	Tertiary	65 -	2	TH	+
37	38,31	74,04	sandstone	Tertiary	65 -	2	AF	+
38	38,50	74,70	diorite	Tertiary ?	65 -	2	AF	+
39	38,51	74,69	diorite	Tertiary ?	65 -	2	TH	+
40	38,47	73,81	red beds	Tertiary	65 -	2	TH	+
41	38,48	73,81	red beds	Tertiary	65 -	2	TH	+
42	38,54	73,73	limestone	Late Cret.	97 -	65	AF	+
43	38,54	73,73	limestone	Late Cret.	97 -	65	AF	+
44	38,54	73,73	limestone	Late Cret.	97 -	65	AF	+

Table 2.1 continued:

site	location lat.	location long.	lithology	geologic age	num. age (Ma)	demag.	k≥10 +/-
45	38,53	73,53	red beds	Tertiary	97 - 65	TH	+
46	38,53	73,53	red beds	Tertiary	97 - 65	TH	+
47	38,53	73,52	red beds	Tertiary	65 - 2	TH	+
48	38,53	73,51	red beds	Tertiary	65 - 2	TH	+
49	38,53	73,53	limestone	Middle to Late Jur.	178 - 146	AF	+
50	38,53	73,53	limestone	Middle to Late Jur.	178 - 146	AF	+
51	38,53	73,53	limestone	Middle to Late Jur.	178 - 146	AF	+
52	38,53	73,54	limestone	Middle to Late Jur.	178 - 146	AF	+
53	38,53	73,55	limestone	Middle to Late Jur.	178 - 146	AF	+
54	38,54	73,53	limestone	Middle to Late Jur.	178 - 146	AF	+
55	38,54	73,53	limestone	Middle to Late Jur.	178 - 146	AF	+
56	38,79	73,29	granite	Triassic?		AF	-
57	38,80	73,30	granite	Triassic?		AF	-
58	38,94	73,45	granite	Triassic?		AF	-
59	38,94	73,45	granite	Triassic?		AF	-
60	39,20	73,45	granite	Triassic?		AF	-
61	39,21	73,43	granite	Triassic?		AF	-
62	39,38	73,33	sandstone	Tertiary	65 - 2	TH	+
63	39,41	73,27	red beds	Tertiary	65 - 2	TH	-
64	39,41	73,27	red beds	Tertiary	65 - 2	TH	+
65	39,50	73,24	limestone	Early Cret.	146 - 97	AF	+
66	39,49	73,22	red beds	Late Cret.	97 - 65	TH	+
67	39,48	73,23	limestone	Early Cret.	97 - 65	AF	+
68	39,48	73,22	red beds	Late Cret.	97 - 65	TH	+
71	39,43	73,20	red beds	Tertiary	65 - 2	TH	+
72	39,43	73,21	red beds	Tertiary	65 - 2	TH	-
74	39,44	73,21	limestone	Early Cret.	146 - 97	AF	+
78	39,71	72,78	red beds	Tertiary	65 - 2	TH	+
79	39,48	72,89	red beds	Late Cret.	97 - 65	TH	+
80	39,48	72,86	red beds	Late Cret.	97 - 65	AF	-
81	39,92	73,35	sandstone	Tertiary	65 - 2	AF	-
82	39,92	73,35	sandstone	Tertiary	65 - 2	TH	+
107	38,26	74,06	red beds	Tertiary	65 - 2	TH	+
113	38,12	74,06	limestone	Middle Jur.	178 - 157	AF	+
115	38,11	73,91	limestone	Early to Middle Jur.	208 - 157	AF	+
122	38,06	73,88	limestone	Early to Middle Jur.	208 - 157	AF	+
127	37,82	73,47	limestone	Middle Jur.	178 - 157	AF	+
140	37,91	73,87	limestone	Early to Middle Jur.	208 - 157	AF	+
142	37,93	73,88	limestone	Early Jur.	208 - 178	AF	+
144	37,96	73,87	limestone	Early Jur.	208 - 178	AF	+
145	37,97	73,93	limestone	Early to Middle Jur.	208 - 157	AF	+
146	37,96	73,97	limestone	Early to Middle Jur.	208 - 157	AF	+
155	38,06	73,95	limestone	Early to Middle Jur.	208 - 157	AF	+
158	38,10	74,36	sandstone	Early Permian	290 - 256	AF	+
161	38,11	74,31	sandstone	Early Permian	290 - 256	AF	+
166	38,29	73,84	red beds	Late Cret.	97 - 65	TH	-
172	38,28	73,75	red beds	Late Cret.	97 - 65	TH	-
174	38,27	73,76	red beds	Late Cret.	97 - 65	TH	-

As guideline for the further considerations and the fold tests, Table 2.2 assigns the sites into groups according to lithology and location.

Table 2.2: Groups of sites according to lithology and location as guideline for further considerations. Sites in rounded brackets have Fisher means with k<10 and, using Fisher statistics, must be excluded as statistically not significant. Sites in edged brackets give a significant site mean, but were not enclosed in a group since they are too distant from the others of the group. Ages are based on geologic maps 1:500.000 of the Russian Geology Ministery (1980, 1984). Numerical age from the time table of Ogg (1995).

location, group	sites	mean coordinates latitude	longitude
Southern Pamirs			
Permian sandstones	1,5,6,9	38,11	74,02
290-256 Ma	[158,161]		
Jurassic limestones	2,3,4,113,115		
208-157 Ma	122,140,142,144, 145,146,155 [22,127]	38,02	73,93
Tertiary sediments	13,14,24,25,27,29		
w estern group, 65-2 Ma	30,31,34,35,37,107 (11,12,32,33, 166,172,174)	38,27	74,05
Tertiary sediments	15,16,17,18,19	38,22	74,34
eastern group, 65-2 Ma	(20,21)		
Central Pamirs			
Jurassic limestones	49,50,51,52	38,53	73,53
178-146 Ma	53,54,55		
Cretaceous limestones	42,43,44	38,54	73,73
97-65 Ma			
Tertiary red beds			
w estern group 65-2 Ma	45,46,47,48	38,53	73,52
eastern group 65-2 Ma	40,41	38,48	73,81
Northern Pamirs and Tien Shan			
Cretaceous limestones and red beds	65,66,67,68,74	39,48	73,22
97-65 Ma	[79],(80)		
Tertiary sediments	62,64,71	39,41	73,27
65-2 Ma	(63,72)		
Tien Shan, Tertiary sediments	78,82		
65-2 Ma	(81)		
Southern and Central Pamirs			
S-Pamirs, volcanic rocks Tertiary(?)	23,28,36	38,27	74,05
S-Pamirs, granites Jurassic(?)	7,10	38,15	73,71
C-Pamirs, granites Tertiary(?)	38,39	38,50	74,70
C-Pamirs, granites Triassic(?)	(56-61)		

2.3 Sample Treatment

The core samples were cut into specimens with a standard length of 2,2 - 2,3 cm. For analysis of the ferrimagnetic minerals, one specimen per site was used for isothermal remanence acquisition (IRM) in a DC-field up to 4,5 Tesla, and subsequent stepwise thermal demagnetisation of the saturation IRM (SIRM). Temperature dependence of susceptibility (KLY-2 susceptibility bridge with CS-2 heating unit, Agico Brno) was used to determine Curie temperatures. Stepwise alternating field (AF) and thermal demagnetisation (TH) were performed for pilot specimens from each site. Susceptibility was monitored after each heating step to detect mineralogical alterations. Depending on the results of the pilot studies and the IRM- and SIRM-curves, the remaining specimens of all sites were demagnetised applying the appropriate procedure, thermally (Magnetic Measurements MMTD1 furnace) or in alternating fields (2G Enterprise degausser). Remanence directions were measured with a RF-SQUID magnetometer with automatic AF-demagnetisation (2G Enterprises). Orthogonal vector plots and equal area projections were used to examine the demagnetisation behaviour of the specimens. Magnetic directions were determined from straight segments of the demagnetisation path with principal component analysis (PCA, modified version after Kirschvink 1980). Calculation of site means used with Fisher statistics (Fisher 1953).

2.4 Palaeomagnetic Results

The rock- and palaeomagnetic results will be presented according to the groups given in Table 2.2. Table 2.3 summarises the rock- and palaeomagnetic results.

Table 2.3 (next page): Rock- and palaeomagnetic results. For ages see also Table 2.1. N: number of specimens measured, spec. (p/n): number of specimens used for statistics with in in-situ coordinates positive (p) and negative (n) inclination. Bedding as dip azimuth and angle of dip; bedding in brackets: dip of adjacent sedimentary beds. Upright/overturned bedding identified from cross bedding or other criteria. Ferrimagnetic minerals as identified from IRM, SIRM-T, susceptibility-temperature measurements and demagnetisation; mt: magnetite, hem: haematite. Goethite occurs occasionally, but is not listed because not relevant in palaeomagnetism. In brackets: minor amounts. If two remanence components are present, x.1 represents the lower coercive/lower temperature unblocking component, x.2 the higher coercive/higher temperature unblocking component. D_{is}/I_{is} D_{bc}/I_{bc}: palaeodeclination and -inclination in in-situ and bedding coordinates, $\alpha 95$: confidence angle; k: precision parameter.

site	lithology	geologic age	mean age	N	spec. p / n	bedding	upright / overturned	ferrimagn. mt	ferrimagn. hem	demag.	in-situ Dis	in-situ Iis	in-situ α95	in-situ k	bedding corrected Dbc	bedding corrected Ibc	bedding corrected α95	bedding corrected k
1	sandstone	Early Permian	273	12	11 / 0	340/67		x		TH	73,1	57,4	10,6	19,7	14,2	23,0	12,3	14,8
2	limestone	Early to Middle Jur.	183	9	8 / 0	326/26;162/35		x	(x)	AF	8,6	39,6	9,5	35	13,4	43,7	27,5	5,0
3	limestone	Early to Middle Jur.	183	10	3 / 5	318/60		x		AF	22,8	36,2	11,0	26,5	5,1	0,1	10,2	30
4	limestone	Early to Middle Jur.	183	8	7 / 1	334/53		x	(x)	AF	43,6	55,9	17,0	11,6	8,4	19,5	18,4	10,0
5.1	sandstone	Early Permian	273	8	8 / 0	333/74	overturned	x		AF	38,8	41,5	10,8	27,4	16,3	-6,3	15,6	13,5
5.2				8	0 / 4	333/74		x		AF	186,4	-47,5	8,1	130	178,8	25,6	7,8	140
6	sandstone	Early Permian	273	12	11 / 0	347/78	overturned	x	x	TH	27,8	35,7	10,0	21,9	24,5	-29,0	10,8	28,7
7	granite	Late Jura.-Early Cret.	122	21	6 / 0			x		AF	314,4	48,2	16,3	15,3				
9	sandstone	Early Permian	273	7	7 / 0	175/61		x		TH	48,3	39,7	15,9	15,4	115,5	45,8	16,7	14,0
10	granite	Late Jura.-Early Cret.	122	8	4 / 3			x		TH	358,0	56,8	5,2	138				
13	red beds	Tertiary	34	9	7 / 2	356/18	upright	x	x	TH	20,4	51,5	12,2	21,5	14,9	35,9	12,1	21,9
14	red beds	Tertiary	34	11	6 / 1	203/68	overturned	x	x	TH	288,3	62,3	18,8	11,3	232,1	17,2	18,8	11,3
15	red beds	Tertiary	34	11	4 / 5	043/45		x	(x)	TH	199,2	-15,2	15,5	12,0	197,2	23,0	16,0	11,3
16	red beds	Tertiary	34	11	0 / 11	0010/48		x	x	TH	60,8	-9,7	13,7	12,1	79,1	-35,2	13,7	12,1
17	red beds	Tertiary	34	8	1 / 6	005/53		x	x	TH	19,6	41,6	8,0	58	16,3	-10,0	8,1	57
18.1	sandstone	Tertiary	34	9	6 / 3	334/42	overturned	x		AF	359,4	45,8	11,6	20,8	351,5	6,4	11,6	20,8
18.2				9	9 / 0	334/42		x		AF	163,5	-9,3	5,2	100	165,1	32,1	5,2	100
19.1	sandstone	Tertiary	34	9	7 / 0	330/36		x		AF	330,6	48,1	14,9	17,3	330,4	12,1	14,9	17,3
19.2				9	9 / 0	330/36		x		AF	128,2	20,6	10,9	23,5	115,1	52,7	10,9	23,5
22	limestone	Early to Middle Jur.	183	6	6 / 0	182/43		x	(x)	AF	71,1	55,6	19,9	12,2	130,2	47,8	19,9	12,2
23	basalt	Tertiary	34	10	1 / 6	(359/47)		x	x	TH	132,8	-49,1	6,6	85				
24	red beds	Tertiary	34	11	11 / 0	029/41		x	x	TH	239,4	24,4	14,7	12,3	264,1	55,7	14,7	12,3
25	red beds	Tertiary	34	10	10 / 0	019/38		x	x	TH	222,0	31,7	9,3	28,0	247,5	63,6	9,3	28,0
27	red beds	Tertiary	34	8	7 / 0	183/68		x	x	TH	320,9	38,7	14,3	18,8	238,2	50,5	14,3	18,8
28	basalt	Tertiary	34	10	0 / 10	(180/70)		x	x	TH	357,7	-48,4	10,2	23,3				
29	red beds	Tertiary	34	9	6 / 2	018/43		x	x	TH	213,9	16,4	16,2	12,7	226,6	56,6	16,2	12,7
30	red beds	Tertiary	34	9	3 / 6	009/71		x	x	TH	345,8	68,0	12,1	19,2	0,9	-1,2	13,4	15,8
31	sandstone	Tertiary	34	9	9 / 0	030/60	upright	x	x	TH	275,7	65,7	17,5	11,0	2,2	38,0	16,6	12,0
34	sandstone	Tertiary	34	11	8 / 0	158/67	overturned	x	x	TH	275,6	74,3	10,8	27,0	173,8	30,0	12,0	22,4
35	sandstone	Tertiary	34	11	9 / 0	343/61	upright	x	x	TH	226,7	59,6	10,1	17,1	308,0	37,9	17,1	10,1
36	basalt	Tertiary	34	11	10 / 1	(188/54)		x	(x)	TH	202,9	19,5	7,5	38				
37	sandstone	Tertiary	34	12	12 / 0	205/45		x	(x)	AF	249,3	54,2	9,6	21,3	230,1	16,1	9,6	21,3
38	granite	Tertiary ?	34	10	8 / 0			x		AF	5,4	44,2	7,7	53				
39	granite	Tertiary ?	34	7	0 / 7			x	x	TH	163,9	-43,1	7,2	71				
40	red beds	Tertiary	34	12	12 / 0	353/51		x	x	TH	345,3	48,4	7,6	34	347,8	-2,5	7,6	34
41	red beds	Tertiary	34	10	10 / 0	340/41		x	x	TH	9,5	36,9	17,8	10,3	2,9	2,7	17,3	9,9
42	limestone	Late Cretaceous	81	9	3 / 3	022/27		x		AF	299,9	50,7	12,7	28,7	326,3	40,5	12,8	28,7
43.1	limestone	Late Cretaceous	81	9	6 / 0	015/30		x		AF	338,6	45,7	14,5	22,2	348,9	19,8	14,5	22,2
43.2				9	0 / 6	015/30		x		AF	97,9	-49,3	11,3	36	130,5	-44,2	11,3	36
44	limestone	Late Cretaceous	81	10	8 / 1	064/30		x		AF	327,2	67,1	5,4	93	21,4	55,1	5,4	93
45	red beds	Tertiary	81	9	0 / 9	011/67		x	x	TH	353,1	-27,6	6,3	68	261,6	-73,2	6,3	68
46	red beds	Tertiary	81	9	0 / 9	011/67		x	x	TH	344,0	-14,0	9,9	32	295,6	-63,0	9,9	32
47	red beds	Tertiary	34	8	0 / 7	005/34		x	x	TH	299,3	-88,4	13,3	21,5	187,6	-56,6	13,3	21,5
48	red beds	Tertiary	34	9	0 / 8	024/40		x	x	TH	65,0	-76,6	10,2	31	186,9	-59,0	10,2	31
49.1	limestone	Middle to Late Jur.	162	8	7 / 0	032/33		x		AF	32,9	53,3	4,5	185	32,6	20,3	4,5	185
49.2								x		AF	0,3	53,7	3,6	286	12,1	23,7	3,6	286
50.1	limestone	Middle to Late Jur.	162	8	8 / 0	022/52		x	(x)	AF	50,9	60,1	13,1	18,9	216,2	-10,9	13,1	18,9
50.2					8 / 0			x		AF	24,7	65,8	2,1	716	23,1	13,9	2,1	716
51.1	limestone	Middle to Late Jur.	162	10	8 / 0	353/76		x		AF	133,4	55,3	15,8	13,2	20,7	38,6	15,8	13,2
51.2				10	10 / 0	353/76		x		AF	16,0	68,3	9,8	25,2	1,3	-6,0	9,8	25,2
52.1	limestone	Middle to Late Jur.	162	9	7 / 0	212/85		x		AF	88,0	54,5	18,2	11,9	180,5	23,2	18,2	11,9
52.2				9	6 / 1			x		AF	4,6	62,4	9,7	40	226,1	29,2	9,7	40
53.1	limestone	Middle to Late Jur.	162	9	7 / 0	167/80		x		AF	50,7	69,5	15,9	13,1	146,5	18,1	15,9	13,1
53.2					8 / 0			x		AF	12,4	38,5	12,5	24,3	130,7	53,0	12,5	24,3
54.1	limestone	Middle to Late Jur.	162	9	7 / 0	020/54		x	(x)	AF	51,7	58,0	11,4	28,9	36,3	7,7	11,4	28,9
54.2					8 / 0			x	(x)	AF	23,1	55,6	8,9	40	21,7	1,6	8,9	40
55.1	limestone	Middle to Late Jur.	162	8	6 / 0	030/61		x		AF	214,1	70,6	18,9	11,2	28,0	48,4	18,9	11,2
55.2					7 / 0			x		AF	354,7	65,8	9,0	46	16,2	8,6	9,0	46
62	sandstone	Tertiary	34	12	11 / 0	040/40	upright	x	x	TH	51,6	74,3	11,3	17,2	43,8	34,6	11,3	17,2
64	red beds	Tertiary	34	10	7 / 0	050/54	upright	(x)	x	TH	219,1	78,6	17,8	12,5	54,3	45,5	17,1	13,4
65.1	limestone	Early Cretaceous	122	10	9 / 0	212/53	overturned	x		AF	124,9	-70,4	10,3	25,9	56,3	-35,3	10,3	25,9
65.2				10	0 / 9			x		AF	354,9	47,4	7,8	44	269,2	61,0	7,8	44
66	red beds	Late Cretaceous	81	12	12 / 0	203/19		(x)	x	TH	21,9	63,9	13,1	11,9	19,0	82,9	13,1	11,9
67	limestone	Early Cretaceous	81	18	17 / 0	279/25		x		AF	349,3	55,3	8,0	30	329,0	45,7	7,8	32
68	red beds	Late Cretaceous	81	12	12 / 0	193/75	upright	x	x	TH	44,6	27,2	9,8	22,9	121,1	57,8	9,9	22,4
71	red beds	Tertiary	34	10	1 / 8	022/85	overturned	x	x	TH	318,9	-32,8	17,1	10,0	257,9	-25,2	17,1	10,0
74	limestone	Early Cretaceous	122	9	7 / 0	032/85	overturned	x	x	TH	207,9	-27,8	17,1	13,5	205,4	57,0	17,1	13,5
78	red beds	Tertiary	34	12	7 / 0	122/68		x	x	TH	323,7	40,4	18,0	12,2	82,7	64,3	18,0	12,2
79	red beds	Late Cretaceous	81	13	10 / 1	150/34		x	x	TH	317,0	38,2	14,4	11,0	298,7	70,2	14,4	11,0
82	sandstone	Tertiary	34	11	10 / 0	140/27		x	(x)	TH	329,5	61,7	10,5	22,1	38,2	85,4	10,5	22,1
107	red beds	Tertiary	34	9	6 / 2	004/27		x	x	TH	6,3	43,2	12,0	22,1	5,7	16,2	12,0	22,1
113	limestone	Middle Jur.	168	9	7 / 0	342/32		x		AF	48,7	51,4	21,4	10,1	24,2	32,5	21,4	10,1
115	limestone	Early to Middle Jur.	183	10	9 / 0	328/64		x		AF	45,5	59,6	16,1	11,2	358,9	16,3	16,1	11,2
122	limestone	Early to Middle Jur.	183	11	8 / 0	179/69		x	(x)	AF	351,7	58,3	18,3	10,1	185,3	52,4	18,3	10,1
127	limestone	Middle Jur.	168	10	10 / 0	144/62		x	(x)	AF	293,9	50,7	5,0	93	180,7	57,9	5,0	93
140	limestone	Early to Middle Jur.	183	14	13 / 0	353/67		x		AF	341,4	36,6	11,5	14,0	342,3	-29,4	11,5	14,0
142	limestone	Early Jur.	193	9	9 / 0	055/23		x		AF	61,9	40,1	12,8	17,1	60,5	17,2	12,8	17,1
144	limestone	Early Jur.	193	10	8 / 0	162/72		x		AF	343,7	54,0	9,6	34	160,3	53,9	9,6	34
145	limestone	Early to Middle Jur.	183	7	7 / 0	327/49		x		AF	4,6	42,8	8,2	55	353,6	0,4	8,2	55
146	limestone	Early to Middle Jur.	183	7	6 / 0	031/42		x		AF	10,2	57,5	8,5	63	19,5	16,9	8,5	63
155	limestone	Early to Middle Jur.	183	9	7 / 0	332/78		x		AF	10,2	54,5	5,4	127	354,0	-16,1	5,4	127
158	sandstone	Early Permian	273	11	10 / 0	006/44		x	(x)	AF	335,7	53,3	6,5	57	348,0	12,6	6,5	57
161	sandstone	Early Permian	273	12	12 / 0	013/59		x	(x)	AF		67,5	2,8	249	41,8	25,1	4,9	80

2.4.2 Southern Pamirs

Permian Sandstones (Sites 1, 5, 6, 9)

In these fine-grained sandstones, IRM-acquisition (Fig. 2.4) and thermal demagnetisation of a SIRM give low coercivities up to 100 mT and blocking temperatures up to 580°C, characteristic for magnetite. The further rise of the IRM-curves of the sites 6 and 9 above 100 mT probably is due to haematite, as evidenced by a small rest intensity above 600°C in the thermal decay curves.

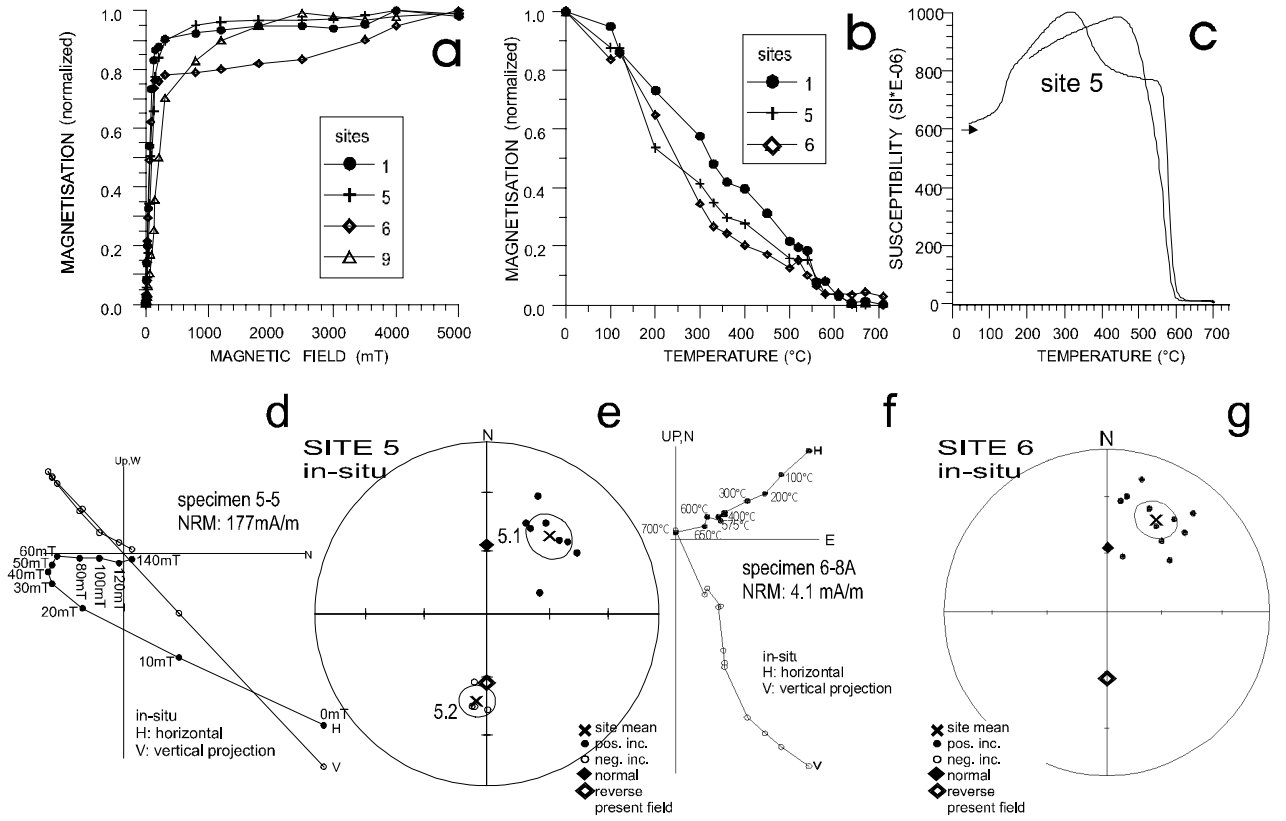

Fig. 2.4: Examples of the rock- and palaeomagnetic investigations for the Permian sandstones of the southern Pamirs. (a) IRM (isothermal remanent magnetisation) acquisition curves, (b) thermal demagnetisation of a saturation IRM (SIRM), (c) susceptibility-temperature curve of site 5, arrow indicates start of heating curve, (d) AF- demagnetisation of a specimen of site 5 in the Zijderveld diagram, (e) site mean of low- (5.1) and high- (5.2) coercive components for site 5, both carried by magnetite, (f) thermal demagnetisation of a specimen of site 6 in the Zijderveld diagram, (g) remanence components of site 6 carried by magnetite.

The susceptibility-temperature curve for site 5 provides a Curie temperature of 580°C, reproduced by the cooling curve. The heating curve exhibits a pronounced Hopkinson peak at 320°C, indicating a single-domain/pseudosingle-domain (SD/PSD) magnetite fraction.

According to the pilot studies, sites 1, 6 and 9 have been demagnetised thermally, and site 5 in the alternating field. Site 5 releases nearly two antipodal components (0 - 20 mT and 60 - 140 mT), both carried by magnetite. The remanence components of site 6 carried by haematite show a strong scatter (not shown), whereas the magnetite components give a site mean with a significant precision parameter (k = 21,9, Fig. 2.4g). All sites of this group provide consistent site means with precision parameters of $k > 10$.

Jurassic Limestones (Sites 2 - 4, 22, 113, 115, 122, 127, 140, 142, 144 - 146, 155)

For all specimens, IRM-acquisition in low fields up to 100 mT (Fig 2.5a) reveals magnetite. The continuous further rise of the curves might be caused by goethite (sites 2 and 22) and/or haematite (sites 3, 4 and 22).

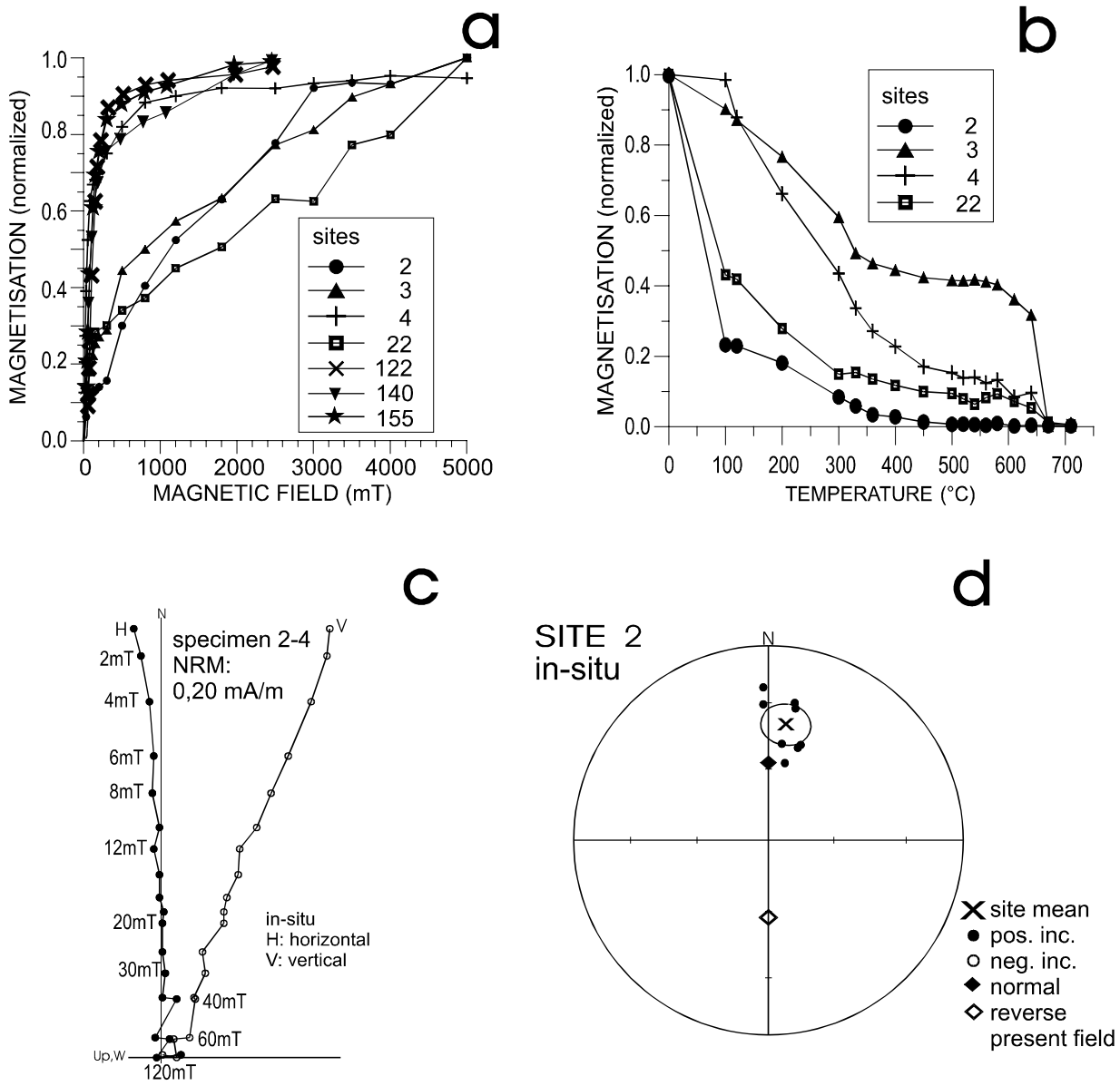

Fig. 2.5: Examples of the rock- and palaeomagnetic investigations for the Jurassic limestones of the southern Pamirs. (a) IRM-acquisition, (b) thermal demagnetisation of a SIRM, (c) AF-demagnetisation of a specimen of site 2 in the Zijderveld diagram, (d) in-situ remanence components of site 2 carried by magnetite.

Thermal demagnetisation of the SIRM (not available for sites 122, 140 and 155) shows goethite, magnetite and haematite in varying amounts. Pyrrhotite could be present as well according to the thermal demagnetisation curves (e.g. site 3, Fig. 2.5a, b). If there, it is always accompanied by magnetite or haematite, and coincides with their remanence components. However, the nearly complete demagnetisation of most of the sites in alternating fields up to 150 mT favours the presence of magnetite. Susceptibility-temperature curves (not shown) failed because of too low intensities. Site 3 has been demagnetised thermally, the other sites in the alternating field after removing goethite remanences by heating to 150°C. Fig. 2.5c shows the demagnetisation of a specimen of site 2, releasing only one remanence component, typical for all sites of this group. Site means with precision parameters of $k > 10$ have been obtained for all sites.

Tertiary Sediments (Sites 11 - 21, 24, 25, 27, 29, 30 - 35, 37, 107)

The rockmagnetic characteristics of the sites of the eastern and western group of the Tertiary sediments are similar and will be treated together. Sites 18 and 19 are dominated by magnetite as evidenced by the IRM-acquisition curves (Fig. 2.6a). This is confirmed by the thermal demagnetisation of the SIRM (Fig. 6b). The other IRM-acquisition curves exhibit much higher coercivities, related to haematite according to the thermal demagnetisation (Fig. 2.6b). Magnetite is present as well, as indicated by blocking temperatures of 580°C. Site 14 additionally shows goethite. The susceptibility-temperature curves (Fig. 2.6c) show magnetite for site 18 and for sites 19, 24 and 37 magnetite and haematite. Cooling curves in all cases are below the heating curves and have been omitted in the figure for clarity.

Fig. 2.6: Examples of the rock- and palaeomagnetic investigations for the Tertiary Red Beds of the southern

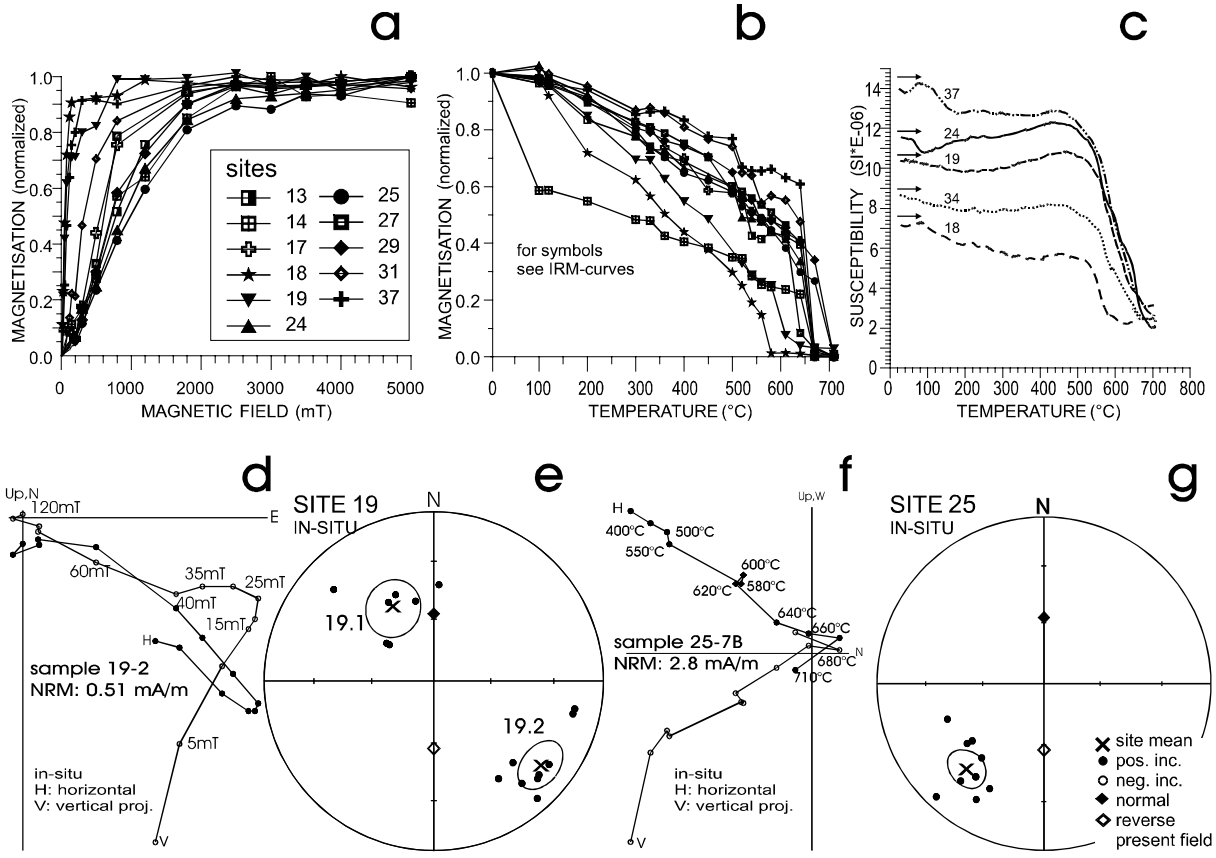

Pamirs. (a) IRM-acquisition, (b) thermal demagnetisation of a SIRM, (c) susceptibility-temperature curves; arrows indicate start of heating curves, (d) AF-demagnetisation of a specimen of site 19, (e) remanence components of site 19 with low (19.1) and high (19.2) coercive components, both carried by magnetite, (f) thermal demagnetisation of a specimen of site 25, (g) remanence components and site mean of site 25.

According to the pilot studies, sites 18, 19 and 37 have been demagnetised in the alternating field, the others thermally. Fig. 2.6d depicts the demagnetisation behaviour of a specimen of site 19. In 7 from 9 specimens of this site, a low-coercive (0 - 20 mT) and a high-coercive (20 - 140 mT) component could be isolated. Both remanence components are carried by magnetite and have site means with precision parameters of $k > 10$ (Fig. 2.6e). Like site 19, the adjacent site 18 carries two components (18.1 and 18.2). Above 500°C site 25 (Fig. 2.6f) yields stable and well grouping components carried by haematite (Fig. 2.6g). Site 21 failed due to low intensities of the NRM. Sites 11, 12, 32 and 33 provide apparently scattering remanence components, giving site means with precision parameters of $k < 10$. As will be shown in section 3, they are not scattering unregularly, but represent small-circle distributions, recording different stages of tectonic displacement.

2.4.3 Central Pamirs

Jurassic Limestones (Sites 49 - 55)

All specimens of this group exhibit a strong IRM-acquisition in low fields, typical for magnetite (Fig. 2.7a). This is confirmed by thermal demagnetisation (Fig. 2.7b), which also would admit pyrrhotite (e.g. site 51). The further rise of the IRM-curves of the sites 50, 53 and 54 is caused by haematite, as shown by thermal demagnetisation (Fig. 2.7b). Pyrrhotite would not be expected in the IRM-acquisition from the low coercivities. Moreover, nearly complete demagnetisation in alternating fields up to 150 mT points to magnetite rather than pyrrhotite.

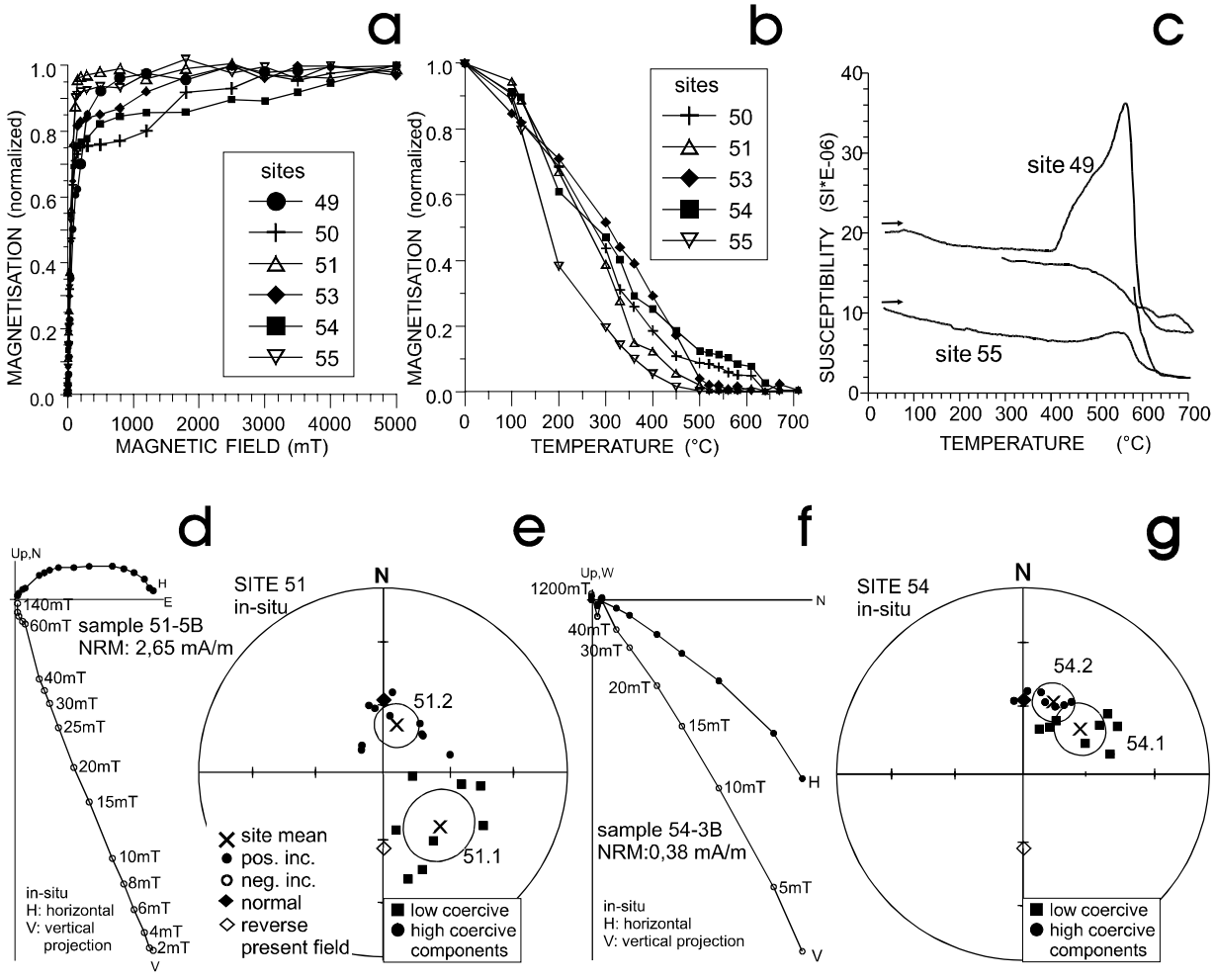

Fig. 2.7: Examples of the rock- and palaeomagnetic investigations for the Jurassic limestones of the central Pamirs. (a) IRM-acquisition, (b) thermal demagnetisation of a SIRM, (c) susceptibility-temperature curves; arrows indicate start of heating curves, (d) AF-demagnetisation of a specimen of site 51 showing at least two components carried by magnetite, (e) two components isolated for site 51, (f) alternating field demagnetisation of a specimen of site 54 showing a similar behaviour, (g) site means for the low- and high-coercive components of site 54.

The susceptibility-temperature curves (Fig. 2.7c) yield Curie temperatures typical for magnetite. There is no evidence for pyrrhotite from the curves, however, its effect could be concealed by the much stronger magnetisation of magnetite. It is unlikely that pyrrhotite is present, however, it cannot be excluded for certainty from the above measurements. All sites have been demagnetised in the alternating field (Fig. 2.7d and 2.7f).

The demagnetisation paths in the Zijderveld plot always show at least two components with apparently overlapping coercivities. Nearly all the sites exhibit this similar continuous change of the remanence directions at least over a part of the demagnetisation. High- and low-coercive components have been isolated over the first two to four steps of the demagnetisation and over the last steps. All sites provide well-defined site means for both high- and low-coercive components (see Fig. 2.7e and 2.7g). For a comparison, analysis of great circles has been carried out (not shown), giving similar results. From this, the coercivity spectra of the remanence components seem to be separated sufficiently to apply component analysis over straight segments.

In all sites, the high-coercive site mean in in-situ coordinates is closer to the present field direction than the low-coercive site mean. The latter always shows a higher declination. In section 3, it will be shown that the change of the remanences during demagnetisation is related to the tectonic displacement. At least three remanence components must be present to explain the demagnetisation behaviour. In some specimens at least four components are seen. The low-coercive components are older and represent the begin of the magnetic record of tectonic displacement, while the high-coercive components have been acquired last. Hence, the site means obtained represent the start and the end of a palaeomagnetically recorded displacement path.

Cretaceous Limestones (Sites 42, 43, 44)

The sites 42, 43 and 44 (no examples shown, similar to the Cretaceous limestones of the northern Pamirs) contain magnetite as the dominating ferrimagnetic mineral. They have been AF-demagnetised after removal of goethite by heating to 150°C. For all sites stable and well-grouping remanence components could be isolated, carried by magnetite. Site 43 gives a low and a high-coercive component, both having a significant site mean.

Tertiary Red Beds (Sites 45 - 48)

IRM-acquisition in fields up to 2 T indicates predominantly haematite (Fig. 2.8a). This is proved by the thermal demagnetisation. Blocking temperatures of 450°C - 580°C also show a magnetite fraction (Fig. 2.8b). The susceptibility-temperature curves have very low intensities. The one of site 40 (Fig. 2.8c) depicts two decays with evidence for haematite and a small fraction of magnetite (see dashed arrows in Fig. 2.8c). Following the pilot studies, all sites have been demagnetised thermally. Demagnetisation above 400°C generally produces one component, carried by magnetite and haematite (Figs. 2.8d and 2.8e). Stable remanence components with significant site means have been obtained for all sites.

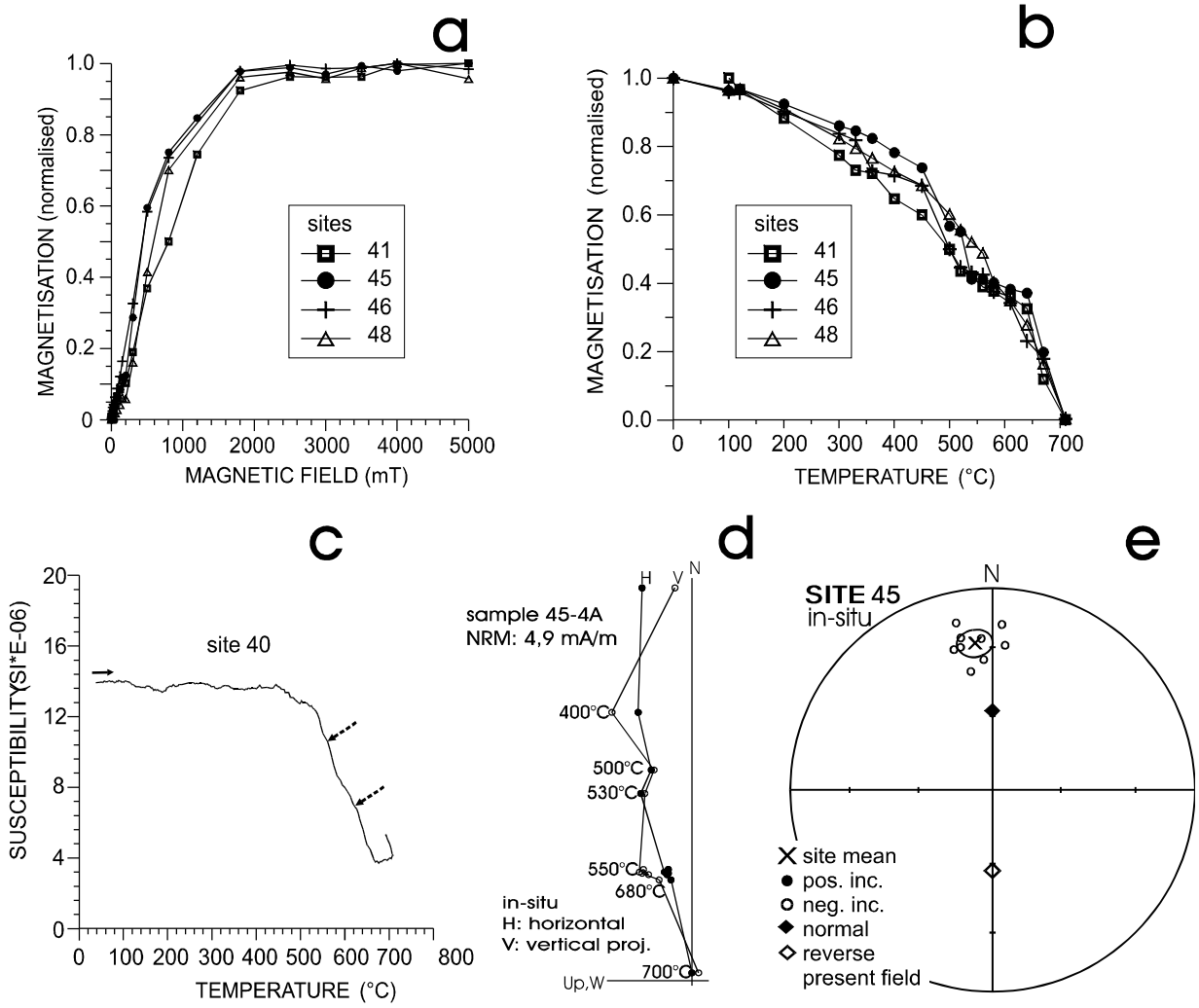

Fig. 2.8: Examples of the rock- and palaeomagnetic investigations for the Tertiary red beds of the central Pamirs. (a) IRM-acquisition, (b) thermal demagnetisation of a SIRM, (c) susceptibility-temperature curve of site 40 with two decays for magnetite and haematite (dashed arrows); left arrow indicates start of heating curve, (d) thermal demagnetisation of a specimen of site 45, (e) remanence components of site 45 and site mean.

2.4.4 Northern Pamirs and Alai range (Sites 62 - 68, 71, 72, 74 and 78 - 82)

From this group, the sites 63, 72, 80 and 81 do not provide significant site means, mostly because of too low intensities of the NRM.

Cretaceous Limestones and Red Beds (Sites 65, 67 and 74; 66, 68, 79 and 80)

IRM-acquisition curves (Fig. 2.9a) identify haematite for the red reds and magnetite for the limestones. This is supported by thermal demagnetisation of the SIRM (Fig. 2.9b). Minor magnetite contents seem to be present in the red beds as well, indicated by the susceptibility-temperature curves of the sites 66 and 68 (Fig. 2.8c).

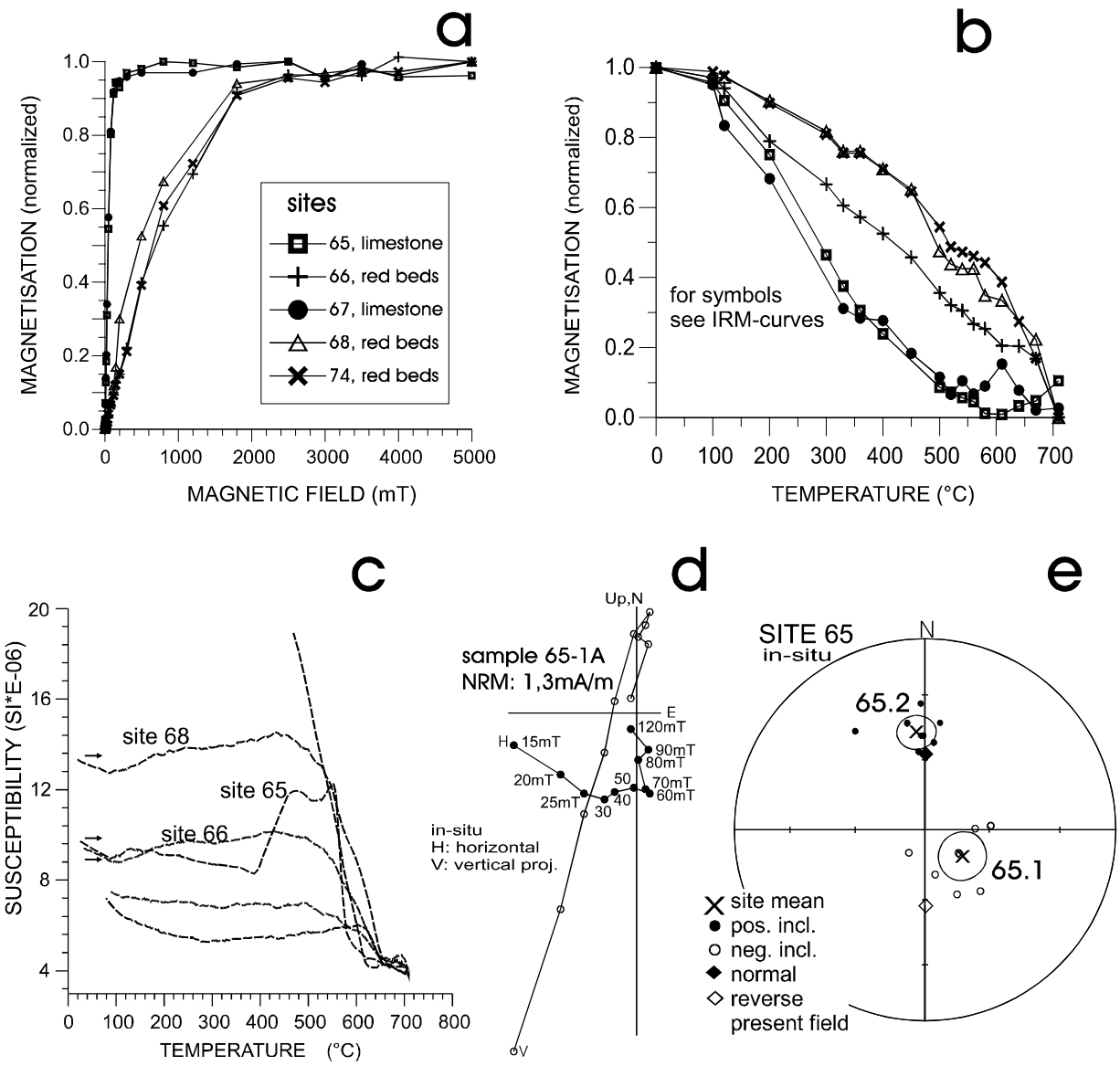

Fig. 2.9: Examples of the rock- and palaeomagnetic investigations for the Cretaceous limestones of the northern Pamirs. (a) IRM-acquisition, (b) thermal demagnetisation of a SIRM, (c) susceptibility-temperature curves; arrows indicate start of heating curves, (d) AF-demagnetisation of a specimen of site 65 releasing two components, (e) two site means of low- and high-coercive components for site 65, carried by magnetite.

The susceptibility-temperature curve of site 65 shows magnetite with two pronounced Hopkinson peaks, characteristic for single-domain/pseudosingle-domain particles. Cooling curves are much higher and therefore have been cut. The red reds have been demagnetised thermally and the limestones in the alternating field. Site 65 (Fig. 2.9d) provides a low-coercive and a high-coercive component (Fig. 2.9e), both having a significant site mean. The high-coercive component is close to the present field direction.

Tertiary Sediments (Sites 62 - 64, 71, 72, 78, 81, 82)

The results of these sites (not shown) are very similar to the previously discussed Cretaceous red beds. The measurements show mainly haematite and small contents of magnetite. Five of eight sites give significant site means (k > 10). The other sites (sites 63, 72 and 81) exhibit very low intensities of the NRM and give randomly scattering remanence components.

2.4.5 Granites and Volcanic Rocks (Sites 7, 10, 38, 39, 56 - 61; 23, 28 and 36)

Most of the IRM is acquired in fields up to 200 mT, typical for magnetite (Fig. 2.10a). Thermal demagnetisation supports this (Fig. 2.10b), but also points to a high fraction of haematite for site 36, not to be seen in the IRM-curve.

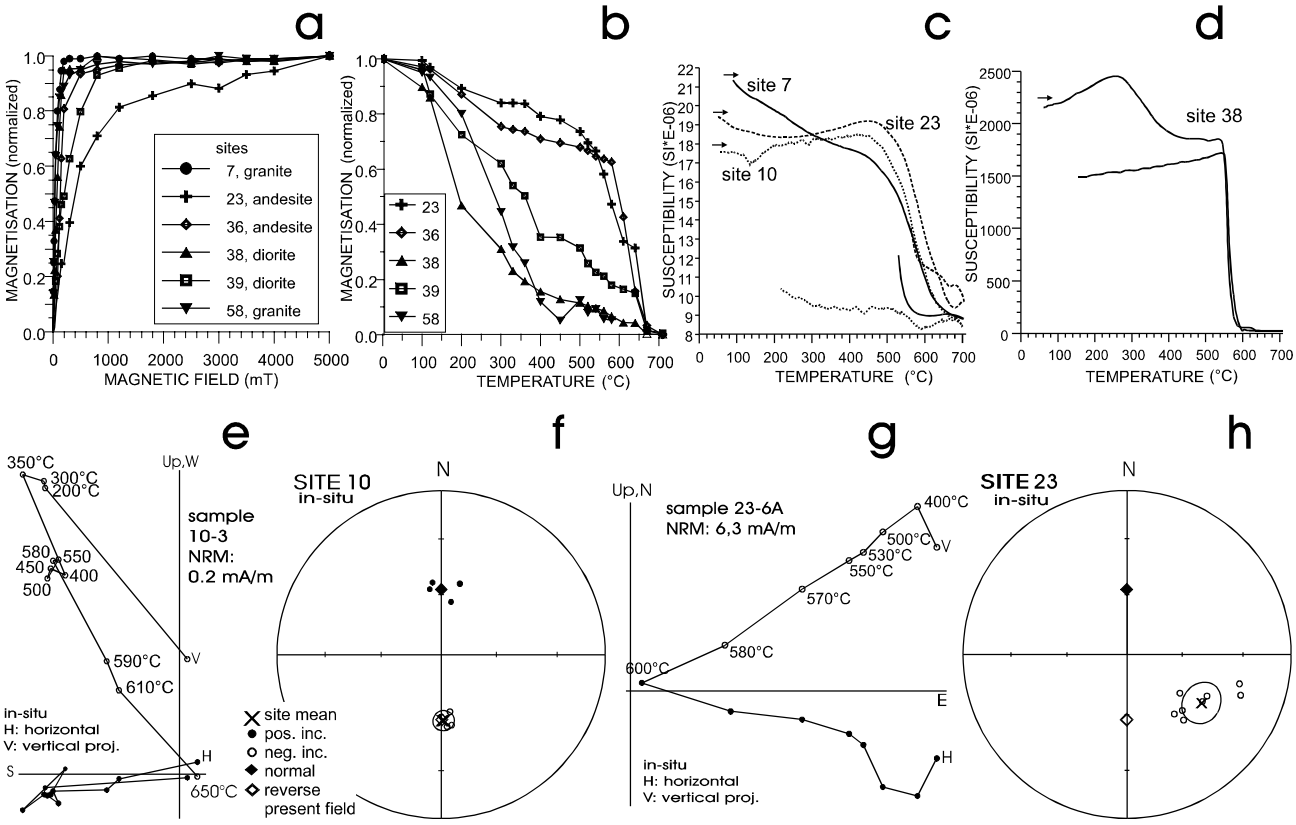

Fig. 2.10: Examples of the rock- and palaeomagnetic investigations for the granites and volcanic rocks from the southern and central Pamirs. (a) IRM-acquisition, (b) thermal demagnetisation of a SIRM, (c) and (d) susceptibility-temperature curves; arrows indicate heating curves, (e) AF-demagnetisation of a specimen of site 10 showing two components, (f) components reverse to each other isolated for site 10 (granite), (g) demagnetisation of a specimen of site 23 (volcanic rock), (h) site mean for site 23.

The susceptibility-temperature curves (Fig. 2.10c) show magnetite for sites 7 and 10, for site 23 predominantly haematite. The granite of site 38 (Fig. 2.10d) exposes a very high susceptibility and a sharply defined Curie temperature of 580°C, reproduced during cooling. Demagnetisation was done thermally or in the alternating field. The Triassic granites of the central Pamirs (sites 56 - 61) have very low intensities and do not give stable remanence components.

Site 10 (granite, southern Pamirs, Fig. 2.10e, f) gives two remanence components, one from 0 - 350°C, probably carried by magnetite, the other from 350 - 650°C, carried by magnetite and haematite. Both components are antiparallel to each other and therefore represent the same direction. The volcanic rock of site 23 also gives a stable remanence component, carried by magnetite and haematite (Fig. 2.10g, h).

2.5. Anisotropy of the Magnetic Susceptibility

The anisotropy of the magnetic susceptibility (AMS) has been measured for a number of sites (mostly sandstones and red beds) in the southern Pamirs and in the Rushan-Pshart zone, where deformation and metamorphism toward the metamorphic dome is obvious. Fig. 2.11 depicts the site mean results of the P- and E-factors.

With P-factors less than 1,05 most of the sites show no significant AMS. For sites 25, 27 and 28, a low anisotropy with P-factors >1,05 is observed. Only the sandstones of sites 34 and 35 close to the metamorphic dome give a significant oblate anisotropy with p-factors up to 1,18. However, a comparison of the directions of the anisotropy axes and the site means of these two sites (not shown) do not point to a change of the remanences by the AMS.

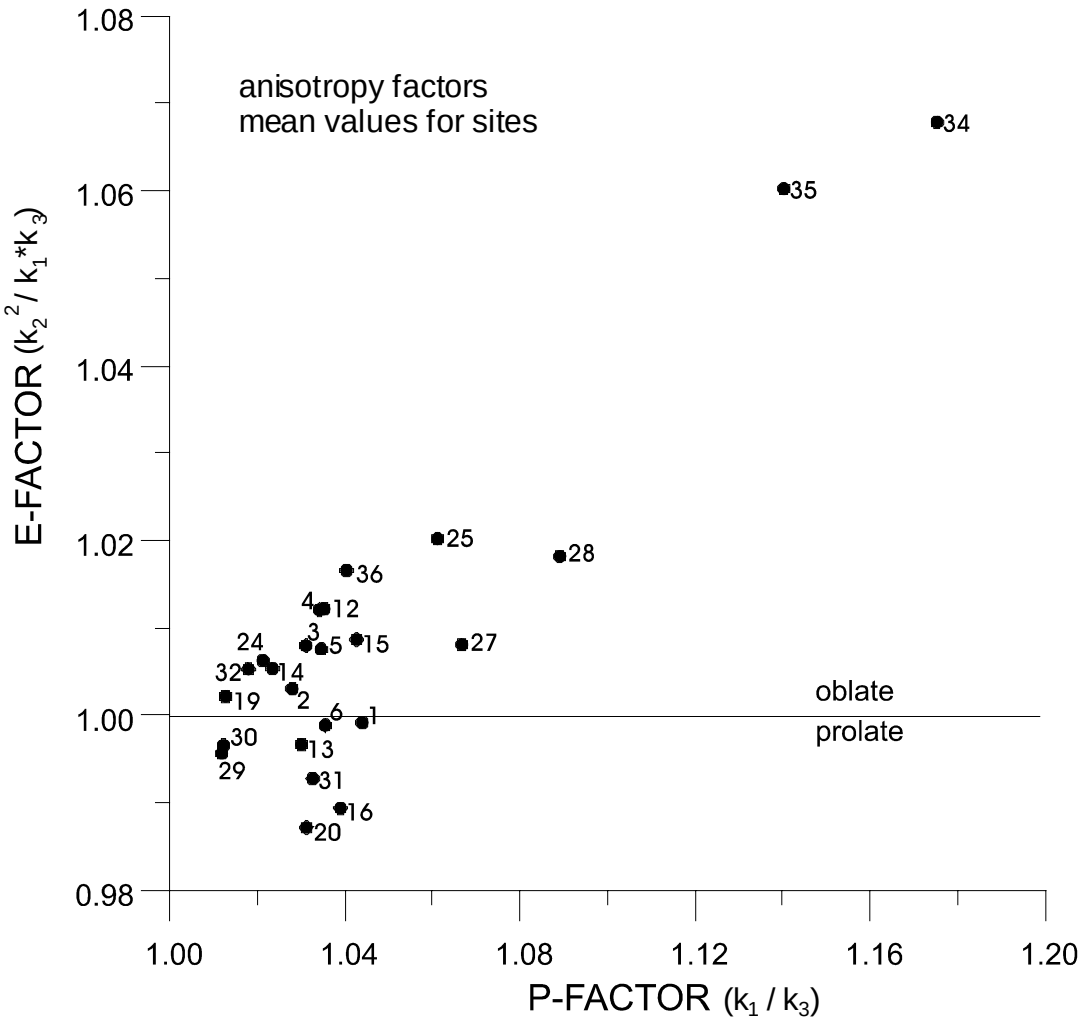

Fig. 2.11: Anisotropy of the magnetic susceptibility for 24 sites from the southern Pamirs, close to the metamorphic dome. Shape of the anisotropy ellipsoid (E-factor) plotted against grade of anisotropy (P-factor). k1, k2, k3: long, intermediate and short axis of anisotropy tensor. Only two sites show a significant oblate anisotropy.

2.6 Fold Tests

Fold tests have been applied according to McElhinny (1964) and McFadden (1990). In most cases, the McElhinny test gives a clear, significant result. For this reason, only this one will be presented in detail. The McFadden test is given additionally where the McElhinny test yields an indifferent or doubtful result.

Moreover, the data sets have been unfolded stepwise from -50% to +150% unfolding with calculation of the precision parameter *k*. This determines the grade of unfolding, where the tightest distribution within a data set is achieved (*k* reaches its maximum). The fold tests have been calculated for the groups of sites as indicated in Table 2.2, using single specimen remanence components and site means. If the fold test using site means already achieves a significant result above the 95% statistical significance, it will be the one to be shown. If not, the test with the remanence components from single specimens is presented. Testing involves at least 4 site means or 20 single specimen remanence components from 3 sites. Calculations account for reverse directions to obtain the maximum precision parameter possible.

The Tertiary sediments of the Rushan-Pshart zone obviously underwent metamorphism and deformation, related to the nearby metamorphic dome to the north. For this reason, primary palaeoremanences in these rocks unlikely have persisted. In the Jurassic and Cretaceous limestones from all parts of the Pamirs, and the Tertiary red beds from the central and northern Pamirs, a macroscopic evidence for metamorphism could not be observed in the field. Thus, primary remanences are more likely to occur there.

2.6.1 Permian Sandstones of the Southern Pamirs (4 Sites)

From site 5, the site mean of the low-coercive components has been used because of its presence in all samples. The fold test with the site means gives a negative result with a significance of 99% (Fig. 2.12a). The precision parameter *k* reaches its maximum for 0% unfolding. The result of the fold test might depend significantly on site 9. However, the fold test with the remanence components of sites 1, 5.1 and 6 (not shown) still is negative with a significance above 95%. Therefore, the remanences are clearly secondary.

2.6.2 Jurassic Limestones of the Southern Pamirs (13 Sites)

The remanence components of site 2 (not shown separately), whose samples are from the opposite limbs of a small fold, already provide a negative fold test at 95% significance. For the further test with site means, site 2 has been subdivided into sites 2a and 2b (see Fig. 2.12b). The fold test of the site means of the Jurassic limestones is clearly negative at the 99% significance level (Fig. 2.12b). As above, the result of the fold test might depend strongly by sites 122 and 144. However, excluding them does not lower the significance below 99% (not shown). The precision parameter *k* achieves its maximum at 0% unfolding. The in-situ site means show up close to the present field direction. Therefore, the remanences are likely to be secondary.

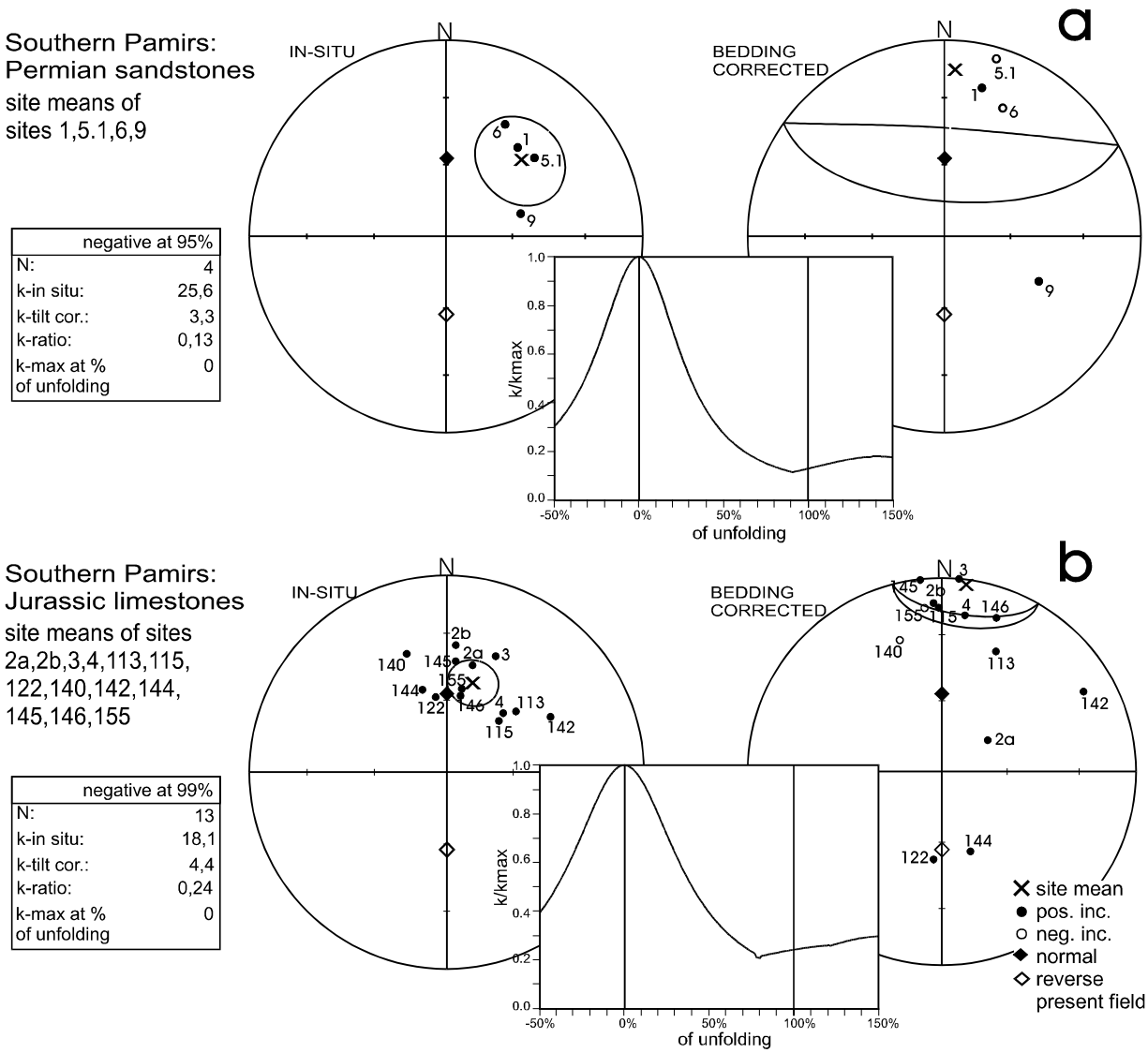

Fig. 2.12: Fold tests according to McElhinny (1964) and stepwise unfolding with calculation of k/k_{max} (small graph) for the Permian sandstones (a), and the Jurassic limestones of the southern Pamirs (b). Groups of sites according to Table 2.2. N: number of site means, n: number of single specimen remanence components, *k*-in situ/*k*-tilt cor.: precision parameter *k* in the in-situ position and bedding corrected position, *k*-ratio: ratio of $k_{tilt\ corrected}$ to $k_{in\text{-}situ}$, k_{max}: maximum of the precision parameter *k* during unfolding.

2.6.3 Tertiary Red Beds and Sandstones of the Southern Pamirs

The geographic distance requires a subdivision of these sites into an eastern and a western group. The western group is at present a unidirectionally folded sequence. The eastern group is on the average more distant from the dome and appears to have undergone less deformation. In both groups the remanences are carried predominantly by magnetite.

Western Group (12 Sites)

Testing the remanence components results in a negative fold test with 95% significance (Fig. 2.13a). The site means give a *k*-ratio of 0,61, not reaching a 95% significance. The *k*-value is largest at 18% unfolding. Hence, an overall secondary character of the sites of this group seems probable. This is also in compliance with the obvious deformation and metamorphism of this rocks, which rapidly increase northward towards the metamorphic dome.

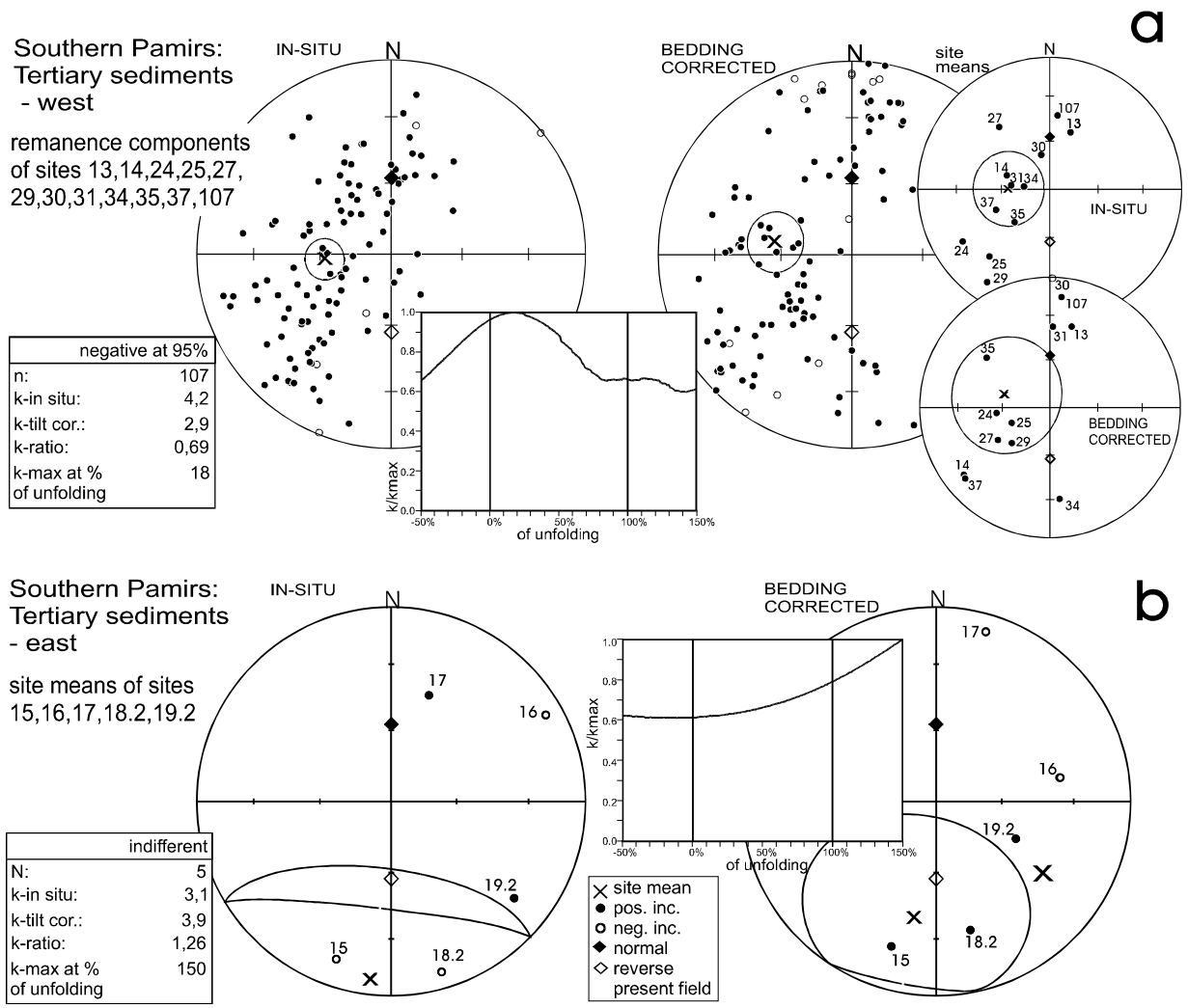

Fig. 2.13: Fold tests according to McElhinny (1964) and stepwise unfolding with calculation of k/k_{max} (small graph) for the Tertiary sediments of the southern Pamirs (a) western group, site means are depicted additionally, (b) eastern group. For symbol conventions see Fig. 2.12.

Eastern Group (5 Sites)

The site means attain a slightly higher *k*-value in bedding coordinates (Fig. 2.13b), but with a *k*-ratio of 1,26 remain well below the 95%-limit for a positive significance (*k*-ratio of 3,44). *k* has not a maximum within the range of unfolding, but continuously rises from 0% to 150% unfolding (Fig. 2.13b). This suggests an unvalid fold test. The single specimen remanence components (not shown) provide a *k*-ratio of 1,22, still well below the 95% limit of a positive fold test (*k*-ratio at 1,43). The McFadden fold test with the site means also does not give a significant result. Hence, neither a primary nor a secondary character can be attributed to these sites. From the visible metamorphism and deformation in the field, a primary character does not seem plausible. Except for site mean 19.2, the inclination in bedding coordinates would also be much below the expected value for a primary remanence in the Tertiary. Therefore, the remanences most likely have a secondary origin.

2.6.4 Jurassic Limestones of the Central Pamirs

For each site low- and high-coercive components - both carried by magnetite and giving significant site means - have been isolated. Testing the low-coercive components yields a negative significance at 99%

when using the remanence components (Fig. 2.14a). The *k*-ratio is highest at 12% unfolding. The site means give an indifferent result (not shown).

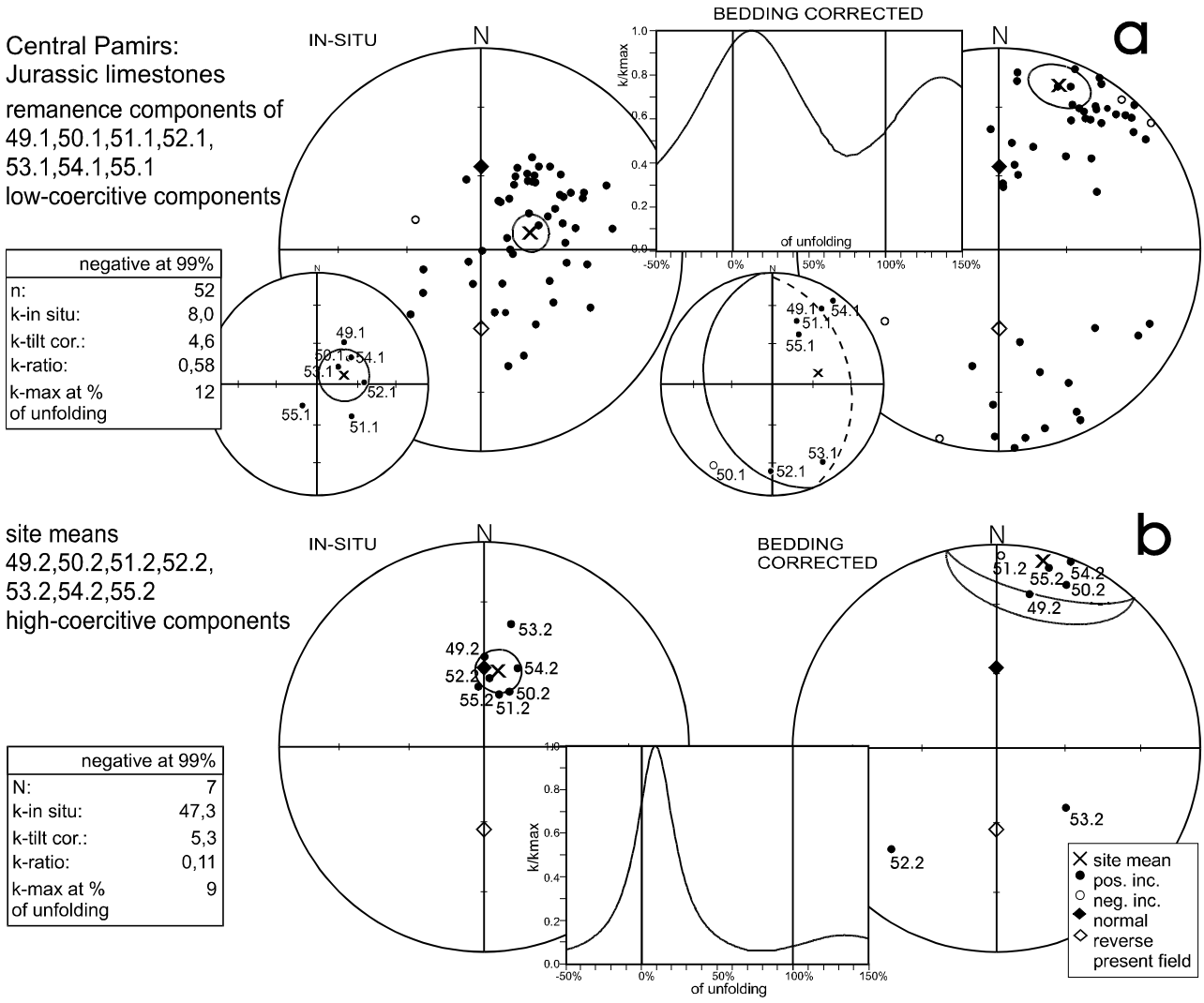

Fig. 2.14: Fold tests according to McElhinny (1964) and stepwise unfolding with calculation of k/k_{max} (small graph) for the low- (a) and high- (b) coercive components of the Jurassic limestones of the central Pamirs. Site means are shown separately. For symbol conventions see Fig. 2.12.

The high-coercive components also yield a negative fold test at 99% significance, already when using the site means (Fig. 2.14b). The *k*-ratio has a sharp maximum at 9% unfolding. The in-situ site means of the high-coercive components are closer to the present field direction than the in-situ site means of the low-coercive components. When bedding correction is applied, all the site means except for 51.1 and 55.1 move away from the present field direction. Hence, both the high- and low-coercive components are most probably secondary.

2.6.5 Cretaceous Limestones of the Central Pamirs (3 Sites)

A fold test is only possible with the single specimen remanence components due to the lack of enough site means. Site 43 has reverse polarity components, and sites 42 and 44 have both normal and reverse polarity remanence components.

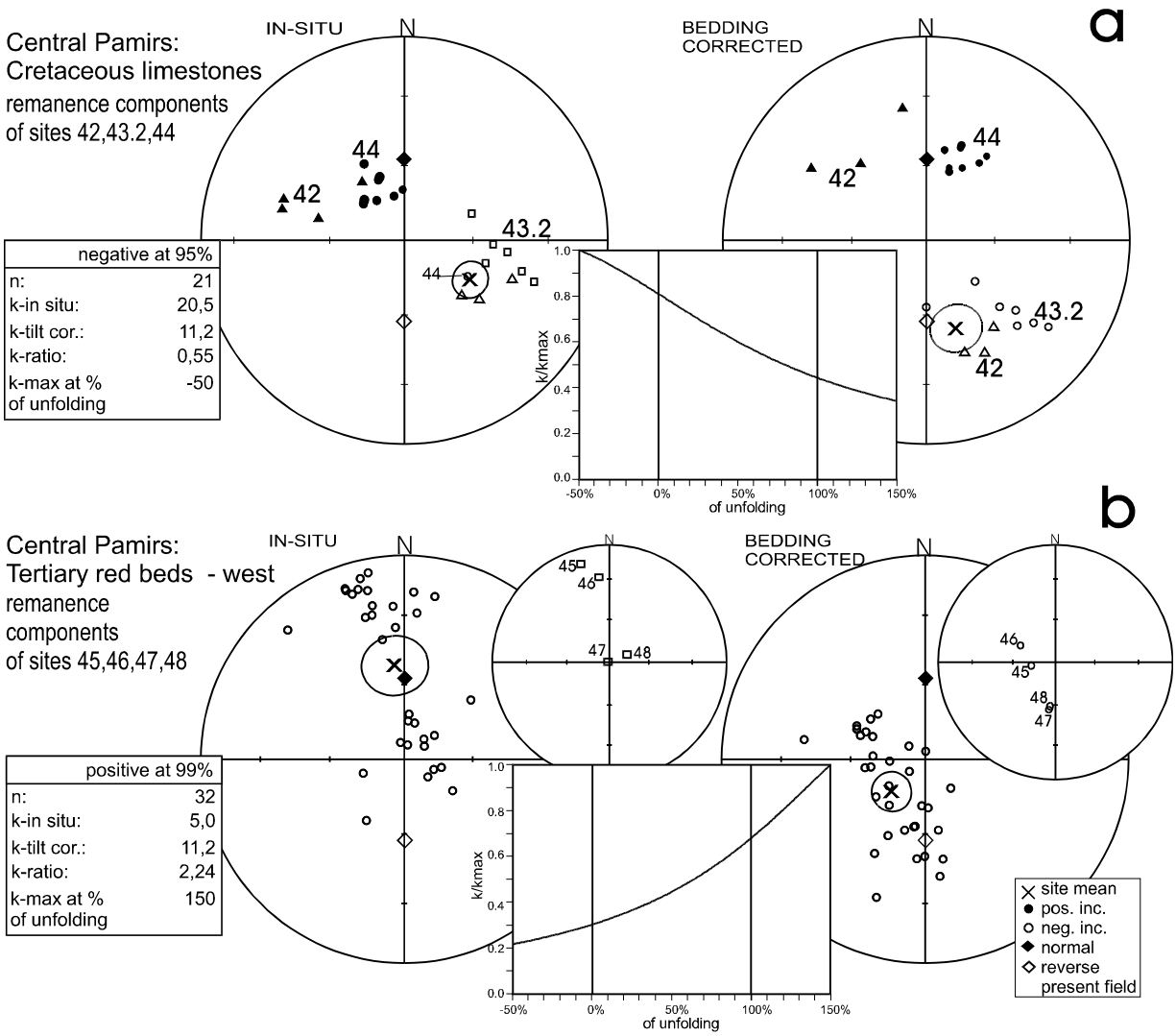

Fig. 2.15: Fold tests according to McElhinny (1964) and stepwise unfolding with calculation of k/k_{max} (small graph) for the Cretaceous limestones (a) and the Tertiary red beds (b) of the central Pamirs. Site means of the Tertiary red beds are shown additionally. For symbol conventions see Fig. 2.12.

The remanences are carried by magnetite and stable in AF-demagnetisation up to 140 mT. The mean inclinations of the sites 42 and 43.2 in bedding coordinates (I_{bc} = 40,5° and I_{bc} = 44,2°) are within the expected range of the palaeofield for this location when Cenozoic shortening of Eurasia (300 - 700 km) is accounted for (see Fig. 2.3). With I_{bc} = 55,1° site 44 is above this expected value. Thus, a primary character of the remanences is possible for site means 42 and 43.2. Nevertheless, the fold test (Fig. 2.15a) is negative at a significance of 95%. However, the *k*-value does not reach a maximum within the range of unfolding, but increases continuously from -50% to 150% unfolding. For this reason, the fold test possibly is unvalid. The McFadden test yields the same negative result with a significance of 95%. Summarising, site 44 probably is secondary, whereas the site means 42 and 43.2 could be primary, although this cannot be confirmed by the fold tests.

2.6.6 Tertiary Red Beds of the Central Pamirs (6 Sites)

The eastern group (sites 40 and 41, fold test not shown) has in-situ remanence components which are close to the present field direction. The fold test is indifferent. Bedding correction results in very low and therefore

unrealistic inclinations (site 40: I_{bc} = -2,5°; site 41: I_{bc} = 2,7°). Hence, a primary character of the remanences can be excluded.

The remanence components of the sites 45, 46, 47 and 48 of the western group provide a primary character with 99% significance (Fig. 2.15b). However, the *k*-value does not reach a maximum at around 100% unfolding, but continuously rises from -50% to 150% unfolding, calling the validity of the test into question. The McFadden test provides an indifferent result. The bedding corrected site means 47 and 48 are close to the expected reverse field direction, whereas the site means 45 and 46 have a much higher declination. This could be due to a relative block rotation in between the sites. Consequently, the McElhinny test involving these four sites is not valid. However, a primary character does not seem unreasonable. Carriers of the palaeoremanences are haematite and magnetite, and the remanence components are stable up to 700°C. Moreover, the rocks do not exhibit macroscopic metamorphism and the inclinations are - except for site 45 with I_{bc} = -73,2° - within the expected range of the Tertiary palaeofield.

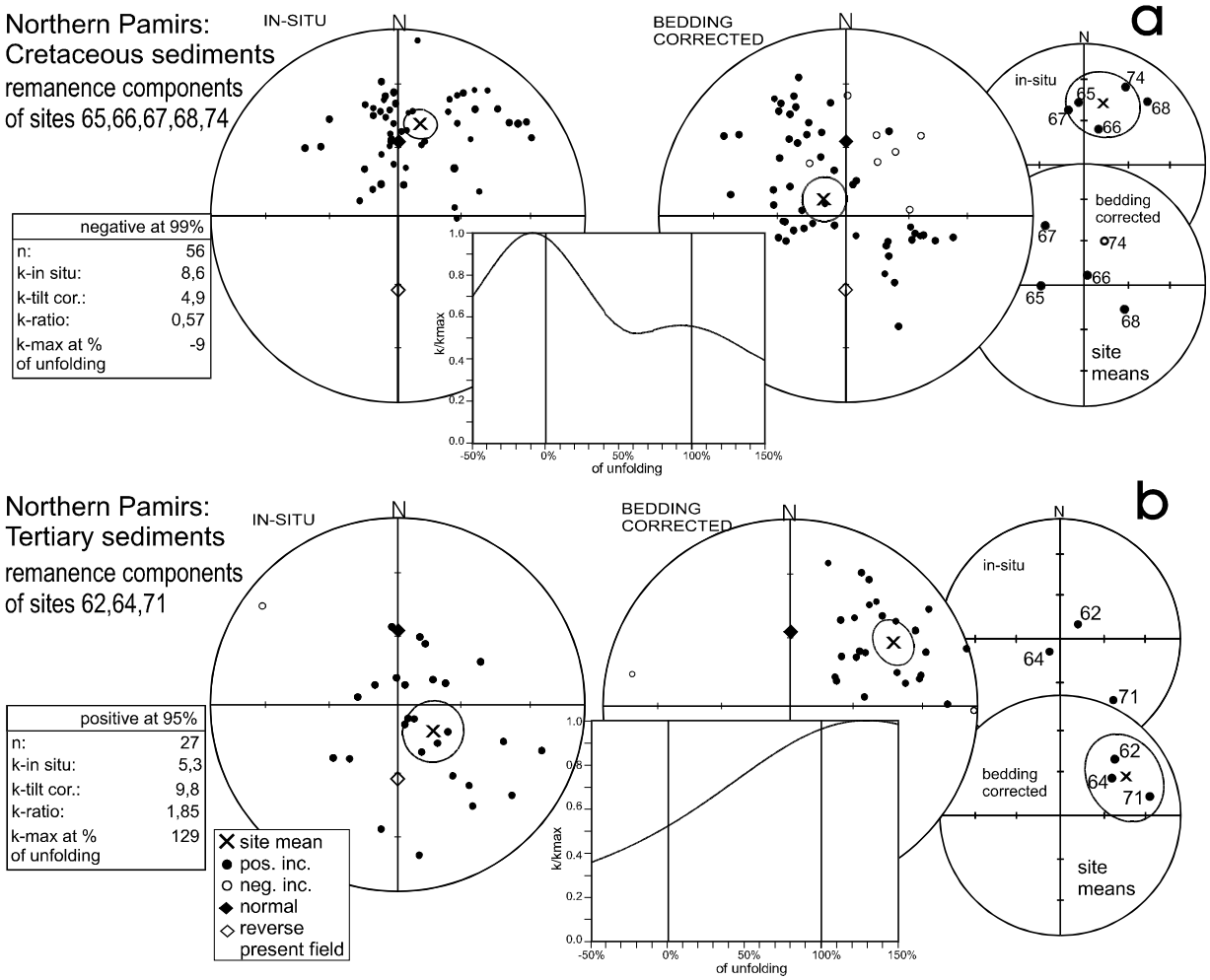

Fig. 2.16: Fold tests according to McElhinny (1964) and stepwise unfolding with calculation of k/k_{max} (small graph) for the Cretaceous limestones (a) and the Tertiary red beds (b) of the northern Pamirs. Site means are shown additionally. For symbol conventions see Fig. 2.12.

2.6.7 Cretaceous Sediments of the Northern Pamirs (5 Sites)

The rocks of this group do not expose macroscopic signs of metamorphism. Despite this, the fold test with the remanence components reveals a negative character at 99% significance (Fig. 2.16a). A test with the

site means (not shown) is indifferent. The *k*-ratio is highest at -9% unfolding. The in-situ site means are close to the present field direction. Hence, also these palaeoremanences most probably are secondary.

2.6.8 Tertiary Sediments of the Northern Pamirs

The fold test with the remanence components is positive at 95% significance. The *k*-ratio is highest at 129% unfolding. Hence, the palaeoremanences which are carried by magnetite and haematite seem to be primary. However, when compared to an expected palaeoinclination of about I_{acq} = 60°, the inclinations in bedding coordinates (site 62: I_{bc} = 34,6°, site 64: I_{bc} = 45,5°, site 71: I_{bc} = 25,2°) are much too low to be primary at all, especially those of sites 62 and 71. Moreover, the McFadden test produces an indifferent result. For this reason, a primary character must be doubted. Either a shallowing of the inclinations occurred, e.g. by sedimentary compaction, or the palaeoremanences are not primary.

Table 2.4 summarises the fold tests.

Table 2.4: Summary of the fold tests according to McElhinny (1964) and of stepwise unfolding. If the fold test with site means (N) already exceeds a significance above 95%, it is the one to be listed. In the other case the fold test with the remanence components (n) is shown. N: number of site means, n: number of single specimen remanence components, Dec.: declination, Inc.: inclination, α95: 95% confidence angle, k: precision parameter, k_{max} at % unfolding: maximum of the k-value over the range of unfolding from -50% to 150%.

Group	Sites	N	n	in-situ				bedding corrected				foldtest	k_{max} at % of unfolding	result
				Dec.	Inc.	α95	k	Dec.	Inc.	α95	k			
Southern Pamirs														
Permian sandstones	1,5.1,6,9	4		44,5	44,6	18,5	25,6	3,8	-15,8	59,9	3,3	neg. 99%	0	secondary
Jurassic limestones	2a,2b,3,4,113, 115,122,140,142 144,145,146,155	9		16,4	50,9	10,0	18,1	7,6	3,0	22,4	4,4	neg. 99%	0	secondary
Tertiary sediments w estern group	13,14,24,25, 27,29,30,31,34, 35,37,107		107	264,6	62,8	7,7	4,2	219,7	37,3	10,0	2,9	neg. 95%	18	secondary
Tertiary sediments eastern group	15,16,17, 18.2,19.2	5		186,5	-8,8	52,9	3,1	190,7	39,2	44,3	3,9	indiff.	not reached w ithin range of unfolding	indifferent
Central Pamirs														
Jurassic limestones	49-55													
low coercitive components			52	71,6	68,7	7,5	8,0	20,4	14,1	10,3	4,6	neg. 95%	12	secondary
high coercitive components		7		10,8	59,8	8,9	47,3	14,2	-5,6	28,8	5,3	neg. 99%	9	secondary
Cretaceous limestones	42,43,44		21	120,8	-59,0	7,2	20,5	161,2	-52,2	9,9	11,2	neg. 95%	not reached w ithin range of unfolding	secondary?
Tertiary red beds w estern group	45,46,47,48		32	354,4	-51,7	12,6	5,0	225,9	-71,4	7,9	11,2	pos. 99%	not reached w ithin range of unfolding	primary?
Northern Pamirs														
Cretaceous limestones & red beds, eastern group	65,66,67,68,74		56	13,7	48,2	6,9	8,6	307,2	78,2	9,6	4,9	neg. 99%	-9	secondary
Tertiary sediments	62,64,71		27	127,0	70,5	13,3	5,3	58,3	35,3	9,3	9,8	pos. 95%	129	primary?

2.7 Summary and Discussion

In 71 from 90 analysed sites, stable remanence components with a significant site mean ($k \geq 10$) could be isolated. In 12 of them, two remanence components - low- and high-coercive - occur both having significant site means. The remanences are carried predominantly by magnetite. Occasionally haematite is

encountered, mainly in sandstones and red beds, but usually together with magnetite. Most of the fold tests reveal a secondary character for the remanences. Only two fold tests (Tertiary sediments in the central and northern Pamirs) indicate a primary character, but either the tests are probably not valid (no maximum of *k* within the range of unfolding) or the obtained inclinations in bedding coordinates are too low compared to the expected value for the location to be primary at all (palaeoinclination not below 55° in the Tertiary). Hence, there is no explicit evidence for primary remanences from the fold tests. The origin of the secondary remanences is most probably related to an Early Miocene metamorphic/deformation event, which is accompanied by the uplift of the metamorphic dome in the central Pamirs and adjacent metamorphism and deformation. According to geochronological ages, this event finished about 20 Ma ago throughout the Pamirs (unpublished data of the same project from L. Ratschbacher, Würzburg, and M. Schwab, Tübingen). Cenozoic overprinting of palaeoremanences has been found throughout the India-Asia collision zone, e.g. in the Tadjik basin (Pozzi & Feinberg 1992), in Chitral, eastern Hindukush (Klootwijk et al. 1994) and in the Tibetan Sedimentary Series of the Himalaya (Appel et al. 1991, 1995). Often, secondary remanences are reported to be carried by pyrrhotite (e.g. Appel et al. 1991 and 1995), but there is no evidence for in the investigated sites in the Pamirs.

If displacement after remanence acquisition is supposed to be negligible, a tectonic interpretation of the secondary remanences can be attempted. For instance, the Permian sandstones and Jurassic limestones of the southern Pamirs (see Fig. 2.12) show a maximum of the *k*-value at 0% unfolding. When the declination values are interpreted in terms of block rotation, similar results will be obtained as in section 3. However, an interpretation of the inclinations of the site means will be rather misleading: For the in-situ remanence components, mean values of D/I = 44,5°/45,4° (Permian sandstones) and D/I = 18,3°/50,1° (Jurassic limestones) are obtained. Assuming a remanence age of about 20 Ma, the difference of these values to the expected value of about 59° for this location on Eurasia would indicate a N-S shortening of Eurasia in the past 20 Ma of about 1500 km and 1000 km, respectively. In comparison, 300 - 700 km of shortening for the whole Cenozoic are reported by Burtman & Molnar (1993). About 440 km of shortening since 20 Ma are obtained from the small-circle reconstruction in section 3, a figure which fits well into the geologic frame.

In the case of the Tertiary sediments of the southern Pamirs (see Fig. 2.13), the interpretation of both declinations and inclinations must fail, because the remanence directions have been changed significantly by tilting after their acquisition.

As will be shown in section 3, some most probably primary remanences indeed occur within the data sets, but are completely concealed by the secondary remanences. Hence, the current analysing procedures of palaeomagnetism (e.g. Piper 1987, Tarling 1971) fail to extract the tectonic information recorded by these secondary remanences.

3. Tectonic Interpretation

This section applies the small-circle reconstruction introduced in section 1 to the palaeomagnetic data from the Pamirs. The inclination of the reference palaeofield will be estimated from the palaeomagnetic data and compared to the expected value derived from the APWP, taking into account Cenozoic shortening of Eurasia. Reconstructions will be performed by considering:

(a) A number of single specimen remanence components within a unidirectionally folded sequence. Reconstructions use the Π-circle as tilting direction and give a mean block rotation for the whole sequence.

(b) Remanence components of single sites and their site means. Reconstructions use the tilting given by the bedding and determine a block rotation for each site individually. For the site mean angles of backtilting can be calculated.

3.1 The Palaeoinclination at the Time of Remanence Acquisition

The palaeoinclination at the time of remanence acquisition is a basic requisite for the reconstruction. Ar-Ar and fission track dating (data from the project, see section 2) reveal cooling ages of about 20 Ma in both metamorphic and igneous rocks throughout the southern, central and northern Pamirs, indicating a metamorphic event associated with deformation. The observed secondary remanences probably have originated at the end of this event around 20 Ma ago. From the APWP for stable Eurasia from Besse & Courtillot (1991; pole at 20 Ma: λ(°N) = 82,3° ϕ(°E) = 147,6° A95 = 3,3°), the corresponding palaeofield for the area of investigation is expected to be D/I = 10°±6°/59°±3° (see Fig. 2.3). The minimum amount of Cenozoic northward movement of the Pamirs due to crustal shortening is estimated to be 300 km (Burtman & Molnar, 1993). If this figure is taken into account, the palaeoinclination 20 Ma ago is expected to be about 56°±3°.

From the palaeomagnetic data, well based primary palaeoremanences are not available, but as outlined in section 1.8, an upper constraint on the palaeofield inclination (maximum I_{acq}) can be obtained from originally E-W or close to E-W folded sites. With this maximum I_{acq}, the maximum northern palaeolatitude for the investigation area 20 Ma ago is given and hence a minimum value for crustal shortening. Fig. 3.1 depicts the distribution and cumulative distribution of the maximum I_{acq} of the site means for all investigated sites of the Pamirs and for the sites of the southern Pamirs. Taking all sites, the cumulative number of sites increases significantly above a maximum I_{acq} of around 55° - 58°. When only the sites in the southern Pamirs are considered, the increase clearly starts at 55°.

The increase starts with the sites 113 and 9, both in the southern Pamirs, having a maximum I_{acq} of 55,0°±21,4° and 55,6°±16,7°. Using a palaeofield of D/I = 0°/55°, sites 113 and 9 turn out with a reconstructed tilting direction of 93° and 82°, which is close to E-W.

Six sites require an I_{acq} lower than 55°. This could indicate older, possibly primary remanences acquired earlier in the course of the northward drift. The lowest maximum I_{acq} has site 16 (Tertiary red beds in the southern Pamirs) with I_{acq} = 40°. A primary character of its remanence can be excluded because the inclination in bedding coordinates of I_{bc} = -35,2° (see Table 2.3 for values) is too low for a primary remanence of the Tertiary. The same is true for site 71 (I_{acq} = 41,4°, I_{bc} = -25,2°), site 3 (I_{acq} = 43,1°, I_{bc} = 0,1°) and site 5.1 (I_{acq} = 46,9°, I_{bc} = -6,3°). Three reasons may account for a too low maximum I_{acq}: Rotation around inclined axes, inclination shallowing or rockmagnetic effects. In contrast, a primary character is

possible for the sites 43.2 and 42 (Cretaceous limestones, I_{acq} = 49,7°, I_{bc} = -44,2° and I_{acq} = 51,1°, I_{bc} = 40,5°), since their bedding corrected inclinations are within the expected range for the area (see Fig. 2.3). The fold test involving sites 42, 43.2 and 44 did not indicate a primary character, but most probably the test is not valid (see section 2.6.5).

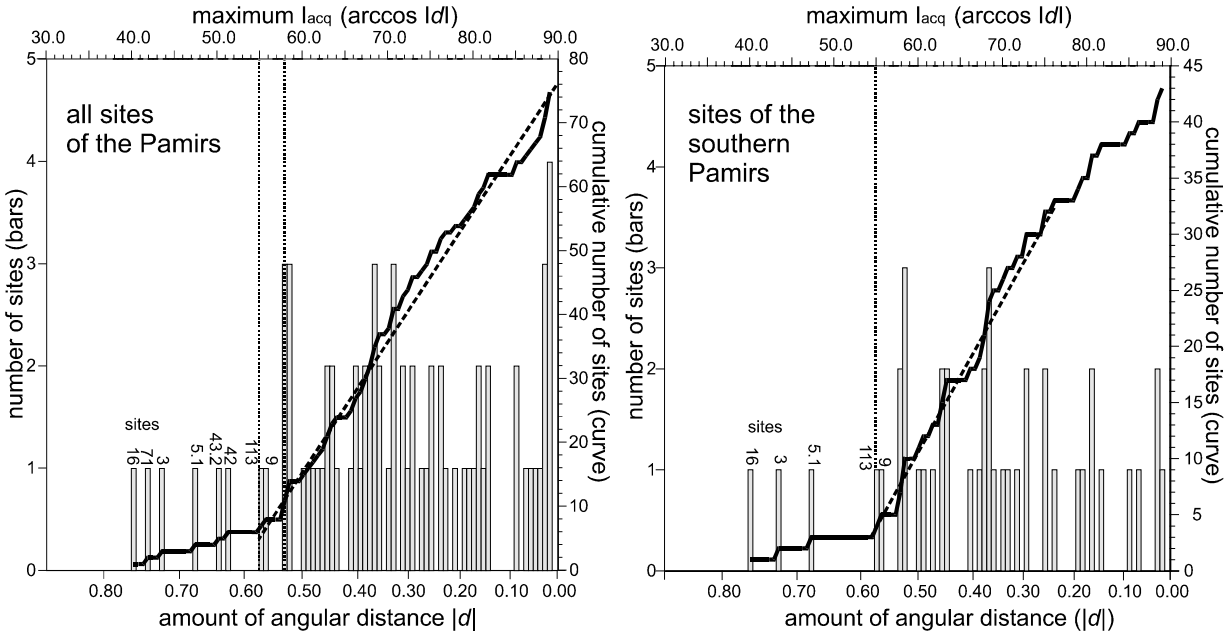

Fig. 3.1: Histogram and cumulative curve for the distribution of the maximum I_{acq} (arccos |*d*|) for all sites of the Pamirs and for the sites of the southern Pamirs. For values see Tables 3.2, 3.4, 3.5, 3.8 and 3.10. Scale of maximum I_{acq} is linear, scale of |*d*| not. Bars refer to the number of sites having a maximum I_{acq} within a class width of 0,5°. The cumulative curve shows a marked increase above 55°. The rise in both cases is nearly linear (dashed lines for comparison) indicating a rather uniform distribution of the reconstructed tilting directions at least between a trend of 0° (N-S) and 90° (E-W). Six sites require the remanence acquisition in a lower I_{acq} than 55°, either due to a possibly primary character of the remanences (Cretaceous sites 42 and 43.2) or due to other effects. According to this, the palaeoinclination at the time of remanence acquisition in the southern Pamirs probably was not above 55°. For discussion see text.

The rise of the cumulative curve for the total of the sites (Fig. 3.1 left) is nearly linear above 55°, indicating a rather uniform distribution of the reconstructed tilting directions, at least between a trend of 0° and 90°. The following reconstructions will show that the distribution ranges even between 270° and 90° (trend of tilt axes between 0° and 180°). This broad variation of the tilting directions is surprising as it is not expected in an overall N-S oriented convergence regime. A detailed discussion of this observation will follow behind.

Summarising, the distribution of the maximum palaeoinclinations of the site means indicates that the palaeoinclination in the southern Pamirs at the time of remanence acquisition - supposedly around 20 Ma ago - unlikely exceeded 55°. The mean inclination difference of 4° to the expected palaeofield inclination of about 59°±3° would imply a minimum northward displacement of the southern Pamirs by 440 km in the past 20 Ma. This amount fits well to the 300 - 700 km of Cenozoic northward displacement of the Pamirs given by Burtman & Molnar (1993).

For the following reconstructions, a palaeofield of D/I = 10°/55° will be taken as the reference for the sites of the southern and central Pamirs. For the northern Pamirs a palaeofield of D/I = 10°/57° will be used and for the Alai range a palaeofield of D/I = 10°/60° (details behind).

3.2 Southern Pamirs

In this part of the investigation area, most of the sites belong to the two approximately unidirectionally folded sequences delineated in Fig. 3.2 (rectangles). The sites in the eastern part cannot be attributed to a unidirectionally folded sequence. Sites 7 and 10 are granites. Sites 9 and 127 are outside the two

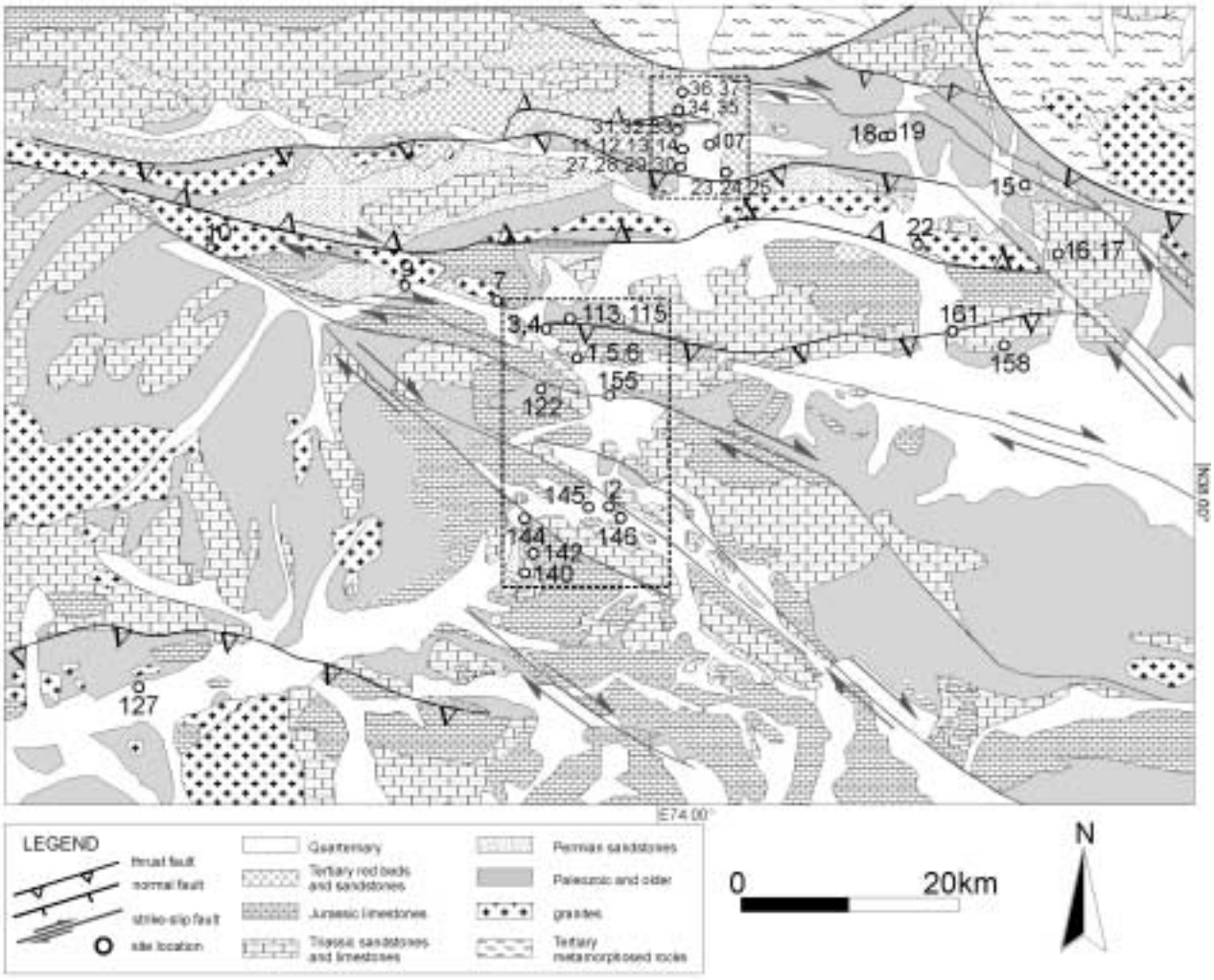

unidirectionally folded sequences.

Fig. 3.2: Geologic map of the southern Pamirs with site locations. Rectangles frame the two sampled unidirectionally folded sequences. The sites outside the rectangles cannot be attributed to a unidirectionally folded sequence. For map overview and references see Fig. 2.2.

3.2.1 Northern Folded Sequence (Sites 11-14, 23-25, 27-37, 107)

In the northern folded sequence 16 sites in Tertiary sediments and 3 volcanic rocks were sampled. The sequence exhibits increasing metamorphism and deformation towards the metamorphic dome to the north. The remanences are carried predominantly by magnetite. 15 sites yield site means with precision parameters of $k \geq 10$. Stepwise unfolding gives a maximum of the k-value at 18% unfolding (see section 2), clearly revealing an overall secondary remanence character. Four sites (11, 12, 32 and 33) do not yield significant site means ($k < 10$), but show small-circle distributions of the remanence components parallel to the Π-circle (see Fig. 3.3b). Site 14 (see Fig. 6.1 in the appendix) gives a significant site mean, but in fact shows a pronounced small-circle distribution.

3.2.1.1 Reconstruction of the Whole Folded Sequence

The pole of the Π-circle (mean tilt axis, Fig. 3.3a) has an azimuth of 112,0° and a plunge of 2,0°. For the calculations, the Π-circle will be assumed to be vertical. The poles of the south-dipping beds are less frequent and show a higher scatter around the Π-circle. Possible reasons for the scatter could be variations in folding, block rotations between the sites or a symmetric second phase of folding perpendicular or at an angle to the first.

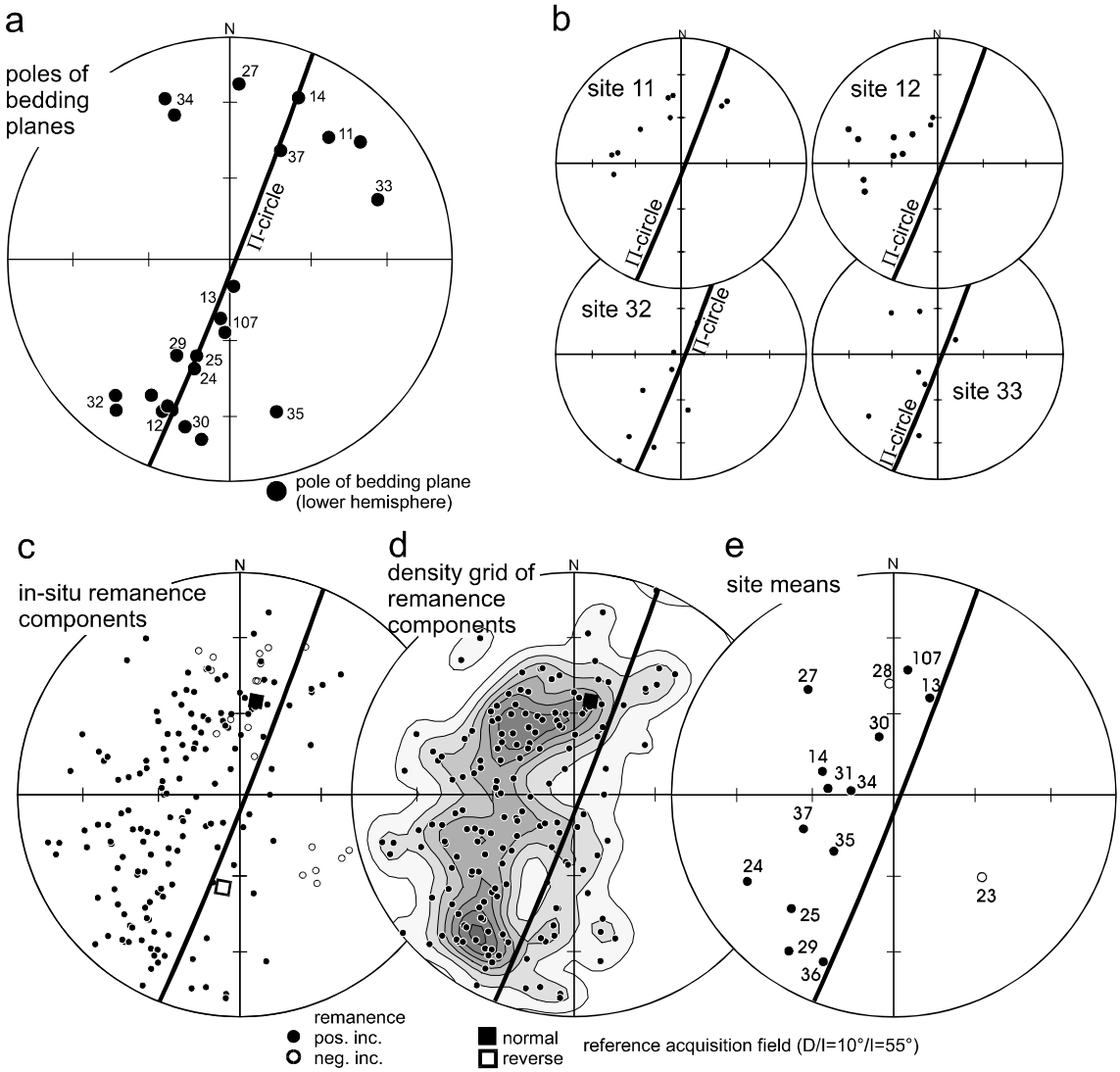

Fig. 3.3: Bedding data and remanences of the northern sequence including the sites 11 - 14, 23 - 25, 27 - 37 and 107. (a) Bedding poles and Π-circle. The mean tilt axis has a strike of 112,0° and a dip of 2,0°. It will be assumed to be vertical. (b) Incorporated sites with small-circle distributions giving site means with *k*-values below 10. (c) The total of 172 remanence components from all sites of the sequence with 149 positive and 23 negative inclinations. (d) Density grid of all remanence components with those of negative inclination inverted, assuming that they did not change the hemisphere through tilting. Distribution is clearly parallel to the Π-circle. (e) Site means.

The remanence components of sites 11, 12, 32 and 33 (Fig. 3.3b) which represent small-circle distributions parallel to the Π-circle, have been incorporated in the small-circle analysis.

Fig. 3.3c depicts all 172 remanence components isolated from the single specimens of the sequence. For the density grid in Fig. 3.3d, the components with negative inclination (mainly site 23 and 28) have been inverted, assuming that they did not change the hemisphere through tilting. The distribution, that can be

seen also in the site means (Fig. 3.3e), is convincingly parallel to the Π-circle. Therefore, the overall distribution is a consequence of folding.

The reconstruction (see section 1) assumes a vertical Π-circle (horizontal mean tilt axis) for the calculation of a mean small circle for the distribution of the remanence components, characterised by the *d*-angle. The remanence components of sites 23 and 28 have been inverted for this calculation (assuming they have reverse polarity and did not change the hemisphere through tilting). The mean small circle is rotated back to intersect the reference field of D/I = 10°/55°. The comparison of the reconstructed mean tilt axis with the present one yields the angle of block rotation. Table 3.1 lists the parameters and the first direct reconstruction which is considered to be the most probable.

Table 3.1: Calculation of a mean small circle for the remanence components of the northern folded sequence. Tectonic reconstruction gives a 20° counterclockwise block rotation for the whole sequence as the shortest and therefore most probable solution. The other three direct reconstructions (not listed, see text) require much higher displacement and therefore are unlikely. For definitions, conventions and equations see section 1.

remanence components of sites 11-14, 23-25,27-37,107			
reference field	D/I = 10°/55°		
number of components		172	
mean *d*		-0,29	
mean *d*-angle (°)		107,6	
standard deviation (°)		17,3	
95% confidence interval (°)		2,6	
azimuth of pole of mean tilt axis (°)			
present	112,0	confidence interval (+)	(-)
reconstructed	131,7	5,2	5,0
block rotation (°)	19,7	5,2	5,0

With a reference field of D/I = 10°/55°, a counterclockwise block rotation of about 20° as the shortest reconstruction is obtained. A palaeoinclination of 50° changes the block rotation from 20° to 16°, a palaeoinclination of 60° gives a block rotation of 25°.

The second solution for the normal reference field is a counterclockwise block rotation by 136°. Relating the small circle to the reverse polarity, block rotations of clockwise -44° and -160° will result. These solutions imply on the average much higher amounts of tilting and block rotation. Remanences, now close to the normal polarity reference field, must be brought to there from a reverse polarity. This is very unlikely. The most probable solution therefore is a mean counterclockwise block rotation by about 20°. In this case, the reconstructed mean tilting direction had a trend of 42° and rotated counterclockwise to its present position of 22°. This amount of block rotation is an average for the whole sequence. Differences in block rotation between the sites are not resolved.

3.2.1.2 Reconstruction of the Single Sites of the Northern Sequence

The reconstruction will now be performed for each site separately. The four direct reconstructions will be determined. In addition, the angles of backtilting to reach the inclination of the reference field are calculated for the sites with a Fisher mean. In the appendix the four direct reconstructions are documented graphically and in tables for each site (Fig. 6.1). Table 3.2 summarises the relevant parameters and the reconstruction for each site chosen as the most probable one.

Table 3.2: Reconstruction of the sites of the southern sequence. Only the most probable reconstruction for each site is listed. For other possible reconstructions and graphical representation see Fig. 6.1 in the appendix. dip az./dip: azimuth and angle of dip, bedding: upright or overturned (overt.) bedding from field evidence, *d*: angular distance, I_{acq} max.: maximum palaeoinclination, % of untilting: percent of untilting related to the present dip assumed to be upright. Remark: upright or overturned bedding as the consequence of the comparison of the present bedding with the sense of untilting (assuming that tilting did not reverse), indiff.: indifferent; used when angle of untilting is below ±10°, >dip: angle of untilting exceeds dip for either upright or overturned position by more than 10°. α95/cos I_{acq}: confidence interval of the declination for sites with Fisher mean. For the small-circle distributions the confidence interval α95 is given (for calculation see section 1). For conventions, definitions and equations see Fig. 1.1 and section 1. For discussion see text.

sites with Fisher mean							back-	block-	reconstruction		% of		α95/
site	dip az.	dip	bedding	*d*	*d*-angle	I_{acq} max.	tilting	rotation	point		untilting	remark	$cosI_{acq}$
	(°)	(°)			(°)	(°)	(°)	(°)	D (°)	I (°)			(°)
13	356	18	upright	0,26	104,9	75,1	4	-13	23	55	-22	indiff.	21,3
23	359	47	-	-0,47	61,8	61,8	9	66	124	-55	-20	indiff.	11,5
24	29	41	-	-0,46	62,6	62,6	-85	34	336	55	207	>dip	25,6
25	19	38	-	-0,33	70,6	70,6	-86	26	344	55	226	>dip	16,2
27	183	68	-	-0,52	58,5	58,5	27	73	297	55	39	upright	24,9
28	180	70	-	0,03	91,5	88,5	103	13	357	55	-109	overt.	17,8
29	18	43	-	-0,26	74,8	74,8	-105	19	351	55	244	>dip	28,2
30	9	71	-	-0,15	81,5	81,5	-14	16	354	55	19	upright	21,1
31	30	60	-	-0,38	68,0	68,0	-39	21	349	55	64	upright	30,5
34	158	67	overt.	-0,24	76,1	76,1	-25	57	313	55	-37	overt.	18,8
35	343	61	upright	-0,45	63,0	63,0	-38	79	291	55	62	upright	17,6
36	180	54	-	-0,37	68,5	68,5	-97	50	320	55	-180	overt.	13,1
37	205	45	-	-0,41	65,9	65,9	-54	30	340	55	-119	overt.	16,7
107	4	27	-	0,03	91,7	88,3	12	3	7	55	-44	overt.	20,9
sites with small circle distribution													
													α95
11	223	64	-	-0,50	60,2	60,2		27				overt.	4,4
12	21	62	upright	-0,49	60,7	60,7		48				upright	10,5
14	203	68	overt.	-0,43	64,5	64,5		36				overt.	6,2
32	39	70	upright	0,03	92,0	88,0		-32				upright	14,3
33	248	61	-	0,03	91,5	88,5		-61				overt.	25,7

Except for sites 24, 25, 29 and 36 (see Fig. 6.1 in the appendix), the shortest reconstruction is the one which fits best to the 20° counterclockwise block rotation determined for the whole sequence. Through comparison of the sense of backtilting with the present bedding, upright and overturned bedding have been determined for the layers (assuming that tilting occurred only in one sense and did not reverse). Upright/overturned bedding is confirmed for all sites where it could be identified in the field from appropriate criteria.

Fig. 3.4 shows the reconstruction of the bedding for the time of remanence acquisition and for the time after folding. The volcanic rocks are incorporated with the bedding of the adjacent sediments. Bedding at the time of remanence acquisition already defined a unidirectionally folded sequence. The bedding poles of the sites 24, 25, 29 and 36 move through the horizontal position to the opposite quadrant, but are not overturned.

Except for the sites 27, 36 and 107, the tilt since remanence acquisition is to the north-east (Fig. 3.4), steepening up the layers.

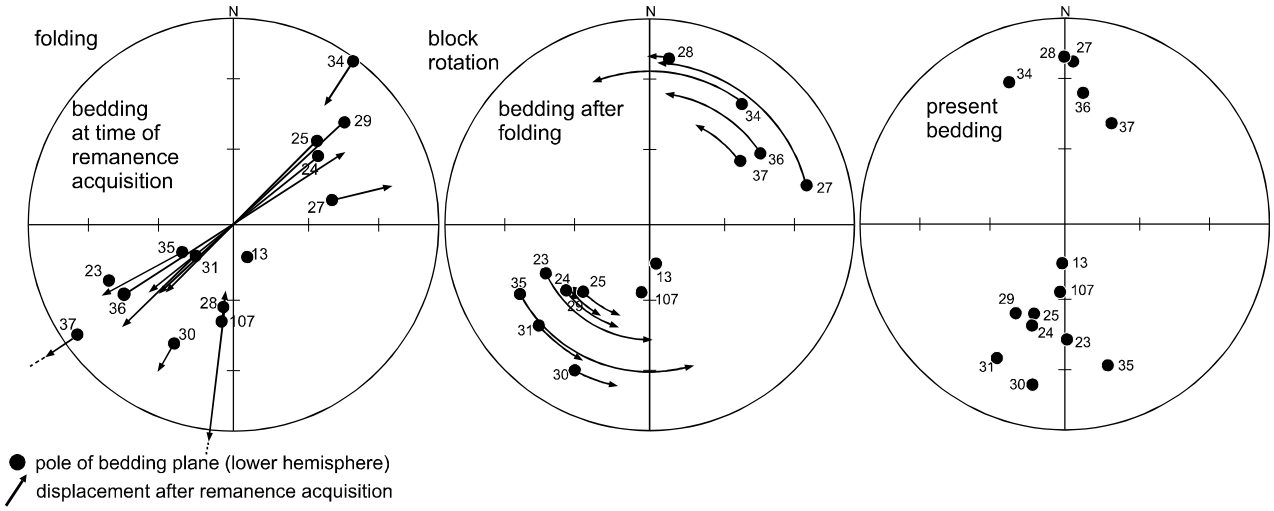

Fig. 3.4: Reconstruction of the bedding for the northern sequence. Left: Bedding at time of remanence acquisition, arrows indicate subsequent tilting. Middle: After folding and before block rotation, arrows indicate subsequent block rotation. Right: Present bedding. For discussion see text.

Variations in block rotation turn out to be rather large, e.g. the -13° clockwise block rotation of site 13 compared to the 79° counterclockwise block rotation of site 35. In the sites 24, 25 and 29 displacements are quite high, thus, the selection of a most probable reconstruction is difficult. To fit the sites 24, 25 and 29 best to the overall counterclockwise block rotation of 20°, the required angle of backtilting will exceed the corresponding dip of an upright bedding. Either the now north-dipping layers have been tilted by more than 180°, or tilting has been first to the south-west, where the remanence was acquired, and then back north-east to the present position. The formation of a vergent fold with one overturned limb indeed implies such a reversal of the tilting sense for the upright limb.

A clear constraint on this reconstruction for the sites 24 and 25 arises from the volcanic sill of site 23, which is some 30 m away, intruded parallel into the beds of sites 24 and 25. Site 23 requires 9° of backtilting to give a 66° counterclockwise block rotation. Whereas the palaeoremanences of the adjacent red beds (sites 24 and 25) are proven to be secondary, the remanence of the volcanic sill is likely to be primary. The low angle of backtilting for site 23 indicates that block rotation mostly occurred after folding. In this case, the sill must have intruded after most of the folding was accomplished, but before block rotation. This is an excellent example of how geologic field information and palaeomagnetic data from neighbouring sites can be put together to resolve geologic events in time.

3.2.2 Southern Folded Sequence (Sites 1-6,113,115,122,140,142,144-146,155)

The southern sequence consists of 12 sites in Jurassic limestones and 3 sites in Permian sandstones. Macroscopically the rocks do not expose signs of metamorphism. The remanences are carried predominantly by magnetite and all sites yield site means with precision parameters of $k \geq 10$ (see section 2). Stepwise unfolding gives a maximum of the k-value at 1% unfolding (see section 2.5.2), clearly revealing an overall secondary remanence character. All sites have significant site means. However, small-circle distributions parallel to the Π-circle may occur in sites 4 and 115. Nevertheless, reconstruction will use their Fisher means.

3.2.2.1 Reconstruction of the Whole Folded Sequence

The pole of the Π-circle of the bedding poles (mean tilt axis, Fig. 3.5a) has an azimuth of 72,9° and a dip of 1,1°. For the calculation of the *d*-angles, the Π-circle is assumed to be vertical.

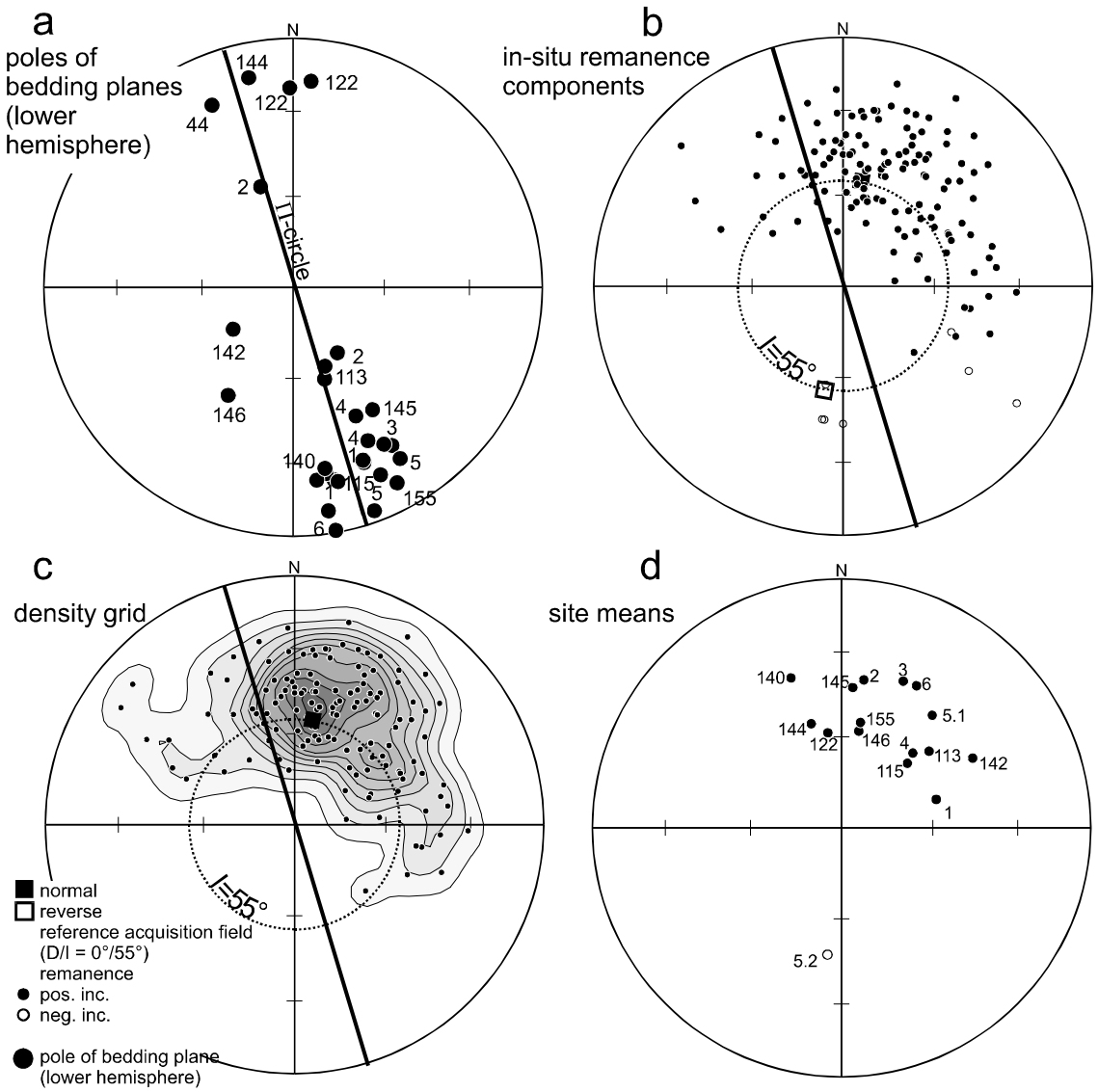

Fig. 3.5: Bedding data and remanences of the northern sequence including the sites 1-4, 5.1, 5.2, 6, 113, 115, 122, 140, 142, 144-146 and 155. (a) Bedding poles and Π-circle. The mean tilt axis has a trend of 72,9° and a dip of 1,1°. (b) 141 in-situ remanence components, 134 with positive and 7 with negative inclination. (c) Density grid of all remanence directions with the directions of negative inclination inverted, assuming that these did not change the hemisphere through tilting. Distribution is not clearly parallel to the Π-circle. (d) Site means.

Most of the in-situ remanences are close to the normal polarity reference field (Fig. 3.5b). The distribution does not clearly reflect a trend parallel to the Π-circle. Hence, folding did not change the in-situ remanences significantly. The distribution itself could be caused as well by differential block rotations between the sites (e.g. sites 1, 142, 115, 113 and 4). This could be suspected from the present position of the bedding poles only in sites 142 and 146, which might have undergone a clockwise block rotation. Nevertheless, if a distribution around a mean small circle parallel to the Π-circle is assumed, the reconstruction yields a mean clockwise block rotation of -11° for the whole sequence. Table 3.3 lists the reconstruction parameters for this most probable solution.

Table 3.3: Calculation of the mean small circle and reconstruction of the southern folded sequence. Remanence components with negative inclination have been inverted for the calculation, assuming that they did not change the hemisphere through tilting. Only the shortest direct reconstruction related to normal polarity is shown. The other three direct solutions require much higher displacement and hence are very unlikely. For definitions, conventions, equations and details see section 1. For discussion see text.

remanence components of sites 1-4,5.1,5.2,6,113,115,122,140,142,144-146,155			
reference field	D/I = 10°/55°		
number of components		135	
mean *d*		0,35	
mean *d*-angle (°)		69,3	
standard deviation (°)		17,3	
95% confidence interval (°)		3,3	
azimuth of pole of fold axis (°)			
present	72,9	confidence interval (+)	(-)
reconstructed	62,0	6,7	7,2
block rotation (°)	-10,9	6,7	7,2

3.2.2.2 Reconstruction of the Single Sites of the Southern Sequence

Table 3.4 summarises the relevant parameters and the reconstruction chosen as the most probable for each site. Fig. 6.2 in the appendix shows the four direct reconstructions. Site 3 requires a maximum I_{acq} of 43,1°, which is more than 10° below the reference field, and will not be considered further. Site mean 5.1, the low-coercive component of site 5, requires a maximum I_{acq} of 47°, and was used for the reconstruction, because it is not too far away from the reference field.

From the four possible direct solutions, the first one for normal polarity in all cases shows the smallest displacement. Resulting block rotations are generally clockwise up to -59° (site 113) except for three sites (122, 140, 144) showing counterclockwise rotations up to 33° (site 140). The angles of backtilting are on the average low (e.g. sites 144, 146 and 155) indicating that most of the folding had already been accomplished at the time of remanence acquisition. For site 5, the high-coercive remanence component (site mean 5.2) takes less backtilting and gives a smaller block rotation than the low-coercive component. It is therefore assumed to be younger recording only part of the displacement.

Table 3.4: Reconstruction of the sites of the northern sequence. Only the most probable reconstruction for each site is listed. For other possible reconstructions and graphical representation see Fig. 6.2 in the appendix. dip az./dip: azimuth and angle of dip. *d*: angular distance, I_{acq} max.: maximum palaeoinclination, % of untilting: percent of untilting related to the present dip assumed to be upright. Remark: upright or overturned (overt.) bedding as the consequence of the comparison of the present bedding with the sense of untilting (assuming that tilting did not reverse), indiff.: indifferent, used when angle of untilting is below ±10°, >dip: angle of untilting exceeds dip for either upright or overturned position by more than 10°. α95/cos I_{acq}: confidence interval of the declination for sites with a Fisher mean. For conventions, definitions and equations see Fig. 1.1 and section 1. For discussion see text.

site	dip az.	dip	bedding	*d*	*d*-angle	I_{acq} max.	back-tilting	block-rotation	reconstruction point		% of untilting	remark	α95/ cosI_{acq}
	(°)	(°)			(°)	(°)	(°)	(°)	D (°)	I (°)			(°)
1	340	67	-	0,54	122,5	57,5	-16	-40	50	55	23	upright	18,5
2a	162	35	-	0,38	112,4	67,6	14	-14	24	55	41	upright	20,6
2b	326	26	-	0,50	120,2	59,8	29	-17	27	55	-112	overt.	16,6
4	334	53	-	0,53	121,7	58,3	-2	-30	40	55	5	indiff.	29,6
5.1	333	74	-	0,68	133,1	46,9	15	-43	53	46	-20	overt.	15,5
5.2	333	74	-	0,37	111,8	68,2	9	-3	193	-55	-13	indiff.	14,1
6	347	78	-	0,53	122,0	58,0	32	-45	55	55	-41	overt.	17,4
113	342	32	-	0,57	125,0	55,0	16	-59	69	55	-49	overt.	37,3
115	328	64	-	0,49	119,6	60,4	-12	-17	27	55	19	upright	28,1
122	179	69	-	-0,07	86,2	86,2	-3	18	352	55	-5	indiff.	31,9
140	353	67	-	-0,16	80,7	80,7	19	33	337	55	-28	overt.	20,0
142	55	23	-	0,09	95,3	84,7	15	-54	64	55	-65	overt.	22,3
144	162	72	-	0,02	91,0	89,0	1	26	344	55	1	indiff.	16,7
145	327	49	-	0,45	116,6	63,4	17	-8	18	55	-34	overt.	14,3
146	31	42	-	-0,19	79,0	79,0	-3	-2	12	55	6	indiff.	14,8
155	332	78	-	0,36	111,0	69,0	1	-1	11	55	-1	indiff.	9,4

The reconstruction of the bedding (Fig. 3.6) reveals that the tilting directions exhibited a much higher variation at the time of remanence acquisition than today. This implies that the now unidirectionally folded sequence is at least partly a product of block rotation.

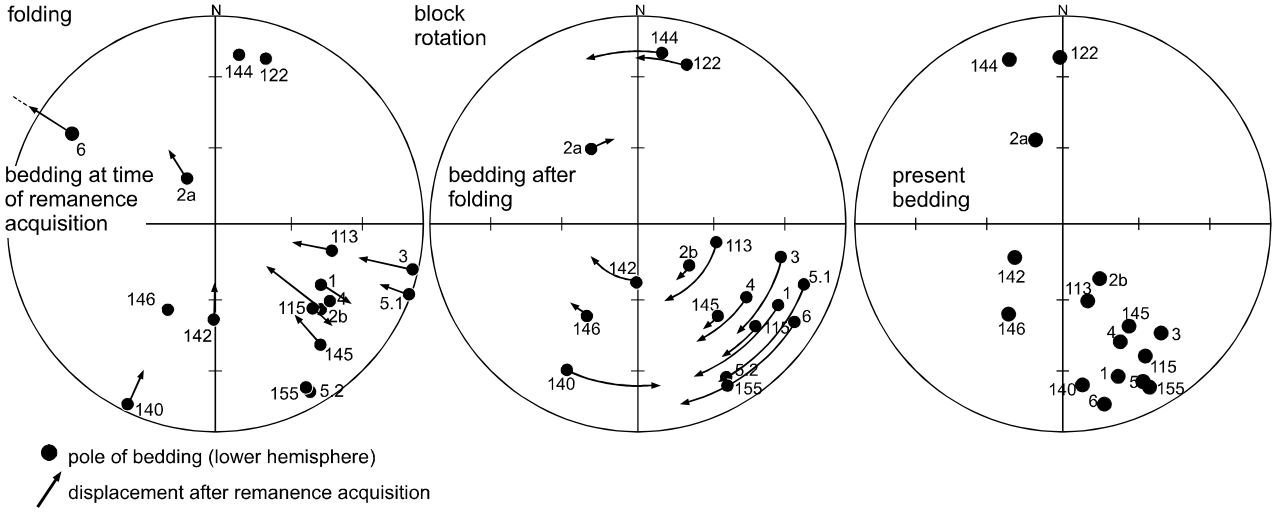

Fig. 3.6: Reconstruction of the bedding for the sites of the southern sequence. Left: Bedding at time of remanence acquisition, arrows indicate subsequent tilting. Middle: After folding and before block rotation, arrows indicate subsequent block rotation. Right: Present bedding. For discussion see text.

The sense of tilting since remanence acquisition is in eight sites against the present dip direction (assumed to be significant if angle > 10°). Hence, they are overturned if tilted only in one sense (information on upright/overturned bedding was not found in the field). Except for sites 1 and 115 and sites with an indifferent sense, all sites have been tilted to the south-east, reducing the dip within the prevalently north-

dipping sequence. This final tilt corresponds to the formation of a vergence to the south, in compliance with the present predominance of north-dipping layers.

3.2.2.3 Reconstruction of the Remaining Sites

The bedding of the sites 17, 18, 19, 22, 158 and 161 in the eastern part of the southern Pamirs does not define a unidirectionally folded sequence. As in the northern sequence, the sites show increasing macroscopic signs of deformation and metamorphism towards the metamorphic dome. The four direct reconstructions are shown in Fig. 6.3 in the appendix. Table 3.5 summarises the relevant parameters and the reconstruction chosen as the most probable for each site.

Except for site means 18.2 and 19.2, the angles of backtilting and block rotation are lowest for the first direct reconstruction related to normal polarity. In both sites 18 and 19 (Tertiary sandstones), AF-demagnetisation provided two components carried by magnetite. The low-coercive components most probably arise from a normal polarity field. With a small angle of backtilting, they give counterclockwise block rotations of 5° and 39°. In contrast, the high-coercive components seem to be of reverse polarity. The reconstruction needs more backtilting and gives counterclockwise block rotations of 20° and 77°, exceeding the block rotation of the low-coercive site means. Thus, the low-coercive components probably are younger recording an increment of the displacement. At site mean 19.2, the more distant reconstruction with 83° of backtilting has been chosen, because otherwise it would be inconsistent (with respect to block rotation) with the results from site 18 nearby. The reconstructions indicate overturned layers for sites 15, 17, 18 and 19 (if tilting sense did not reverse).

Table 3.5: Reconstruction of the remaining sites outside the two folded sequences. Only the most probable solution for each site is listed. For other possible reconstructions and graphical representation see Fig. 6.3 in the appendix. dip az./dip: azimuth and angle of dip. *d*: angular distance, I_{acq} max.: maximum palaeoinclination, % of untilting: percent of untilting related to the present dip assumed to be upright. Remark: upright or overturned (overt.) bedding as the consequence of the comparison of the present bedding with the sense of untilting (assuming that tilting did not reverse), indiff.: indifferent, used when angle of untilting is below ±10°, >dip: angle of untilting exceeds dip for either upright or overturned position by more than 10°. $\alpha 95/\cos I_{acq}$: confidence interval of the declination for sites with a Fisher mean. For conventions, definitions and equations see Fig. 1.1 and section 1. For discussion see text.

site	dip az.	dip	bedding	*d*	*d*-angle	I_{acq} max.	back-tilting	block-rotation	reconstruction point		% of untilting	remark	$\alpha 95/\cos I_{acq}$
	(°)	(°)			(°)	(°)	(°)	(°)	D (°)	I (°)			(°)
9	181	61	-	0,57	124,4	55,6	33	-71	81	55	53	upright	32,5
15	43	45	-	-0,39	67,1	67,1	46	10	0	55	-103	overt.	27,0
17	5	53	-	0,19	100,9	79,1	14	-14	24	55	-26	overt.	13,9
18.1	334	42	-	0,30	107,4	72,6	10	5	5	55	-25	overt.	20,2
18.2	334	42	-	0,16	99,4	80,6	47	20	170	-55	-111	overt.	9,1
19.1	330	36	-	0,01	90,4	89,6	7	39	331	55	-19	indiff.	26,0
19.2	330	36	-	0,35	110,3	69,7	83	77	113	-55	-230	overt.	19,0
22	182	43	-	0,53	121,9	58,1	-2	-59	69	55	-4	indiff.	34,7
127	144	62	-	-0,32	71,5	71,5	5	80	290	55	8	indiff.	8,7
158	6	44	-	-0,30	72,5	72,5	2	36	334	55	-5	indiff.	11,3
161	13	59	-	0,38	112,4	67,6	-26	-45	55	55	44	upright	4,9

As in the southern sequence, the tilting directions show a much higher variation at the time of remanence acquisition and now exhibit a preferred orientation around north (Fig. 3.7). Hence, also here the block rotations seem to have rotated the tilting directions due north. As in the southern sequence, an overall tilting to the south occurred after remanence acquisition, reducing the dip of the predominantly north-dipping layers.

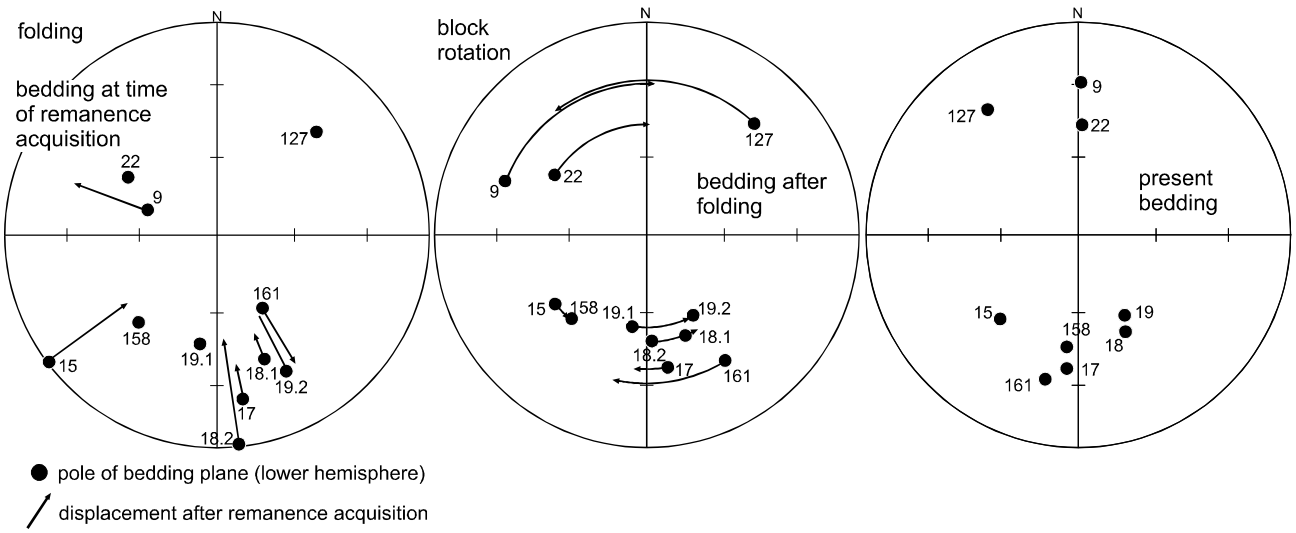

Fig. 3.7: Reconstruction of the bedding for the remaining sites of the southern Pamirs. Left: Bedding at time of remanence acquisition, arrows indicate subsequent tilting. Middle: After folding and before block rotation, arrows indicate subsequent block rotation. Right: Present bedding.

3.2.3 Compilation of Results

For each site, a reconstructed tilt axis and a block rotation have been obtained from the small-circle reconstruction. For clearness, the tilting directions rather than the tilt axes will be under further consideration.

Fig. 3.8a shows block rotations and Fig. 3.8b both present and reconstructed tilting directions. In Fig. 3.8a block rotations of the granites as declination deviation to the reference declination of D = 10° have been incorporated, because they depict site means close to the reference field (see Table 2.3), hence tilting cannot have changed them significantly. However, there is no tectonic control on them regarding the displacement axes and no certain constraint on their age. If the remanences are primary, they are Lower Cretaceous, if secondary, they are probably around 20 Ma as indicated by the geochronological ages (see section 2). Their block rotations with respect to the 20 Ma reference field will be shown with a question mark.

Fig. 3.8 (following pages): (a) Block rotations as the angular difference between the reconstructed and the present tilt axes. The granites (GR) of the sites 7 and 10 are incorporated with their declination difference to the reference declination of D = 10°. The dashed arrows of site means 5.2 (high-coercive component), 18.1 and 19.1 (low-coercive components) are probably younger than 5.1, 18.2 and 19.2, each indicating an increment of block rotation. Confidence intervals $\pm\alpha 95/\cos I_{acq}$ or from small circle statistics as given by Tables 3.2, 3.4 and 3.5 (see also Fig. 6.1, 6.2 and 6.3). (b) Present and reconstructed tilting directions as determined from the reconstructions. Tilting directions are shown separately in equal-area plots for the two unidirectionally folded sequences and for the total of the sites with number (n), azimuth of a resultant mean and standard deviation (Sd, calculated without incremental tilting directions). Tilting directions in each sequence as well as on the whole show a higher variation at the time of remanence acquisition, indicating a close relationship to the block rotations. For discussion see text.

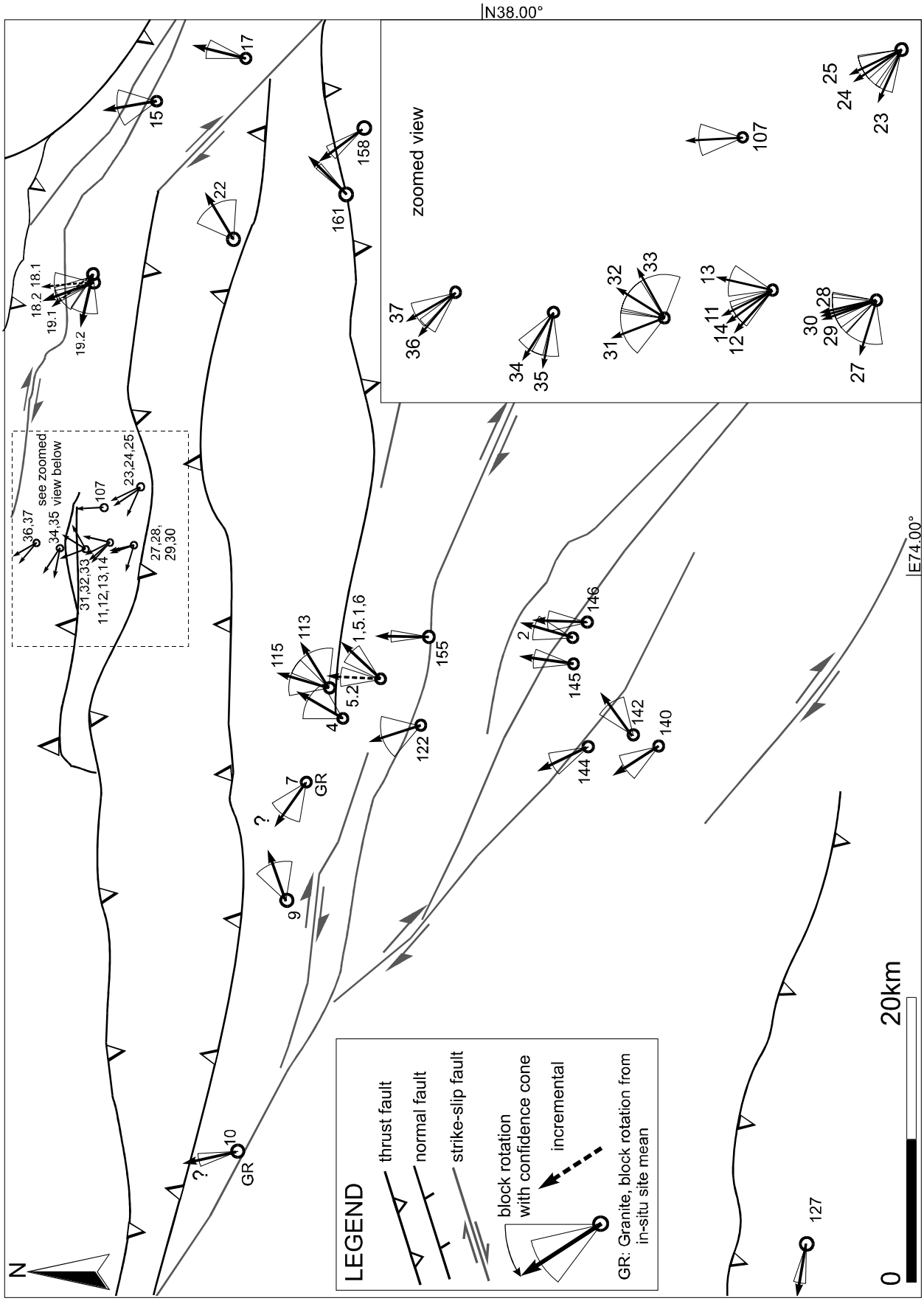
N38.00°
E74.00°
zoomed view
see zoomed view below
LEGEND
thrust fault
normal fault
strike-slip fault
block rotation with confidence cone
incremental
GR: Granite, block rotation from in-situ site mean
N
0
20km

Fig. 3.8a

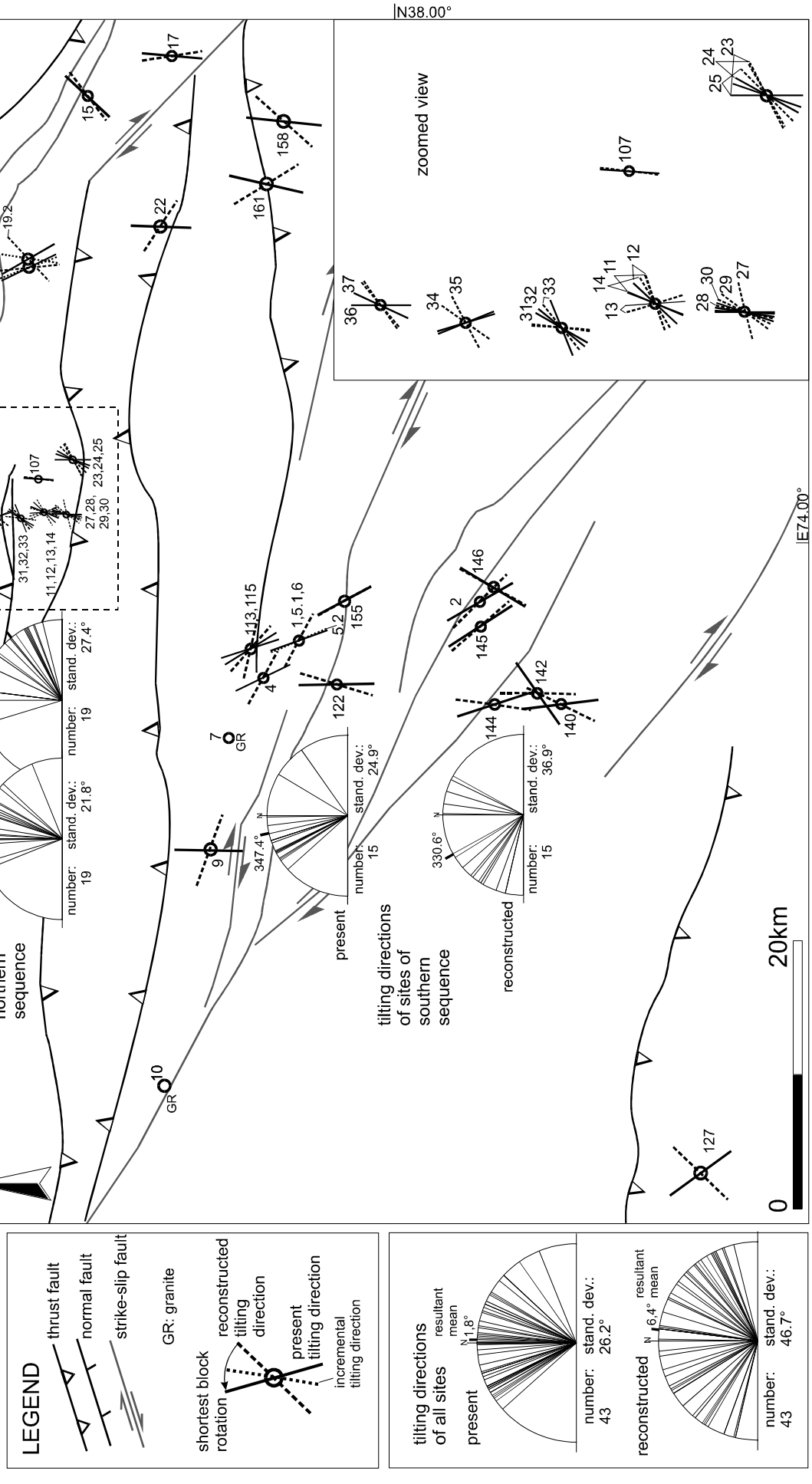
N38.00°
E74.00°
zoomed view
see zoomed view below
tilting directions of sites of northern sequence
present
reconstructed
number: 19
stand. dev.: 21.8°
15.1°
number: 19
stand. dev.: 27.4°
41.0°
tilting directions of sites of southern sequence
present
number: 15
stand. dev.: 24.9°
347.4°
reconstructed
number: 15
stand. dev.: 36.9°
330.6°
GR
0
20km
LEGEND
thrust fault
normal fault
strike-slip fault
GR: granite
shortest block rotation
reconstructed tilting direction
present tilting direction
incremental tilting direction
tilting directions of all sites
present
resultant mean
1.8°
number: 43
stand. dev.: 26.2°
reconstructed
resultant mean
6.4°
number: 43
stand. dev.: 46.7°

Fig. 3.8b

In the northern sequence, located close to the metamorphic dome, the rotations turn out to be predominantly counterclockwise. In the southern sequence which is more distant from the dome, the rotations vary and are smaller on the average, as are the amounts of backtilting. In the eastern part of the investigated area which is more distant to the metamorphic dome and closer to the Pamir-Karakorum fault, the sites do not show a general trend of block rotation. The granites of sites 7 and 10 indicate counter-clockwise block rotations. On the whole, counterclockwise block rotations may prevail close to the metamorphic dome. In the other areas no general trend of rotation can be observed. Summarising, the block rotations in the southern Pamirs do not seem to follow an overall tectonic behaviour, such as oroclinal bending or dextral shear.

In contrast, it is the tilting directions that clearly indicate an general behaviour:

While the present tilting directions exhibit a clear orientation around north (resultant vector at 1,8°, see Fig. 3.8b), the reconstructed tilting directions are oriented more due north-east for the northern folded sequence and more due north-west for the southern folded sequence. Altogether, the reconstructed tilting directions are nearly uniformly distributed between a trend of 270° and 90° (tilt axes trending between 0° and 180°). Within both the two folded sequences and the total of the sites, the variation of the tilting directions at the time of remanence acquisition is much higher than at present, as shown by the standard deviations (see Fig. 3.8b). This is most pronounced in the southern sequence. This quite uniform distribution of the reconstructed tilting directions is also evident from the distribution of the maximum I_{acq} values (Fig. 3.1). The cumulative distribution curve depicts a rather linear rise above a maximum I_{acq} of 55°.

The comparison of the present with the reconstructed tilting directions shows that, on the whole, the block rotations rotated the tilting directions due north. This observation probably reflects a general mechanism in the process of folding: With increasing amount of shortening the layers in a folded sequence must line up perpendicular to the shortening direction.

Under the assumption that the tilting directions have been aligned predominantly by the overall N-S shortening of the area, a quantification of shortening can be attempted. Since the resultant mean of the present tilting directions of all sites in the southern Pamirs is oriented at 2° (see Fig. 3.8b), a N-S oriented shortening regime is reasonable. The simplest approach to a quantification is considered to be the following procedure:

The reconstructed tilt axes are subjected to uniaxial N-S shortening until their standard deviation around a mean direction reaches the present value. N-S shortening is assumed to be taken up completely by folding, giving vertical extension (Fig. 3.9).

The azimuth *t´´* of a tilt axis after N-S shortening is:

$$t'' = \arctan\left(\frac{\tan t'}{l/l_o}\right) \qquad (8)$$

t´ azimuth of reconstructed tilt axis, *t´´* azimuth of tilt axis after N-S shortening, l_o original length, *l* length after shortening.

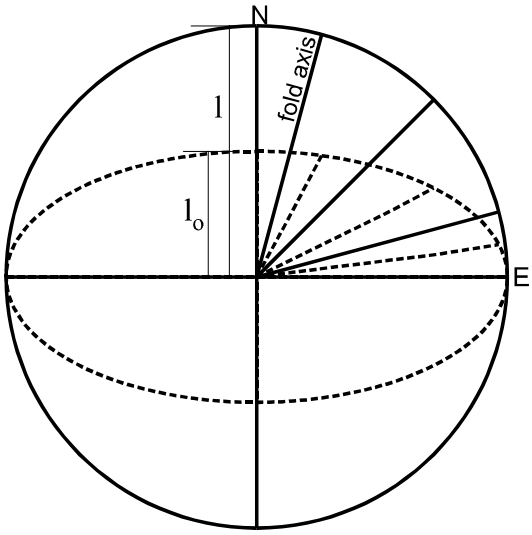

Fig. 3.9: Rotation of tilt axes by N-S shortening taken up completely by folding (vertical extension). Solid line: initial geometry (circle). Dashed line: N-S shortened by 0.5.

This procedure is applied to the data set of reconstructed tilt axes iteratively until the value of the standard deviation of the azimuths of the tilt axes reaches the present value. Table 3.6 lists the result.

Table 3.6: Finite N-S oriented uniaxial shortening ($1-l/l_0$; l_0 original length, l length after shortening) to reduce the standard deviation of the reconstructed tilt axes to the one of the present tilt axes for 43 sites of the southern Pamirs. Incremental tilt axes are excluded. Involved site means: 1, 2a, 2b, 4, 5.1, 6, 9, 11-15, 17, 18.2, 19.2, 22-25, 27-37, 107, 113, 115, 122, 127, 140, 142, 144-146, 155, 158 and 161.

	standard deviation (°)		finite shortening by
tilt axes from	at present	reconstructed	$(1-l/l_0)$
43 sites of the southern Pamirs	46,7	26,2	0,64

The distribution of the total of 43 tilt axes has to be N-S shortened by 0,64 to reach the present standard deviation. This procedure is not a strictly correct approach accounting for the rotation of each site. Since tilting directions become rotated across north (e.g. in sites 15, 19.2, 34 and 35) or even rotate away from north (e.g. in sites 142 and 144), a simple alignment due to N-S shortening cannot be the sole process to account for the observed block rotations. Local effects such as space accomodation and block rotation near faults must be involved as well. Therefore, it is not appropriate to explain each rotation by N-S shortening, neither does it seem adequate to apply the procedure in more detail, i.e. to the block rotation of single sites. The value obtained must be considered as a rough estimate for the total of the sites.

3.3 Central Pamirs

In this part of the investigation area, fourteen sites were taken from Jurassic, Cretaceous and Tertiary sedimentary rocks north of the metamorphic dome and two sites from two granites intruded into the metamorphic rocks of the dome (Fig. 3.10). The sites 45 - 55 belong to a unidirectionally folded sequence, from here on called *Muzkol zone*. In the field the sampled rocks do not exhibit macroscopic signs of metamorphism. Nevertheless, in the fold tests most of the remanences turn out to be secondary.

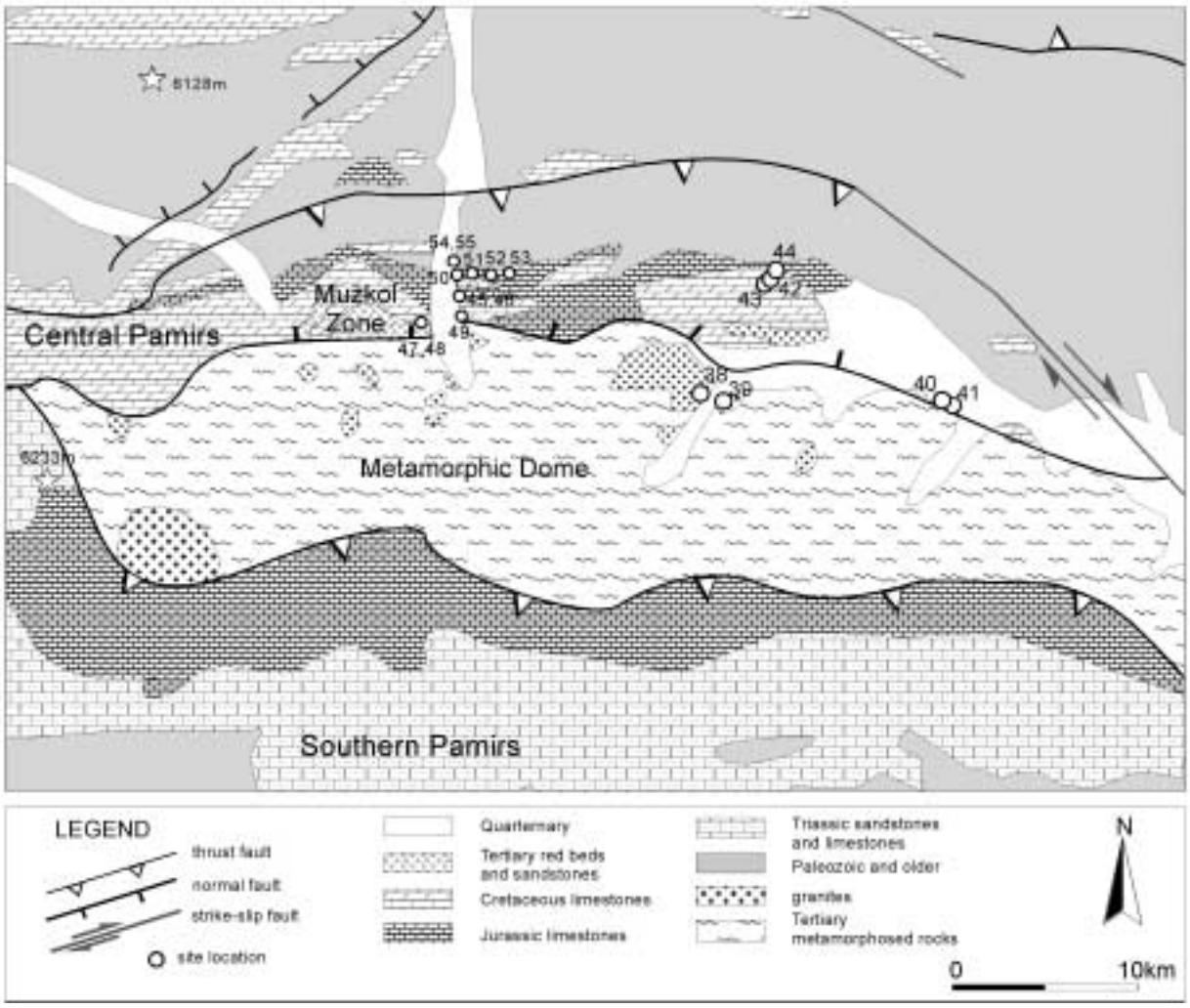

Fig. 3.10: Geologic map of the central Pamirs with site locations. Sites 45 - 55 belong to a unidirectionally folded sequence (Muzkol zone). For map overview and references see Fig. 2.2.

3.3.1 Reconstruction of the Sites from the Muzkol Zone

The Muzkol zone has been sampled with 11 sites, 4 of them in Tertiary red beds and 7 in Jurassic limestones. The palaeoremanences in the limestones are carried by magnetite, in the red beds by haematite and magnetite (see section 2.4.3). For all sites of the Jurassic limestones, a low- and a high-coercive component have been isolated, both having a significant site mean with $k \geq 10$. The fold tests clearly show a secondary character for both remanence components. For the low-coercive components, the *k*-value is highest at 12% unfolding and for the high-coercive components at 9% unfolding. Thus, the remanences have been acquired at a late stage of folding in the area. The negative significance of the fold test is much higher for the high-coercive components, which in in-situ coordinates are closer to the

reference field direction (Fig. 3.11c, d). The low-coercive components generally exhibit the higher declination. These observations suggest that the low-coercive components are older than the high-coercive components. If the high-coercive components are unfolded by 9%, where the *k*-value is largest, a site mean of D_{is}/I_{is} = 11,7°/57,7° is obtained. This value fits well to the 20 Ma reference palaeofield of D/I = 10°/55°, assumed for this area.

In the Tertiary red beds of sites 45 - 48 the remanences are carried by haematite and magnetite. The fold test is positive with 99% significance. However, the continuous rise of the *k*-value during stepwise unfolding up to 150% unfolding calls its validity into question (see section 2.6.6 and Fig. 2.15).

The pole of the Π-circle of the bedding poles (mean tilt axis, Fig. 3.11a) has an azimuth of 105,2° and a dip of 0,9°. For the calculations, the Π-circle is assumed to be vertical. North-dipping layers (sites 52 and 53) are much less frequent, therefore, additional bedding data measured within the sequence had to be incorporated to define a Π-circle accurately.

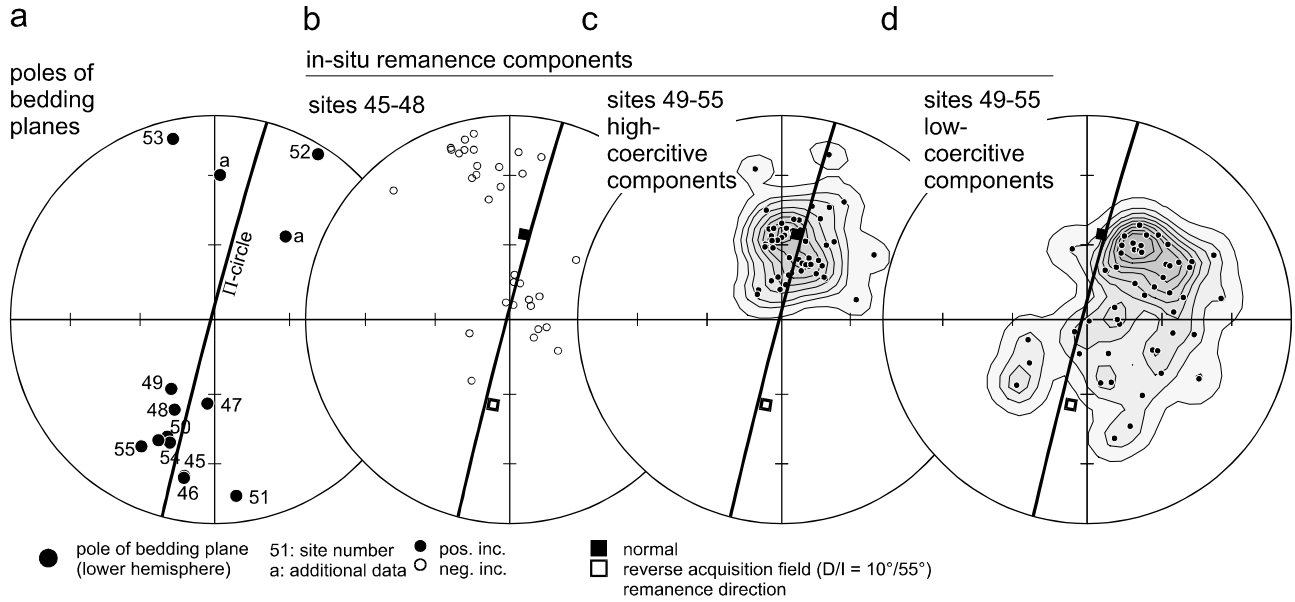

Fig. 3.11: Bedding data and remanences of the Muzkol zone including the Tertiary red beds of sites 45 - 48 and the Jurassic limestones of sites 49 - 55. (a) Bedding poles and Π-circle. The mean tilt axis has a strike of 105,2° and a dip of 0,9°. (b) In-situ remanence components of the Tertiary red beds (sites 45 - 48) showing no clear small-circle distribution parallel to the Π-circle. Remanence components probably relate to a reverse polarity field and have not changed the hemisphere through tilting. (c) High-coercive in-situ remanence components of the Jurassic limestones (sites 49 - 55) with density grid showing no relation to folding. (d) Low-coercive in-situ remanence components of the Jurassic limestones with density grid. A few directions with negative inclination occur and have been inverted for gridding. Both high- and low-coercive components most likely relate to a normal polarity field. A relation to folding seems to be given for the low-coercive components. The high-coercive components record less displacement and therefore must be younger.

The in-situ remanence components of the Tertiary red beds (Fig. 3.11b) and the high-coercive components of the Jurassic limestones (Fig. 3.11c) do not show a clear small-circle distribution parallel to the Π-circle (Fig. 3.11b). The low-coercive components of the Jurassic limestones (Fig. 3.11d) might reflect such a trend. If a mean small circle is calculated for the low-coercive components and reconstructed with a reference field of D/I = 10°/55°, a clockwise block rotation of -32° is obtained as the shortest solution (see Table 3.7).

low-coercive remanence components of sites 49 - 55			
reference field	D/I = 10°/55°		
number of components		52	
mean α		0,26	
mean α-angle (°)		75,1	
standard deviation (°)		17,8	
95% confidence interval (°)		5,0	
azimuth of pole of mean tilt axis (°)			
present	105,2	confidence interval	
		(+)	(-)
reconstructed	73,4	9,1	9,7
block rotation (°)	-31,8	9,1	9,7

Table 3.7: Small-circle reconstruction of the low-coercive components of the Jurassic limestones (sites 49 - 55). Reconstruction gives a -32° clockwise block rotation as the shortest and therefore most probable solution. The other three direct solutions require much higher displacements and thus are unlikely. For definitions, conventions and equations see Fig. 1.1 and section 1. For discussion see text.

3.3.2 Reconstruction of the Single Sites of the Central Pamirs

Table 3.8 summarises the relevant parameters and the reconstruction chosen as the most probable for each site. Fig. 6.4 in the appendix depicts the four direct reconstructions for each site. On the whole, net displacements seem to be moderate, and mostly one reconstruction can be chosen, which shows by far the smallest displacement. The site means 42 and 43.2 (Late Cretaceous limestones) require an I_{acq} of 49,7° and 51,1°, somewhat below the reference inclination of I_{acq} = 55°. This could indicate a primary character of the remanences. Indeed, the bedding corrected inclinations of I_{bc} = 40,5° and I_{bc} = 44,2° (see Table 2.3) would fit to an expected Late Cretaceous palaeofield inclination of about 43° (see APWP in Fig. 2.3), with about 440 km of Cenozoic shortening of Eurasia taken into account. Consequently, these sites might be primary. Site 44 in the same rocks seems to be primary as well, since it reaches the I_{acq} at 101% untilting, however, the bedding corrected inclination of I_{bc} = 55,1° is above the expected value for the Cretaceous. Summarising, a primary character for the remanences of the Cretaceous limestones may be given, although the fold test indicates the opposite (see section 2.6.5). As the primary character is not proven, the site means 42 and 43.2 will be reconstructed using their corresponding maximum I_{acq} and a declination of 10°. If the bedding corrected site means of the three sites were taken, referenced to the Cretaceous palaeofield in the area, the resulting block rotations would be some degrees lower, however, with the tectonic result basically remaining the same.

In site 43 the senses of backtilting of the low- and high-coercive site mean oppose each other, indicating a reversal of the tilting sense. The Tertiary red beds of sites 47 and 48 reach the reference inclination of 55° at 105% and 111% untilting. Thus, these seem to be primary as also indicated by the fold test. The site mean in bedding coordinates for the remanence components of both sites is with D_{bc}/I_{bc} = 187,2°/-57,9° close to the reference palaeofield. In contrast, the adjacent sites 45 and 46 in the same rocks require much higher untilting of 139% and 147%, and also show a much higher inclination in bedding coordinates (mean D_{bc}/I_{bc} = 281,4°/-69,3°). Consequently, a primary remanence in these sites does not seem plausible, intensifying the doubts on the validity of the fold test involving the sites 45 - 48.

Site means 51.1 (74% untilting) and 55.1 (89% untilting) also could have preserved primary (Jurassic) remanences. Their inclinations in bedding coordinates (I_{bc} = 38,6° and 48,4°) are within the expected range

for the Middle to Late Jurassic, assuming a location on Eurasia and Cenozoic convergence of about 440 km (see expected values in Fig. 2.3).

Table 3.8: Reconstruction of the sites of the Muzkol zone. Only the most probable reconstruction for each site is listed. For other possible reconstructions and graphical representation see Fig. 6.4 in the appendix. dip az./dip: azimuth and angle of dip. *d*: angular distance, I_{acq} max.: maximum palaeoinclination, % of untilting: percent of untilting related to the present dip assumed to be upright. Remark: upright or overturned (overt.) bedding as the consequence of the comparison of the present bedding with the sense of untilting (assuming that tilting did not reverse), indiff.: indifferent, used when angle of untilting is below ±10°, >dip: angle of untilting exceeds dip for either upright or overturned position by more than 10°. α95/cos I_{acq}: confidence interval of the declination for sites with Fisher mean. For conventions, definitions and equations see Fig. 1.1 and section 1. For discussion see text. Note that site means 42 and 43.2 call for an I_{acq} lower than 55°.

site	dip az.	dip	bedding	*d*	*d*-angle	I_{acq} max.	back-tilting	block-rotation	reconstruction point		% of untilting	remark	α95/ cosI_{acq}
	(°)	(°)			(°)	(°)	(°)	(°)	D (°)	I (°)			(°)
40	353	51	-	-0,09	84,9	84,9	7	26	344	55	-13	indiff.	13,3
41	340	41	-	0,39	113,2	66,8	22	-13	23	55	-54	overt.	31,0
42	22	27	-	-0,63	51,1	51,1	3	73	297	51	-10	indiff.	20,2
43.1	15	30	-	-0,41	65,5	65,5	12	41	329	55	-41	overt.	25,3
43.2	15	30	-	-0,65	49,7	49,7	-14	76	114	-49	47	upright	17,2
44	64	30	-	-0,39	67,3	67,3	-30	-12	22	55	101	upright	9,4
45	11	67	-	0,27	105,8	74,2	-93	-29	219	-55	139	>dip	11,0
46	11	67	-	0,44	116,1	63,9	-99	-51	241	-55	147	>dip	17,3
47	5	34	-	0,03	91,5	88,5	-36	2	188	-55	105	upright	23,2
48	24	40	-	-0,15	81,3	81,3	-44	1	189	-55	111	upright	17,8
49.1	32	33	-	0,01	90,5	89,5	-2	-23	33	55	5	indiff.	7,8
49.2	32	33	-	-0,31	71,9	71,9	2	11	359	55	5	indiff.	6,3
50.1	22	52	-	0,24	103,9	76,1	-6	-37	47	55	11	indiff.	22,8
50.2	22	52	-	0,02	91,1	88,9	-11	-14	24	55	21	upright	3,7
51.1	353	76	-	0,36	111,3	68,7	-57	-22	32	55	74	upright	27,5
51.2	353	76	-	0,14	98,3	81,7	-14	2	8	55	18	upright	17,1
52.1	212	85	-	0,48	118,8	61,2	1	-79	89	55	1	upright	31,7
52.2	212	85	-	-0,21	77,7	77,7	-8	0	10	55	-10	indiff.	16,9
53.1	167	80	-	0,31	108,3	71,7	-21	-10	20	55	-26	overt.	27,7
53.2	167	80	-	0,34	109,6	70,4	19	-13	23	55	24	upright	21,8
54.1	20	54	-	0,28	106,2	73,8	-4	-39	49	55	6	indiff.	19,9
54.2	20	54	-	0,03	91,8	88,2	-1	-13	23	55	1	indiff.	15,5
55.1	30	61	-	-0,02	88,6	88,6	-54	-18	28	55	89	upright	33,0
55.2	30	61	-	-0,24	76,3	76,3	-12	4	6	55	20	upright	15,7

Fig. 3.12 depicts the displacement of the bedding poles, assuming that block rotation performed after tilting. Block rotation in sites 40 - 44 seems to be rather high compared to the tilt angles (Fig. 3.12a). In the Muzkol zone the poles of sites 45 and 46 change to the opposite quadrant, implying either tilting by more than 180° in one sense, or successive tilting in two opposite senses. In comparison, the incremental bedding poles of the high-coercive components of the Jurassic limestones give much smaller angles of tilting and block rotation than those of the low-coercive components. Like in the sites immediately south of the dome, the sense of tilting since remanence acquisition has been predominantly to the north, steepening up the overall north-dipping layers.

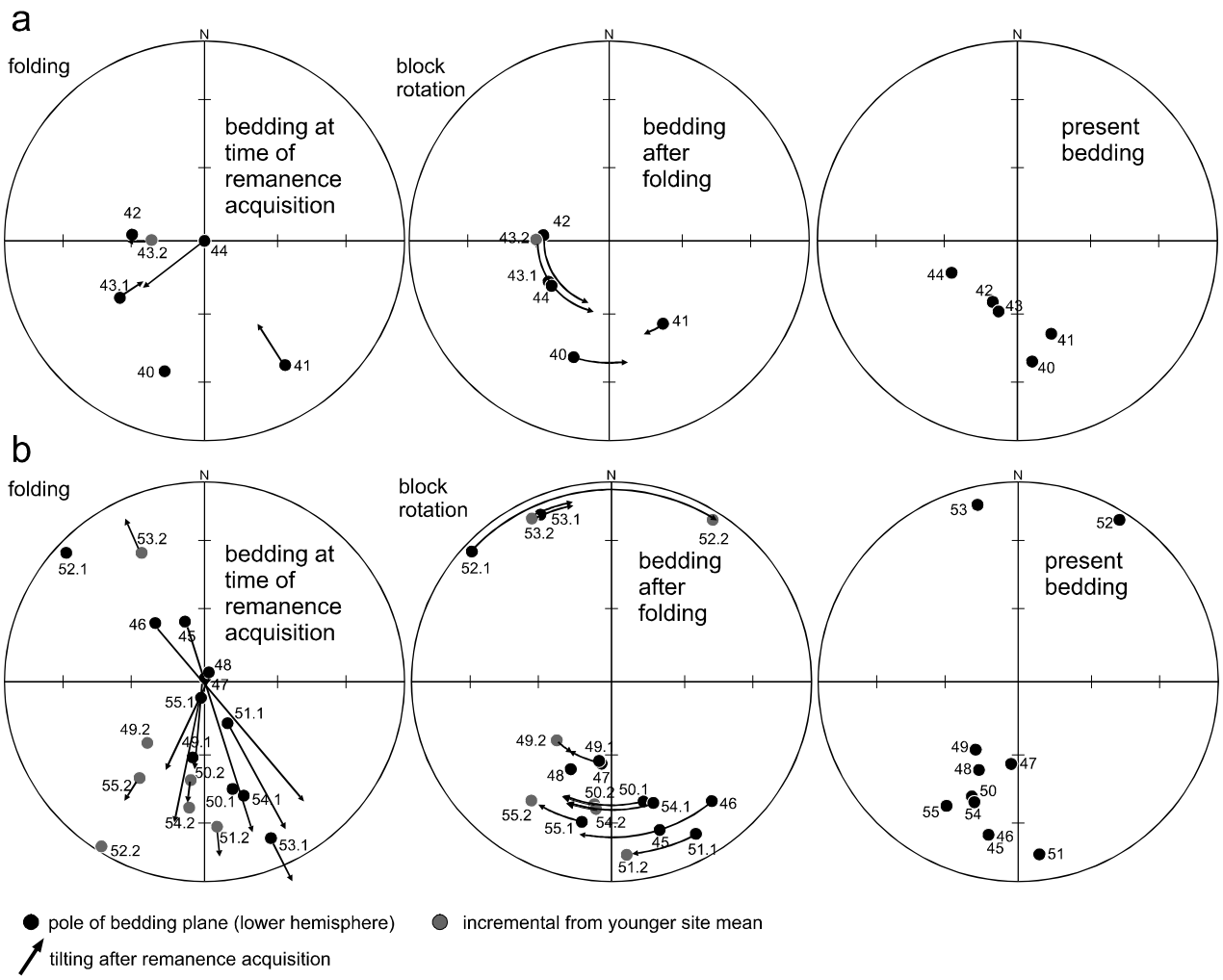

Fig. 3.12: Reconstruction of the bedding for sites 40 - 44 (a) and sites 45 - 55 (b) . Note that incremental bedding poles have been incorporated, representing part of the displacement. (b). Left: Bedding at time of remanence acquisition, arrows indicate subsequent tilting. Middle: After folding and before block rotation, arrows indicate subsequent block rotation. Right: Present bedding. For discussion see text.

On the whole, the bedding poles of all sites seem to be closer together in the present orientation than at the time of remanence acquisition, showing the same behaviour like in the sites of the southern Pamirs: Rotation of strata towards an orientation perpendicular to the shortening direction.

3.3.3 Record of Displacement in Individual Specimens of the Jurassic Limestones

The remanences in the Jurassic limestones depict a very well-defined AF-demagnetisation behaviour. From the rockmagnetic investigations and the demagnetisation, there is no clear evidence for other ferrimagnetic minerals besides magnetite. For each site, a low-coercive and a high-coercive site mean has been obtained, both clearly giving an overall secondary character in the fold tests. For the Muzkol zone, a mean clockwise block rotation by -32° has been obtained from the low-coercive components (see section 3.3.1). As already noted in section 1.4.3, small-circle distributions of remanences related to tectonic displacement occur within the individual specimens. The well-defined demagnetisation behaviour allows the calculation of differential vectors, which enables a detailed examination of the change of remanences during demagnetisation. Fig. 3.13 shows the demagnetisation behaviour of some exemplary specimens.

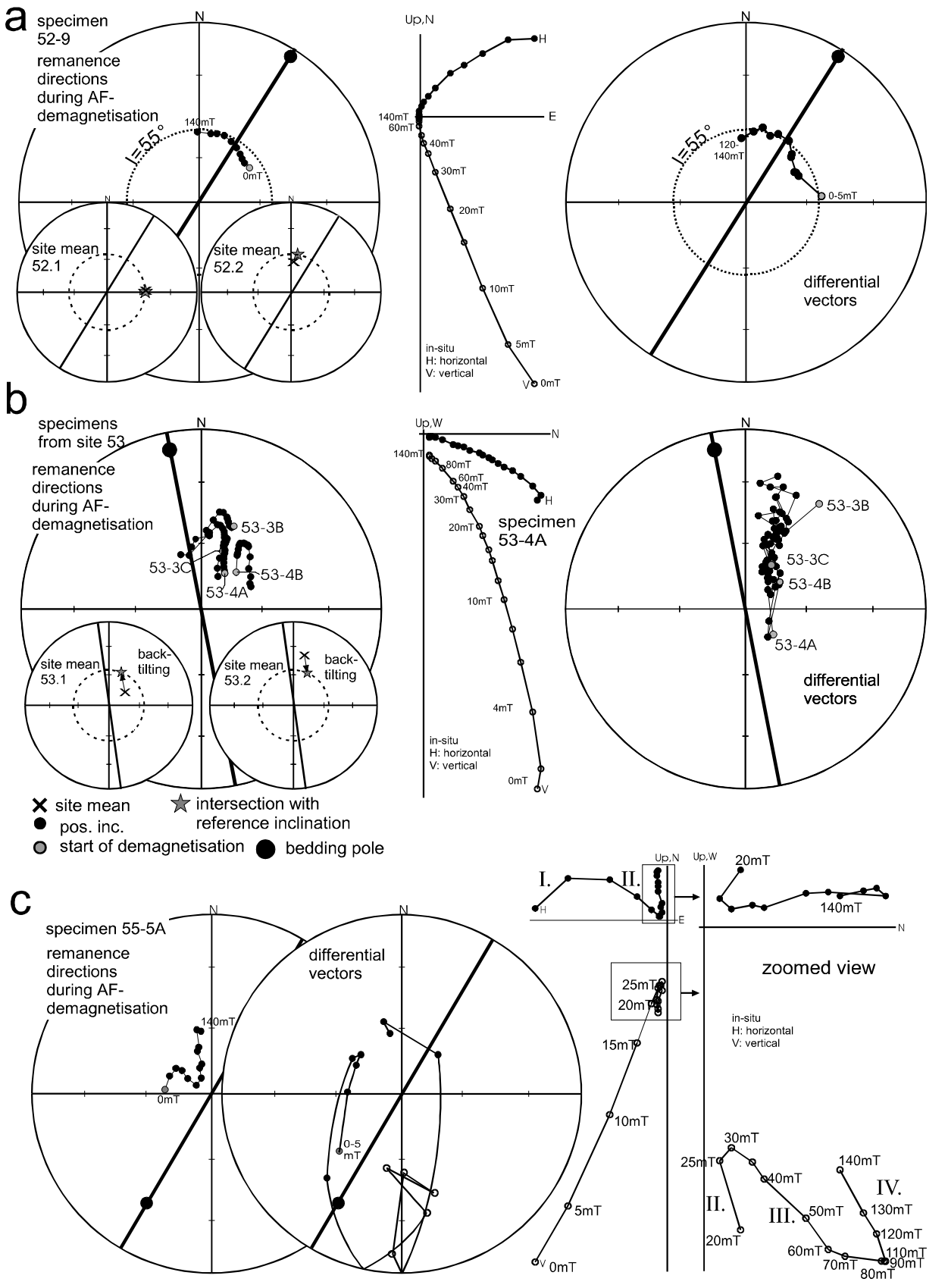

Fig. 3.13: Small-circle distributions of remanences during AF-demagnetisation in individual specimens of the Jurassic limestones of the central Pamirs. Demagnetisation behaviour in equal-area plots for the remanence directions (sum vectors) and differential vectors, and in the Zijderveld plot. Site means with reconstruction as chosen (see Fig. 6.4) are also given for (a) and (b). Stars mark the intersection of the remanence small circle with the small circle of constant field inclination (I = 55°) for the reconstruction chosen as the most probable. For discussion see text.

The differential vectors of specimen 52-9 (Fig. 3.13a) move on a horizontal small circle of approximately I = 55°. A relation to tilting is not evident, instead, the record seems to reflect a clockwise block rotation. At least three different remanence components are necessary to define the small circle. The displacement path ends up close to the reference field direction, therefore, the highest-coercive component is the youngest component added to the record.

The differential vectors of specimens from the nearby site 53 (Fig. 3.13b) move on a well-defined vertical small circle parallel to the Π-circle, thus they are clearly related to tilting. As before, at least three components must be present to define the small circle. If examined in detail, the remanence directions reflect a reversal of the tilting sense, as also indicated by the opposite angles of backtilting of the low- (53.1) and high-coercive (53.2) site means. Tilting as recorded has been first to the north and then back to the south. In both sites 52 and 53, the demagnetisation path constrains the small-circle reconstruction to one solution, related to normal polarity. According to these displacement paths, block rotation occurred mostly after tilting.

In specimen 55-5A (Fig. 3.13c) the remanence directions start moving parallel to the Π-circle, then turn aside towards south and eventually return to their previous path. This behaviour requires at least four different remanence components (I...IV, Zijderveld plots of Fig. 3.13c). The differential vectors scatter, but some of them clearly move to the reverse polarity field direction. PCA-analysis from 300 - 600 mT provides a component of D_{is}/I_{is} = 169°/-46°, which is close to a reverse polarity field. This behaviour is interpreted as the change of the magnetic field to reverse polarity and back within the time interval of remanence acquisition during the tectonic displacement. It is also observed in other specimens of site 55 (55-4A and 55-4B) and in some specimens of site 52 (52-4A, -5, -7, -8; see following section 3.3.3.1). In these specimens the duration of remanence acquisition and folding must have covered at least the time necessary for a reversal.

Since the AF-demagnetisation reveals the temporal sequence of displacement, the coercivity and hence the spectrum of grain sizes of the magnetite particles must somehow be related to the age of the remanences. This again points to a continuous process of remanence acquisition during displacement, rather than the subsequent acquisition of single discrete remanence components.

3.3.3.1 Compilation of the Data

For 5 specimens from each of the sites 49 - 55, Fig. 3.14 compiles the site means, the remanence directions and corresponding differential vectors during AF-demagnetisation.

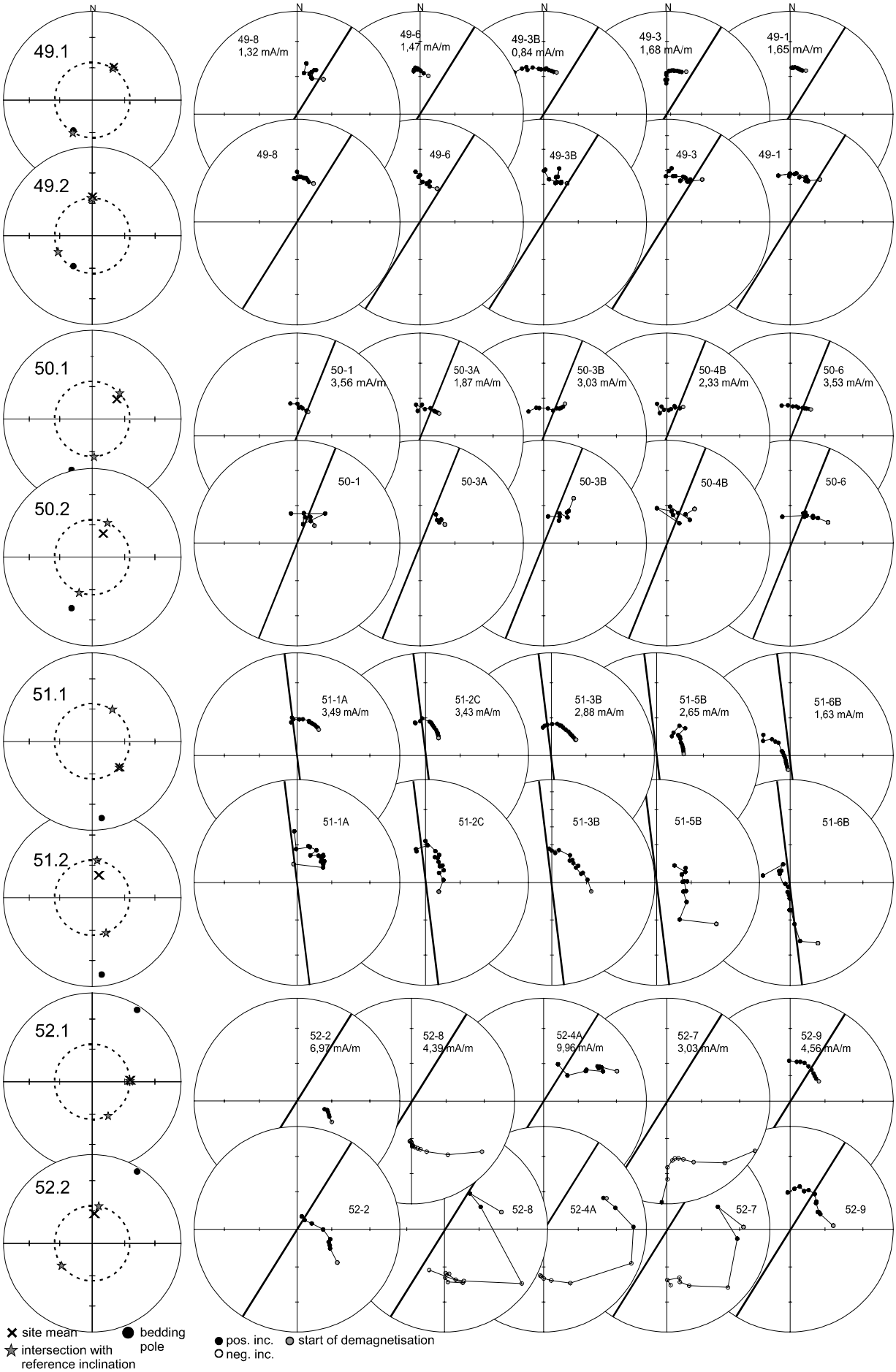

Fig. 3.14, continued on next page

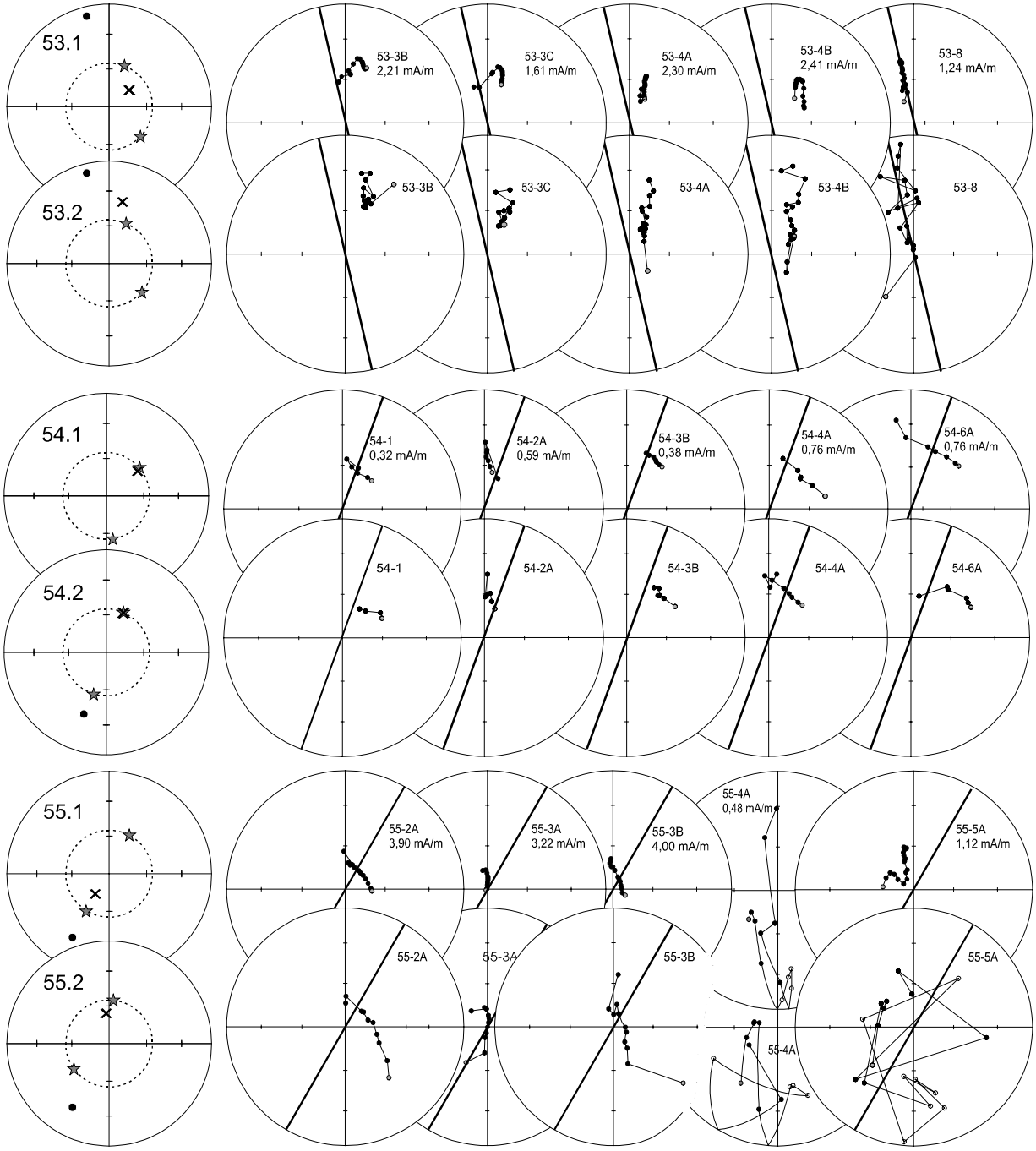

Fig. 3.14: Demagnetisation behaviour of five exemplary specimens from each of the sites 49 - 55 from the Jurassic limestones of the central Pamirs. Site means of low- and high-coercive components (x.1 and x.2) are given left. Stars mark the intersections of the remanence small circle with the small circle of constant field inclination (I = 55°) according to the reconstructions. Demagnetisation directions (sum vectors) are given in the upper row and corresponding differential vectors in the lower row. Π-circle is for individual bedding of each site. Natural remanent magnetisation (NRM) is given for each specimen. For discussion see text.

In sites 49 and 50 the remanences change only slightly during demagnetisation. The angles of block rotation and backtilting of the site means are small. There is no evidence for a relation to tilting. The demagnetisation paths in the equal-area plots probably record a clockwise block rotation up to about 30°, which is in compliance with the reconstruction of the site means 49.1 and 50.1.

In site 51 more displacement has been recorded. The specimens give a path mostly parallel to the Π-circle, hence a relation to tilting. The clockwise block rotation has still been recorded, as reflected by the higher-

coercive remanence directions at the end of the demagnetisation path. The reconstruction with backtilting by 56° giving a -22° clockwise block rotation is the correct solution for the site mean 51.1. The tilt since remanence acquisition has been to the north. According to specimens 51-2C, 51-5B and 51-6B, whose distributions are rather parallel to the Π-circle, block rotation seems to have occurred mostly after folding, and not simultaneously.

In site 52 the behaviour is more complex. A reversal of the magnetic field seems to have occurred during the remanence acquisition. From the reconstruction of the site means, the angles of backtilting are low, hence, tilting is not expected to have a major influence. Specimens 52-2 and 52-9 show a clockwise block rotation. In contrast, the remanence directions of the remaining specimens start with a normal polarity and move towards the reverse polarity field during progressive demagnetisation. This is best reflected by the differential vectors. The reconstruction of the low-coercive site mean is in compliance with the clockwise block rotation recorded by the specimen 52-9.

In site 53, the differential vectors move predominantly parallel to the Π-circle and therefore are related to tilting. The angles of backtilting for the site means are low (19° and -21°) and have opposite senses: The low-coercive site mean implies a tilt to the north after remanence acquisition, whereas the high-coercive site mean indicates a tilt to the south by about the same amount. The reversing sense of tilting is better reflected by the change of the remanence directions (upper row) during demagnetisation.

Site 54 does not show significant changes. The path of the remanence directions during demagnetisation is most probably related to clockwise block rotation, as also indicated by the small angles of backtilting for the site means.

Site mean 55.1 requires the highest amount of untilting (89%) and therefore might be primary (see section 3.3.2). If so, there is at least one discrete remanence component which is much older than the others, and to which the later secondary record has been added. Except for specimen 55-3A and maybe 55-5A, the demagnetisation paths do not clearly reflect tilting. A reasonable explanation for the demagnetisation paths requires a tilt axis different from the one defined by the present bedding, e.g. a tilt to the west around a N-S oriented axis. Therefore, the demagnetisation path cannot be related clearly to tilting or block rotation.

Specimens 55-5A, 55-4A and 55-4B (similar to 55-4A, not shown in Fig. 3.14) are interpreted to show a reversal within the time interval of remanence acquisition during the tectonic displacement. In this case, the duration of remanence acquisition and folding must be in the order of the time necessary for a field reversal.

Summarising, the majority of the specimens depicts remanences that during demagnetisation seem to move on small circles. This directional change most probably is related to tilting or block rotation, thus defining a displacement path. In most specimens, at least three different remanence components must be present, in some of them a minimum of four is required to explain the demagnetisation behaviour. There are several observations that point to a (partly) continuous remanence acquisition:

- The palaeomagnetic displacement path in most specimens seems to be complete, ending up close to the reference field direction.
- The complete record of a reverse field polarity interval in the course of tectonic displacement in several specimens of different sites.
- The record of a reversal of the sense of tilting during folding.

3.3.3.2 Overprinting Due to the Metamorphic Dome

Site 49 which is closest to the dome, yields no significant tilting and only a small block rotation. The other sites generally reflect higher changes of the in-situ remanences, i.e. related to tilting. The largest record is given by the site 55, whose low-coercive components may be of primary character. There seems to be a relation to the distance to the metamorphic dome: The more distant from the dome, the more extensive is the magnetic record of the tectonic displacement in a site, especially of folding. Therefore, overprinting and tectonic displacement are probably associated with the rise of the dome. Consequently, the geochronological ages of about 20 Ma for the dome place an upper limit on the age of the secondary remanences. Assuming that folding occurred approximately at the same time throughout the sequence, later followed by block rotation, the magnetic record within the sequence must have ended a little earlier in the distant sites.

3.3.3.3 Implications on the Process of Magnetic Overprinting

Overprinting is often related to temperature producing thermal remanences. Within the scale of an outcrop, the temperature is not expected to differ by more than a few degrees. Thus, the remanences in the specimens of one site should not differ much beyond the effect of secular variation. However, the variation of the magnetic record within the specimens of the sites is surprisingly high. For instance, in sites 52 and 55 some specimens recorded a reversal and others not. Obviously, the ages of the remanences from specimens a few metres apart differ significantly. Heating and cooling in a temperature field hardly can account for such variations, because a temperature field is homogeneous within the scale of a few metres. The reason for the heterogeneity must be found in the process of overprinting, which did not add new components to an existing remanence, but seems to have faded out or replaced the primary remanences. A chemical process with fluids migrating through the rocks, changing the ferrimagnetic minerals and producing new chemical remanences (CRM) is likely to be responsible. Such a process should account for several observations:

- A (possibly) continuous remanence acquisition.
- A fading out of existing remanences.
- The presence of a spectrum of coercivities.
- The decreasing age of the secondary remanences with increasing coercivity.

A continuous remanence acquisition implies an also continuous formation and blocking of ferrimagnetic grains, which in a chemical process is likely to perform. If migrating fluids are considered acting on existing magnetite particles, it is plausible that smaller particles alterate easier and faster than larger ones. This could explain the low coercivities of the possibly primary remanences of site means 51.1 and 55.1 and the fading out of the primary remanences in the other sites.

Low-coercive components usually are carried by larger magnetite grains with a few or more domains (pseudosingle domain particles, PSD), whereas high-coercive remanences relate to smaller (single-domain, SD) particles. The secondary remanences - be it a continuous record or three to four discrete components - encompass a spectrum of coercivities and therefore must be carried by magnetite particles with a spectrum of grain sizes. According to the recorded displacement paths, particles with increasing grain size (decreasing coercivity) have an increasing age.

The following scenario could be an explanation for this:

Chemical processes produce small ferrimagnetic particles that continuously grow. As they pass from a superparamagnetic into a singledomain status, they acquire a remanence. The growth continues lowering the coercivity, but does not change the remanence direction acquired. This process of grain formation and growth must act over the time interval of remanence acquisition. The result will be a spectrum of grain sizes in which the larger grains carry the older remanence.

3.3.3.4 Constraints on the Time of Overprinting and Folding in the Muzkol Zone

This last topic addresses the duration of overprinting and hence folding, which in turn is connected to the uplift of the dome. The upper age limit on the secondary remanences is given by the geochronological cooling ages of about 20 Ma for the rocks from the dome (see section 2.1). The specimens that record significant tilting and block rotation and thus enclose a certain time interval, have predominantly remanences with a normal polarity. Several specimens from sites 52 and 55 are thought to have recorded a reversal in the course of tectonic displacement and remanence acquisition. In the Miocene around 20 Ma ago, normal and reverse polarity chrons alternate with about the same duration (magnetic polarity time scale from Ogg 1995). The largest normal polarity chron is from about 20 Ma to 19 Ma. The other normal and reverse chrons around are much shorter. Hence, assuming that the palaeomagnetic data are representative, the acquisition of the secondary remanences and thus the recorded displacement are constrained to a time duration of not more than 2 Ma.

3.3.3.5 Summary of the Above Observations

The following conclusions can be drawn from the observations:

- Uplift of the metamorphic dome went along with remanence acquisition and tectonic deformation of the adjacent sediments.
- Block rotation performed after folding.
- The rise of the metamorphic dome probably is associated with magnetic overprinting, thus also placing an upper limit of about 20 Ma on the age of the secondary remanences.
- The relation of the change of the remanences and the tectonic displacement with the occurrence of at least three to four discrete remanence components during AF-demagnetisation and the relation between coercivity and age of the secondary remanence point to a (partly) continuous process of remanence acquisition.
- The frequency of normal and reverse polarity remanences constrains the remanence acquisition and hence the record of folding to a narrow time interval of probably not more than 2 Ma.
- There has been no further tilting subsequent to the rise of the dome 20 Ma ago, because the magnetic record probably ended at that time and today the high-coercive remanences are still close to the reference field direction.

3.3.4 Compilation of Results

Fig. 3.15a shows the block rotations and Fig. 3.15b both reconstructed and present tilting directions, according to the reconstructions listed in Table 3.8. The site means of the granites within the metamorphic rocks have been incorporated (block rotation as declination difference to reference field), since their remanences show reasonable values (see Table 2.3), that cannot have been changed significantly by tilting. Biotites of these granites give Ar-Ar cooling ages of about 20 Ma (see section 2.1). However, the in-situ

inclinations of about 44° appear too low for this age. Since there is no tectonic control on these remanences, they are shown with a question mark (see Fig. 3.15).

The block rotations of sites 38 - 44 scatter, but on the whole tend to be counterclockwise like those of the sites south adjacent to the metamorphic dome.

In contrast, the sites of the Muzkol zone reveal clockwise block rotations. The mean block rotation for the whole sequence as determined from the low-coercive components is -32°. The site means 47 and 48 (Tertiary red beds), which could be primary, do not have undergone block rotation, whereas the sites 45 and 46 support the overall trend in the area.

The present tilting directions of all sites exhibit a mean orientation of about 15° (see Fig. 3.15b), thus close to north. The reconstructed tilting directions are more to the west (mean trend of 347°) reflecting this overall clockwise block rotation. For the total of the sites, the variation of the reconstructed tilting directions is twice as high as today. There seems to be the same relationship as in the southern Pamirs: Strata line up perpendicular to the shortening direction in the course of further convergence (see section 3.2.3). Oroclinal bending, however, would have rotated the tilting directions away from north.

The complete data set of the central Pamirs appears to be too heterogeneous to assess shortening from the block rotations like in the southern Pamirs. The folded sequence of the Muzkol zone (sites 45 - 55) seems to appropriate. Table 3.9 lists the results.

Table 3.9: Finite N-S oriented uniaxial shortening ($1-l/l_0$; l_0 original length, l length after shortening) to reduce the standard deviation of the reconstructed tilt axes to the one of the present tilt axes for the sites of the Muzkol zone. Incremental tilt axes are excluded. Involved site means: 45 - 48, 49.1, 50.1, 51.1, 52.1, 53.1, 54.1 and 55.1.

	standard deviation (°)		finite shortening by
tilt axes from	at present	reconstructed	$(1-l/l_0)$
sites 45 - 55	23,1	15,4	0,39

Assuming N-S oriented convergence, a shortening by 0,39 (to 0,61) is required to reduce the standard deviation of the reconstructed tilt axes to the one of the present tilt axes. This figure is significantly below the shortening amount of 0,64 derived for the southern Pamirs.

Fig. 3.15 (following page): (a) Block rotations as the angular difference between the reconstructed and the present tilt axes. Block rotation for site means of the granites of sites 38 and 39 as declination difference to the expected declination value (see Table 2.3) is incorporated with a question mark. Dashed arrows indicate incremental block rotation as inferred from younger remanence components. Confidence intervals as $\pm\alpha 95/\cos I_{acq}$. (b) Present and reconstructed tilting directions. Dotted lines for incremental tilting directions. Tilting directions are shown in equal-area plots separately for all sites together and for the sites of the Muzkol zone with number (n), azimuth of a resultant mean and standard deviation (Sd). Reconstructions listed in Table 3.8. Map overview in Fig. 2.2. For discussion see text.

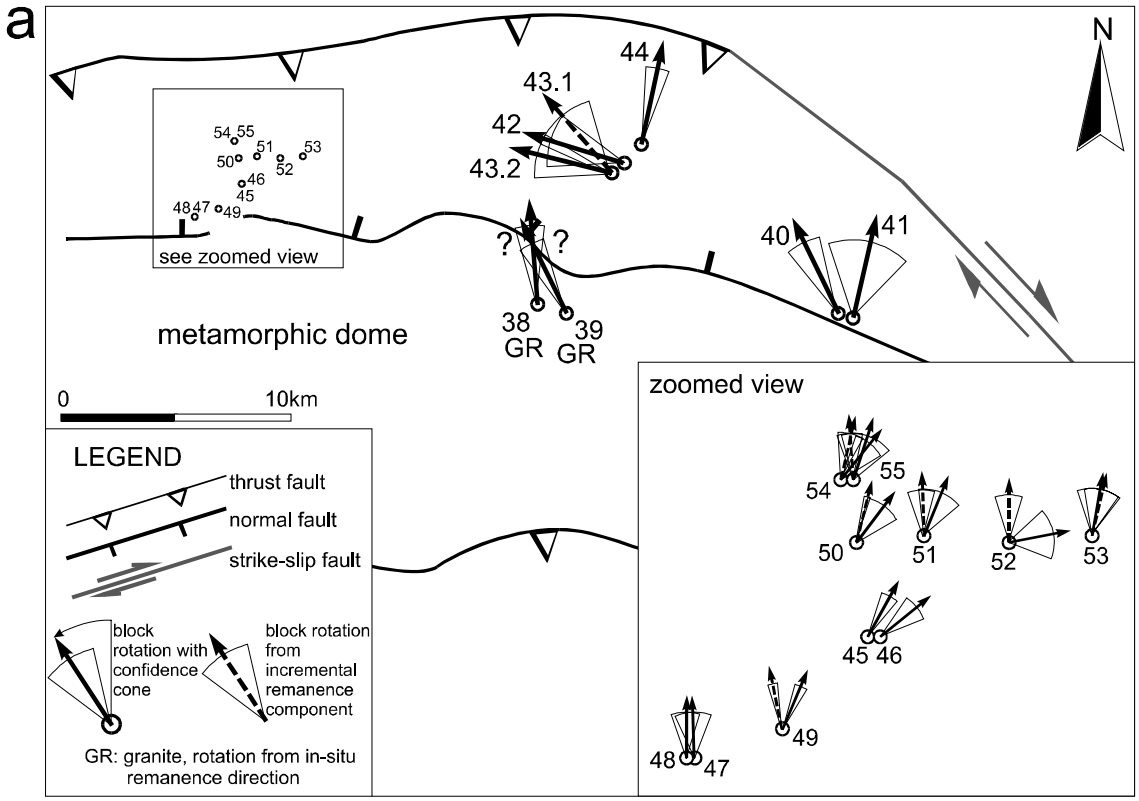
a
N
44
43.1
42
43.2
54 55
50 51 53
52
46
45
48 47 49
see zoomed view
?
?
40
41
metamorphic dome
38 GR
39 GR
0
10km
zoomed view
LEGEND
thrust fault
normal fault
strike-slip fault
block rotation with confidence cone
block rotation from incremental remanence component
GR: granite, rotation from in-situ remanence direction
54
55
50
51
52
53
45 46
48 47
49

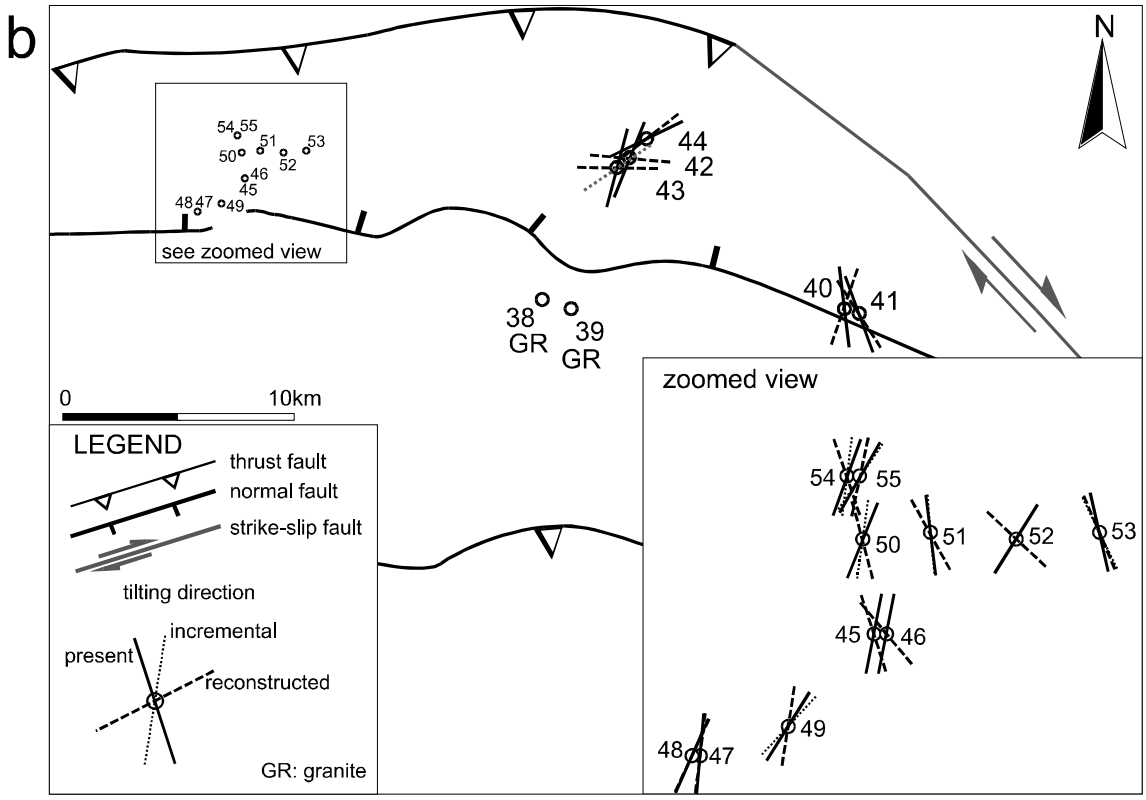
b
N
54 55
50 51 53
52
46
45
48 47 49
see zoomed view
44
42
43
40
41
38 GR
39 GR
0
10km
zoomed view
LEGEND
thrust fault
normal fault
strike-slip fault
tilting direction
present
incremental
reconstructed
GR: granite
54 55
50
51
52
53
45 46
48 47
49

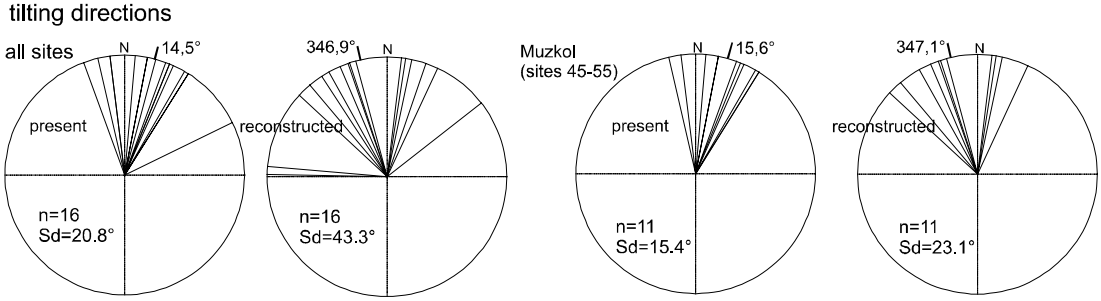
tilting directions
all sites
N
14,5°
present
n=16
Sd=20.8°
346,9°
N
reconstructed
n=16
Sd=43.3°
Muzkol
(sites 45-55)
N
15,6°
present
n=11
Sd=15.4°
347,1°
N
reconstructed
n=11
Sd=23.1°

3.4. Northern Pamirs and Alai range

In the northern Pamirs 10 sites have been taken from Early Cretaceous limestones, Late Cretaceous red beds and Tertiary sediments (Fig. 3.16). Two sites are situated in Tertiary sediments of the Alai range. The sites 62 - 74 belong to a unidirectionally folded sequence. None of the rocks shows macroscopic signs of metamorphism.

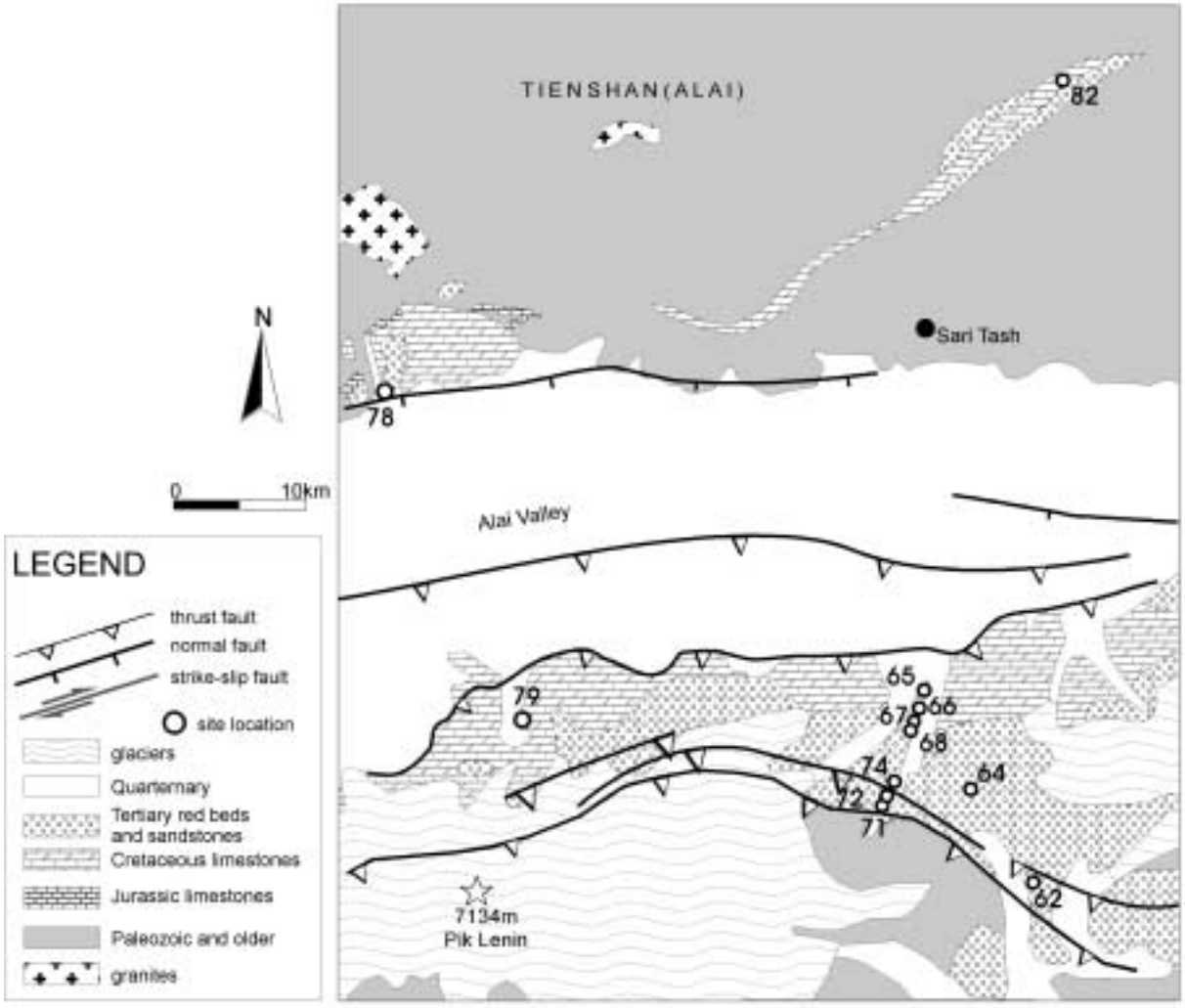

Fig. 3.16: Geologic map of the northern Pamirs with site locations. Sites 62 - 74 belong to a unidirectionally folded sequence. For map overview and references see Fig. 2.2.

The fold tests show a secondary character for the remanences of the Cretaceous sites. The positive fold test for the Tertiary sites 62, 64 and 74 is doubtful, because the bedding corrected inclination values are too low to be primary (see section 2). Again, the remanences have an overall secondary character. There are no geochronological constraints on the age of the remanences from immediately adjacent rocks as in the southern and central Pamirs. The nearest rocks dated are Triassic granites at the Karakul lake, where fission tracks in apatites give cooling ages around 20 Ma (see section 2.1). Overprinting might be associated with the same metamorphic event as in the southern and central Pamirs. The age of the remanences is supposed to be about 20 Ma, coinciding with the begin of thrusting as given by Wang et al. (1992).

Assuming about 300 km of shortening between the northern Pamirs and Eurasia in the past 20 Ma (see Burtman & Molnar 1993), the reference palaeoinclination 20 Ma ago (see Fig. 2.3) was about 57°. This

estimate is supported by the d-angle of site mean 67: Now having a dip to nearly west (bedding 279°/25°), its *d*-angle implies a maximum I_{acq} of 57,6°. Thus, for the reconstructions a reference palaeofield of D/I = 10°/57° will be assumed.

For the Tertiary sites in the Alai range, there is no constraint on the remanence age besides the age of the rocks. As the reference, a palaeofield of D/I = 10°/60° will be taken for the Alai range, corresponding to a Miocene age.

3.4.1 Reconstruction of the Folded Sequence of Sites 62 - 74

The sequence consists of 5 Cretaceous and 5 Tertiary sites. The palaeoremanences in the limestones are carried predominantly by magnetite, and in the red beds by haematite and magnetite. Only site 65 yields two remanence, each providing a significant Fisher mean. Small-circle distributions within the individual sites or single specimens during demagnetisation are not evident. Sites 63 and 72 have been rejected, because their remanences scatter beyond significance. The bedding poles define a unidirectionally folded sequence (Fig. 3.17a). The pole of the Π-circle (mean tilt axis) has an azimuth of 121,0° and a dip of 2,0°. For the reconstruction, the Π-circle is assumed to be vertical.

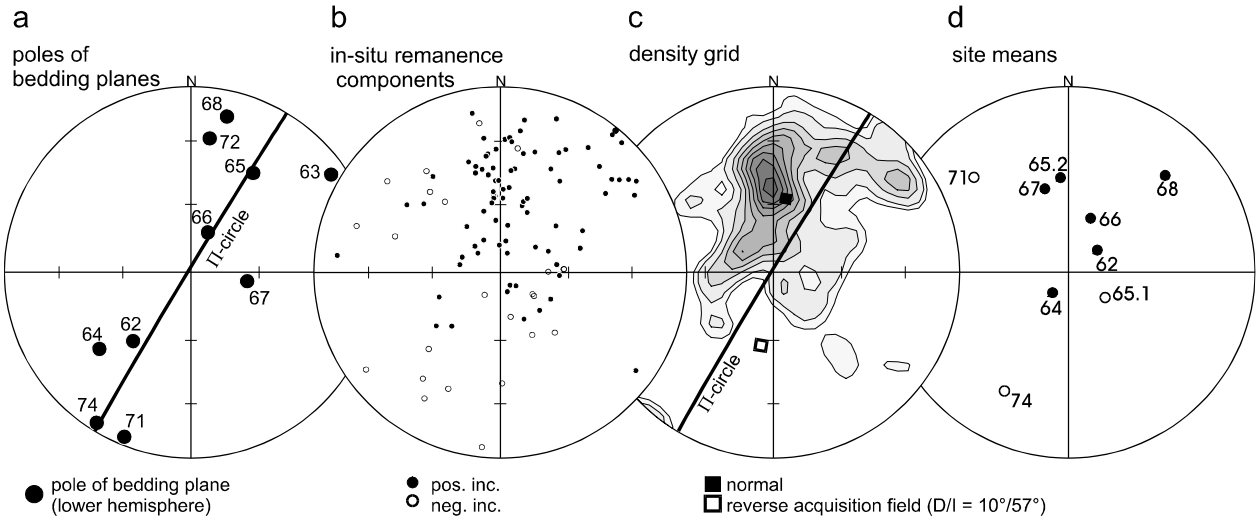

Fig. 3.17: Bedding data and remanences of the folded sequence in the northern Pamirs. (a) Bedding poles and Π-circle. The pole of the Π-circle (mean tilt axis) has an azimuth of 121,0° and a dip of 2,0°. (b) 92 in-situ remanence components of site means 62, 64, 65.1, 65.2, 66 - 68, 71 and 74. (c) Density grid of the remanence components. Components of sites 65.1, 71 and 74 with negative inclination have been inverted, assuming they did not change the hemisphere through tilting. Distribution shows a trend parallel to the Π-circle. (d) Site means.

For the calculation of the density grid, the components of sites 65.1, 71 and 74 with a negative inclination have been inverted, assuming that these remanences did not change the hemisphere through tilting. The distribution shows a concentration near the reference field direction. A relation to tilting might be given, according to the scatter parallel to the Π-circle, but the tilt angles are small. The small-circle reconstruction gives a clockwise block rotation of -14° as the shortest reconstruction (see Table 3.9).

remanence components of sites 62,64,65.1,65.2,66,67,68,71			
reference field D/I = 10°/57°			
number of components	92		
mean *d*	-0,07		
mean *d*-angle (°)	93,9		
standard deviation (°)	24,0		
95% confidence interval (°)	5,0		
azimuth of pole of mean tilt axis (°)			
present	121,0	95% confidence interval (°)	
		(+)	(-)
reconstructed	107,2	9,3	13,8
block rotation (°)	-13,8	9,3	13,8

Table 3.9: Small-circle reconstruction of the remanence components of the folded sequence in the northern Pamirs, giving a -14° clockwise block rotation as the shortest and therefore most probable solution. The other three direct solutions require much higher amounts of backtilting and block rotation and hence are unlikely. For definitions, conventions and equations see section 1.

3.4.2 Reconstruction of the Single Sites

Table 3.10 summarises the relevant parameters and the reconstruction chosen as the most probable for each site. Fig. 6.5 in the appendix shows all four direct reconstructions.

Site 71 which contributes to a positive fold test (see section 2.6.8), gives a maximum I_{acq} of 41,4°, which is far below the reference field inclination. Hence, this site will be discarded.

Table 3.10: Reconstruction of the sites of the northern Pamirs. Only the most probable reconstruction is listed. For other possible reconstructions and graphical representation see Fig. 6.5 in the appendix. dip az./dip: azimuth and angle of dip, upright and overturned bedding is given where identified in the field. *d*: angular distance, I_{acq} max.: maximum palaeoinclination, % of untilting: percent of untilting related to the present dip assumed to be upright. Remark: upright or overturned (overt.) bedding as the consequence of the comparison of the present bedding with the sense of untilting (assuming that tilting did not reverse), indiff.: indifferent, used when angle of untilting is below ±10°, >dip: angle of untilting exceeds dip for either upright or overturned position by more than 10°. $\alpha 95/\cos I_{acq}$: confidence interval of the declination. For conventions, definitions and equations see Fig. 1.1 and section 1. Site 71 (not listed) has been discarded because it requires a much too low maximum I_{acq} of 41,4°. Site 78 (not listed) yields two reconstructions with the same probability. For bedding data and palaeomagnetic results see Table 2.3.

site	dip az.	dip	bedding	*d*	*d*-angle	I_{acq} max.	back-tilting	block-rotation	reconstruction point		% of untilting	remark	$\alpha 95/\cos I_{acq}$
	(°)	(°)			(°)	(°)	(°)	(°)	D (°)	I (°)			(°)
62	40	40	upright	0,05	93,1	86,9	-18	-36	46	57	44	upright	20,7
64	50	54	upright	0,04	92,1	87,9	-44	-44	54	57	82	upright	32,7
65.1	212	53	overt.	-0,34	70,4	70,4	-26	16	174	57	-49	overt.	18,9
65.2	212	53	overt.	-0,41	65,9	65,9	13	27	343	57	25	upright	14,3
66	203	19	-	-0,01	89,5	89,5	-7	-12	22	57	-36	indiff.	24,1
67	279	25	-	0,54	122,4	57,6	7	11	359	57	12	indiff.	14,7
68	193	75	upright	0,47	117,8	62,2	40	-62	72	57	54	upright	18,0
74	32	85	overt.	-0,06	86,4	86,4	29	-29	205	-57	-34	overt.	31,4
79	150	34	-	-0,18	79,8	79,8	20	59	311	57	57	upright	26,4
82	140	27	-	0,08	94,5	85,5	-2	41	329	60	-7	indiff.	21,0

On the whole, the net displacements are moderate. Thus, mostly one reconstruction can be chosen, which shows by far the smallest displacement. Upright and overturned bedding - where identified in the field - are confirmed by the reconstructions in all cases, except for site 65, whose two site means have opposite senses of untilting. In the field, overturned bedding has clearly been identified from cross bedding. The reconstruction of site mean 65.1 is in compliance with that, but site mean 65.2 exposes the opposite sense

of tilting. As the block rotation of site mean 65.2 is higher, it should be older than 65.1. Thus, tilting has changed its sense after acquisition of site mean 65.2.

Site 67 offers two reconstructions which are close to each other with respect to both backtilting and block rotation (see Fig. 6.5). This is the consequence of tilting close to an original E-W orientation. The reconstruction with the smallest angle of backtilting has been chosen.

The sites 62, 64 and 71 give a positive fold test (see section 2.6.8). However, considering the angles of backtilting, only site 64 might be close to a primary character with 82% of untilting. Having 44% of untilting, site 62 is far away from that. Site mean 71 cannot be explained by tilting and block rotation of a remanence acquired in the reference field. Consequently, the fold test involving these sites cannot be valid.

Site 78 offers two equivalent reconstructions (see Fig. 6.5) which are thought to have the same level of probability. Both are related to a normal polarity field. The first has a much smaller displacement, however, the second solution with 106% of untilting implies a primary character of the remanence. Both solutions are equally reasonable. Since they are contradictory with opposite block rotations, the site will be discarded until further evidence is available.

Fig. 3.18 illustrates the displacement of the bedding poles, assuming that block rotation occurred after tilting. The layers are now generally steeper. There is no predominant sense of tilting and the obtained block rotations are both clockwise and counterclockwise.

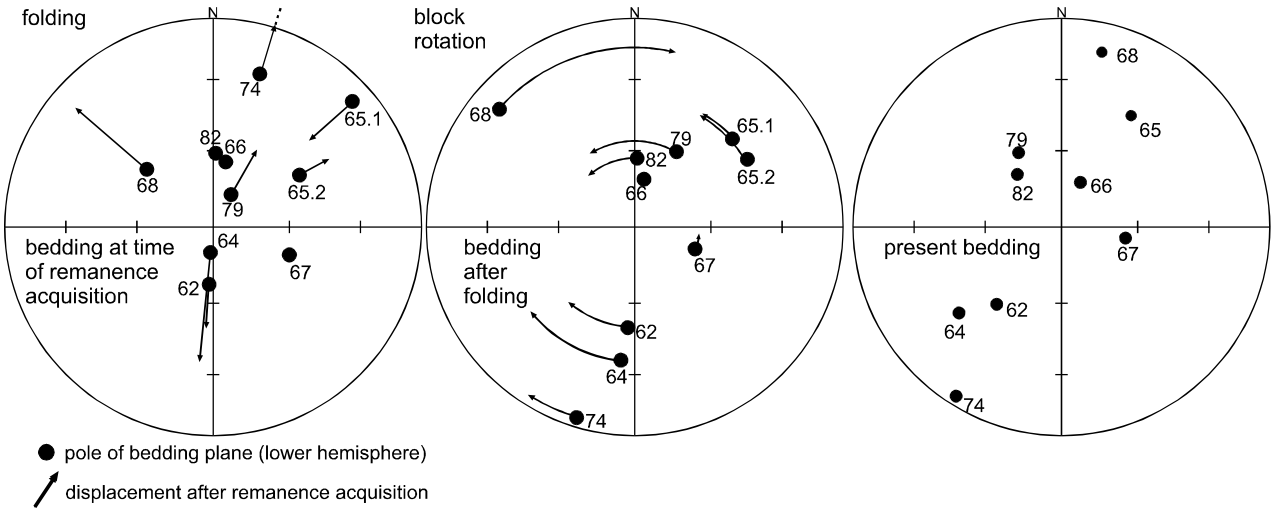

Fig. 3.18: Reconstruction of the bedding for the sites of the northern Pamirs. Left: Bedding at time of remanence acquisition, arrows indicate subsequent tilting. Middle: After folding and before block rotation, arrows indicate subsequent block rotation. Right: Present bedding. For discussion see text.

3.4.3 Compilation of Results

Fig. 3.19a shows the block rotations and Fig. 3.19b both reconstructed and present tilt directions. Within the folded sequence, the rotations turn out to be predominantly clockwise, except for sites 65 and 67. Site 79 and site 82 in the Alai range give counterclockwise block rotations.

Unlike the sites in the central and southern Pamirs, the reconstruction reduces the variation of the tilting directions (Fig. 3.19b). The reconstructed tilting directions are close to N-S for the sites 62, 64, 66 and 74, and the site 82 in the Alai range. Block rotation turned them away from north indicating oroclinal bending. In contrast, at sites 65 and 68 the tilting directions rotated due north, indicating the same behaviour as in the southern Pamirs: Tilt axes rotate due an orientation perpendicular to shortening during progressive convergence. This is reasonable for these two sites, because their reconstructed tilting directions are far off north. Hence, block rotations are predominantly controlled by oroclinal bending, but block rotation of "incompatible" layers within the folded sequence occurs as well.

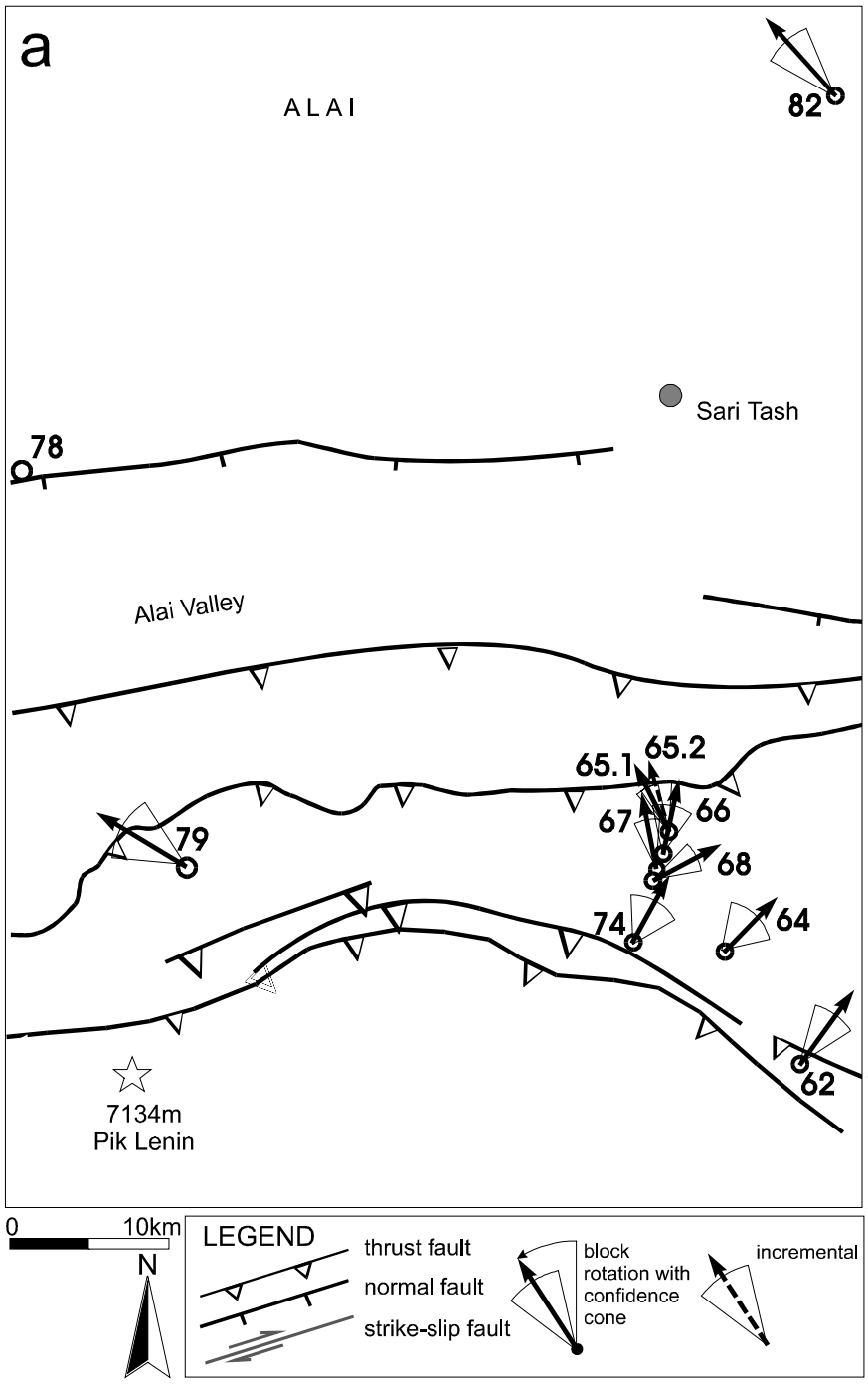

Fig. 3.19a: Block rotations as the angular difference between the reconstructed and the present tilt axes. Site mean 65.1 most probably is younger, reflecting an increment of block rotation. Confidence intervals as ±α95/ cos I_{acq}. Fig. 3.19b see next page.

On the whole, the arrows of the block rotations seem to be perpendicular to the strike of the adjacent thrusts, indicating oroclinal bending.

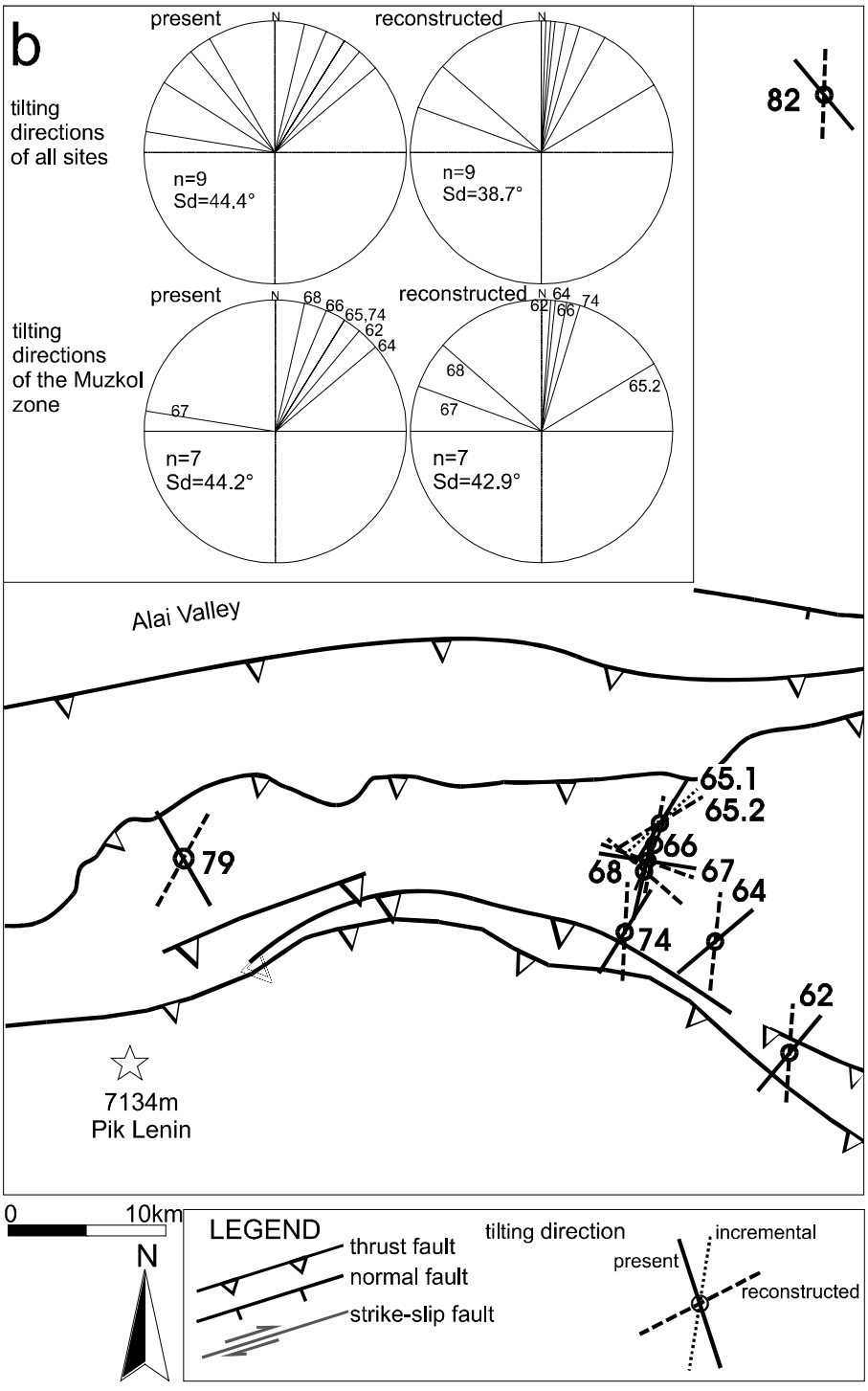

Fig. 3.19: (b) Present and reconstructed tilting directions. Dashed lines for incremental tilting directions. Tilting directions are shown separately in equal-area plots. Sd: standard deviation around a resultant mean. For discussion see text.

3.5 Synthesis

3.5.1 Primary or Secondary - Fold Tests and Small-Circle Reconstruction

The small-circle reconstruction shows that among the remanences with overall secondary character - as shown by the fold tests - a few primary remanences occur. On the other hand, remanences that seem to be primary according to fold tests (sites 62, 64 and 71), turn out to be undoubtedly secondary according to the small-circle reconstruction. Hence, the small-circle reconstruction shows the remanence character for each site individually, while the fold tests give an overall either primary, secondary or indifferent character for a number of sites. Combining both methods, the maximum of information regarding the remanence character will be obtained.

3.5.2 Palaeofield Inclination and Drift Constraints

The maximum angular distances of the site means indicate that the palaeoinclination in the southern Pamirs at the time of remanence acquisition 20 Ma ago unlikely exceeded 55° (see section 3.1). The difference of 4° to the expected mean value of 59° from the APWP of stable Eurasia (see Fig. 3.20) implies a mean shortening between the southern Pamirs and Eurasia of about 440 km since remanence acquisition. This is in good agreement with the 300 - 700 km of Cenozoic shortening given by Burtman & Molnar (1993).
Supposedly primary remanences that could give information about the Mesozoic drift history, have been obtained from the Late Cretaceous sites 42 and 43.2 and the Middle to Late Jurassic sites 51.1 and 55.1 in the central Pamirs. Fig. 3.20 compares the inclinations of these sites to the expected value from the APWP for stable Eurasia.

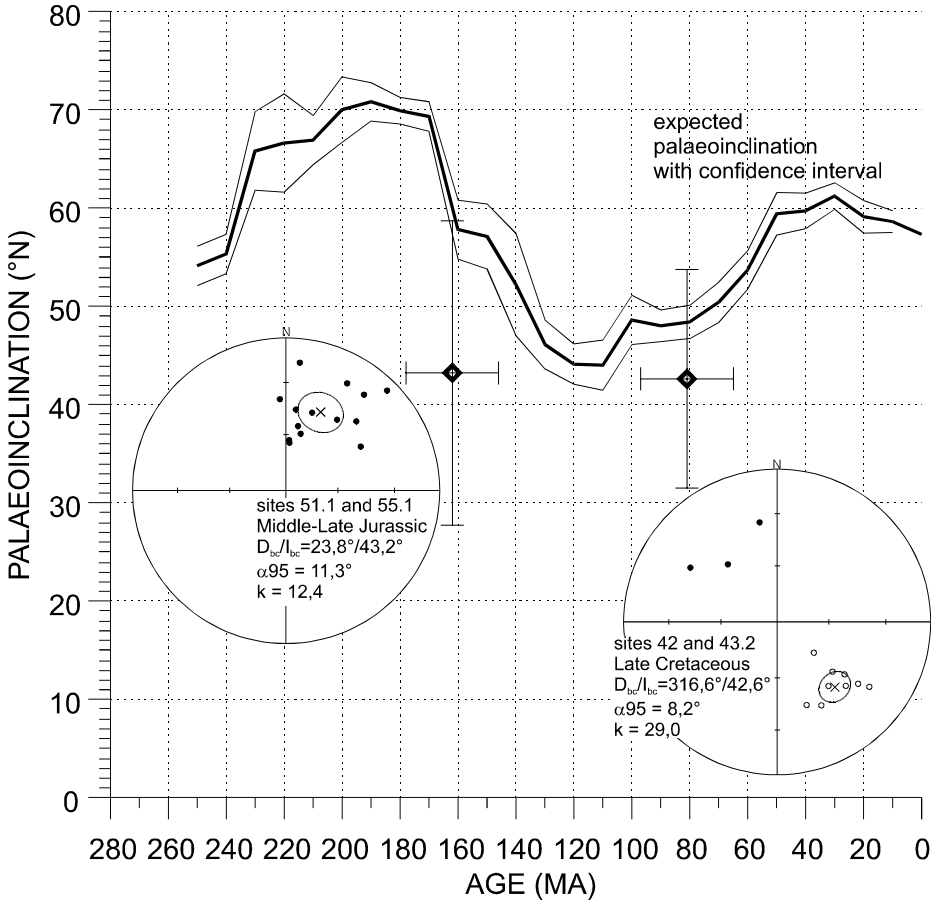

Fig. 3.20: Palaeoinclination of supposedly primary sites from the central Pamirs in comparison to the expected value for a location at long./lat. E74.00°/N38.00° on Eurasia (calculated using APWP for stable Eurasia from Besse & Courtillot, 1991). Sites 42 and 43.2, and 51.1 and 55.1 have been taken together for calculation of a Fisher mean. For discussion see text.

The mean inclination of sites 42 and 43.2 is on the average about 5° south of the expected value for the corresponding mean age of the sites. Taking into account northward Cenozoic shortening of 300 - 700 km as given by Burtman & Molnar (1993), the mean inclination of these sites corresponds well with the expected value.

The mean inclination of the Jurassic sites 51.1 and 55.1 is about 15° (for the mean age) below the expected value. The inclination difference could reflect a more southern position of these rocks in the Jurassic. As the site location is north of the Mesozoic suture (see Fig. 3.21), this observation would imply significant crustal shortening of Eurasia before the India-Asia collision, probably associated with the accretion of the southern Pamirs to Eurasia in the Late Jurassic - Early Cretaceous. However, the few data (14 remanence components from 2 sites) and the large changes of the expected inclination over the time interval do not allow for a reliable statement.

3.5.3 The Tectonic Setting

Fig. 3.21 compiles block rotation, tilt after remanence acquisition, and present and reconstructed tilting directions for the investigated area. Tilting directions and tilt for groups of sites are given separately in equal-area plots together with the calculation of the standard deviation around a resultant mean.

In the northern Pamirs, the arrows for the block rotation mostly are arranged perpendicular to the strike of the thrusts. The standard deviation of the tilting directions is lower at the time of remanence acquisition than today. Hence, oroclinal bending is likely to have occurred there, rotating the original tilting directions away from north. Thrusting apparently started along a straight E-W trending thrust that later became bent in the course of further shortening. This is in compliance with the present arrangement of thrust faults in the area. The northernmost frontal thrust is straight, while towards south the curvature of the thrusts increases. This observation represents progressive oroclinal bending on the scale of a few kilometres.

In the central and southern Pamirs the block rotations scatter and do not give an overall consistent pattern. The tilting directions, however, yield a consistent behaviour for all data sets (see equal-area plots in Fig. 3.21):

1. The standard deviation of the reconstructed tilting directions is higher than the standard deviation of the present tilting directions.
2. The present tilting directions are, on the whole, closer to north than the reconstructed ones.

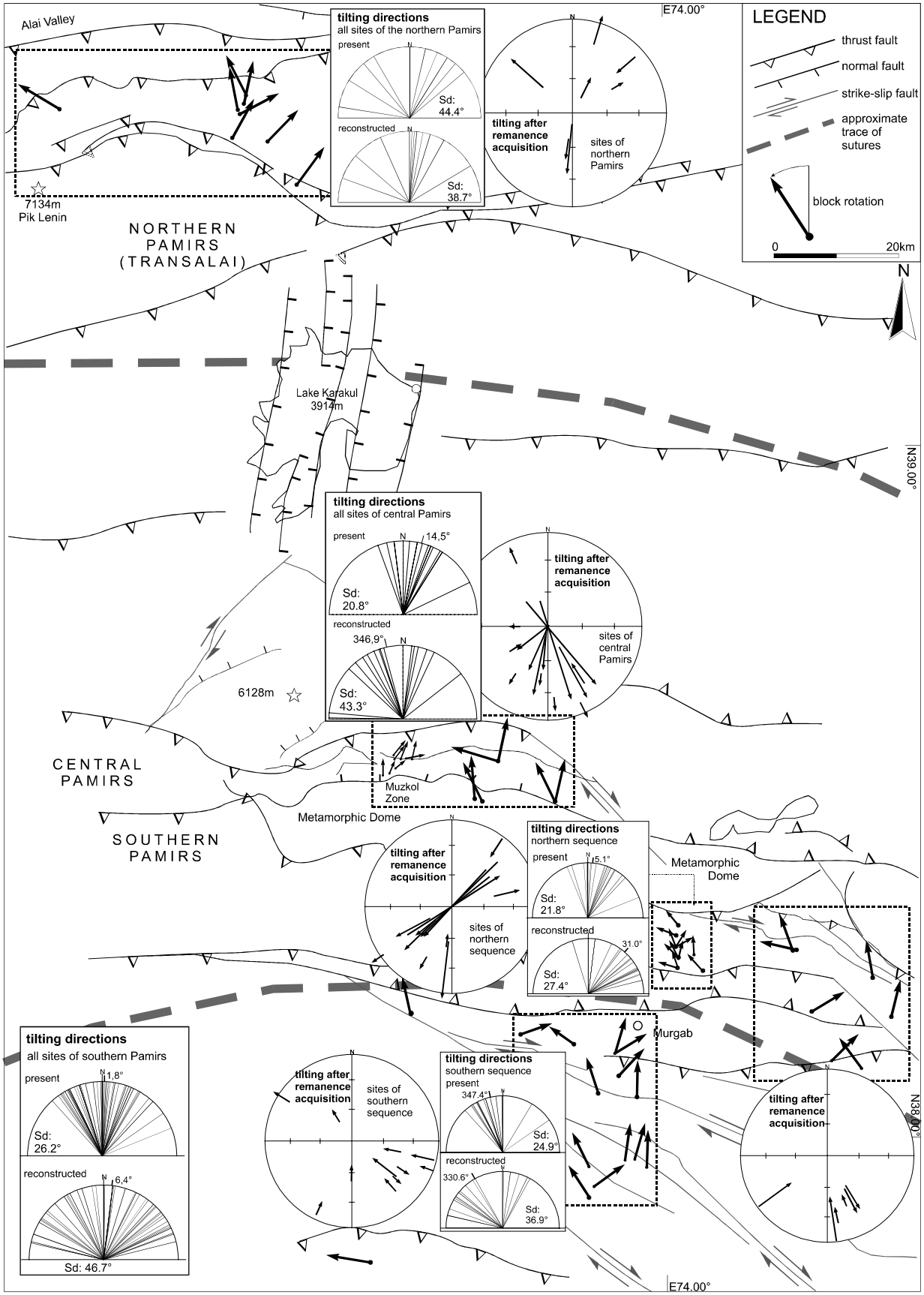

Fig. 3.21: Compilation of present and reconstructed tilting directions, block rotation and tilting since remanence acquisition. Tilting directions and tilting are given in equal-area plots for a number of sites as framed by the rectangles. Tilting in equal-area plots is shown in the orientation before block rotation. Tilting directions for the Muzkol zone are not shown separately (see Fig. 3.15b). Approximate traces of Palaeozoic (northern one) and Mesozoic (southern one) sutures as given by Burtman & Molnar (1993). For geologic map and references see Fig. 2.2. See text for discussion.

This behaviour is found in the total of the tilting directions as well as in each of the unidirectionally folded sequences. In contrast to oroclinal bending which rotates the tilting directions away from the overall convergence direction, they have been rotated towards the convergence direction (Fig. 3.22). Thus, a rather uniform regime of N-S shortening is likely to have caused the block rotations in the southern and central Pamirs. In such a process block rotation and tilting must have performed simultaneously or in alternating increments.

This observation is furthermore supported by field evidence from the geologic map: The thrusts in the southern Pamirs and also the metamorphic dome are trending rather straight from west to east until they are cut by the strands of the Pamir-Karakorum fault. Oroclinal bending would have bent them.

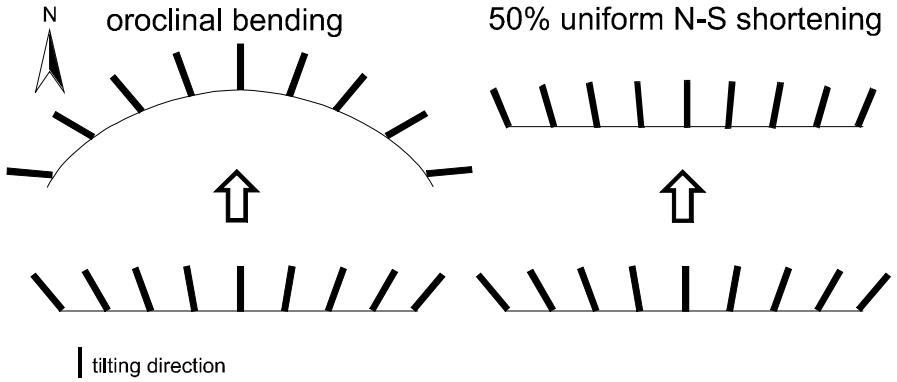

Fig. 3.22. Oroclinal bending in a N-S convergence regime rotates the tilting directions away from north increasing their scatter. Uniform N-S shortening rotates them due north reducing the scatter. This process probably has occurred in the southern and central Pamirs.

As the block rotations depend on the initial tilting directions and the direction and amount of the overall convergence, shortening can be quantified if its direction is known. Such a quantification has been carried out for the data set of the southern Pamirs, giving finite shortening by 64% (see section 3.2.3), and for the Muzkol zone, giving shortening by 39% (see section 3.3.4). These figures can be compared to the amounts of Cenozoic shortening given by Burtman & Molnar (1993): The whole southern Pamirs including the Rushan-Pshart zone have a present N-S extent of about 100 km. From fault displacements and balanced cross sections, shortening is reported to be at least 240 km (Burtman & Molnar 1993 and references therein), giving an original N-S extent of 340 km. If 100 km are the result of shortening by about 60%, the original length was about 250 km, thus, below the minimum estimate of 340 km. While the shortening obtained by Burtman & Molnar (1993) accounts for the total effect of folding and fault displacements in the Cenozoic, the palaeomagnetic record started at a time where folding already had achieved a significant degree. For this reason, a shortening by about 4° of palaeolatitude since about 20 Ma ago seems to be a reasonable estimate.

Tilting after remanence acquisition in the southern part of the southern Pamirs has been predominantly to the south or south-east, reducing the predominant northward dip of the layer, thus, intensifying the south-vergence. To both sides of the metamorphic dome, tilting has been predominantly to the north or north-east, steepening up the strata in the folded sequences. Tilting apparently has been more intense close to the metamorphic dome than in the other areas investigated, suggesting a relation of the dome to folding of the adjacent sediments. Surprisingly, to both sides of the dome tilting has the same sense. A simple upward rise of the dome with northward tilting at its northern boundary and southward tilting to the south of it cannot have taken place.

In the Muzkol zone remanence acquisition performed simultaneously with tilting over a certain time interval, thus providing a tape-like record of tectonic displacement. It is evident from these displacement paths that tilting and remanence overprinting are closely related to the rise of the metamorphic dome, hence, an upper age limit of around 20 Ma (fission track cooling ages from the dome) can be assumed for the secondary remanences. Information about the duration of remanence acquisition is given by the frequency of normal (most of them) and reverse (a few) polarities of the remanences acquired during displacement. When compared to the magnetic polarity time table (Ogg 1995), the process of remanence acquisition and thus tilting around 20 Ma ago unlikely enclosed more than 2 Ma. Most of the younger in-situ remanences, acquired at the end of overprinting, are still close to the reference field. Thus, tilting in the Muzkol zone performed around 20 Ma ago over a short time interval of probably not more than 2 Ma. Since then there was no further folding, probably because the sequence with its now nearly vertical layers has been locked up. The only tectonic movements in the Muzkol zone since then can have been rigid fault displacements and/or an overall en-bloc displacement to the north.

Fig. 3.23 sketches a restoration of the original N-S extent of the southern and central Pamirs, and the amounts of shortening. About 440 km of total N-S convergence since 20 Ma between the southern Pamirs and stable Eurasia have been derived from the maximum angular distances of the site means. From this amount, about 160 km have been taken up by internal shortening in the southern and central Pamirs. If shortening within the metamorphic dome and the northern Pamirs is neglected, the remaining 280 km constitute a maximum estimate for overthrusting of the Pamirs onto the Alai range since about 20 Ma ago.
Most of the northern Pamirs consist of granites and metamorphic rocks consolidated in the Palaeozoic and therefore unlikely took up much internal shortening. It appears plausible that they acted as a rigid block, against which the central and southern Pamirs have been pushed in the course of progressive indentation of Eurasia. This could explain the high amounts of N-S shortening and the absence of oroclinal bending in the southern Pamirs.
In the Muzkol zone in the central Pamirs folding ended in the Early Miocene. Since then the only major movement in this region could have been an en-bloc N-translation.
The amounts of shortening given must be treated as rough estimates, however, independent from their statistical significance, the following sequence of events seems plausible:

- Northward convergence affects first the southern and central Pamirs, pushes them against the rigid block of the northern Pamirs and causes intense internal N-S shortening. At least in the central Pamirs internal shortening ends already in the Early Miocene.
- Subsequently, active shortening shifts to the northern frontal thrust zone and the whole Pamirs become thrusted onto the Alai range.

Fig. 3.23 (next page): Schematic sequence of tectonic events. Total shortening between the southern Pamirs and stable Eurasia is assumed to be 440 km corresponding to 4° of palaeolatitude. Convergence first pushes the southern and central Pamirs against the northern Pamirs causing internal shortening by about 160 km (A). Then the whole Pamirs are displaced northward by about 280 km (B). Shortening amounts given must be considered as rough estimates. Shortening within the metamorphic dome and the northern Pamirs has been assumed to be negligible.

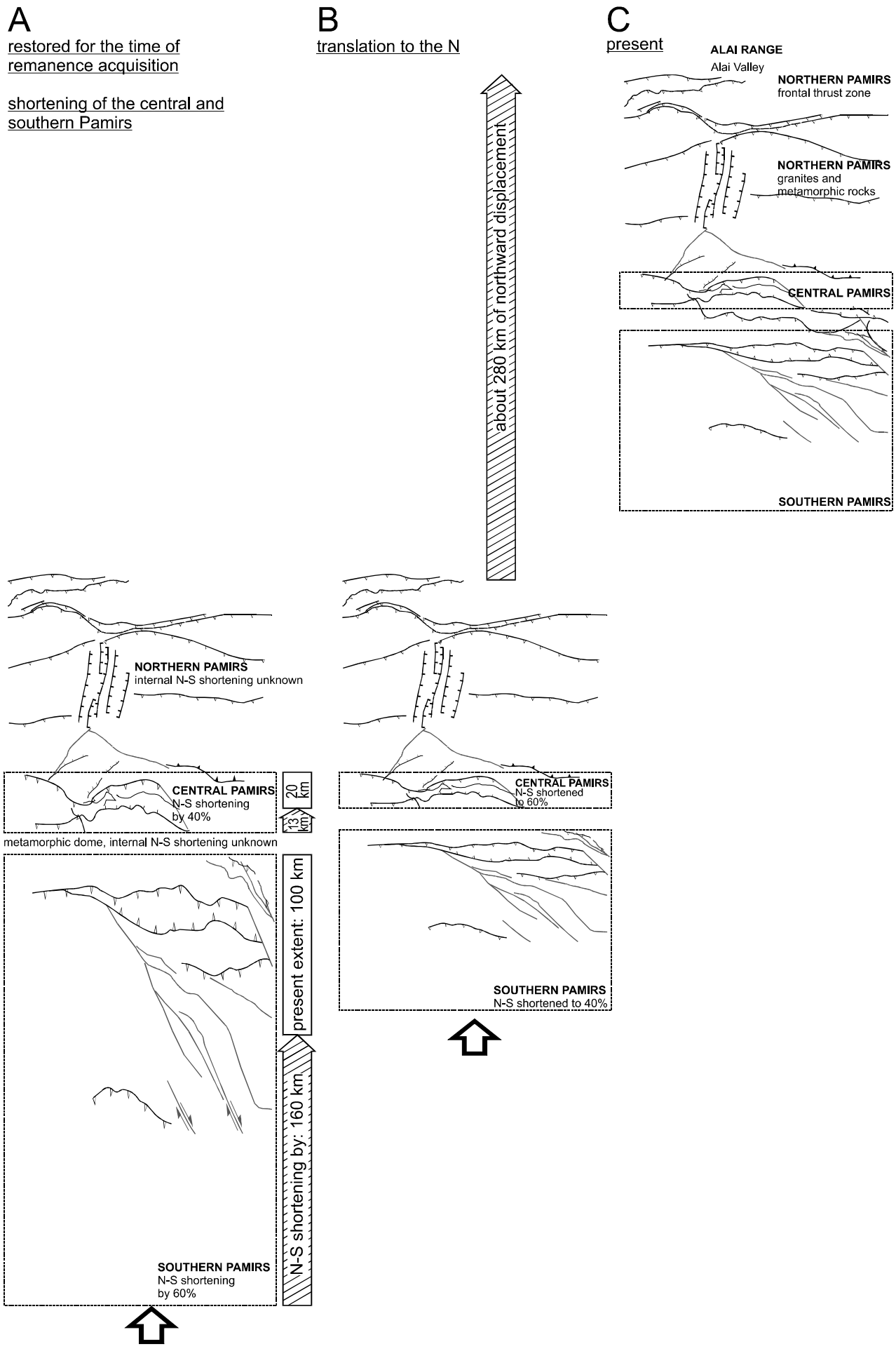
A
restored for the time of remanence acquisition
shortening of the central and southern Pamirs
B
translation to the N
about 280 km of northward displacement
C
present
ALAI RANGE
Alai Valley
NORTHERN PAMIRS
frontal thrust zone
NORTHERN PAMIRS
granites and metamorphic rocks
CENTRAL PAMIRS
SOUTHERN PAMIRS
NORTHERN PAMIRS
internal N-S shortening unknown
CENTRAL PAMIRS
N-S shortening by 40%
20 km
13 km
metamorphic dome, internal N-S shortening unknown
present extent: 100 km
N-S shortening by: 160 km
SOUTHERN PAMIRS
N-S shortening by 60%
CENTRAL PAMIRS
N-S shortened to 60%
SOUTHERN PAMIRS
N-S shortened to 40%

4. Glossary of New and Frequently Used Terms and Abbreviations

AF, TH	Demagnetisation methods, in alternating field (AF) and thermal (TH).
AMS	Anisotropy of the magnetic susceptibility.
angular distance *d*	Distance of a remanence to its corresponding tilting direction or Π-circle as a fraction of the radius. Depending on the direction of tilting, its amount varies between 0 (N-S tilting) and cos I_{acq} (E-W tilting).
APWP	Apparent polar wander path.
bedding corrected remanence (tilt corrected remanence, remanence in bedding coordinates)	Remanence in the horizontal orientation of a rock layer at the time of acquisition. Bedding correction tilts a rock layer back to the horizontal around the strike of the layer by the angle of the dip. Bedding correction can only be applied to primary remanences.
CRM	Chemical remanent magnetisation, acquired during growth of a ferrimagnetic mineral above a critical size (blocking volume).
D_{acq}, I_{acq}	Declination and inclination of the Earth's magnetic field at the site location at the time of remanence acquisition.
$D_{is}/I_{is,}$ D_{bc}/I_{bc}	Declination and inclination in in-situ and bedding coordinates.
d-angle	arccos *d*, can vary between 0° and 180° (see angular distance *d*).
differential vectors	Calculated from the remanence directions during demagnetisation by component analysis from one demagnetisation step to the next.
direct reconstruction	Each Fisher site mean or remanence small-circle has four direct reconstructions with angles of block rotation and backtilting below 180°. Two reconstructions relate to normal and two to reverse field polarity.
displacement/displacement path	**Here:** Refers only to tectonic tilting and block rotation.
Fisher distribution	Two-dimensional Gaussian distribution of vectors around a mean direction on the sphere (Fisher 1953).
Fisher (site) mean (usually called *site mean*)	Mean direction for a number of remanence components (vectors), calculated on the assumption of a two-dimensional Gaussian distribution around a mean direction on the sphere (Fisher 1953).
tilting direction	**Here:** Projection of the dip vector of a layer to the horizontal. Tilting direction is perpendicular to tilt axis.
in-situ remanence (remanence in in-situ coordinates)	Remanence in the present day orientation of the rock in the field. Shows the net tectonic displacement since remanence acquisition.
IRM	Isothermal remanent magnetisation.

maximum I_{acq}	arccos $\|d\|$. The highest inclination, to which a remanence can be moved by tilting around its corresponding tilt axis. The maximum I_{acq} depends on the tilting direction and on the inclination of the acquisition field, and is an upper constraint on the field inclination at the time of remanence acquisition.
mean small circle	Small circle fitted to a distribution of remanences, assumed to represent a small circle distribution caused by tilting and therefore perpendicular to the corresponding tilt axis.
NRM	Natural remanent magnetisation.
Π-circle	Mean great circle for a distribution of bedding poles.
palaeofield, palaeofield inclination	Earth magnetic field/field inclination at the time of the acquisition of a palaeomagnetic remanence.
PCA	Principal component analysis according to Kirschvink (1980).
PSD-particle	Pseudosingle domain particle; ferrimagnetic particle with several magnetic domains. Usually with medium to low coercivity.
remanence/palaeoremanence	**Here:** All kinds of palaeomagnetic directional remanence data (sum vectors, differential vectors, remanence components).
remanence component	**Here:** Palaeomagnetic remanence vector isolated by component analysis in a single rock specimen.
remanence direction	**Here:** Remanence measured during the demagnetisation of single specimens. Sum vector of all remanence components in a specimen.
reference field/palaeofield	Earth magnetic field at the time of remanence acquisition.
remanence small circle	Small circle on which remanences are distributed by tectonic tilting (vertical small circle) or block rotation (horizontal small circle).
SD-particle	Single domain particle; ferrimagnetic particle ideally with one magnetic domain, having high coercivity.
SIRM	Saturation isothermal remanent magnetisation.
small circle of constant field/ palaeofield inclination	Small circle normal to the z-axis with a constant field inclination (e.g. I = 60°). The intersections of the remanence small circle with the small circle of constant field inclination give the possible tectonic reconstructions.
site mean	See *Fisher mean*.
TRM	Thermal remanent magnetisation, acquired in the course of cooling of a ferrimagnetic particle below its blocking temperature.

5. References

Appel, E., Müller, R. & Widder, R.W. (1991). Palaeomagnetic results from the Tibetan Sedimentary Series of the Manang area (north central Nepal), Geophys. J. Int., 104, 255-266.

Appel, E., Patzelt, A. & Chouker, C. (1995). Secondary palaeoremanence of Tethyan sediments from the Zanskar Range (NW Himalaya). Geophys. J. Int., 122, 227-242.

Beck, R.A., Burbank, D.W., Sercombe, W.J., Riley, G.W., Barndt, J.K., Berry, J.R., Afzal, J., Khan, A.M., Jurgen, H., Metje, J., Cheema, A., Shafique, N.A., Lawrence, R.D. & Khan, M.A. (1995). Stratigraphic evidence for an early collision between northwest India and Asia. Nature, 373, 55-58.

Besse, J. & Courtillot, V. (1991). Revised and synthetic apparent polar wander paths of the African, Eurasian, North American and Indian plates, and true polar wander paths since 200 Ma. J. Geophys. Res., 96, 4029-4050.

Burtman, V.S. & Molnar, P. (1993). Geological and geophysical evidence for deep subduction of continental crust beneath the Pamir. Spec. Pap. Geol. Soc. Am., 281, 76 pp.

Chen, Y.,Courtillot, V., Cogne, J.P., Besse, J., Yang, Z. & Enkin, R. (1993a). The configuration of Asia prior to the collision of India: Cretaceous paleomagnetic constraints. J. Geophys. Res., 98, 21927-21941.

Chen, Y., Cogne, J.P., Courtillot, V., Tapponnier, P. & Zhu, X.Y.(1993b). Cretaceous paleomagnetic results from Western Tibet and tectonic implications. J. Geophys. Res., 98, 17981-17999.

Crouzet, C., Ménard, G. & Rochette, P. (1996). Post-Middle Miocene rotations recorded in the Bourg d'Oisans area (Western Alps, France) by paleomagnetism. Tectonophysics, 263, 137-148.

DeMets, C., Gordon, R.G., Argus, D.F, & Sein, S. (1990). Current plate motions. Geophys. J. Int., 101, 425-478.

Fisher, N.I., Lewis, T. & Embleton B.J.J. (1987). Statistical analysis of spherical data. Cambridge University Press, New York, 329pp.

Fisher, R. A. (1953). Dispersion on a sphere. Proc. Roy. Soc., A, 217, 295-305.

Gray, N.H., Geiser, P.A. & Geiser, J.R. (1980). On the least-squares fit of small and great circles to spherically projected orientation data. J. Math. Geol., 12, 173-184.

Hamburger, M.W., Sarewitz, D.R., Pavlis, T.L. & Papandopoulo, G.A. (1992). Structural and seismic evidence for intracontinental subduction in the Peter The First Range, Central Asia. Geol. Soc. Am. Bull., 104, 397-408.

Kirschvink, J.L. (1980). The least-squares line and plane and the analysis of palaeomagnetic data. Geophys. J. R. Astron. Soc., 62, 699-718.

Klootwijk, C.T., Nazirullah, R. & DeJong, K.A. (1986). Palaeomagnetic constraints on formation of the Mianwali reentrant, Trans Indus and Western Salt Range, Pakistan. Earth Planet. Sci. Lett., 80, 394-414.

Klootwijk, C.T., Gee, J.S., Peirce, J.W. & Smith, G.M. (1991). Constraints on the India-Asia Convergence: Paleomagnetic Results from Ninetyeast Ridge, in: Proc. ODP, Sci. Results, 121, 777-881, eds.: J. Weissel, J. Peirce, et al., College Station, TX (Ocean Drilling Program).

Klootwijk, C.T., Conaghan, P.J., Nazirullah, R. & Jong K.A. (1994). Further palaeomagnetic data from Chitral (Eastern Hindukush): evidence for an early India-Asia contact. Tectonophysics, 237, 1-25.

Le Fort, P. (1975). Himalayas: the collided range. Present knowledge of the continental arc. Am. J. Sci., 275A, 1-44.

MacDonald, W.D. (1980). Net tectonic rotation, apparent tectonic rotation, and the structural tilt correction in paleomagnetic studies. J. Geophys. Res., Vol. 85, No. B7, 3659-3669.

Mardia, K.V. & Gadsden, R.J. (1977). A small circle of best fit for spherical data and areas of vulcanism. Appl. Statist. 26, 238-245.

Ménard, G. & Rochette, P. (1992). Utilisation de réaimantations postmétamorphiques pour une étude de l'évolution tectonique et thermique tardive dans les Alpes occidentales (France). Bull. soc. géol. France, t. 163, n. 4, 381-392.

McElhinny, M.W. (1964). Statistical significance of the fold test in palaeomagnetism. Geophys. J. R. Astron. Soc., 8, 338-340.

McFadden, P.L. (1990). A new foldtest for palaeomagnetic studies. Geophy. J. Int., 103, 163-169.

Molnar, P. & Tapponnier, P. (1975). Cenozoic tectonics of Asia; effects of a continental collision. Science, 189, 419-426.

Ogg, J. (1995). Magnetic polarity time scale of the Phanerozoic, in: T. Ahrens (ed.) Global Earth Physics: A Handbook of Physical Constants, AGU Reference Shelf series, 1, Am. Geophys. Union, 240-270.

Patzelt, A., Huamei, L., Wang, J., & Appel, E. (1996). Palaeomagnetism of Cretaceous to Tertiary sediments from southern Tibet: evidence for the extent of the northern margin of India prior to the collision with Eurasia. Tectonophysics, 259, 259-284.

Piper, J.D.A. (1987). Palaeomagnetism and the continental crust. Open Univ. Press, Milton Keynes.

Pozzi, J.-P. & Feinberg, H. (1994). Paleomagnetism in Tajikistan: continental shortening of European margin in the Pamirs during Indian Eurasian collision. Earth Planet. Sci. Lett., 103, 365-378.

Russian Geology Ministery (1980). Geological Map of Kyrgyzstan, scale 1:500.000, sheet J-43-A, St. Petersburg.

Russian Geology Ministery (1984). Geological Map of the Tadjik SSR and adjoining territories, scale 1:500.000, St. Petersburg.

Strecker, M.R., Frisch, W., Hamburger M.W., Ratschbacher, L., Semiletkin, S., Zamoruyev, A., & Sturchio, N. (1995). Quaternary deformation in the Eastern Pamirs, Tadzhikistan and Kyrgyzstan. Tectonics, Vol. 14, No. 5, 1061-1079.

Tarling, D.H.. (1971). Principles and applications of paleomagnetism. Chapman and Hall, London, 164p.

Thomas, J.C., Chauvin, A., Gapais, D., Bazhenov, M.L., Perroud, H., Cobbold, P.R. & Burtman, V.S. (1994). Paleomagnetic evidence for Cenozoic block rotations in the Tadjik depression (Central Asia). J. Geophys. Res., 99, B8, 15141-15160.

Wang, Q.M., Nishidai, T. & Coward, M.P. (1992). The Tarim Basin, NW China: Formation and aspects of petroleum geology. Journal of Petroleum Geology, 15, 5-34.

6. Appendix

Sites with Fisher mean (k>10)

s. 13	backt.	bl.rot.	% unt.	sns.	remark	pol.
bed. (°)	4	-13±21	-22	-	indiff.	n
356	68	-139±21	-378	-	overt.	n
18	-112	41±21	622	+	>dip	r
upright	-176	167±21	978	+	>dip	r

s. 30	backt.	bl.rot.	% unt.	sns.	remark	pol.
bed. (°)	-14	16±21	19	+	upr.	n
9	55	166±21	-77	-	overt.	n
71	-126	-164±21	177	+	>dip	r
	166	-14±21	-234	-	>dip	r

s. 23	backt.	bl.rot.	% unt.	sns.	remark	pol.
bed. (°)	9	66±12	-20	-	indiff.	r
359	53	136±12	-112	-	overt.	r
47	-127	-114±12	271	+	>dip	n
	-171	-44±12	363	+	>dip	n

s. 31	backt.	bl.rot.	% unt.	sns.	remark	pol.
bed. (°)	-39	21±31	64	+	upr.	n
30	17	119±31	-29	-	overt.	n
60	-163	-159±31	271	+	>dip	r
upright	142	-61±31	-236	-	>dip	r

s. 24	backt.	bl.rot.	% unt.	sns.	remark	pol.
bed. (°)	-85	34±26	207	+	>dip	n
29	-40	108±26	97	+	upr.	n
41	140	-140±26	-342	-	>dip	r
	95	-72±26	-232	-	overt.	r

s. 34	backt.	bl.rot.	% unt.	sns.	remark	pol.
bed. (°)	-25	57±19	-37	-	overt.	n
158	40	-173±19	60	+	upr.	n
67	-140	-123±19	-209	-	>dip	r
overt.	155	7±19	231	+	>dip	r

s. 25	backt.	bl.rot.	% unt.	sns.	remark	pol.
bed. (°)	-86	26±16	226	+	>dip	n
19	-26	136±16	69	+	upr.	n
38	154	-154±16	-404	-	>dip	r
	94	-44±16	-248	-	overt.	r

s. 35	backt.	bl.rot.	% unt.	sns.	remark	pol.
bed. (°)	-38	79±18	62	+	upr.	n
343	9	155±18	-14	-	indiff.	n
61	-171	-101±18	281	+	>dip	r
upright	142	-25±18	-233	-	>dip	r

s. 27	backt.	bl.rot.	% unt.	sns.	remark	pol.
bed. (°)	27	73±25	39	+	upr.	n
183	59	121±25	86	+	upr.	n
68	-121	-107±25	-178	-	overt.	r
	-153	-59±25	-225	-	>dip	r

s. 36	backt.	bl.rot.	% unt.	sns.	remark	pol.
bed. (°)	-97	50±13	-180	-	overt.	n
180	-41	150±13	-75	-	overt.	n
54	139	-130±13	258	+	>dip	r
	83	-30±13	153	+	>dip	r

s. 28	backt.	bl.rot.	% unt.	sns.	remark	pol.
bed. (°)	-77	7±18	-109	-	overt.	r
180	-7	-167±18	-9	-	indiff.	r
70	173	-173±18	248	+	>dip	n
	103	13±18	148	+	>dip	n

s. 37	backt.	bl.rot.	% unt.	sns.	remark	pol.
bed. (°)	-54	30±17	-119	-	overt.	n
205	-1	120±17	-2	-	indiff.	n
45	179	-150±17	398	+	>dip	r
	127	-66±17	281	+	>dip	r

s. 29	backt.	bl.rot.	% unt.	sns.	remark	pol.
bed. (°)	-105	19±28	244	+	>dip	n
18	-41	145±28	96	+	upr.	n
43	139	-101±28	-323	-	overt.	r
	75	-35±28	-175	-	overt.	r

s. 107	backt.	bl.rot.	% unt.	sns.	remark	pol.
bed. (°)	12	3±21	-44	-	overt.	n
4	82	-171±21	-303	-	overt.	n
27	-98	-177±21	364	+	>dip	r
	-168	9±21	623	+	>dip	r

Fig. 6.1, continued on next page

Sites with small-circle distribution

s.11	bl.rot.	cf.int.	sns.	remark	pol.
bed. (°)	27	-12+21	-	overt.	n
223	87	-21+12	-	overt.	n
64	-153	-12+21	+	>dip	r
	-93	-21+12	+	>dip	r

s.14	bl.rot.	cf.int.	sns.	remark	pol.
bed. (°)	36	-14+18	-	overt.	n
203	118	-18+14	-	overt.	n
68	-62	-14+18	+	>dip	r
overt.	-144	-18+14	+	>dip	r

s.12	bl.rot.	cf.int.	sns.	remark	pol.
bed. (°)	48	-24+?	+	upr.	n
21	110	+24-?	+	upr.	n
62	-132	-24+?	-	overt.	r
upright	-70	+24-?	-	overt.	r

s.32	bl.rot.	cf.int.	sns.	remark	pol.
bed. (°)	-32	-26+25	+	upr.?	n
39	154	-25+26	+	upr.?	n
70	148	-26+25	-	overt.	r
upright	-26	-25+26	-	overt.	r

s.33	bl.rot.	cf.int.	sns.	remark	pol.
bed. (°)	-61	-50+48	-	overt.	n
248	125	-48+50	-	overt.	n
61	119	-50+48	+	>dip	r
	-55	-48+50	+	>dip	r

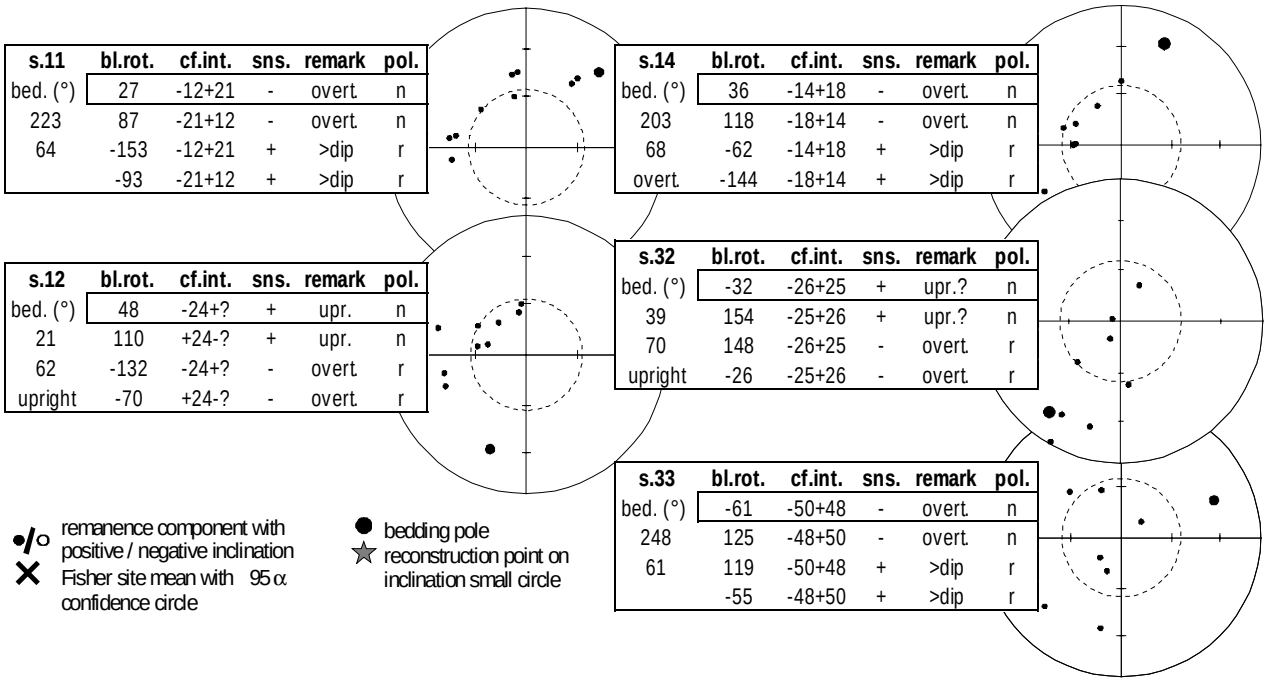

Fig. 6.1: The four direct reconstructions for the sites of the northern sequence. Reference palaeofield D/I = 10°/55°. For conventions see Fig. 1.1. Sites 23, 28 and 36 are volcanic rocks and bedding is from adjacent sediment layers. 14 sites have Fisher distributions and means with $k \geq 10$ (above). Five sites have small-circle distributions. bed (°): dip azimuth and dip angle with upright/overturned bedding where identified in the field. backt.: angle of backtilting (only for sites with site mean). bl.rot.: resulting angle of block rotation with the confidence interval $\pm\alpha 95/\cos I_{acq}$. For sites with small-circle distribution, the asymmetric confidence interval (cf.int.) is given. At site 12 one limit is outside the possible range and cannot be calculated (question mark). % unt.: percent of untilting related to the present dip assumed to be upright. sns: sense of tilting since remanence acquisition with respect to present bedding; + : with present upright bedding, - : against. Remark refers to upright (upr.) or overturned (overt.) bedding as the consequence of the comparison of present bedding with sense of backtilting (assuming that tilting did not reverse), indiff. : indifferent; used when angle of backtilting is below ±10°, >dip: angle of backtilting exceeds dip for either upright or overturned position by more than 10°. Except for sites 24, 25, 29 and 36, the shortest solution is the one which fits best to the overall result of a 20° counterclockwise block rotation determined for the whole sequence. The reconstruction thought to be the most probable within the general frame of a 20° counterclockwise block rotation for each site is framed.

Fig. 6.2 (next page): The four direct reconstructions for the sites of the southern sequence. Reference field D/I = 10°/55°. For conventions and symbols see Fig. 6.1 and Fig. 1.1. All sites have site means with a precision parameter of $k \geq 10$. Site 3 requires a too low I_{acq} of 43° and has been rejected. Site 5.1 demands a field inclination of 47° which was used for its reconstruction because its is not much below 55°. The shortest and most probable reconstruction within the general frame of a -10° clockwise block rotation for each site is framed.

s. 1	backt.	bl.rot.	% unt.	sns.	remark	pol.
bed. (°)	-16	-40±19	23	+	upr.	n
340	12	-80±19	-17	-	overt.	n
67	164	140±19	-245	-	>dip	r
	-168	100±19	251	+	>dip	r

s. 115	backt.	bl.rot.	% unt.	sns.	remark	pol.
bed. (°)	-12	-17±28	19	+	upr.	n
328	27	-79±28	-42	-	overt.	n
64	-153	163±28	239	+	>dip	r
	168	101±28	-262	-	>dip	r

s. 2a	backt.	bl.rot.	% unt.	sns.	remark	pol.
bed. (°)	14	-14±21	41	+	upr.	n
162	70	-110±21	199	+	>dip	n
35	-110	70±21	-315	-	overt.	r
	-166	166±21	-473	-	>dip	r

s. 122	backt.	bl.rot.	% unt.	sns.	remark	pol.
bed. (°)	-3	18±32	-5	-	indiff.	n
179	66	-176±32	96	+	upr.	n
69	-114	-162±32	-165	-	overt.	r
	177	4±32	256	+	>dip	r

s. 2b	backt.	bl.rot.	% unt.	sns.	remark	pol.
bed. (°)	29	-17±17	-112	-	overt.	n
326	67	-75±17	-256	-	overt.	n
26	-151	163±17	580	+	>dip	r
	-114	105±17	437	+	>dip	r

s. 140	backt.	bl.rot.	% unt.	sns.	remark	pol.
bed. (°)	19	33±20	-28	-	overt.	n
353	87	-179±20	-129	-	overt.	n
67	-93	-147±20	139	+	>dip	r
	-161	1±20	240	+	>dip	r

s. 4	backt.	bl.rot.	% unt.	sns.	remark	pol.
bed. (°)	-2	-30±30	5	+	indiff.	n
334	29	-78±30	-55	-	overt.	n
53	-151	102±30	285	+	>dip	r
	178	150±30	-335	-	>dip	r

s. 142	backt.	bl.rot.	% unt.	sns.	remark	pol.
bed. (°)	15	-54±22	-65	-	overt.	n
55	84	144±22	-367	-	overt.	n
23	-96	126±22	416	+	>dip	r
	-165	-36±22	717	+	>dip	r

s. 5.1	backt.	bl.rot.	% unt.	sns.	remark	pol.
bed. (°)	15	-43±16	-20	-	overt.	n
333	35	-63±16	-47	-	overt.	n
74	-145	117±16	196	+	>dip	r
	-165	137±16	223	+	>dip	r

s. 144	backt.	bl.rot.	% unt.	sns.	remark	pol.
bed. (°)	1	26±17	1	+	indiff.	n
162	71	-150±17	99	+	upr.	n
72	-109	-154±17	-151	-	overt.	r
	-179	30±17	-249	-	>dip	r

s. 5.2	backt.	bl.rot.	% unt.	sns.	remark	pol.
bed. (°)	9	-3±14	-13	-	indiff.	r
333	66	-103±14	-89	-	overt.	r
74	-115	77±14	155	+	>dip	n
	-171	177±14	231	+	>dip	n

s. 145	backt.	bl.rot.	% unt.	sns.	remark	pol.
bed. (°)	17	-8±14	-34	-	overt.	n
327	64	-86±14	-131	-	overt.	n
49	-116	172±14	236	+	>dip	r
	-163	94±14	333	+	>dip	r

s. 6	backt.	bl.rot.	% unt.	sns.	remark	pol.
bed. (°)	32	-45±17	-41	-	overt.	n
347	61	-89±17	-79	-	overt.	n
78	-119	91±17	152	+	>dip	r
	-148	135±17	190	+	>dip	r

s. 146	backt.	bl.rot.	% unt.	sns.	remark	pol.
bed. (°)	-3	-2±15	6	+	indiff.	n
31	64	140±15	-153	-	overt.	n
42	-116	178±15	276	+	>dip	r
	177	-40±15	-422	-	>dip	r

s. 113	backt.	bl.rot.	% unt.	sns.	remark	pol.
bed. (°)	16	-59±37	-49	-	overt.	n
342	19	-65±37	-60	-	overt.	n
32	-161	121±37	502	+	>dip	r
	-164	115±37	513	+	>dip	r

s.155	backt.	bl.rot.	% unt.	sns.	remark	pol.
bed. (°)	1	-1±9	-1	-	indiff.	n
332	58	-103±9	-74	-	overt.	n
78	-122	179±9	157	+	>dip	r
	-179	77±9	230	+	>dip	r

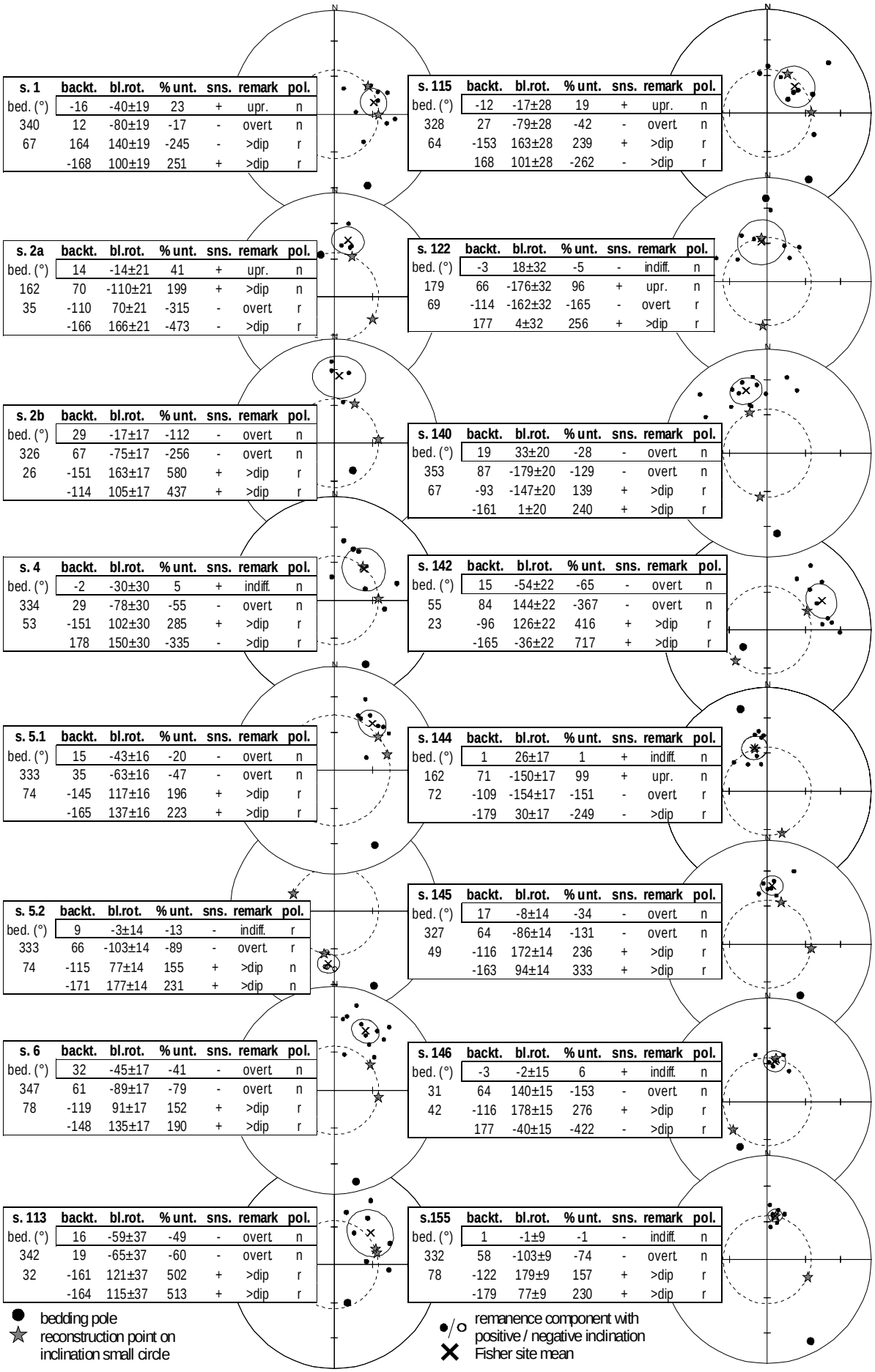

● bedding pole
★ reconstruction point on inclination small circle

●/○ remanence component with positive / negative inclination
✕ Fisher site mean

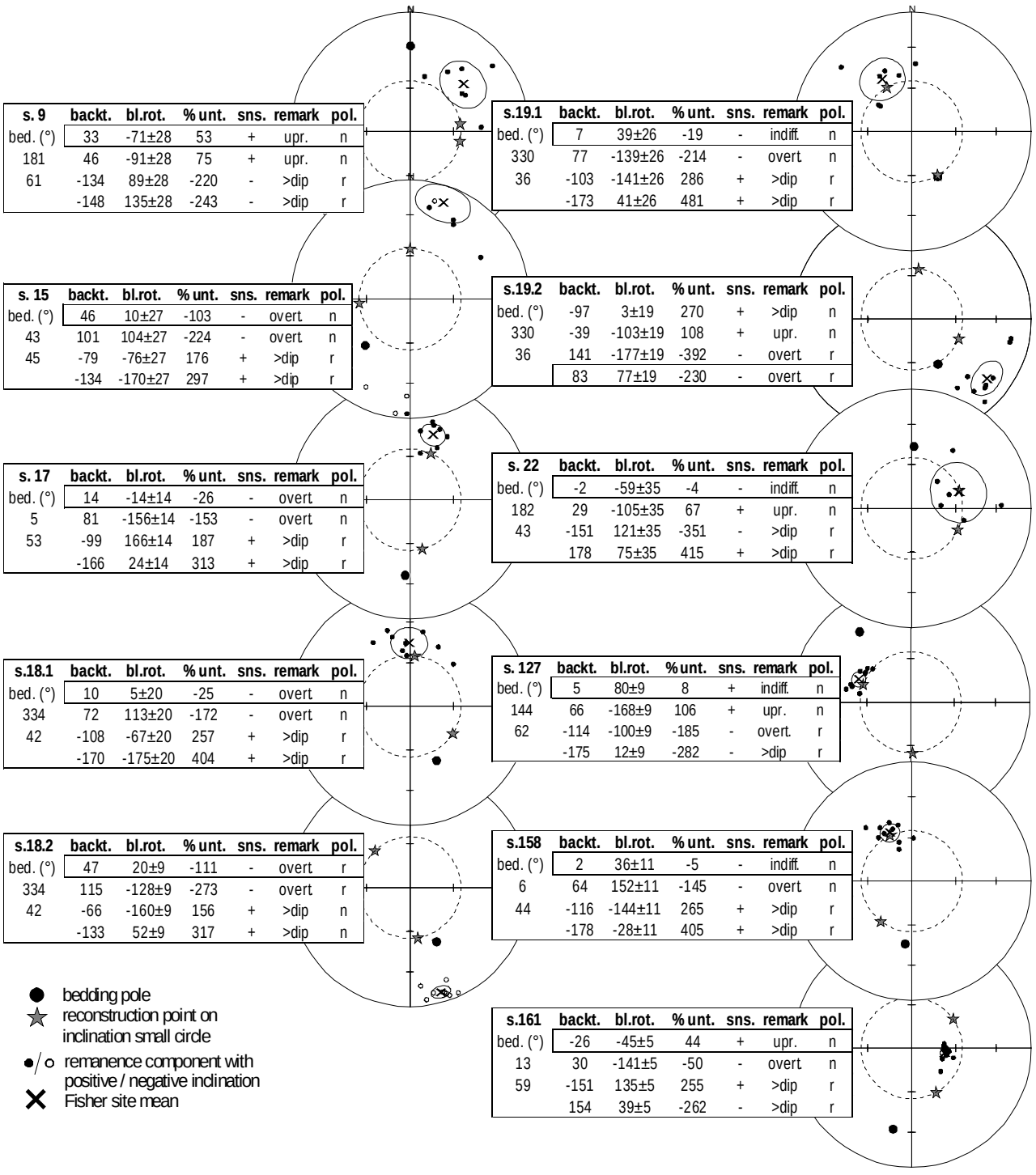

s. 9	backt.	bl.rot.	% unt.	sns.	remark	pol.
bed. (°)	33	-71±28	53	+	upr.	n
181	46	-91±28	75	+	upr.	n
61	-134	89±28	-220	-	>dip	r
	-148	135±28	-243	-	>dip	r

s.19.1	backt.	bl.rot.	% unt.	sns.	remark	pol.
bed. (°)	7	39±26	-19	-	indiff.	n
330	77	-139±26	-214	-	overt.	n
36	-103	-141±26	286	+	>dip	r
	-173	41±26	481	+	>dip	r

s. 15	backt.	bl.rot.	% unt.	sns.	remark	pol.
bed. (°)	46	10±27	-103	-	overt.	n
43	101	104±27	-224	-	overt.	n
45	-79	-76±27	176	+	>dip	r
	-134	-170±27	297	+	>dip	r

s.19.2	backt.	bl.rot.	% unt.	sns.	remark	pol.
bed. (°)	-97	3±19	270	+	>dip	n
330	-39	-103±19	108	+	upr.	n
36	141	-177±19	-392	-	overt.	r
	83	77±19	-230	-	overt.	r

s. 17	backt.	bl.rot.	% unt.	sns.	remark	pol.
bed. (°)	14	-14±14	-26	-	overt.	n
5	81	-156±14	-153	-	overt.	n
53	-99	166±14	187	+	>dip	r
	-166	24±14	313	+	>dip	r

s. 22	backt.	bl.rot.	% unt.	sns.	remark	pol.
bed. (°)	-2	-59±35	-4	-	indiff.	n
182	29	-105±35	67	+	upr.	n
43	-151	121±35	-351	-	>dip	r
	178	75±35	415	+	>dip	r

s.18.1	backt.	bl.rot.	% unt.	sns.	remark	pol.
bed. (°)	10	5±20	-25	-	overt.	n
334	72	113±20	-172	-	overt.	n
42	-108	-67±20	257	+	>dip	r
	-170	-175±20	404	+	>dip	r

s. 127	backt.	bl.rot.	% unt.	sns.	remark	pol.
bed. (°)	5	80±9	8	+	indiff.	n
144	66	-168±9	106	+	upr.	n
62	-114	-100±9	-185	-	overt.	r
	-175	12±9	-282	-	>dip	r

s.18.2	backt.	bl.rot.	% unt.	sns.	remark	pol.
bed. (°)	47	20±9	-111	-	overt.	r
334	115	-128±9	-273	-	overt.	r
42	-66	-160±9	156	+	>dip	n
	-133	52±9	317	+	>dip	n

s.158	backt.	bl.rot.	% unt.	sns.	remark	pol.
bed. (°)	2	36±11	-5	-	indiff.	n
6	64	152±11	-145	-	overt.	n
44	-116	-144±11	265	+	>dip	r
	-178	-28±11	405	+	>dip	r

s.161	backt.	bl.rot.	% unt.	sns.	remark	pol.
bed. (°)	-26	-45±5	44	+	upr.	n
13	30	-141±5	-50	-	overt.	n
59	-151	135±5	255	+	>dip	r
	154	39±5	-262	-	>dip	r

Fig. 6.3: The four direct reconstructions for the sites of the southern Pamirs outside the two folded sequences. Site 16 is not considered because it requires a too low maximum I_{acq} of 40°. Reference palaeofield D/I = 10°/55°. For terminology, conventions and symbols see Fig. 6.1 and Fig. 1.1. All sites have site means with $k \geq 10$. The shortest and/or most probable reconstruction within the general framework for each site is framed.

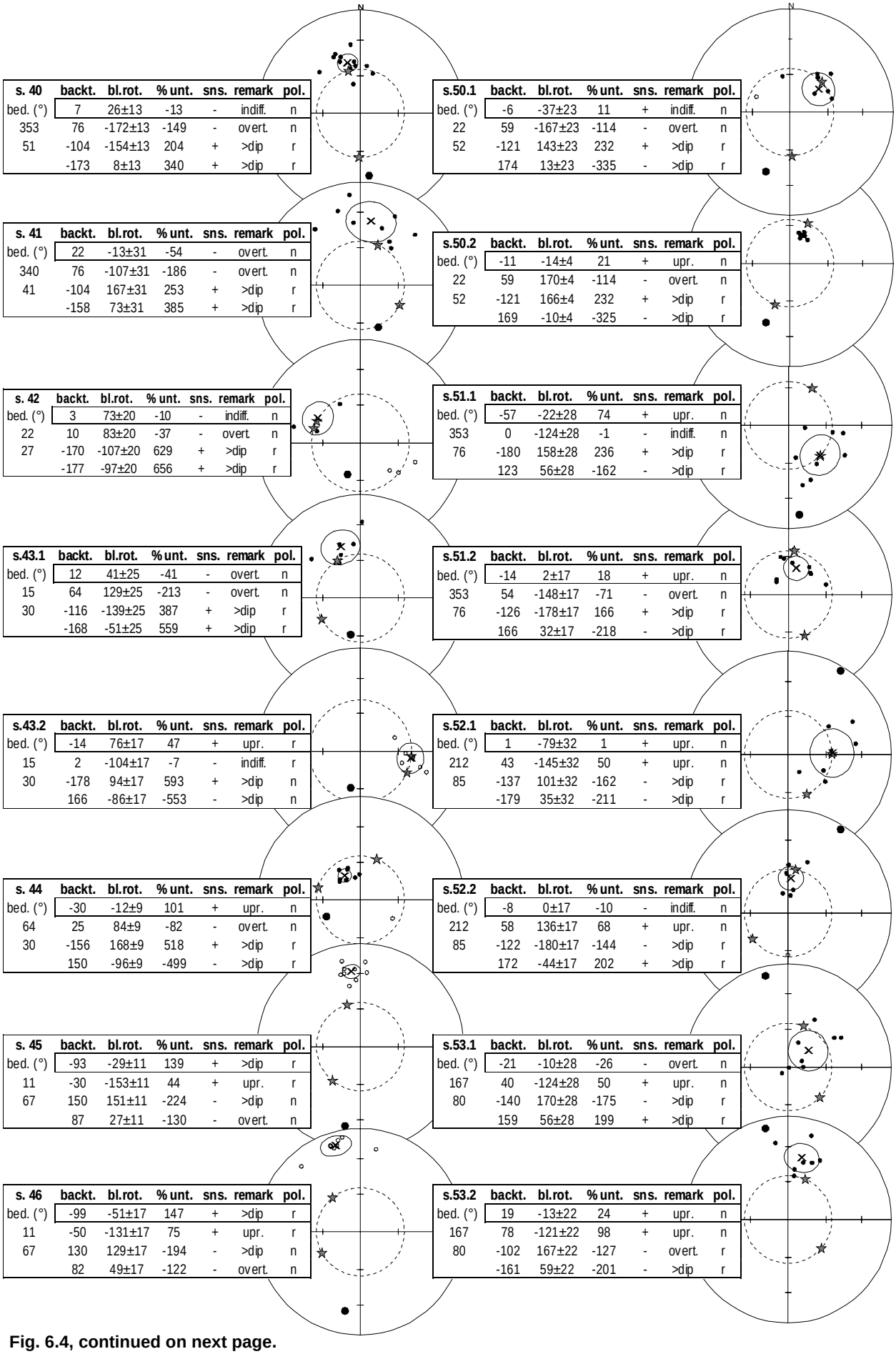

s. 40	backt.	bl.rot.	% unt.	sns.	remark	pol.
bed. (°)	7	26±13	-13	-	indiff.	n
353	76	-172±13	-149	-	overt.	n
51	-104	-154±13	204	+	>dip	r
	-173	8±13	340	+	>dip	r

s.50.1	backt.	bl.rot.	% unt.	sns.	remark	pol.
bed. (°)	-6	-37±23	11	+	indiff.	n
22	59	-167±23	-114	-	overt.	n
52	-121	143±23	232	+	>dip	r
	174	13±23	-335	-	>dip	r

s. 41	backt.	bl.rot.	% unt.	sns.	remark	pol.
bed. (°)	22	-13±31	-54	-	overt.	n
340	76	-107±31	-186	-	overt.	n
41	-104	167±31	253	+	>dip	r
	-158	73±31	385	+	>dip	r

s.50.2	backt.	bl.rot.	% unt.	sns.	remark	pol.
bed. (°)	-11	-14±4	21	+	upr.	n
22	59	170±4	-114	-	overt.	n
52	-121	166±4	232	+	>dip	r
	169	-10±4	-325	-	>dip	r

s. 42	backt.	bl.rot.	% unt.	sns.	remark	pol.
bed. (°)	3	73±20	-10	-	indiff.	n
22	10	83±20	-37	-	overt.	n
27	-170	-107±20	629	+	>dip	r
	-177	-97±20	656	+	>dip	r

s.51.1	backt.	bl.rot.	% unt.	sns.	remark	pol.
bed. (°)	-57	-22±28	74	+	upr.	n
353	0	-124±28	-1	-	indiff.	n
76	-180	158±28	236	+	>dip	r
	123	56±28	-162	-	>dip	r

s.43.1	backt.	bl.rot.	% unt.	sns.	remark	pol.
bed. (°)	12	41±25	-41	-	overt.	n
15	64	129±25	-213	-	overt.	n
30	-116	-139±25	387	+	>dip	r
	-168	-51±25	559	+	>dip	r

s.51.2	backt.	bl.rot.	% unt.	sns.	remark	pol.
bed. (°)	-14	2±17	18	+	upr.	n
353	54	-148±17	-71	-	overt.	n
76	-126	-178±17	166	+	>dip	r
	166	32±17	-218	-	>dip	r

s.43.2	backt.	bl.rot.	% unt.	sns.	remark	pol.
bed. (°)	-14	76±17	47	+	upr.	r
15	2	-104±17	-7	-	indiff.	r
30	-178	94±17	593	+	>dip	n
	166	-86±17	-553	-	>dip	n

s.52.1	backt.	bl.rot.	% unt.	sns.	remark	pol.
bed. (°)	1	-79±32	1	+	upr.	n
212	43	-145±32	50	+	upr.	n
85	-137	101±32	-162	-	>dip	r
	-179	35±32	-211	-	>dip	r

s. 44	backt.	bl.rot.	% unt.	sns.	remark	pol.
bed. (°)	-30	-12±9	101	+	upr.	n
64	25	84±9	-82	-	overt.	n
30	-156	168±9	518	+	>dip	r
	150	-96±9	-499	-	>dip	r

s.52.2	backt.	bl.rot.	% unt.	sns.	remark	pol.
bed. (°)	-8	0±17	-10	-	indiff.	n
212	58	136±17	68	+	upr.	n
85	-122	-180±17	-144	-	>dip	r
	172	-44±17	202	+	>dip	r

s. 45	backt.	bl.rot.	% unt.	sns.	remark	pol.
bed. (°)	-93	-29±11	139	+	>dip	r
11	-30	-153±11	44	+	upr.	r
67	150	151±11	-224	-	>dip	n
	87	27±11	-130	-	overt.	n

s.53.1	backt.	bl.rot.	% unt.	sns.	remark	pol.
bed. (°)	-21	-10±28	-26	-	overt.	n
167	40	-124±28	50	+	upr.	n
80	-140	170±28	-175	-	>dip	r
	159	56±28	199	+	>dip	r

s. 46	backt.	bl.rot.	% unt.	sns.	remark	pol.
bed. (°)	-99	-51±17	147	+	>dip	r
11	-50	-131±17	75	+	upr.	r
67	130	129±17	-194	-	>dip	n
	82	49±17	-122	-	overt.	n

s.53.2	backt.	bl.rot.	% unt.	sns.	remark	pol.
bed. (°)	19	-13±22	24	+	upr.	n
167	78	-121±22	98	+	upr.	n
80	-102	167±22	-127	-	overt.	r
	-161	59±22	-201	-	>dip	r

Fig. 6.4, continued on next page.

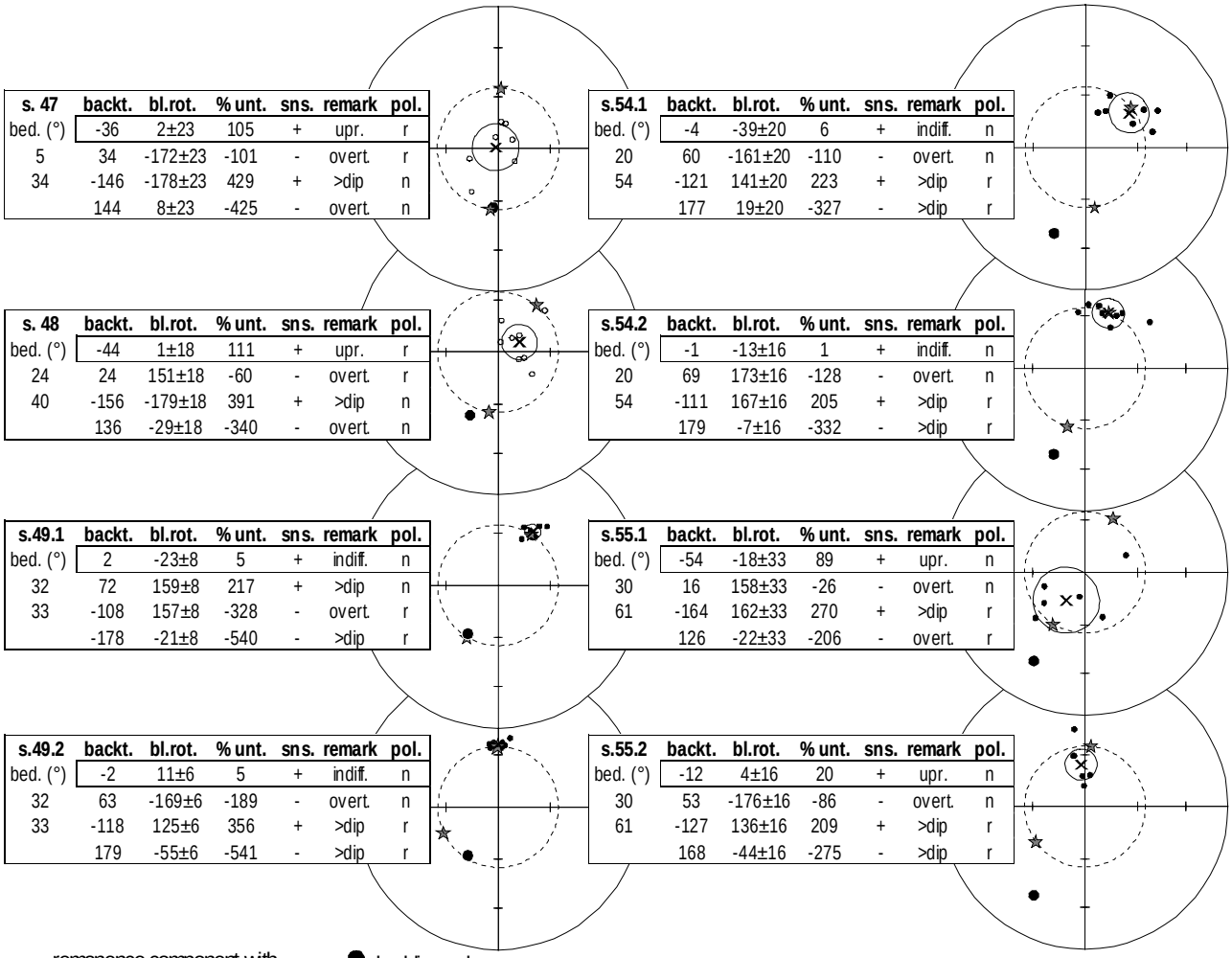

s. 47	backt.	bl.rot.	% unt.	sns.	remark	pol.
bed. (°)	-36	2±23	105	+	upr.	r
5	34	-172±23	-101	-	overt.	r
34	-146	-178±23	429	+	>dip	n
	144	8±23	-425	-	overt.	n

s.54.1	backt.	bl.rot.	% unt.	sns.	remark	pol.
bed. (°)	-4	-39±20	6	+	indiff.	n
20	60	-161±20	-110	-	overt.	n
54	-121	141±20	223	+	>dip	r
	177	19±20	-327	-	>dip	r

s. 48	backt.	bl.rot.	% unt.	sns.	remark	pol.
bed. (°)	-44	1±18	111	+	upr.	r
24	24	151±18	-60	-	overt.	r
40	-156	-179±18	391	+	>dip	n
	136	-29±18	-340	-	overt.	n

s.54.2	backt.	bl.rot.	% unt.	sns.	remark	pol.
bed. (°)	-1	-13±16	1	+	indiff.	n
20	69	173±16	-128	-	overt.	n
54	-111	167±16	205	+	>dip	r
	179	-7±16	-332	-	>dip	r

s.49.1	backt.	bl.rot.	% unt.	sns.	remark	pol.
bed. (°)	2	-23±8	5	+	indiff.	n
32	72	159±8	217	+	>dip	n
33	-108	157±8	-328	-	overt.	r
	-178	-21±8	-540	-	>dip	r

s.55.1	backt.	bl.rot.	% unt.	sns.	remark	pol.
bed. (°)	-54	-18±33	89	+	upr.	n
30	16	158±33	-26	-	overt.	n
61	-164	162±33	270	+	>dip	r
	126	-22±33	-206	-	overt.	r

s.49.2	backt.	bl.rot.	% unt.	sns.	remark	pol.
bed. (°)	-2	11±6	5	+	indiff.	n
32	63	-169±6	-189	-	overt.	n
33	-118	125±6	356	+	>dip	r
	179	-55±6	-541	-	>dip	r

s.55.2	backt.	bl.rot.	% unt.	sns.	remark	pol.
bed. (°)	-12	4±16	20	+	upr.	n
30	53	-176±16	-86	-	overt.	n
61	-127	136±16	209	+	>dip	r
	168	-44±16	-275	-	>dip	r

Fig. 6.4: The four direct reconstructions for the sites of the central Pamirs. Reference palaeofield D/I = 10°/55°. Site means 42 and 43.2 have been reconstructed using their maximum I_{acq} (see Table 3.8). For terminology and conventions see Fig. 6.1 and Fig. 1.1. All site means seem to have Fisher distributions with site means of $k \geq 10$. The reconstruction thought to be the most probable for each site is framed.

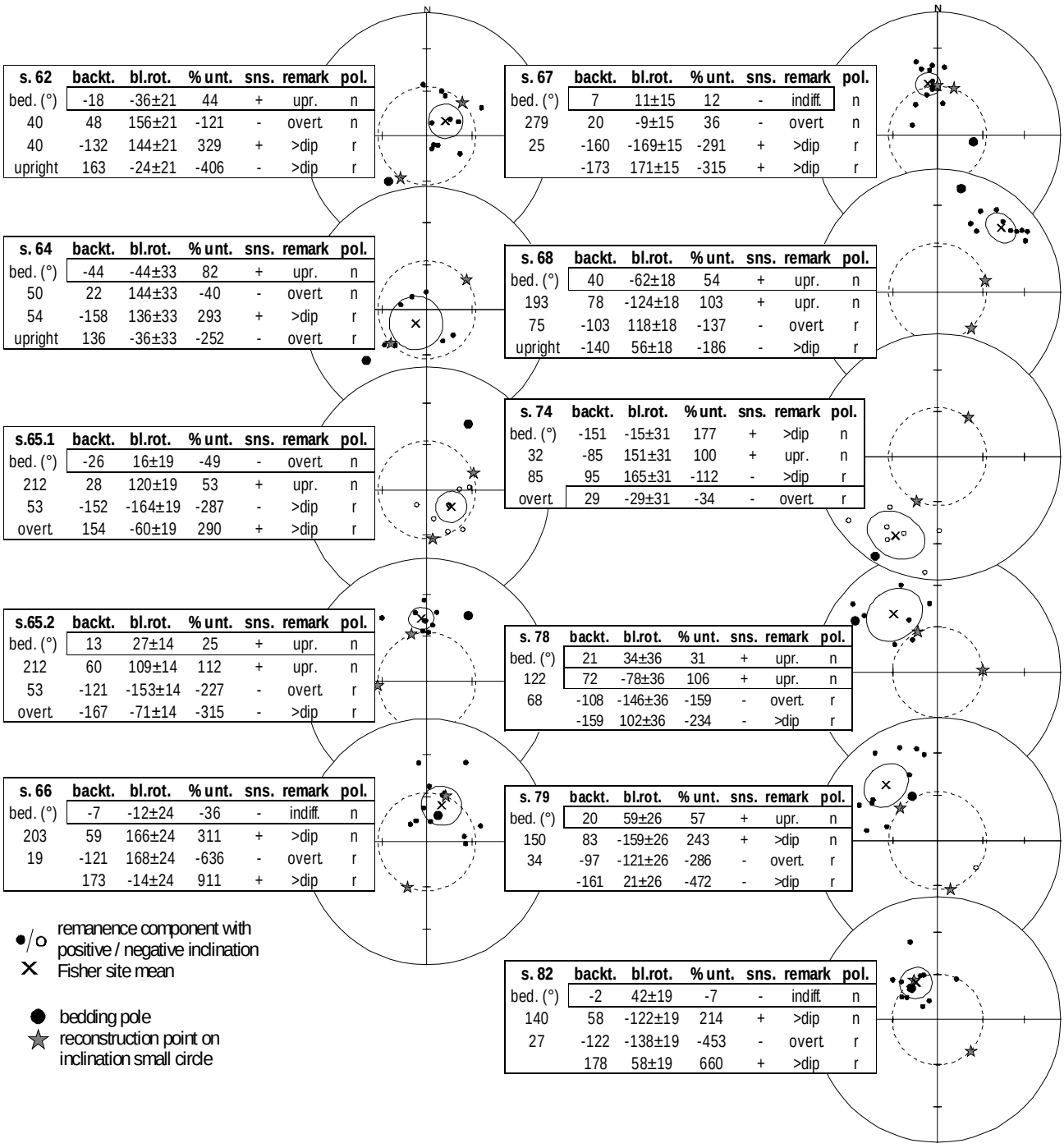

s. 62	backt.	bl.rot.	% unt.	sns.	remark	pol.
bed. (°)	-18	-36±21	44	+	upr.	n
40	48	156±21	-121	-	overt.	n
40	-132	144±21	329	+	>dip	r
upright	163	-24±21	-406	-	>dip	r

s. 67	backt.	bl.rot.	% unt.	sns.	remark	pol.
bed. (°)	7	11±15	12	-	indiff.	n
279	20	-9±15	36	-	overt.	n
25	-160	-169±15	-291	+	>dip	r
	-173	171±15	-315	+	>dip	r

s. 64	backt.	bl.rot.	% unt.	sns.	remark	pol.
bed. (°)	-44	-44±33	82	+	upr.	n
50	22	144±33	-40	-	overt.	n
54	-158	136±33	293	+	>dip	r
upright	136	-36±33	-252	-	overt.	r

s. 68	backt.	bl.rot.	% unt.	sns.	remark	pol.
bed. (°)	40	-62±18	54	+	upr.	n
193	78	-124±18	103	+	upr.	n
75	-103	118±18	-137	-	overt.	r
upright	-140	56±18	-186	-	>dip	r

s.65.1	backt.	bl.rot.	% unt.	sns.	remark	pol.
bed. (°)	-26	16±19	-49	-	overt.	n
212	28	120±19	53	+	upr.	n
53	-152	-164±19	-287	-	>dip	r
overt.	154	-60±19	290	+	>dip	r

s. 74	backt.	bl.rot.	% unt.	sns.	remark	pol.
bed. (°)	-151	-15±31	177	+	>dip	n
32	-85	151±31	100	+	upr.	n
85	95	165±31	-112	-	>dip	r
overt.	29	-29±31	-34	-	overt.	r

s.65.2	backt.	bl.rot.	% unt.	sns.	remark	pol.
bed. (°)	13	27±14	25	+	upr.	n
212	60	109±14	112	+	upr.	n
53	-121	-153±14	-227	-	overt.	r
overt.	-167	-71±14	-315	-	>dip	r

s. 78	backt.	bl.rot.	% unt.	sns.	remark	pol.
bed. (°)	21	34±36	31	+	upr.	n
122	72	-78±36	106	+	upr.	n
68	-108	-146±36	-159	-	overt.	r
	-159	102±36	-234	-	>dip	r

s. 66	backt.	bl.rot.	% unt.	sns.	remark	pol.
bed. (°)	-7	-12±24	-36	-	indiff.	n
203	59	166±24	311	+	>dip	n
19	-121	168±24	-636	-	overt.	r
	173	-14±24	911	+	>dip	r

s. 79	backt.	bl.rot.	% unt.	sns.	remark	pol.
bed. (°)	20	59±26	57	+	upr.	n
150	83	-159±26	243	+	>dip	n
34	-97	-121±26	-286	-	overt.	r
	-161	21±26	-472	-	>dip	r

s. 82	backt.	bl.rot.	% unt.	sns.	remark	pol.
bed. (°)	-2	42±19	-7	-	indiff.	n
140	58	-122±19	214	+	>dip	n
27	-122	-138±19	-453	-	overt.	r
	178	58±19	660	+	>dip	r

Fig. 6.5: The four direct reconstructions for the sites of the northern Pamirs and the Alai range. Reference palaeofield D/I = 10°/57° for the northern Pamirs and D/I = 10°/60° for the Alai range. For terminology and conventions see Fig. 6.1 and Fig. 1.1. The reconstruction thought to be the most probable for each site is framed. Site 78 has two solutions having the same probability.